



# Development of Smart Parabolic Trough Solar Collector for Water Heating and Hybrid Polymeric Composite Water Storage Tank

Idowu David Ibrahim

## ► To cite this version:

Idowu David Ibrahim. Development of Smart Parabolic Trough Solar Collector for Water Heating and Hybrid Polymeric Composite Water Storage Tank. Automatic Control Engineering. Université Paris-Saclay; Tshwane University of Technology, 2020. English. NNT : 2020UPASG049 . tel-03220701

**HAL Id: tel-03220701**

**<https://theses.hal.science/tel-03220701>**

Submitted on 7 May 2021

**HAL** is a multi-disciplinary open access archive for the deposit and dissemination of scientific research documents, whether they are published or not. The documents may come from teaching and research institutions in France or abroad, or from public or private research centers.

L'archive ouverte pluridisciplinaire **HAL**, est destinée au dépôt et à la diffusion de documents scientifiques de niveau recherche, publiés ou non, émanant des établissements d'enseignement et de recherche français ou étrangers, des laboratoires publics ou privés.



Développement d'un Système Chauffe-Eau Solaire Avec Poursuite  
Pour la Maximisation du Rendement et Réservoir de Stockage avec  
Isolation en Matériaux composites

Development of Smart Parabolic Trough Solar Collector for Water  
Heating and Hybrid Polymeric Composite Water Storage Tank

**Thèse de doctorat de l'université Paris-Saclay et de Tshwane  
University of Technology**

École doctorale n°580, Sciences et technologies de l'information et de la  
communication (STIC)

Spécialité de doctorat: Automatique

Unité de recherche : Université Paris-Saclay, UVSQ, LISV, 78124, Vélizy -Villacoublay,  
France

Référent : Université de Versailles -Saint-Quentin-en-Yvelines

**Thèse présentée et soutenue à Paris-Saclay, le 17 décembre 2020,  
par**

**Idowu David IBRAHIM**

## Composition du Jury

**François ROCARIES**

Professeur des universités, Tshwane Université of Technology

Président

**Abdulkarim AHMED**

Professeur, Ahmadu Bello Université

Rapporteur & Examineur

**Onyemaechi EKECHUKWU**

Professeur, Université of Nigeria

Rapporteur

**Anish KURIEN**

Professeur, Tshwane Université of Technology

Examineur

**Fadila MAROTEAUX**

Professeur, Université Paris-Saclay

Examinatrice

**Yasser ALAYLI**

Professeur, Université Paris-Saclay

Directeur de thèse

**Yskandar HAMAM**

Professeur, ESIEE Paris, Noisy-Le-Grand

Co-Directeur de thèse

**Rotimi SADIKU**

Professeur, Tshwane Université of Technology

Directeur de thèse

**Tamba JAMIRU**

Maître de Conférence, Tshwane Université of Technology

Invité

## DEDICATION

This project is dedicated first to God Almighty, the one who created the heaven and earth, the giver of life, knowledge, wisdom and understanding; the God who made it possible for me to embark on this research and finish it successfully. I also dedicate this research work to my wonderful, supportive, adorable and loving wife Barr. (Mrs.) Oluwaseyitan Solademi Ibrahim and my Family.

*"Now unto him that is able to do  
exceeding abundantly above all that we  
ask or think, according to the power  
that worketh in us"*

*Ephesians 3:20 KJV*

Thank you Lord

## **ACKNOWLEDGEMENTS**

My profound gratitude goes first to God Almighty, the creator of the universe, for His grace, mercy, love, provision, protection and help throughout my dual doctoral research. May His name be praised forever.

I wish to express my sincere appreciation to my France supervisor, Prof. Yasser Alayli from the Laboratoire d'Ingénierie des Systèmes de Versailles, Université de Versailles Saint-Quentin-en-Yvelines, France, for his understanding and continuous support during the process of my research.

I wish to express my sincere appreciation to my supervisor in South Africa, Prof. Emmanuel Rotimi Sadiku of the Department of Chemical, Metallurgical and Materials Engineering for making available the materials for the research. Thank you for your continuous guidance in both theoretical and practical experiences, throughout the study.

My earnest gratitude to my co-supervisor, Prof. Yskandar Hamam from the Department of Electrical Engineering. Thank you for all the support, encouragement, training and guidance given to me, and the interpretation and analysis of my research work.

To my entire supervisory team, I wish to express my deepest appreciation for your fatherly succour and absolute belief in me.

My sincere appreciation goes to TUT, the Dean of Faculty of Engineering and the Built Environment, Prof. Josiah Munda and the HOD of the Department of Mechanical and Mechatronics Engineering, Dr. Lodewyk Willem Beneke, for providing the platform and suitable environment to carry out this research.



I would also like to thank all the staff members of the Department of Mechanical and Mechatronics Engineering, for all the time we spent together as colleagues in the Department, and the wonderful experience.

I want to appreciate the entire members of the French South African Institute of Technology Institute (F'SATI) at the Tshwane University of Technology (TUT). My sincere appreciation goes to the F'SATI TUT Institute Node Director in the person of Prof Anish Kurien for bringing me into the dual doctoral program.

I would to appreciate the members of the Jury for this doctoral thesis for their valuable time and comments: Prof. François Rocaries (Président), Prof. Abdulkarim Ahmed (Rapporteur), Prof. Onyemaechi Ekechukwu (Rapporteur), Prof. Anish Kurien (Examineur), and Prof. Fadila Maroteaux (Examineur).

My sincere appreciation goes to the former Dean of the Faculty of Engineering and the Built Environment, Prof. Barend van Wyk, for the valuable suggestion towards the selection of one of the components for the research.

I would like to acknowledge and sincerely appreciate the Council for Scientific and Industrial Research (CSIR) and the Department of Science and Technology (DST), under the umbrella name of CSIR DST-Interbursary Support (IBS), South Africa, for the financial support during this research.

My gratitude goes to my father, Mr. Yusuf Ibrahim (late) and my mother Mrs. Maria Ibrahim for their efforts, support and godly upbringing since my birth to this moment, God bless you.

I wish to use this occasion to acknowledge my brothers: Sunday, Segun, Bidemi, Ayodele; sisters: Mrs. SE Igugu, Mrs. AH George and Kehinde Ibrahim; nephews and

niece: Henry Igugu, Maxwell Igugu, Ewaoluwa Ibrahim for all their contributions, encouragement, support and prayers for me. God bless you.

Best appreciation to Prof. and Dr. (Mrs.) Kupolati for being a father and a mother to me in South Africa, and for always checking on the wellbeing of my family. I would also like to thank Halleluyah Kupolati and to my “learned colleague” since my wife is also a lawyer, Fiyinfooluwa Kupolati. Thank you all.

I would like to acknowledge my adopted family, friends and fellow postgraduate colleagues, Rev. (Dr.) Amos Adeniyi and Family, Mrs. René Janse van Vuuren, Dr. T.A. Oloruntoba, Dr. O. Agboola and Family, Dr. T.K. Bello and Family, Dr A.A. Eze and Family, Dr. S. Owonubi and Family, Dr. S.O Adekomaya, Mr. Fameso and Family, Mr. Oyesola and Family, Mr. T.W. Olagbenro, Dr. G. Ogunbiyi, Dr. G. Adesina, Mr O.A. Ogunmefun, Thank you all.

Lastly, I wish to sincerely acknowledge and appreciate my adorable and beautiful wife, Barr. (Mrs.) Oluwaseyitan Solademi Ibrahim for being a pillar of support and encouragement for me throughout this study and always. I also appreciate my son, Joshua David Ibrahim for the joy you give to me. I will always love and cherish you all.

## LIST OF PUBLICATIONS

### Journal Articles (Published)

- 1 **Ibrahim I.D.**, Sadiku E.R., Jamiru T., Hamam Y., Alayli Y., Eze A.A., **2020**. Prospects of Nanostructured Composite Materials for Energy Harvesting and Storage. *Journal of King Saud University-Science*. 32: 758-764.
- 2 **Ibrahim I.D.**, Hamam Y., Alayli Y., Jamiru T., Sadiku R. **2020**. Design and Modification of Parabolic Trough Solar Collector for Performance Effectiveness. *IEEE Xplore* 1-5. **DOI:** [10.1109/REDEC49234.2020.9163896](https://doi.org/10.1109/REDEC49234.2020.9163896)
- 3 **Ibrahim ID**, Jamiru T, Sadiku ER, Hamam Y, Alayli Y, Kupolati WK, Eze AA. **2020**. Development and Application of Nanocomposite for Sustainable Rail Vehicle with Low Environmental Footprint. *International Journal of Lightweight Materials and Manufacture*. 3:193-197.
- 4 **ID Ibrahim**, T Jamiru, ER Sadiku, Y Hamam, Y Alayli, AA Eze. **2019**. Application of nanoparticles and composite materials for energy generation and storage. *IET Nanodielectrics*. 2(4): 115-122

### Journal Articles (Submitted)

- 5 **ID Ibrahim**, Y Hamam, Y Alayli, T Jamiru, ER Sadiku, WK Kupolati, AA Eze. A review on Africa energy supply through renewable energy production: Nigeria, Cameroon, Ghana and South Africa as case study. *Energy Strategy Reviews*. Manuscript No.: ESR-D-19-00231.R4
- 6 **ID Ibrahim**, Y Alayli, Y Hamam, T Jamiru, ER Sadiku. Performance Evaluation of Parabolic Trough Solar Collector and Comparison with other Solar Concentrating Technologies: A Critical Review. *Renewable and Sustainable Energy Reviews*. Manuscript No.: RSER-D-19-02937.

### Journal Articles (To be submitted)

- 7 **ID Ibrahim**, Y Hamam, ER Sadiku, T Jamiru, Y Alayli, Energy consumption reduction in residential buildings through the use of solar water heating system: A case study of South Africa. Proposed journal: *Renewable and Sustainable Energy Reviews*.

- 8 **ID Ibrahim**, ER Sadiku, Y Hamam, T Jamiru, Y Alayli, Design and performance analysis of improved parabolic trough solar collector. Proposed journal: *Renewable Energy*.
- 9 **Idowu David Ibrahim**, Tamba Jamiru, Yasser Alayli, Yskandar Hamam, Emmanuel Rotimi Sadiku. Modelling and performance evaluation of a parabolic trough solar water heating system in various weather conditions in South Africa. Proposed journal: *Applied Energy*.

### **Chapters in an Edited Book (Published)**

- 10 **ID Ibrahim**, ER Sadiku, Y Hamam, Y Alayli, T Jamiru, WK Kupolati, AA Eze, SC Agwuncha, CA Uwa, MO Oyesola, OO Daramola, MJ Mochane. **2019**. Advancement in Material Coating for Engineering Applications. In: Liang Li and Qing Yang, *Photoenergy and Thin Film Materials*, 473-498. Wiley.
- 11 **ID Ibrahim**, ER Sadiku, T Jamiru, Y Hamam, Y Alayli, AA Eze, WK Kupolati. **2019**. Biopolymer Composites and Bionanocomposites for Energy Applications. In: Dhorali Gnanasekaran, *Green Biopolymer & its Nanocomposites*, 313-341. Springer, Singapore.

### **Presented Conference Papers**

- 12 **ID Ibrahim**, Y Hamam, Y Alayli, T Jamiru, ER Sadiku. Design and Modification of Parabolic Trough Solar Collector for Performance Effectiveness. Proceeding: 5<sup>th</sup> International Conference on Renewable Energies for Developing Countries, 29–30 June **2020** (online presentation). Mohammed VI Polytechnic University, Lot 660, Hay Moulay Rachid Ben Guerir, 43150, Morocco.
- 13 **ID Ibrahim**, ER Sadiku, T Jamiru, Y Hamam, Y Alayli. Nanostructured and Composite Materials for Energy Applications. Proceeding in European Advanced Energy Materials and Technology Congress. 25–28 March **2018**, Stockholm, Sweden.
- 14 **ID Ibrahim**, ER Sadiku, T Jamiru, Y Hamam, Y Alayli, AA Eze. Application of nanoparticles and composite materials for energy generation and storage. Proceeding in European Advanced Energy Materials and Technology Congress. 25–28 March **2018**, Stockholm, Sweden.

## THESIS SUMMARY IN ENGLISH

In recent years, various energy sources and methods have been used to heat water in domestic and commercial buildings. The known sources for water heating include electrical energy and solar radiation energy in the urban regions or burning of firewood in rural areas. Several water heating methods may be used such as electrical heating elements, solar concentrators, flat plate collectors and evacuated tube collectors. This thesis focuses on ways to further improve the system's performance for water heating through the combined use of solar energy and solar concentrator technique. Furthermore, the study proposed an alternative design method for the hot water storage tank.

The solar collector-supporting frame was designed and analysed using Solidworks®. The forces acting on the structural members were simulated to determine the capacity of the frame to sustain the load, and the possible regions on the supporting frame, which could potentially fail while in operation.

Energy performance was simulated for five years of operation using Matlab Simulink® software. This simulation was based on the use of three different data. The first is a five-year weather database of the City of Tshwane in South Africa. The second is a hot water consumption profile for a typical household. The third is the cost of additional heating with electricity depending on the time of use. This simulation allowed the validation of the choices of the different elements of the heating system.

This study allowed the development of an approach for the design of a solar heating system by optimising the dimensions of the different elements for a typical household and a specific region.

In addition, the use of polymeric materials and other materials like polyurethane, salt and aluminium can be explore possibly for the development of a hot water storage tank based on their inherent properties.

Extending the findings in this thesis will further improve the designs for solar concentrator technologies and solar water heating systems. Therefore, some recommendations and suggestions are highlighted in order to improve the overall system design, analysis and performance. This includes but not limited to Life cycle analysis of the entire system based on the working conditions of the solar collector and the hot water storage tank.

## RÉSUMÉ DE LA THÈSE EN FRANÇAIS

Les sources d'énergies utilisées pour le chauffage de l'eau dans les bâtiments commerciaux et résidentielles sont multiples. Ces ressources sont essentiellement électriques dans les milieux urbains et utilisent le bois dans les milieux ruraux. Le pourcentage de l'énergie solaire utilisé reste assez faible. Les méthodes les utilisées pour produire l'eau chaude sont pour basés pour l'essentielle sur l'utilisation des résistances électrique ou des capteurs solaire plat. Le travail présenté dans cette thèse est basé sur l'utilisation des concentrateurs solaires pour chauffer des collecteurs d'énergie. Le rendement est augmenté par le développement de nouveau matériaux pour le stockage.

La structure pour le support du collecteur a été conçue et analysée utilisant le logiciel Solidworks<sup>®</sup>. Les forces agissant sur les éléments de la structure sont simulées pour assurer la fiabilité du support lors des différentes conditions de fonctionnement. L'analyse par la méthode des éléments finis a permis la vérification de la structure utilisée pour le réflecteur et son support.

Les performances énergétiques ont été simulées pour cinq ans d'opération utilisant le logiciel Matlab Simulink<sup>®</sup>. Cette simulation a été basée sur l'utilisation de trois données différentes. La première est une base de données météorologique de cinq ans en Afrique du Sud dans la Ville de Tshwane. La deuxième est un profil d'utilisation pour un foyer type. La troisième est le coût de complément de chauffage en électricité dépendant de l'heure de l'utilisation. Cette simulation a permis la validation des choix de dimensions de différents éléments du système de chauffage.

Cette étude a permis le développement d'une approche pour la conception d'un système de chauffage solaire en optimisant les dimensions des différents éléments pour un foyer type et une région spécifique.

De plus, nous avons conçu un autre réservoir d'eau chaude. Nous avons démontré que l'utilisation de matériaux polymères et d'autres matériaux comme le polyuréthane, le sel et l'aluminium est possible pour le développement d'un réservoir de stockage d'eau chaude en fonction de leurs propriétés inhérentes.

L'extension des résultats de cette thèse améliorera encore les conceptions des technologies de concentrateurs solaires et des systèmes de chauffage solaire de l'eau. Par conséquent, certaines recommandations et suggestions sont mises en évidence afin d'améliorer la conception, l'analyse et les performances globales du système.



## RESUMÉ

Les ressources énergétiques renouvelables ont joué un rôle important dans la réduction de la dégradation de l'environnement et la réduction des émissions de gaz à effet de serre. Ces sources d'énergie renouvelables ont été récoltées, converties et utilisées pour diverses applications en fonction des sources d'énergie. Ces applications comprennent, parmi d'autres, le chauffage, le séchage. Ces dernières années, diverses sources d'énergie et méthodes ont été utilisées pour chauffer l'eau dans les bâtiments domestiques et commerciaux. Les ressources principales pour le chauffage de l'eau comprennent l'énergie électrique et l'énergie de rayonnement solaire dans les régions urbaines ou la combustion de bois de chauffage dans les régions rurales.

Les méthodes utilisées pour le chauffage de l'eau sont parmi d'autres des éléments chauffants électriques, des concentrateurs solaires, un collecteur à plaque plate ou collecteur à tube sous vide. Cette thèse s'est concentrée sur les moyens d'améliorer les performances du système de chauffage de l'eau grâce à l'utilisation combinée de l'énergie solaire et de la technique du concentrateur solaire. De plus, l'étude propose une méthode de conception alternative pour le ballon d'eau chaude.

Dans cette thèse, le concentrateur solaire proposé est un réflecteur solaire à cylindre parabolique (PTSC). Le châssis porteur du capteur solaire a été conçu et analysé à l'aide du logiciel Solidworks®. Les forces agissant sur les éléments de structure ont été simulées pour déterminer la capacité de charge du cadre de support et la partie possible du cadre de support, qui pourrait potentiellement tomber en panne pendant le fonctionnement. L'ensemble des performances du système a été modélisé à l'aide du logiciel Matlab Simulink®.

La simulation est basée sur l'utilisation de trois données différentes. Le premier est une base de données météo quinquennale de la ville de Tshwane en Afrique du Sud. Le second est un profil

de consommation d'eau chaude pour un ménage type. Le troisième est le coût du chauffage supplémentaire à l'électricité en fonction de l'heure de l'utilisation. Cette simulation a permis de valider les choix des différents éléments du système de chauffage.

La base de données météorologiques a été utilisée pour obtenir la température de sortie de l'absorbeur et la température du de l'eau dans le réservoir. L'étude a permis de développer une approche pour la conception d'un système de chauffage solaire en optimisant les dimensions des différents éléments pour un ménage type et une région donnée. Le comportement du système dans les différentes saisons en Afrique du Sud a été simulé pour une période de cinq ans ainsi le coût supplémentaire de l'électricité nécessaire pour un profil type s'un habitat pendant.

Le comportement du système variait chaque mois en raison du changement d'intensité solaire. D'après l'analyse du modèle pour l'année 2019, janvier semblait avoir la plus haute intensité solaire directe tandis que mai 2019, avait l'intensité solaire la plus faible. D'après les données météorologiques 2018/2019, la température moyenne de sortie de l'absorbeur de l'ordre de grandeur était de 333, 332, 328 et 325 K pendant les saisons d'automne, d'été, de printemps et d'hiver respectivement. De même, la température moyenne des réservoirs de stockage de l'ordre de grandeur était de 366, 364, 363 et 360 K respectivement au printemps, en été, en automne et en hiver. D'après les résultats observés, compte tenu des tarifs journaliers d'électricité par système de facturation de la ville de la municipalité de Tshwane, le coût supplémentaire maximal d'électricité était très faible pour la durée considérée. Par conséquent un système bien entretenu est autosuffisant.

Au delà du développement d'une stratégie pour la conception et dimensionnement du système du chauffage d'eau une contribution au développement des différents éléments physique du système a été menée. Le dimensionnement physique du concentrateur et son support ainsi que

sa commande pour optimiser le captage énergétique et de sa sécurité de fonctionnement ont été étudiés.

Nous avons également étudié l'isolation thermique du réservoir. De plus, l'utilisation de matériaux polymères et d'autres matériaux comme le polyuréthane, le sel et l'aluminium est possible pour le développement d'un réservoir de stockage d'eau chaude en fonction de leurs propriétés inhérentes.

Nous avons également étudié l'isolation thermique du réservoir. De plus, l'utilisation de matériaux polymères et d'autres matériaux comme le polyuréthane, le sel et l'aluminium est possible pour le développement d'un réservoir de stockage d'eau chaude en fonction de leurs propriétés inhérentes.

L'extension des résultats de cette thèse améliorera encore les conceptions des technologies de concentrateurs solaires et des systèmes de chauffage solaire de l'eau. Par conséquent, certaines recommandations et suggestions sont mises en évidence afin d'améliorer la conception, l'analyse et les performances globales du système. Cela comprend, mais sans s'y limiter, l'analyse du cycle de vie de l'ensemble du système en fonction des conditions de fonctionnement du capteur solaire et du ballon de stockage d'eau chaude. En outre, la construction et le test d'un modèle physique basé sur les résultats de cette recherche pour étudier les performances par rapport aux prédictions du modèle.

## TABLE OF CONTENTS

DEDICATION .....	i
ACKNOWLEDGEMENTS .....	ii
LIST OF PUBLICATIONS .....	v
THESIS SUMMARY IN ENGLISH .....	vii
RÉSUMÉ DE LA THÈSE EN FRANÇAIS .....	ix
RESUMÉ .....	xi
TABLE OF CONTENTS.....	xiv
LIST OF FIGURES .....	xx
LIST OF TABLES.....	xxiv
LIST OF ABBREVIATIONS.....	xxvi
NOMENCLATURE .....	xxix
<b>CHAPTER ONE .....</b>	<b>1</b>
1.0 BACKGROUND OF THE STUDY .....	1
1.2 Introduction.....	1
1.3 Problem Statement.....	4
1.4 Objectives of the Research.....	5
1.4.1 Broad objective .....	5
1.4.2 Specific objectives .....	5
1.5 Significance of the Research.....	5
1.6 Study Area .....	6
1.7 Structure of the Thesis .....	7
<b>CHAPTER TWO .....</b>	<b>9</b>
2.0 LITERATURE REVIEW .....	9
2.1 Introduction.....	9

2.2	Renewable Energy .....	10
2.2.1	Hydropower .....	16
2.2.2	Wind energy.....	16
2.2.3	Bioenergy.....	19
2.2.4	Geothermal energy.....	22
2.2.5	Solar energy .....	25
2.2.5.1	Solar Angles.....	28
2.2.5.2	Incident Angle.....	31
2.2.5.3	Solar energy potentials in South Africa .....	31
2.3	Solar Energy Collectors for Household Water Heating.....	33
2.3.1	Evacuated tube solar collector .....	33
2.3.2	Flat plate collectors .....	34
2.3.3	Glazed and unglazed solar collector .....	35
2.4	Solar Water Heating for Electrical Power Generation.....	36
2.4.1	Linear Fresnel reflector.....	37
2.4.2	Heliostat field solar collector .....	42
2.4.3	Parabolic dish solar collector .....	45
2.4.4	Parabolic trough solar collector .....	46
2.5	Importance of Solar Water Heating Systems.....	55
2.5.1	Improvement of solar water collector .....	60
2.6	Hailstones Damages as a Result of Heavy Rainfall.....	64
2.6.1	Hailstones damages in South Africa .....	64
2.7	Sun Chaser .....	67
2.8	Hot Water Storage Tank .....	67
2.9	Insulation.....	70
2.10	Conclusion .....	71

<b>CHAPTER THREE .....</b>	<b>73</b>
3.0 MODELLING AND SIMULATION .....	73
3.1 Introduction.....	73
3.2 Mathematical Modelling of Parabolic Trough Solar Collector Geometry .....	73
3.3 Heat Production, Transferred and Losses by the PTSC to the Glass Cover .....	75
3.4 Heat Losses from the Glass Cover to the Environment.....	78
3.5 Effective Solar Energy Absorbed .....	79
3.6 Solar Absorber Tube (Amount of Heat Transferred to the Fluid and Heat Loss) .....	79
3.6.1 Heat transfer by convection from the receiver pipe internal wall to the heat transfer fluid (HTF) .....	79
3.6.2 Heat transfer by conduction through the absorber pipe .....	80
3.7 Heat Transfer from the Absorber to the Glass Cover .....	80
3.7.1 Heat transfer by convection .....	80
3.8 Heat Transfer from the Glass Cover to the Environment .....	82
3.8.1 Heat transfer by convection .....	82
3.8.2 Heat transfer by radiation.....	84
3.9 Heat Exchanger Chamber (Heat Transfer Rate and Amount of Heat Transferred).....	85
3.10 Numerical Model Summary for the Entire System.....	87
3.10.1 Thermal storage model .....	89
3.10.2 Dynamic model of a concentrated solar absorber.....	92
3.10.3 Weather history .....	94
3.10.4 Control systems.....	95
3.10.5 Considering the different response times of the various parts of the system.....	97
3.10.6 A scenario for the use of domestic hot water.....	97
3.11 Conclusion .....	98

<b>CHAPTER FOUR.....</b>	<b>99</b>
4.0 DESIGN METHODOLOGY .....	99
4.1 Introduction.....	99
4.2 Design of Parabolic Trough Solar Collector.....	99
4.2.1 Materials .....	102
4.3 Solar Tracking Development and Calibration .....	103
4.3.1 Rain sensor installation and calibration .....	105
4.3.2 Temperature sensor installation and calibration .....	107
4.3.3 Light dependent resistor sensor installation and calibration.....	108
4.4 Design of the Hot Water Storage Tank.....	109
4.5 Storage Tank Sizing.....	112
4.5.1 General water demand estimation.....	113
4.5.2 Estimating the indoor water demand .....	114
4.5.3 Estimating the hot water storage tank size.....	114
4.6 Conclusion .....	115
 <b>CHAPTER FIVE .....</b>	 <b>116</b>
5.0 RESULTS AND DISCUSSION .....	116
5.1 Introduction.....	116
5.2 Collector Supporting Frame Design Analysis .....	116
5.3 Weather Data Analysis .....	120
5.4 Performance Evaluation of the Model .....	123
5.5 System Performance During the Four Weather Seasons in South Africa .....	127
5.5.1 Autumn .....	129
5.5.2 Winter .....	130
5.5.3 Spring.....	131
5.5.4 Summer .....	132

5.6	Effect of Solar Radiation on Absorber Outlet Temperature and Storage Tank Temperature .....	134
5.7	Collector Aperture Area.....	137
5.8	System Evaluation of Additional Cost of Electricity for Heating During Low Solar Intensity.....	140
5.9	Conclusion .....	142

## **CHAPTER SIX ..... 143**

6.0	CONCLUSION AND RECOMMENDATIONS .....	143
6.1	Summary .....	143
6.2	Conclusion .....	144
6.3	Contribution to the Body of Knowledge.....	148
6.4	Recommendations for Future Work.....	148

## **REFERENCES..... 150**

## **APPENDICES ..... 176**

Appendix 1: CAD Orthographic Drawing of Parabolic Trough Solar Collector .....	176
Appendix 2: Datasheet for the temperature sensor .....	177
Appendix 3: Solar collector beam body information.....	179
Appendix 4: Solar collector beam forces .....	188
Appendix 5: Solar collector beam stresses. ....	192
Appendix 6: Impact of solar intensity on the absorber and storage temperature for each month in year 2019.....	196
Appendix 7: Impact of solar intensity on the absorber and storage temperature for five years (January 2015 – December 2019).....	208
Appendix 8: Impact of solar intensity on the absorber and storage temperature for three years (January 2015 – December 2017).....	209



Appendix 9: Impact of solar intensity on the absorber and storage temperature for one years (January – December 2015). .....	210
Appendix 10: Absorber and storage temperature during autumn (mid-February to April 2019)... ..	211
Appendix 11: Absorber and storage temperature during winter (May to July 2019). .....	212
Appendix 12: Absorber and storage temperature during spring (August to mid-October 2019)... ..	213
Appendix 13: Absorber and storage temperature during summer (mid-October 2018 to mid- February 2019). .....	214

## LIST OF FIGURES

<b>Figure 1.1:</b> Available renewable energy resources. ....	2
<b>Figure 1.2:</b> Amount of solar collectors installed in some countries. ....	3
<b>Figure 2.1:</b> Renewable energy annual average growth rate capacity from 2002–2006. ....	11
<b>Figure 2.2:</b> Region-based investments into renewable energy from 2004 to 2015. ....	13
<b>Figure 2.3:</b> Wind turbines installation between buildings (Bahrain World Trade Centre Towers). ....	19
<b>Figure 2.4:</b> Schematic diagram of the sustainable cycle of anaerobic co-digestion of organic wastes and animal manure. ....	20
<b>Figure 2.5:</b> Power conversion technologies for biomass. ....	22
<b>Figure 2.6:</b> Operating capacity of geothermal power generation by country. ....	23
<b>Figure 2.7:</b> Geothermal power generation under development per country. ....	24
<b>Figure 2.8:</b> Utilization of geothermal energy for different applications. ....	25
<b>Figure 2.9:</b> Earth motion about the sun. ....	26
<b>Figure 2.10:</b> Solar declination angle throughout the year. ....	27
<b>Figure 2.11:</b> Illustration of overall solar radiation that passes through the earth's surface. ....	28
<b>Figure 2.12:</b> Coordinate system earth surface showing solar altitude angle, azimuth angle and zenith angle. ....	30
<b>Figure 2.13:</b> Fundamental sun angles. ....	30
<b>Figure 2.14:</b> Provincial distribution of renewable energy resources in South Africa. ....	32
<b>Figure 2.15:</b> Solar energy potentials of South Africa. ....	32
<b>Figure 2.16:</b> Schematic diagram of evacuated solar tube collector. ....	34
<b>Figure 2.17:</b> Schematic diagram of a glazed flat plate solar collector. ....	35
<b>Figure 2.18:</b> Linear Fresnel solar power concentrated (a) and Saudi Arabia linear Fresnel solar power concentrated (b). ....	39
<b>Figure 2.19:</b> Working principle of a heliostat solar thermal plant. A ....	43
<b>Figure 2.20:</b> Shadowing and blocking the loss of solar flux (a) and radial stagger heliostat layout (b). ....	45
<b>Figure 2.21:</b> Parabolic dish collector: (a) typical PDC and (b) working principle of PDC. ....	46
<b>Figure 2.22:</b> Real-world installed PTC (a) and schematic diagram of the working principle of PTC (b). ....	47
<b>Figure 2.23:</b> Schematic diagram of the linear parabolic solar collector. ....	59

<b>Figure 2.24:</b> Schematic diagram of a parabolic solar collector. ....	60
<b>Figure 2.25:</b> Photo of buildings and cars damaged due to hailstones.....	65
<b>Figure 2.26:</b> Photo of hailstones as big as a tennis ball. ....	66
<b>Figure 2.27:</b> Damages caused by hailstones to evacuated glass tubes.....	66
<b>Figure 2.28:</b> Schematic cross-sectional view of a hot water storage tank with PCM containers insert.....	68
<b>Figure 2.29:</b> Conventional hot water storage tank showing the cross-sectional layers: (a) steel tank and (b) steel tank with glass lining.....	69
<b>Figure 2.30:</b> Schematic diagram of a hot water storage tank with heat exchanger and heating element. ....	71
<b>Figure 3.1:</b> Schematic design of: (a) a parabolic trough solar collector and (b) rim angle evaluation.....	74
<b>Figure 3.2:</b> Schematic diagram of the heat exchanger pipe .....	85
<b>Figure 3.3:</b> Main algorithm for the entire system. ....	88
<b>Figure 3.4:</b> Solar heating and auxiliary heating system algorithm. ....	96
<b>Figure 4.1:</b> Schematic representation of the entire solar water heating system.....	100
<b>Figure 4.2:</b> Schematic 3D model of a modify parabolic trough solar collector.....	102
<b>Figure 4.3:</b> Schematic circuit diagram for the control system .....	104
<b>Figure 4.4:</b> Pictorial view of the mini prototype.....	104
<b>Figure 4.5:</b> Pictorial images of (a) water-drop sensor board, (b) rain sensor module and (c) connecting cables .....	106
<b>Figure 4.6:</b> Pictorial image of a temperature sensor with cable labelling.....	108
<b>Figure 4.7:</b> Light dependent resistor .....	109
<b>Figure 4.8:</b> Schematic image of a hot water storage tank in layers .....	110
<b>Figure 5.1:</b> Structural force loading and nodes of the supporting frame .....	117
<b>Figure 5.2:</b> Stress analysis of the solar collector-supporting frame.....	119
<b>Figure 5.3:</b> Typical static displacement resultant .....	120
<b>Figure 5.4:</b> Change in wind speed, humidity and ambient temperature with a corresponding change in time .....	121
<b>Figure 5.5:</b> Solar intensity variation with time of the day .....	123

<b>Figure 5.6:</b> Influence of solar intensity on the absorber and storage temperature for six months (January–June 2015) .....	124
<b>Figure 5.7:</b> Influence of solar intensity on the absorber and storage temperature for three months (January–March 2015) .....	124
<b>Figure 5.8:</b> Impact of solar intensity on the absorber and storage temperature for one month (January 2015) .....	125
<b>Figure 5.9:</b> Impact of solar intensity on the absorber and storage temperature for one day (1 January 2015).....	126
<b>Figure 5.10:</b> Absorber and storage tank temperature during autumn. Note: y min, y max and y mean represent the minimum, maximum and mean temperatures.....	129
<b>Figure 5.11:</b> Absorber and storage tank temperature during winter. Note: y min, y max and y mean represent the minimum, maximum and mean temperatures .....	131
<b>Figure 5.12:</b> Absorber and storage tank temperature during spring. Note: y min, y max and y mean represent the minimum, maximum and mean temperatures.....	132
<b>Figure 5.13:</b> Absorber and storage tank temperature during summer. Note: y min, y max and y mean represent the minimum, maximum and mean temperatures.....	134
<b>Figure 5.14:</b> Influence of solar intensity on absorber output and storage tank temperature.	136
<b>Figure 5.15:</b> Influence of solar intensity on absorber efficiency .....	136
<b>Figure 5.16:</b> Effect of increasing collector aperture area on absorber outlet temperature....	138
<b>Figure 5.17:</b> Effect of increasing collector aperture area on storage tank temperature .....	139
<b>Figure 5.18:</b> Interaction between the ambient, absorber and storage temperature for an aperture area of 6 m <sup>2</sup> .....	139
 <b>Appendix 6.1:</b> Impact of solar intensity (SI) on the absorber and storage temperature for January 2019 (a) without and (b) with solar intensity relationship. ....	196
<b>Appendix 6.2:</b> Impact of solar intensity (SI) on the absorber and storage temperature for February 2019 (a) without and (b) with solar intensity relationship. ....	197
<b>Appendix 6.3:</b> Impact of solar intensity (SI) on the absorber and storage temperature for March 2019 (a) without and (b) with solar intensity relationship. ....	198
<b>Appendix 6.4:</b> Impact of solar intensity (SI) on the absorber and storage temperature for April 2019 (a) without and (b) with solar intensity relationship. ....	199
<b>Appendix 6.5:</b> Impact of solar intensity (SI) on the absorber and storage temperature for May 2019 (a) without and (b) with solar intensity relationship. ....	200

<b>Appendix 6.6:</b> Impact of solar intensity (SI) on the absorber and storage temperature for June 2019 (a) without and (b) with solar intensity relationship. ....	201
<b>Appendix 6.7:</b> Impact of solar intensity (SI) on the absorber and storage temperature for July 2019 (a) without and (b) with solar intensity relationship. ....	202
<b>Appendix 6.8:</b> Impact of solar intensity (SI) on the absorber and storage temperature for August 2019 (a) without and (b) with solar intensity relationship. ....	203
<b>Appendix 6.9:</b> Impact of solar intensity (SI) on the absorber and storage temperature for September 2019 (a) without and (b) with solar intensity relationship. ....	204
<b>Appendix 6.10:</b> Impact of solar intensity (SI) on the absorber and storage temperature for October 2019 (a) without and (b) with solar intensity relationship. ....	205
<b>Appendix 6.11:</b> Impact of solar intensity (SI) on the absorber and storage temperature for November 2019 (a) without and (b) with solar intensity relationship. ....	206
<b>Appendix 6.12:</b> Impact of solar intensity (SI) on the absorber and storage temperature for December 2019 (a) without and (b) with solar intensity relationship. ....	207

## LIST OF TABLES

<b>Table 2.1:</b> Geographical location and energy consumption due to water heating. ....	10
<b>Table 2.2:</b> Renewable energy scenario global by 2040. ....	12
<b>Table 2.3:</b> Annual global carbon-related death <sup>a</sup> .....	14
<b>Table 2.4:</b> South Africa estimated renewable energy resources net green jobs.....	15
<b>Table 2.5:</b> Renewable energy generation by an independent producer in SA. ....	18
<b>Table 2.6:</b> Comparison of linear Fresnel collector with a parabolic trough collector. A.....	40
<b>Table 2.7:</b> Performance evaluation of CSP* plants based on PTC and LFC.....	42
<b>Table 2.8:</b> Performance improvement analysis of parabolic trough collector .....	49
<b>Table 2.9:</b> Performance evaluation of solar trough concentrating system by using water as working fluid in an evacuated tube with increasing flow rate. A .....	62
<b>Table 2.10:</b> Performance evaluation of solar trough concentrating system by using water as working fluid in an evacuated tube with decreasing flow rate. ....	63
 <b>Table 3.1:</b> Constant for computing Nusselt number with wind influence .....	84
 <b>Table 4.1:</b> Luz Cermet coating emittance at various temperatures.....	101
<b>Table 4.2:</b> Mechanical properties of the square tubing.....	103
<b>Table 4.3:</b> Justification for selected materials.....	111
<b>Table 4.4:</b> Indoor daily hot water estimation per single-family household. ....	115
 <b>Table 5.1:</b> Weather station data source. ....	116
<b>Table 5.2:</b> Overall resultant forces for the supporting frame.....	118
<b>Table 5.3:</b> Square-tubing properties from Solidworks <sup>®</sup> analysis.....	118
<b>Table 5.4:</b> Daily weather data for 01, January 2017 .....	122
<b>Table 5.5:</b> Statistical data for absorber outlet temperature and storage tank temperature for a period of 5, 3 and 1 year(s) .....	127
<b>Table 5.6:</b> Periods of various weather seasons in South Africa.....	128
<b>Table 5.7:</b> Statistical data for absorber outlet temperature and storage temperature during winter. ....	130
<b>Table 5.8:</b> Statistical data for absorber outlet temperature and storage temperature during summer.....	133

<b>Table 5.9:</b> Effect of solar intensity on absorber outlet temperature and storage tank temperature .....	135
<b>Table 5.10:</b> Input data for modelling the influence of increasing solar concentration area..	138
<b>Table 5.11:</b> Varying electricity tariffs showing the effective periods.....	140
<b>Table 5.12:</b> Impact of aperture area on additional cost of electricity .....	141
 <b>Table 6.1:</b> Conventional systems/models and improvements made. ....	 147

## LIST OF ABBREVIATIONS

Aluminium mirror reflector	AMR
Carbon dioxide	CO <sub>2</sub>
City of Tshwane	CoT
Department of higher education and training	DHET
Direct current	DC
Displacement resultant	URES
Evacuated tube solar collector	ETSC
Finite element analysis	FEA
Flat plate collectors	FPCs
Flat plate solar collector	FPSC
Geothermal energy	GTE
Giga watt hour	GWh
Giga watt thermal	GWth
Greenhouse gases	GHG
Heat transfer fluid	HTF
Heating, ventilation, and air-conditioning	HVAC
Hot water storage tank	HWST
Light dependent resistor	LDR



Linear Fresnel Collector	LFC
Mass flow rate	MFR
Maximum peak power tracking	MPPT
Megawatt	MW
National Energy Regulator of South Africa	NERSA
Parabolic dish collector	PDC
Parabolic trough collectors	PTCs
Parabolic trough solar collector	PTSC
Phase change material	PCM
Polypropylene	PP
Polyurethane	PU
Rand	ZAR
Research and innovation	RnI
Solar water heating	SWH
Solar water heating systems	SWHSs
South Africa	SA
Stainless steel reflector	SSR
Terawatt hour	TWh
United Arab Emirates	UAE
United Kingdom	UK

United States of America

USA

Water closet

WC

World Health Organization

WHO

## NOMENCLATURE

		Unit
$a$	Accommodation coefficient	-
$A$	Area of a cylinder	$m^2$
$A_a$	Collector aperture area	$m^2$
$A_{eq}$	Equivalent surface area	$m^2$
$A_{ao}$	Absorber area	$m^2$
$AST$	Apparent solar time	day
$A_{eff}$	Effective receiver area	$m^2$
$a_s$	Solar azimuth angle	degree
$b$	Interaction coefficient	-
$C$	Concentration ratio	-
$c_p$	Specific heat capacity of water	$J/(kg \cdot K)$
$EqT$	Equation of time	day
$DM$	Ratio of mirror area to overall heliostat area	-
$D$	Diameter	$m$
$D_o$	Average earth-sun distance	$m$
$DS_r(t)$	Direct solar radiation data with respect to time	$W/m^2$
$f$	Focal distance	$m$
$f_{ai}$	Frictional factor for the inner surface of the absorber pipe	$kg/(m \cdot s)$

$F_g$	Geometric parameter	-
$g$	Acceleration due to gravity	$m/s^2$
$G$	Volume exchange coefficient	$W/(m^3 \cdot K)$
$G_b$	Direct beam irradiation	$W/m^2$
$h$	Hour angle	degree
$h_f$	Convection heat transfer coefficient	$W/(m^2 \cdot K)$
$h_{in}$	Inner heat transfer coefficient	$W/(m^2 \cdot K)$
$I_b$	Solar intensity	$W/m^2$
$K$	Surface of the heat exchange coefficient	$W/(m^2 \cdot K)$
$k_a$	Thermal conductivity of the absorber pipe	$W/(m \cdot K)$
$k_{air}$	Thermal conductivity of air	$W/(m \cdot K)$
$k_{an}$	Thermal conductivity of the annulus gas at STP	$W/(m \cdot K)$
$k_{eff}$	Effective thermal conductivity	$W/(m \cdot K)$
$k_f$	Thermal conductivity of the working fluid	$W/(m \cdot K)$
$h$	Heat transfer coefficient	$W/(m^2 \cdot K)$
$HM$	Height of the heliostat	$m$
$h_{out}$	Coefficient of heat transfer	$W/(m^2 \cdot K)$
$i$	Portion of the absorber considered	-
$I_o$	Solar constant	$W/m^2$

$LL$	Local solar time meridian	<i>day</i>
$M$	Mass of the storage	<i>kg</i>
$n$	Particular day's number	-
$n_1$ and $n_2$	Refractive indices	-
$Nu$	Nusselt number	-
$P_{an}$	Annular gas pressure	<i>N/m<sup>2</sup></i>
$Pr$	Prandtl number	-
$PT_{Cu}$	Thickness of heat exchanger pipe	<i>m</i>
$q_r$	Heat flux	<i>W/m<sup>2</sup></i>
$\dot{Q}$	Heat energy	<i>watt</i>
$Q_{abs}$	Solar energy absorbed	<i>W/m<sup>2</sup></i>
$\dot{Q}_{loss}$	Thermal losses	<i>watt</i>
$\dot{Q}_u$	Useful heat	<i>joule</i>
$r$	Normalized distance between the tower and the heliostat location	
$Ra$	Rayleigh number	-
$Re$	Reynolds number	-
$S$	Surface area of the exchanger	<i>m<sup>2</sup></i>
$SL$	Standard solar time meridian	
$T_a$	Absorber temperature	<i>°C</i>

$T_{am}$	Ambient temperature	$^{\circ}\text{C}$
$T_{ext}$	Outdoor temperature	$^{\circ}\text{C}$
$T_f$	Temperature of heat transfer fluid	$^{\circ}\text{C}$
$T_{gi}$	Glass inner temperature	$^{\circ}\text{C}$
$T_{go}$	Glass outer temperature	$^{\circ}\text{C}$
$T_{ai}$	Absorber inner temperature	$^{\circ}\text{C}$
$T_{ao}$	Absorber outer temperature	$^{\circ}\text{C}$
$T_{in}$	Inlet temperature to the absorber	$^{\circ}\text{C}$
$T_{lim}$	Temperature limit	$^{\circ}\text{C}$
$T_{limS}$	Safe temperature limit	$^{\circ}\text{C}$
$T_{min}$	Minimum temperature	$^{\circ}\text{C}$
$T_{out}$	Outlet temperature from the absorber	$^{\circ}\text{C}$
$T_s$	Average temperature of storage tank	$^{\circ}\text{C}$
$T_{sky}$	Sky temperature	$^{\circ}\text{C}$
$TI_{abs}$	Thermal inertia of absorber	$\text{J}/(\text{m}^2 \cdot \text{K}^1 \cdot \text{s}^{1/2})$
$U_L$	Thermal loss coefficient	$\text{W}/(\text{m}^2 \cdot \text{K})$
$V$	Velocity of wind	$\text{m/s}$
$V_{Cu}$	Volume of copper in the absorber pipe	$\text{m}^3$
$V_s$	Volume of the repository	<i>litre</i>

$V_{wabs}$	Volume of standing water contained in the absorber	<i>litre</i>
$P_{an}$	Annular gas pressure	$N/m^2$
$W$	Aperture width	$m$
$WM$	Width of the heliostat	$m$
$z$	Solar zenith angle	<i>degree</i>
$\dot{m}$	Flow rate	$kg/s$
$\rho_F$	Ratio of mirror area to land area at a specific point in the solar field	
$\theta_1$	Incidence angle	<i>degree</i>
$\theta_2$	Refraction angle	<i>degree</i>
$\theta_c$	Critical angle	<i>degree</i>
$\theta_L$	Altitude angle to the receiver from the heliostat location of interest	
$\delta_s$	Solar declination angle	<i>degree</i>
$\Delta A$	Azimuthal spacing	$m$
$\Delta R$	Radial spacing	$m$
$\varphi_r$	Rim angle	<i>degree</i>
$\eta_{th}$	Solar collector thermal efficiency	%
$\varepsilon_r$	Emittance of cermet coating	-

## Greek Symbols

$\alpha$	Solar altitude angle	<i>degree</i>
$\alpha_s$	Emissivity of the absorber	-
$\varepsilon$	Emittance	-
$\rho$	Mirror reflectivity	-
$\pi$	Pi	-
$\eta$	Solar concentrating system efficiency	%
$\delta$	Molecular diameter of the annular gas	<i>m</i>
$\gamma$	Ratio of specific heat for the annular gas	<i>K/N</i>
$\sigma$	Stefan-Boltzmann constant	<i>W/(m<sup>2</sup>·K<sup>4</sup>)</i>
$\nu$	Air kinematic viscosity	<i>m<sup>2</sup>/s</i>
$\mu$	Air thermal diffusivity	<i>m<sup>2</sup>/s<sup>2</sup></i>
$\psi$	Water demand	<i>litre</i>
$\vartheta$	Volume of water usage per plumbing fixture per time	<i>litre</i>
$\omega$	Number of person per household	-
$\varphi$	Number of usage of a plumbing fixture per day	-
$\propto$	Factor of uncertainty	-
$\nabla$	Actual hot water storage tank volume	<i>litre</i>



## Superscript

*in* Inlet

*out* Outlet

## Subscript

*a* Aperture

*abs* Absorb

*ai* Absorber inner

*ai – ao* Absorber inner to absorber outer

*ao* Absorber outer

*ao – gi* Absorber out to glass inner

*cond* Conduction

*conv* Convection

*Cu* Copper

*go – s* Glass outer to sky

*f* Working fluid

*gi* Glass inner

*go* Glass outer

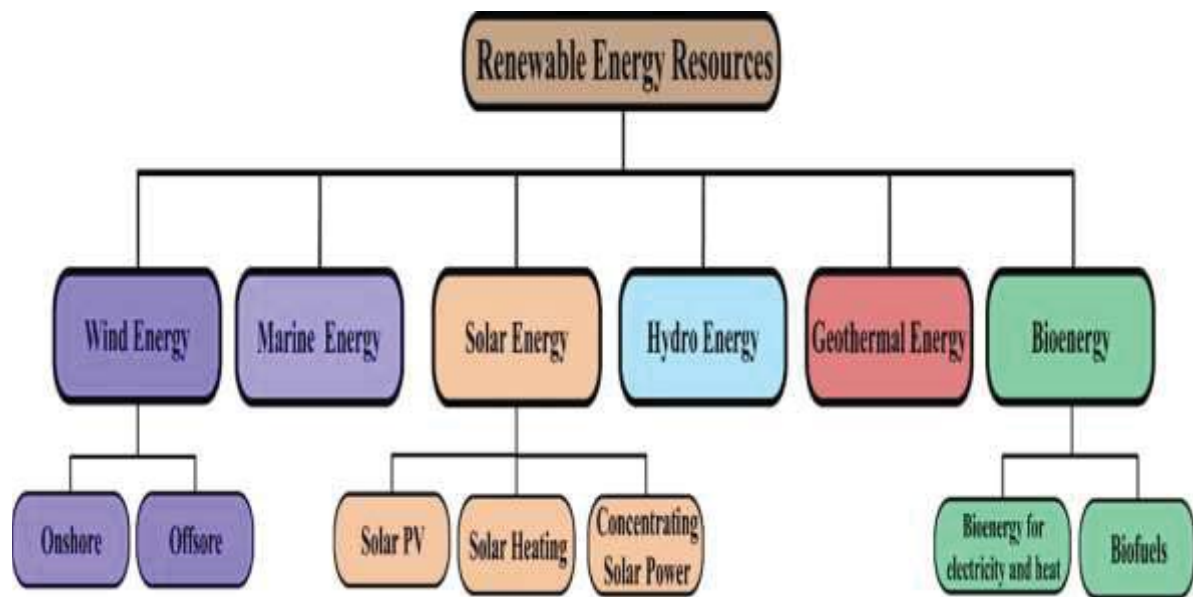
*rad* Radiation

## CHAPTER ONE

### 1.0 BACKGROUND OF THE STUDY

#### 1.2 Introduction

The rapid global growth in population has led to high energy demand, especially in developing countries. One of the major challenges of many nations is how to generate and store, when not needed and adequately supply clean and sustainable energy to their citizens. Currently, some of the major sources for energy production involves the use of environmental pollutants, such as: fossil fuel, nuclear fuel, etc. (Ramirez *et al.*, 2019, Lodhi *et al.*, 1997). The increase in population, commutative energy requirement and concern for the environment globally have prompted the need to facilitate the development of a sustainable environment (Shahzad *et al.*, 2020). Furthermore, this has led to the development of alternative renewable, sustainable and environmentally friendly energy to address the need created by global population growth. Meeting this demand means solving a major global crisis and may attract relevant foreign investors to such a country like South Africa. The availability of affordable and reliable energy facilitates economic growth because most manufacturing and service industries, including large-scale and small-scale businesses, depend on it to help produce and/or store their products. The available forms of alternative renewable energy resources are shown in **Figure 1.1**.

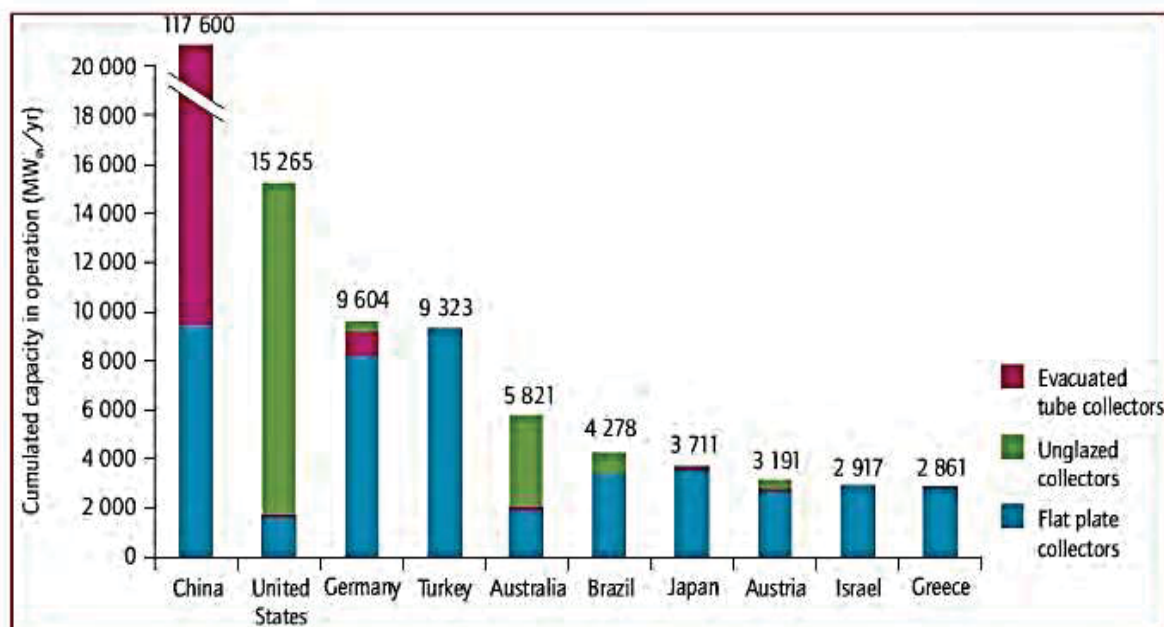


**Figure 1.1:** Available renewable energy resources. Adopted from Ellabban *et al.* (2014)

The impact on health, the environmental effects and the possible depletion of fossil fuel, have also necessitated the shift to renewable and sustainable alternative energy (Joubert *et al.*, 2016). In South Africa, the current electrical energy generated mainly from fossil fuels is used for industrial, agricultural, or domestic purposes. In terms of domestic applications, electricity is, mainly used for lighting, cooking, and heating. Heating in this context can either be for space (house) or water heating. The load on the power grid, as a result of water heating in domestic and commercial buildings, can be minimized by other means, e.g., solar water heating systems (SWHSs).

The installed solar thermal projects, all over the world, grew in 2007 by about 9%, which accounts for the total output of 88 845 GWh globally. This achievement led to the prevention of approximately 39.3 million tons of greenhouse gases (carbon dioxide (CO<sub>2</sub>)) being released into the atmosphere. Based on the statistical analysis, in 2010, the total solar collectors in operation globally, was 195.8 GWth, accounting for 279.7 million m<sup>2</sup> collectors. The capacity grew by 25% (245 GWth) in 2011. The flat plate and evacuated tube collectors' installation accounted for 88.3%, while 11% are

unglazed water collectors and air collectors accounted for 0.7%. The highest amount of unglazed and glazed water and air collectors are used in China, totalling approximately 117.6 GWth, with Europe at 36 GWth, while 16 GWth is found in Canada and the United States of America (Cullen, 2012). **Figure 1.2** shows the total amount of solar collectors installed in several countries. The countries that have taken advantage of SWHSs and have significantly benefited from it, include but are not limited to: China, India, Turkey, USA, Germany, Brazil and Australia (Gautam *et al.*, 2017, Weiss and Mauthner, 2010).



**Figure 1.2:** Amount of solar collectors installed in some countries. (Weiss and Mauthner, 2010, Gautam *et al.*, 2017)

Based on the current standards of design, a product should have the beauty of line, texture, high efficiency, durability, and safety of operation. A basic feature to be considered in achieving a good design is the factor of good material selection. Besides the artistic ability, an effective design requires the combined knowledge of engineering ethical standards and materials, production techniques, cost and market status (Encarta 2009). In any design, the choice of material is very important because it

significantly influences the life span of such a design or product. The material selection process is based on narrowing down a list of technically compliant materials for a specified purpose. The most economical option is then selected in the context of operational life within the constraints of health, safety, environmental and sustainable development.

Many of our recent technologies require materials with remarkable combinations of properties that are not present in conventional metal, ceramics, and polymeric materials. This is expressly true for materials that are required in the aerospace, transportation and underwater applications. Thus, increasing the general strength and/or stiffness results in a reduction in impact strength.

A composite material is a material consisting of two or more micro- or macro-constituents that vary in chemical and/or physical compositions and which are insoluble in each other. Composites generally have enhanced characteristics than those of the individual components. Usually, the reinforcing component(s) is/are distributed in the matrix component. Majority of composites were developed to improve mechanical properties such as strength, stiffness, toughness, impact resistance, etc.

### **1.3 Problem Statement**

Much of the energy consumed (25 – 40%) in the South African households has to do with the heating of hot water for various functions. A study conducted in one of the rural areas (Mamelodi) in South Africa showed that many households do not readily have access to hot water due to the lack of access to safe and sustainable energy for heating. The operation of a geyser is quite expensive, constituting a lump sum of the electrical bills for most households. Furthermore, many households in the settlement do not have access to electricity, which is the most common form of energy supply. In

addition, the current solar water heaters' (flat plate and evacuated tubes) performance are significantly ineffective due to the aperture area and lack of solar concentration. The evacuated glass tubes are often damaged during thunderstorms with hailstones. From research, there is a need for a cheaper, cleaner, and sustainable source of energy for domestic water heating. This could help mitigate the increased energy demand and environmental concerns due to the use of fossil fuels for energy generation. Solar energy is clean, sustainable, and readily available. However, harnessing the energy for water heating will require a suitable solar collector and an insulated hot water storage tank.

## **1.4 Objectives of the Research**

### **1.4.1 Broad objective**

The main objective of the research is to develop a sustainable integrated system for domestic water heating, comprising of a smart parabolic trough solar collector and a hot water storage tank for both the rural and peri-urban areas.

### **1.4.2 Specific objectives**

The specific objectives of the research are:

- a. To design and evaluate the performance improvement of a parabolic trough solar collector for water heating in domestic buildings.
- b. To model and simulate the performance of the system using Matlab Simulink®.
- c. To propose a novel hybrid polymeric composite material for the storage tank.

## **1.5 Significance of the Research**

The research seeks to bridge the gap that exists in the high demand for fossil fuels-based energy, which is exacerbated through domestic water heating needs.

Furthermore, it aims to promote further research into environmentally friendly, renewable, sustainable and clean energy that is readily available for our use.

Therefore, the study contributed to the body of knowledge in the following ways:

- a) Improved solar water heating system to meet the needs of the people in the townships with and without electricity, ultimately reducing the electricity demand.
- b) Ability to regulate the temperature and pressure within the hot water storage tank. This is achievable by introducing a temperature sensor linked to the cover of the collector, thereby minimizing the overheating of the system.
- c) Design of a laminated hybrid composite, which can serve as the hot water storage container.
- d) Development of a model that can analyse historical weather data over a long period.
- e) The integration of various components (parabolic trough collector, MPPT, and hybrid storage container) into a single working unit.
- f) Articles published in high-impact journals accredited by the Department of Higher Education and Training (DHET) and peer-reviewed conference papers presented in both local and international conferences.

## **1.6 Study Area**

The current study was carried out on solar water heating systems to help reduce the reliance on the national power grid and to mitigate the release of carbon dioxide (CO<sub>2</sub>) into the atmosphere. The solar water heating system is based on renewable energy, which is readily available, especially during the summer season of the year. Basic materials that will lead to the optimal performance of the system are of paramount consideration, so that the intensity of the sun can be, fully harnessed. In addition, the intensity of the solar radiation was trailed for efficiency and performance by using an

existing system known as maximum peak power tracking (MPPT). Furthermore, polypropylene and polyurethane materials with very low thermal conductivity were proposed for the storage tank in order for the water in the tank to retain the heat for a longer period.

## **1.7 Structure of the Thesis**

The thesis is made up of six chapters, which are described as follows:

**Chapter 1:** The chapter introduced the research work, the problem statement, objectives and the significance of the research.

**Chapter 2:** The chapter discussed in detail the background to the research work. This entails an in-depth analysis of previous works in this area of research until date. An extensive literature review on the different designs of the current solar collectors for water heating and various methods of improving the performance of the system is also conducted. In addition, the current hot water storage tanks are succinctly reviewed in order to understand the problem that exists. Furthermore, possible ways to address the problems are identified from the literature.

**Chapter 3:** The chapter presented the mathematical modelling and simulation aspects of the research. The entire system was simulated with due consideration for all fixed variables and changing variables.

**Chapter 4:** In the chapter, the design and analysis of the solar collector were done by using a CAD model. Furthermore, the control system analysis was explained in detail with a mini prototype. An alternative method of developing a hot water storage tank, sizing of a storage tank and daily water usage are also discussed succinctly.

**Chapter 5:** The chapter gave an in-depth discussion of the performance of the developed solar collector and the hot water storage tank. The impact of South African



varying weather seasons and the influence it has on the overall performance of the solar absorber and storage tank were analysed and discussed. Cost implications of downtimes for direct solar intensity are also presented.

**Chapter 6:** In the chapter, the summary, the conclusions as a result of the research that was conducted and the recommendations for future research work, which could potentially, improve the present research are highlighted.

## CHAPTER TWO

### 2.0 LITERATURE REVIEW

#### 2.1 Introduction

The depletion of fossil fuel and environmental concern has led researchers to investigate other forms and sources of energy generation and utilization. Renewable and sustainable energy sources have shown great merit, in which solar energy is among the leading forms of energy, where extensive research works, have been done. The energy of the sun has been harnessed for various applications, such as: solar panels, steam boilers, solar water heating, etc. (Zaimi *et al.*, 2019, Araújo and Silva, 2020, Alotaibi *et al.*, 2020). The emphasis of the current research work is on solar water heating systems (SWHSs). SWHS is a device that utilizes the energy from the sun for the benefit of heating water, which could either be used domestically or commercially in places like hospitals, schools, industries, etc. Hot water is essential for bathing, washing, and other domestic uses in both the urban and rural areas of society. Before the increased interest in the use of solar energy, water heating was, mainly done by burning of wood in the rural communities and by the use of fossil fuel such as gas, oil, peat, and coal in the urban or metropolitan areas (Deng *et al.*, 2019, Xie *et al.*, 2018). Electrical energy is also another means of heating water in areas with access to electricity.

In commercial and residential buildings, a substantial amount of energy is used, contributing majorly to the high greenhouse gas emissions globally. According to Pang and O'Neill (2018), residential and commercial buildings together contribute about 39% of the United States' annual greenhouse gas emission. From research, the major energy consumption in buildings is building heating, ventilation, and air-conditioning (HVAC) systems, lighting sector, major appliances and water heating. Previously,

most studies on energy consumption focused mainly on the first three, while excluding the impact of the last on the list for energy consumption, which is water heating. However, several studies in recent times have accounted for the amount of energy consumption due to water heating as explained by Hiller and Johnson (2017) and Pang and O'Neill (2018). **Table 2.1** shows the different energy consumption levels due to water heating from various geographical locations.

**Table 2.1:** Geographical location and energy consumption due to water heating. Adapted from (Pang and O'Neill, 2018, EREN)

Location	Energy consumption <sup>a</sup> (%)
United States	15 – 25
Canada	8 – 19
Hong Kong <sup>b</sup>	–
European Union	14
United Kingdom	22
Spain	26

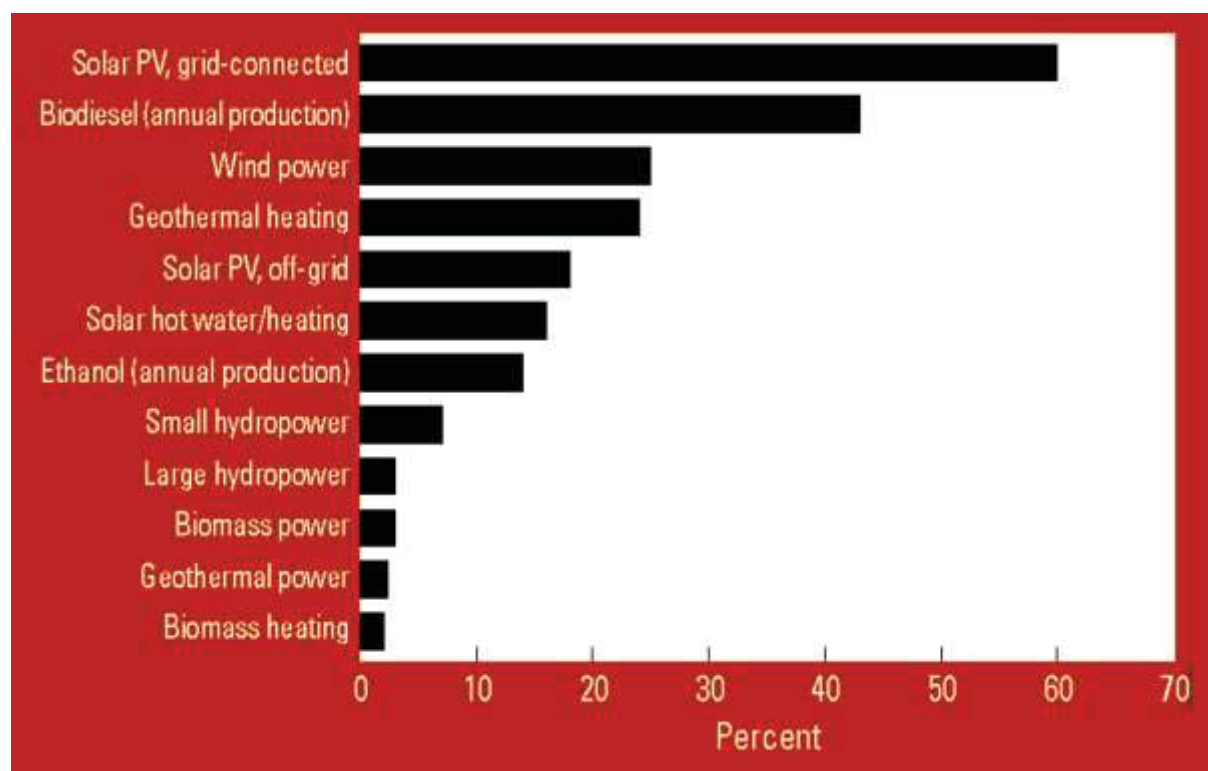
a:Percentage of energy consumption by water heater from the total energy consumed;

b:50 percentage higher of hot water usage in five-star hotels compared with three-star hotels

## 2.2 Renewable Energy

The increase in global energy consumption especially in countries like China, Brazil, India, Germany, the United States of America, etc., has led to the advancement of renewable and sustainable energy research. The environmental concern is another important factor responsible for the increase in the energy mix. Renewable energies such as biofuel, biomass, wind energy, solar energy, hydro energy, geothermal energy, wave energy and tidal energy have greatly attracted researchers. Governments of nations who are aware of the importance of harnessing these

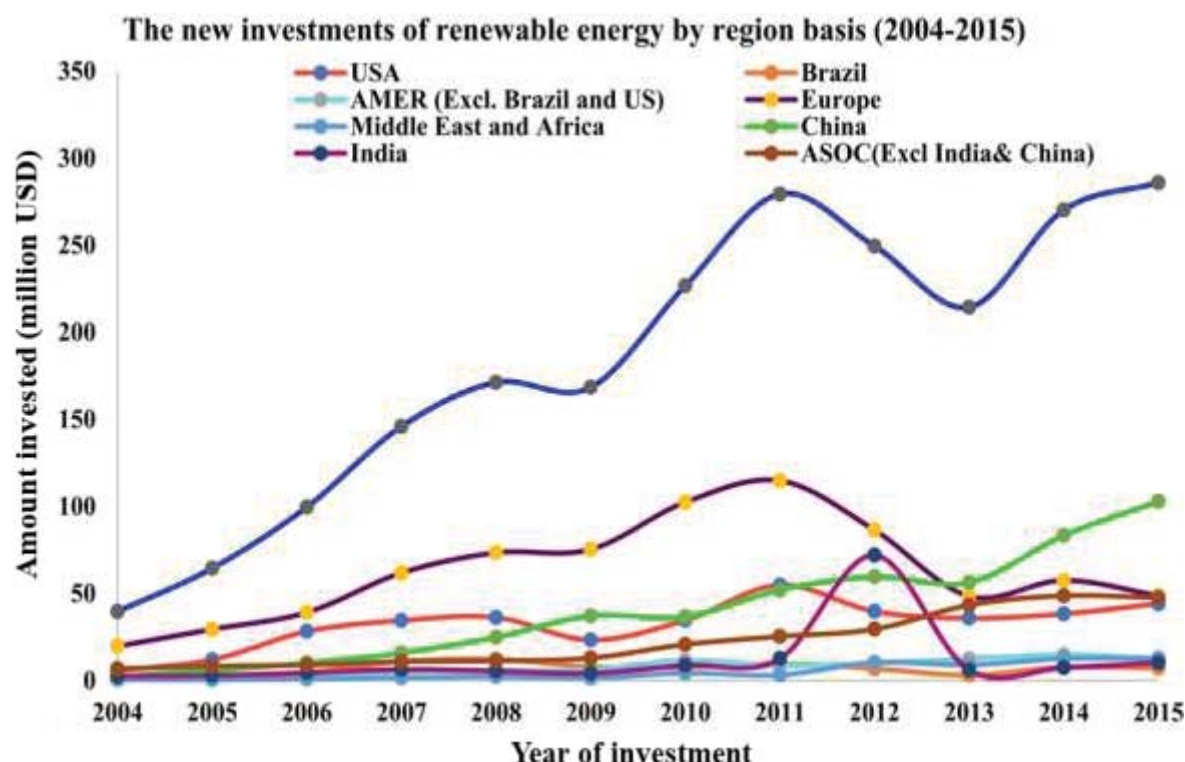
alternative energy resources are also taking conscious effort to add them to their energy mix. **Table 2.2** shows the worldwide renewable and sustainable energy scenario by 2040. The sources of these energies can be traced directly or indirectly to the sun. Tidal energy can also be produced by the combination of the sun and the moon with the rotation of the Earth movement, which is then used to turn the turbine and generate energy (Sánchez Herranz, 2009). Solar energy is generated from the sun and it is the only form of energy that comes directly from the sun solar radiation. **Figure 2.1** shows the annual growth rates of renewable energy between 2002 and 2006. **Figure 2.2** shows the level of investments into renewable energy by various regions from 2004 to 2015.



**Figure 2.1:** Renewable energy annual average growth rate capacity from 2002–2006. (Global Status Report 2007)

**Table 2.2:** Renewable energy scenario global by 2040. Adopted from Kralova and Sjöblom (2010)

	2001	2010	2020	2030	2040
Total consumption (million tons oil equivalent)	10038	10549	11425	12352	13310
Biomass	1080	1313	1791	2483	3271
Geothermal	43.2	86	186	333	493
Large hydro	22.7	266	309	341	358
Marine (tidal/wave/ocean)	0.05	0.1	0.4	3	20
Photovoltaic	0.1	2	24	221	784
Small hydro	9.5	19	49	106	189
Solar thermal	4.1	15	66	244	480
Solar thermal electricity	0.1	0.4	3	16	68
Wind	4.7	44	266	542	688
Total RES	1,365.5	1,745.5	2,964.4	4289	6351
Renewable energy source contribution (%)	13.6	16.6	23.6	34.7	47.7



**Figure 2.2:** Region-based investments into renewable energy from 2004 to 2015. Adopted from Sahu (2018)

One of the potential solutions to meet the prevailing issues surrounding climate change and environmental pollution as a result of carbon dioxide (CO<sub>2</sub>) emission is to develop and enforce and/or execute policies which support the adoption of renewable energy sources over fossil fuels like coal, natural gas, etc. (Abd-ur-Rehman and Al-Sulaiman, 2016). The increasing cost of fossil fuels due to increasing demand is also a significant contributing factor to the shift toward renewable energy because they are clean and readily available (Gautam *et al.*, 2017). According to a report in 2014 by World Health Organization (WHO), about 4 million people die prematurely due to illnesses associated with household air pollution which emanate from burning of solid fuel (paper, charcoal, wood, etc.) (World\_Health\_Organization\_(WHO)). **Table 2.3** presents the various illnesses resulting in death, which are traceable to household air pollution; the observation is an extract of the study reported by WHO in 2014.

Continuous dependence on fossil fuels with little interest in renewable energy resources will continue to destroy the ozone layer due to the large emission of greenhouse gases (GHG) into the environment (atmosphere). The continued engagement in this unhealthy environmental practice could further exacerbate the challenge of climate change. Therefore, to increase energy generation and reduce the hazards associated with carbon-based energy sources, there is a need to investigate alternative energy sources, which bear little or no impact on the environment. Another significant merit of renewable energy is the creation of green jobs. The potential green jobs that can be created are presented in **Table 2.4** in the case of South Africa's green job generation.

**Table 2.3:** Annual global carbon-related death<sup>a</sup>. Adapted from (World\_Health\_Organization\_(WHO))

Nature of death	Number of reported cases (%)
Chronic obstructive pulmonary disease	22
Ischaemic heart disease	26
Lung cancer	6
Pneumonia	12
Stroke	34

<sup>a</sup>: the total number of people involved is 4.3 million

**Table 2.4:** South Africa estimated renewable energy resources net green jobs.  
Adapted from Borel-Saladin and Turok (2013)

Source	Harvesting Method	Long-Term	Long-Term
		Manufacturing Jobs	Jobs
Biofuels	Biodiesel	6641	52729
	Bioethanol		
Hydropower	Large hydropower	111	272
	Marine power	0	197
	Micro/small hydro	0	100
	power		
Solar power	Concentrated solar	608	3014
	power		
	Photovoltaic power	608	13541
Waste to energy	Anaerobic digestion	591	1429
	Biomass combustion	154	37270
	Co-generation	1050	10789
	Landfills	180	1178
	Pyrolysis/gasification	2663	4348
Wind power	Offshore wind power	2105	5156
	Onshore wind power		



### **2.2.1 Hydropower**

The hydropower plant is a source of energy generation that exploits the energy of water falling from a height or down the hill. The water falls on the turbine blades and transfers the energy due to the height of the fall to turn the turbine blades, which then generates electricity. The water after turning the turbine flows downstream to smaller water bodies. The water source for the hydropower generation can be either artificial (dam) or natural. The dam is a barrier made of concrete or earth to control water flow to create water storage known as a reservoir (Microsoft®, 2009).

Dams are fed by water from rivers, streams, and direct rainfall. The main sources of rivers and streams are rain and underground water. Furthermore, the rain is produced as a result of water evaporation into the atmosphere under the influence of solar heating (Breeze, 2018b). The amount of energy that can be generated from hydropower is a function of the quantity of rainfall over a region, which successfully flows into a dam, and can be allowed to flow downhill under a controlled process referred to as dam opening. The explanation gives a rough estimate for the gross theoretical hydropower potential per location. Technically, approximately 38% of the hydropower potential globally has been exploited (Breeze, 2018b). Hydropower plants are categorised based on their size either small or large (Breeze, 2018c). In terms of energy type, hydropower is categorised as renewable energy resources. In addition, it is regarded to be environmentally friendly. Hydropower remains one of the most important and efficient renewable sources to date, contributing approximately 16% of the total electricity generation globally (Breeze, 2018a).

### **2.2.2 Wind energy**

Wind energy has been reported to be one of the highly sustainable renewable energies which are crucial for the growth of a country (Hernández-Escobedo *et al.*, 2018). The

application of wind power ranges from the milling of grain to sailing of ships and pumping of water. Wind energy is currently regarded as the major alternative sources of energy to fossil fuels (Stathopoulos *et al.*, 2018). Wind energy can either, be harvested onshore or offshore, depending on the wind speed at the location (Zheng *et al.*, 2018, Stathopoulos *et al.*, 2018). Wind energy can be converted to electrical energy, simply by installing a wind vane.

South Africa is one of the developing Nations that have tapped into the potential of wind energy for electricity generation. Approximately 562 MW is currently generated, based on the 2016 report by the International Energy Agency of South Africa, while 2098 MW is under construction. **Table 2.5** shows the amount of electricity generated from wind energy among other renewable energy and further capacity under construction. The installation of the wind vane is best implemented in an open field with no obstructions, which could reduce the wind speed that is hitting the turbine blades. The available open land field is usually far from the urban centres where the energy generated is used. This has necessitated the installation of wind turbines on high-rise buildings as exemplified in Bahrain (Bahrain World Trade Centre Towers). The pictorial view of the installation is shown in **Figure 2.3**. Wind energy has shown good promises in complementing the energy mix of any society (Ahmad and Derrible, 2018, Ashfaq and Ianakiev, 2018, François *et al.*, 2016). The initial installation for commercial power generation is usually capital intensive. However, it is cost-effective in the long-term. Wind energy is a viable substitute or complement for fossil fuel-based energy generation because it is readily available and environmentally friendly.

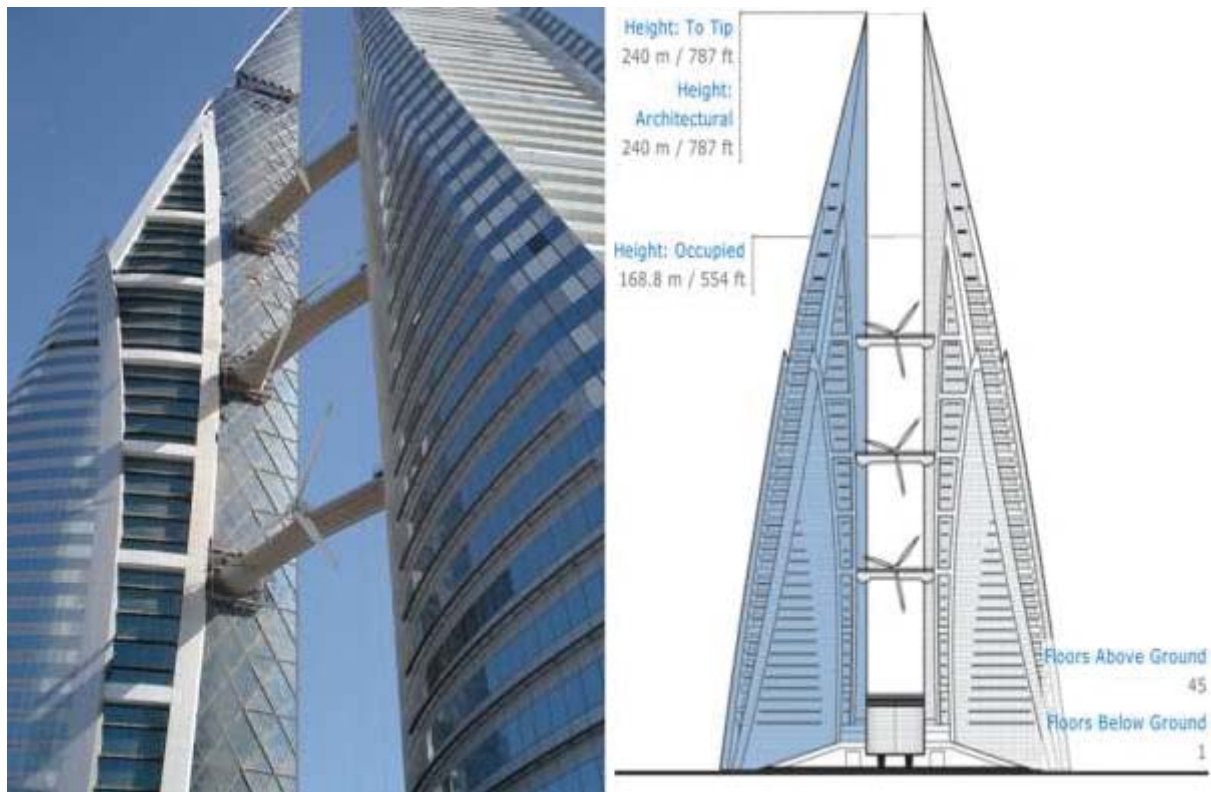
According to Dupont *et al.* (2018), by the year 2050 many countries will utilize wind as a major energy source, which will include onshore and offshore wind energy sources. The achievement of this plan will inform new and improved technology, policy design,

investment modalities, job creation, foreign investment collaborations, among others. The United Arab Emirates (UAE) government's plan is to reduce greenhouse gas emission (CO<sub>2</sub>) by 2030 through renewable energy mix while maintaining the price of electricity to a minimum. In the global markets, countries like the USA, China, Germany, Spain, and India are the major leading countries with respect to wind energy installation capacity. From these countries, China has been reported to have the highest installed capacity in the world (Sahu, 2018).

**Table 2.5:** Renewable energy generation by an independent producer in SA. Source: (International-Energy-Agency, 2016)

Energy Source	Status	Capacity (MW) <sup>a</sup>	Average Expected Capacity Factor (%)
Concentrated solar	Operational	100	36
	Under construction	400	46
Solar PV	Operational	941	23
	Under construction	958	23
Wind	Operational	562	15–37
	Under construction	2098	15–43
<b>Total</b>		<b>5069</b>	

<sup>a</sup>: megawatt



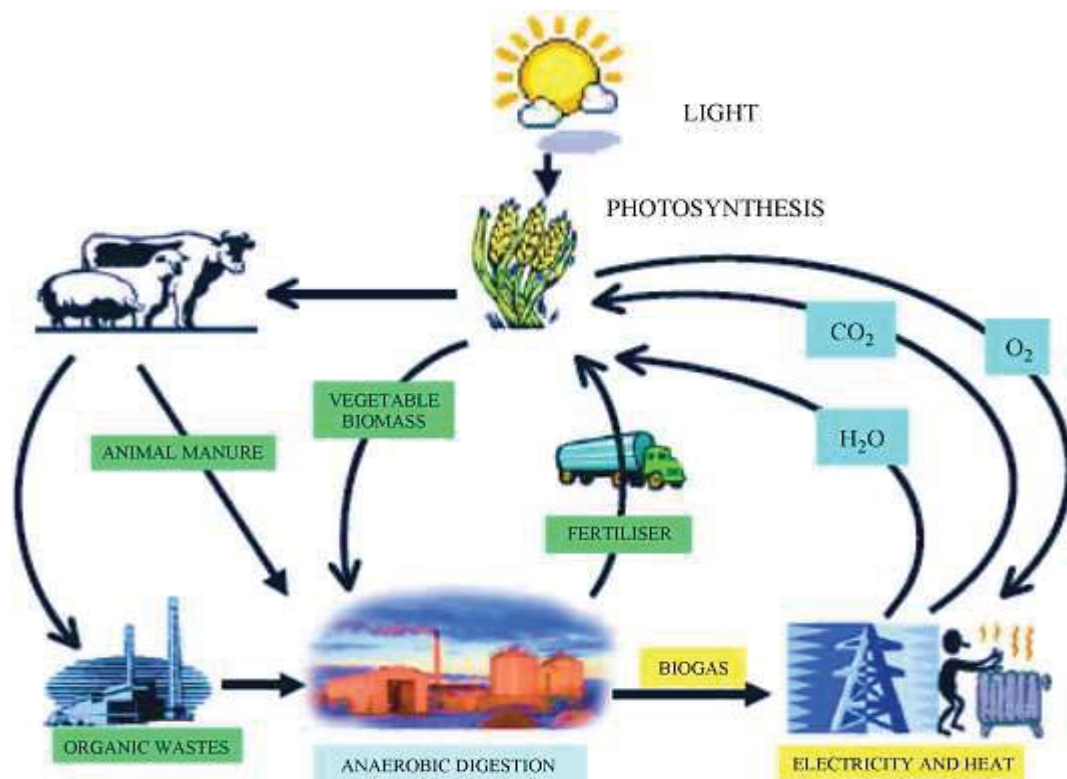
<http://www.skyscrapercenter.com/building/bahrain-world-trade-center1/998>

**Figure 2.3:** Wind turbines installation between buildings (Bahrain World Trade Centre Towers). Adopted from Stathopoulos *et al.* (2018)

### 2.2.3 Bioenergy

The global total energy usage originates mainly from fossil fuels, accounting for approximately 80% while renewable energy sources account for 20% (Devi *et al.*, 2003). In the last decade, based on primary energy consumption, biomass is responsible for approximately 14% of the global primary energy consumption, and it is expected to reach 50% by 2050 (Kamel *et al.*, 2018). Biomass has the potential to meet the global energy requirement since the raw material is readily available in all countries of the world. The raw materials can be obtained from various sources ranging from domestic waste to industrial and agricultural waste (Panwar *et al.*, 2011). The raw materials include but are not limited to wheat straw (Townsend *et al.*, 2018), palm oil (Papilo *et al.*, 2018), dairy manure (Chowdhury *et al.*, 2018), and forest residues (Jin and Sutherland, 2018). **Figure 2.4** represents the process of generating

electricity and heat from biomaterials through anaerobic digestion. The global production of biomass has been valued at 146 billion metric tons (Kamel *et al.*, 2018).



**Figure 2.4:** Schematic diagram of the sustainable cycle of anaerobic co-digestion of organic wastes and animal manure. Adopted from Panwar *et al.* (2011)

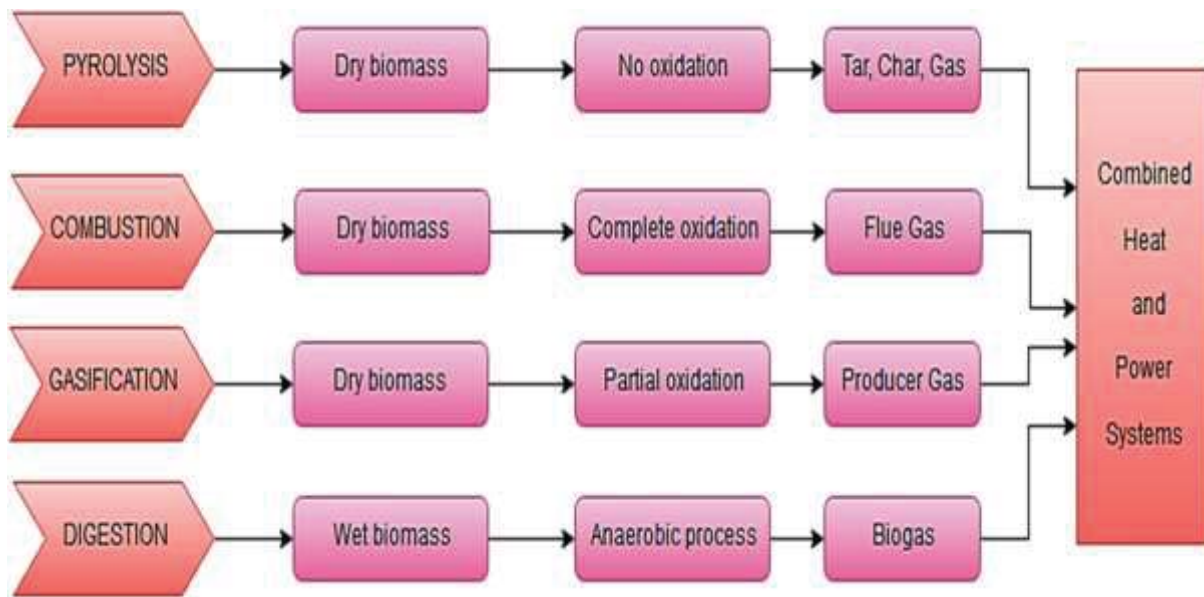
Africa and Asia have the highest biomass conversion to thermal energy rate of approximately 79% of the world's total. While in developed countries, liquid energy and/or electricity are produced from biomass (Cook and Beyea, 2000, World\_Bioenergy\_Association, 2017). Europe on the other hand generates approximately 196 TWh of electricity from biomass (Slade *et al.*, 2011). Electricity generation and the use of bioenergy are observed to differ from one region to another, which equally depends on the nature of waste generation per time (Parikka, 2004). The complexity behind the energy conversion process for biomass is the main drawback when it comes to this form of renewable energy generation. Understanding the process of energy conversion for bioenergy will contribute to global energy

generation and reduce the amount of CO<sub>2</sub> emission to the environment. Therefore, this will significantly contribute to the decrease in the negative impact of fossil fuel-based energy generation and conversion. Countries with advanced experience in biomass energy generation and conversion include Germany, America, Denmark, and Spain (Varela *et al.*, 1999). According to Kamel *et al.* (2018), the three largest practical biomass power plants in the world from the least to the greatest respectively are:

- (i) The Polaniec biomass power plant located at Polaniec in South-East Poland with a capacity of 205 MW.
- (ii) The bio-fuelled power plant located in Finland with a capacity of 265 MW.
- (iii) The Ironbridge power plant located in the UK with a capacity of 740 MW.

Bioenergy is a viable renewable energy resource that can be implemented in African countries. This will require the importation of existing technologies on how to convert biomass into bioenergy from Europe and other parts of the world where the technology is already in place. The leaders of the African countries have a significant part to play in ensuring the possibility of diversifying into this form of renewable energy. One of the ways to achieve this diversification is to create a conducive and enabling environment that will attract foreign investors and private sector establishments. One approach that the governments can implement is to reduce the tariff or tax payable by such operators within the country. The viability of biomass conversion to various forms of energy like heat, electricity and biofuels has been reported in many studies (Zhu and Pan, 2010, Gai and Dong, 2012, Ozonoh *et al.*, 2018). Various conversion processes can be used to generate bioelectricity as shown in **Figure 2.5**.



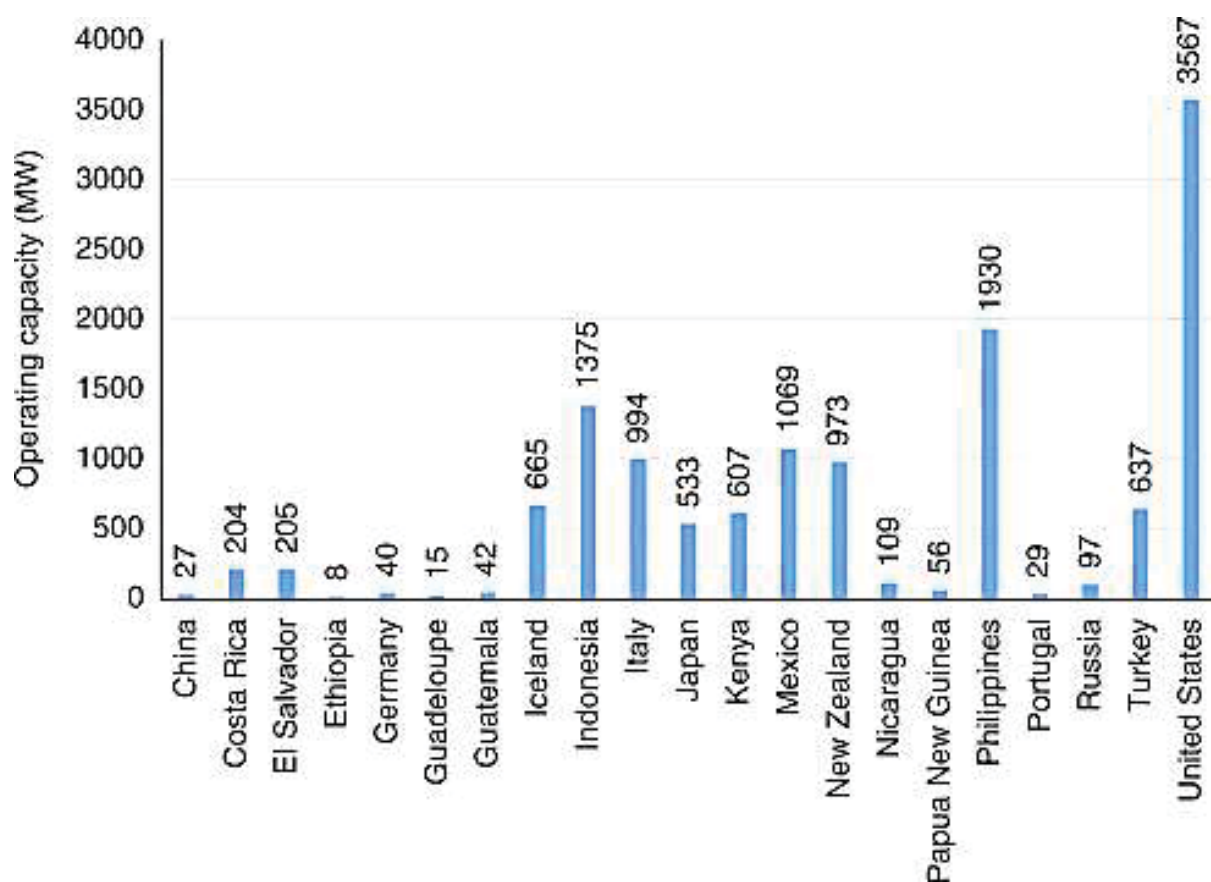


**Figure 2.5:** Power conversion technologies for biomass. Adopted from Kamel *et al.* (2018)

#### 2.2.4 Geothermal energy

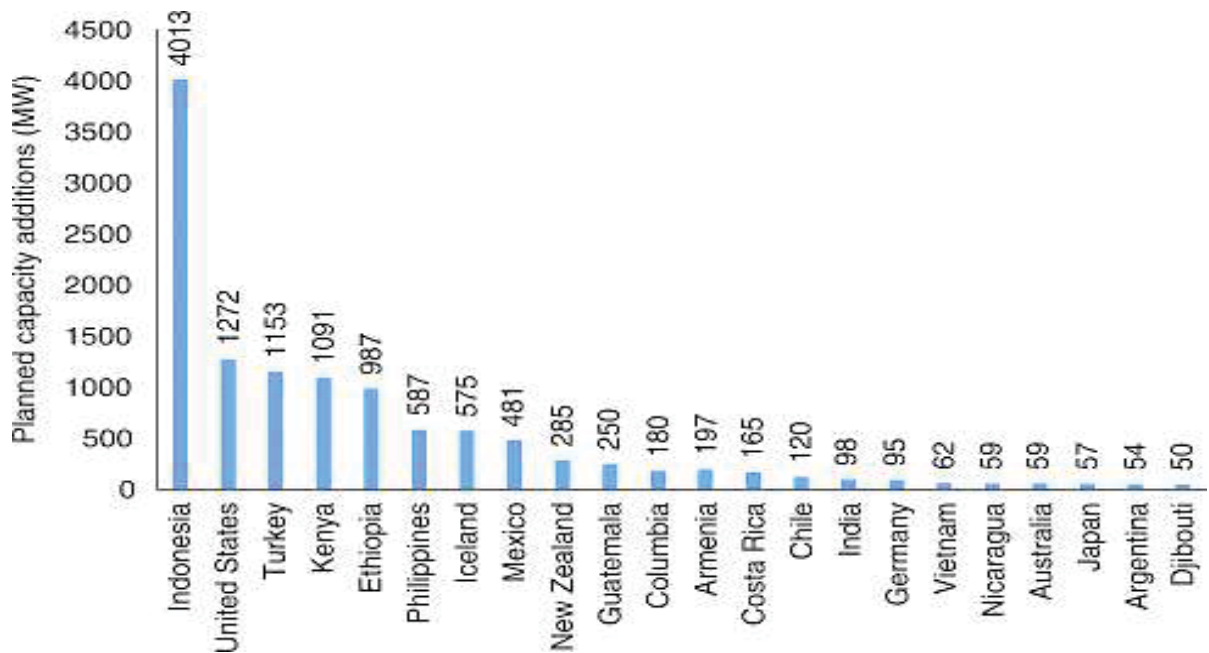
The energy that is generated and stored in the Earth's crust, is known as geothermal energy (GTE). Lay *et al.* (2008), referred to geothermal energy as the earth's internal heat energy that is generated from radioactive decayed materials. The temperature of any organic and/or inorganic matter can be determined by the thermal energy. Radioactive decaying of plants and animals and the planet formation is responsible for the geothermal energy source of the earth's crust (Dye, 2012). According to Gando *et al.* (2011), approximately 50% of the total heat flux of the earth crust is a result of heat from radioactive decay of materials. Among the renewable energy resources, geothermal energy is the largest untapped energy resources. The International Energy Agency projects the geothermal energy could contribute about 1400 TWh annually to electricity generation by the year 2050, accounting for approximately 3.5% of total global electricity generation (Zheng *et al.*, 2015, Pan *et al.*, 2019). Several countries are already generating a significant amount of electrical energy. Of these, the United States America generates the highest, followed by the Philippines, Indonesia, in that

order as shown in **Figure 2.6**. African countries such as Ethiopia and Kenya generate approximately 8 and 607 MW respectively from a geothermal energy source (Dincer and Ezzat, 2018). Most countries already generating energy from a geothermal source are planning to increase the production capacity, while some new countries like Vietnam, Argentina, Djibouti, Armenia, etc. are equally focusing on geothermal power as shown in **Figure 2.7**.



**Figure 2.6:** Operating capacity of geothermal power generation by country. Adopted from Dincer and Ezzat (2018)





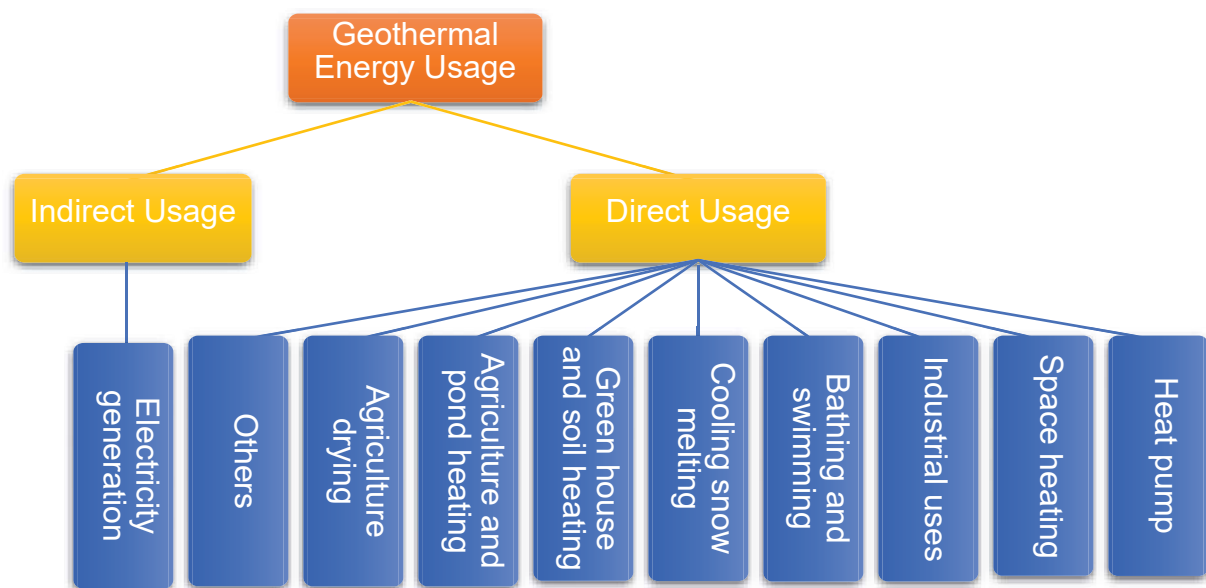
**Figure 2.7:** Geothermal power generation under development per country. Adopted from Dincer and Ezzat (2018)

Geothermal energy has a wide range of useful applications. The area of geothermal application will determine the design method. These applications could be indirect or direct usage as shown in **Figure 2.8**. The direct usage seems to have more applications unlike the indirect usage, which is only for electricity generation.

Power generation through geothermal energy is sustainable, cost-effective, reliable and environmentally friendly, but is historically limited to areas that are close to tectonic plate boundaries (Glassley, 2010). The advancement in technology has significantly broadened the size and range of feasible resources, particularly for applications such as pool heating, home heating, and water heating. This leads to global exploitation due to the huge energy potential. Geothermal energy has some setbacks such as the following:

- (i) The release of greenhouse gases that are trapped deep within the wells of the earth; although, this is below the emissions release per energy unit for fossil fuels,

- (ii) Harvesting geothermal energy requires drilling and exploration that are characterized by high cost,
- (iii) Lack of adequate technologies for exploration of geothermal energy,
- (iv) Insufficient government contribution and support, despite the potential decrease in geothermal energy generation cost, by ~25% due to government interventions.



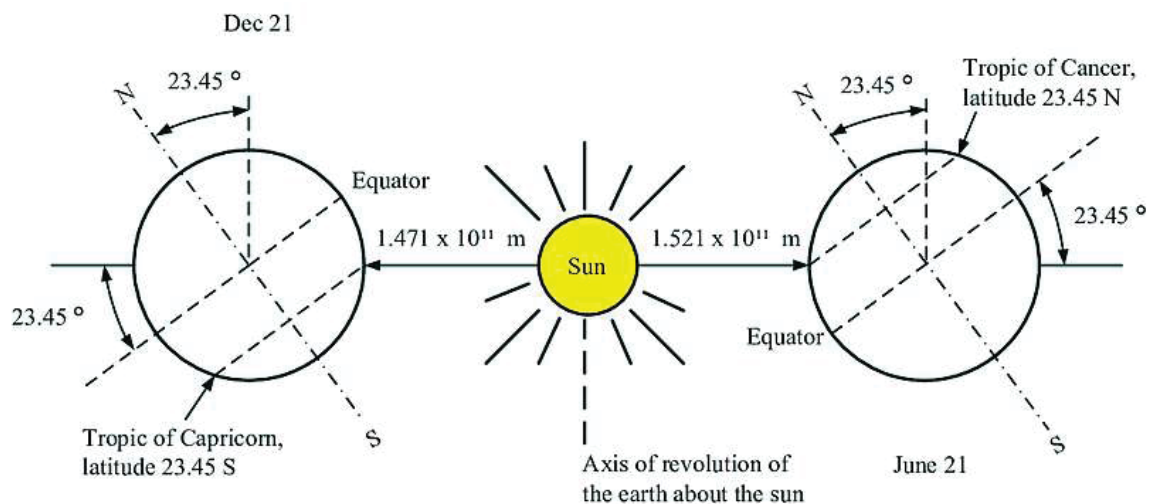
**Figure 2.8:** Utilization of geothermal energy for different applications. Adapted from Dincer and Ezzat (2018)

### 2.2.5 Solar energy

Solar energy can be regarded to be in the same form with electromagnetic radiation having wavelengths varying from approximately  $0.3 \times 10^{-6}$  to over  $3 \times 10^{-6}$  m, which tally with ultraviolet (less than  $0.4 \times 10^{-6}$  m), infrared (over  $0.7 \times 10^{-6}$  m) and visible ( $0.4 \times 10^{-6}$  m and  $0.7 \times 10^{-6}$  m). This form of energy is predominantly concentrated in the visible wavelength and close to the infrared wavelength range (Padilla, 2011). Incident solar radiation, also known as insolation, is calculated in irradiance or  $\text{kW/m}^2$ . The average total amount of solar radiation striking the earth's surface, normal to the sun incident rays outside the earth atmosphere, extra-terrestrial insolation and at an average earth-

sun distance ( $D_o$ ), is known as the solar constant ( $I_o$ ). This constant was recently measured to have a value of  $1366.10 \text{ W/m}^2$  (Gueymard, 2004).

Solar energy is the energy from the sun that falls on the earth's surface. The intensity of the energy is a result of the distance between the sun and the earth. The minimum intensity occurs on December 21 (winter solstice) and the maximum on June 21 (summer solstice). The distances between the sun and earth during the minimum and maximum intensity scenarios are respectively  $1.471 \times 10^{11} \text{ m}$  and  $1.521 \times 10^{11} \text{ m}$ . Therefore, the amount of solar radiation that the earth intercepts varies per time throughout the year depending on the earth-sun distance having an average of  $1.496 \times 10^{11}$ , i.e.,  $(\text{max} + \text{min})/2$  (see **Figure 2.9**).



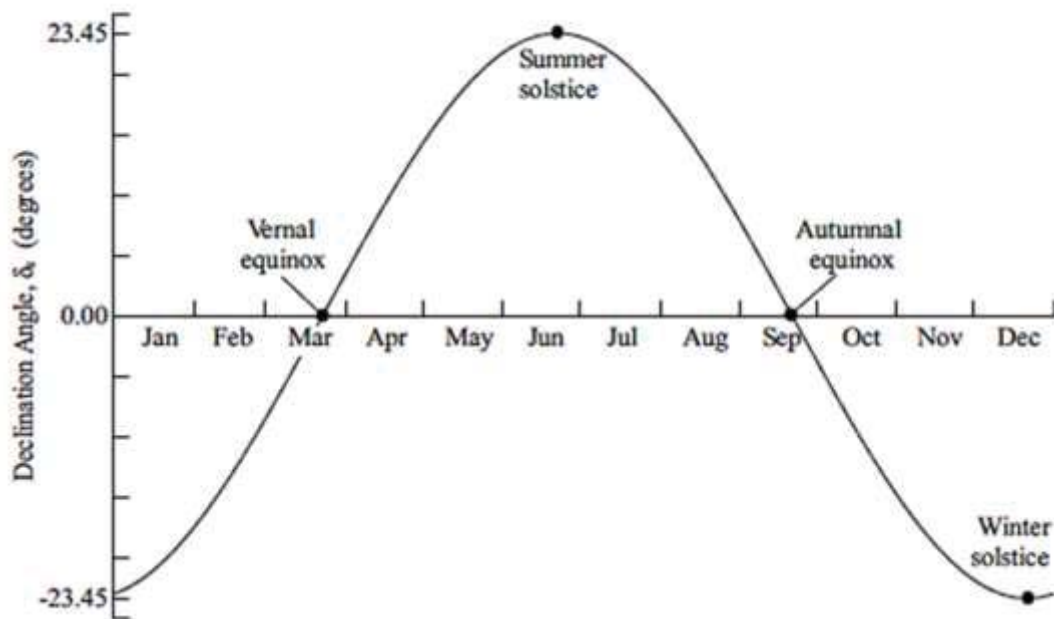
**Figure 2.9:** Earth motion about the sun. Adopted from Goswami *et al.* (2000)

Daily, the earth rotates about its axis, at an angle of  $23.45^\circ$ , to its ecliptic orbital plane axis around the sun. This angle is called the tilt angle and it is responsible for the solar radiation's seasonal variation observable at any given location across the earth's surface. The angle formed by the sun line and the equatorial plane, which is between the earth-sun line and the equatorial plane is known as the solar declination angle ( $\delta_s$ ). Solar declination angle varies from  $-23.45^\circ$  to  $+23.45^\circ$  on December 21 and June 21

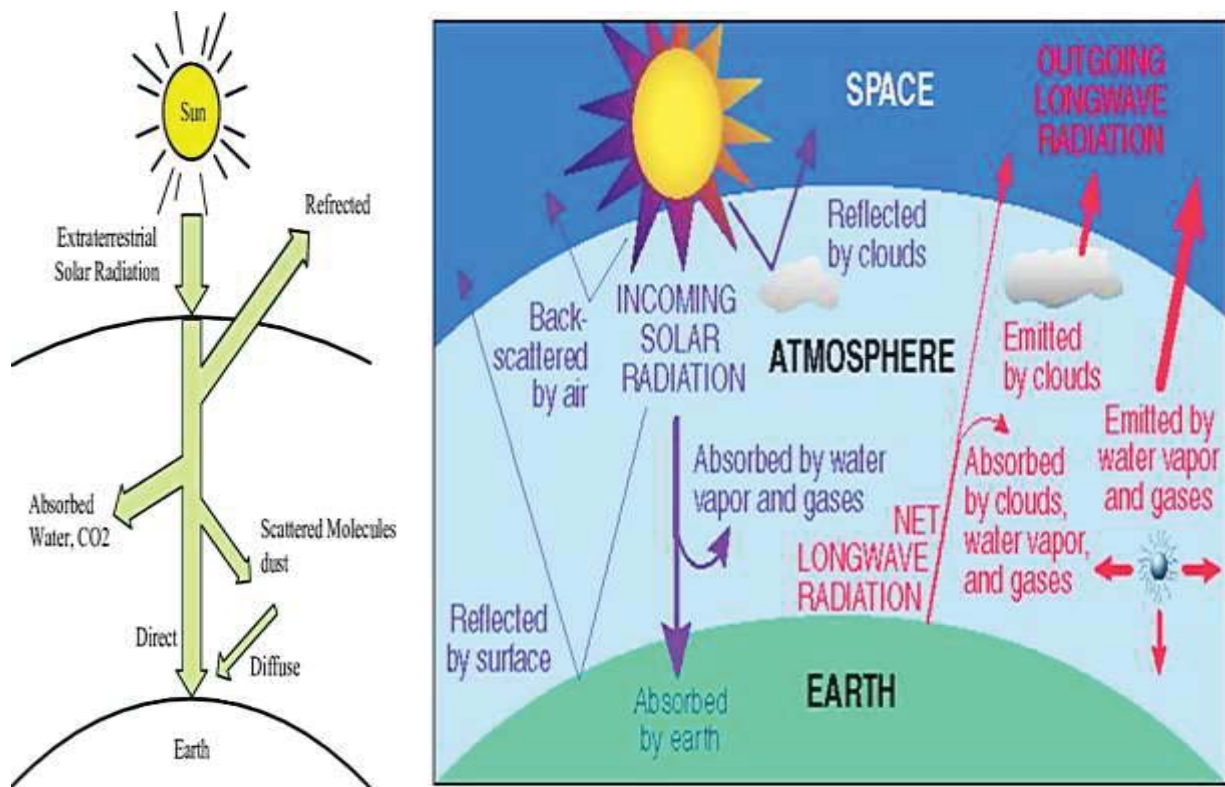
respectively as shown in **Figure 2.10**. The solar declination angle can be determined using Equation 2.1. As solar radiation travels from the sun to the earth, only a certain amount of the extra-terrestrial solar radiation can go through the atmosphere. Some of the solar radiations are reflected, while air and water vapour absorb a portion of it. A part of the solar radiation is also scattered by water vapour, aerosols, air molecules, and dust particles as shown in **Figure 2.11**. The amount of solar radiation, which eventually reaches the earth's surface directly are the rays, which experience no change in direction. This is known as the beam or the direct radiation. Furthermore, the scattered diffuse radiation that eventually reaches the earth's surface is known as sky diffuse radiation (Padilla, 2011). **Figure 2.11** shows each of the solar radiation types explained above.

$$\delta_s = 23.45^\circ \sin \left[ \frac{360(284+n)}{365} \right] \quad (2.1)$$

Where  $n$  is the day number, when  $n = 1$ : meaning January 1.



**Figure 2.10:** Solar declination angle throughout the year. Adopted from Padilla (2011)



**Figure 2.11:** Illustration of overall solar radiation that passes through the earth's surface. Adopted from Padilla (2011), (AssignmentPoint)

### 2.2.5.1 Solar Angles

As the sun moves during the day, its position at any given time is a function of two angles, namely: the azimuth angle and the altitude angle. As presented in **Figure 2.12** the solar azimuth angle ( $a_s$ ), is the angle that lines between the projected horizontal line that is joining the site to the sun and due south plane, while the solar altitude angle ( $\alpha$ ) is the angle between the horizontal projection plane and the collinear line with the ray of the sun (Goswami *et al.*, 2000). The azimuth angle shows a positive value when the sun is directed towards the West of South and indicates negative values whenever the Sun is directed toward East of South. From **Figure 2.12**, the solar zenith angle ( $z$ ), is the angle that is between the vertical at the site location and the site to the line of the sun. The relationship between the solar altitude angle and the solar zenith angle is presented in Equation 2.2. The solar altitude and solar azimuth angles are not

classified as fundamental. Therefore, they are linked to fundamental angles like hour angle ( $h$ ), latitude angle ( $L$ ) and declination angle ( $\delta_s$ ) as shown in **Figure 2.13** (Padilla, 2011). The hour angle ( $h$ ) at noon at local solar ( $LL$ ) noon is zero, provided that 1 hour equals to  $15^\circ$  of the sun traveling across the sky.

$$z + \alpha = 90^\circ \quad (2.2)$$

$$\alpha = \sin^{-1} [\cos(L) \cos(\delta_s) \cos(h) + \sin(L) \sin(\delta_s)] \quad (2.3)$$

$$h = (AST - 12) \times 15^\circ \quad (2.4)$$

Where  $AST$  represent the apparent solar time that can be obtained from Equation 2.5.

$$AST = LST + EoT \pm 4(SL - LL) - DS \quad (2.5)$$

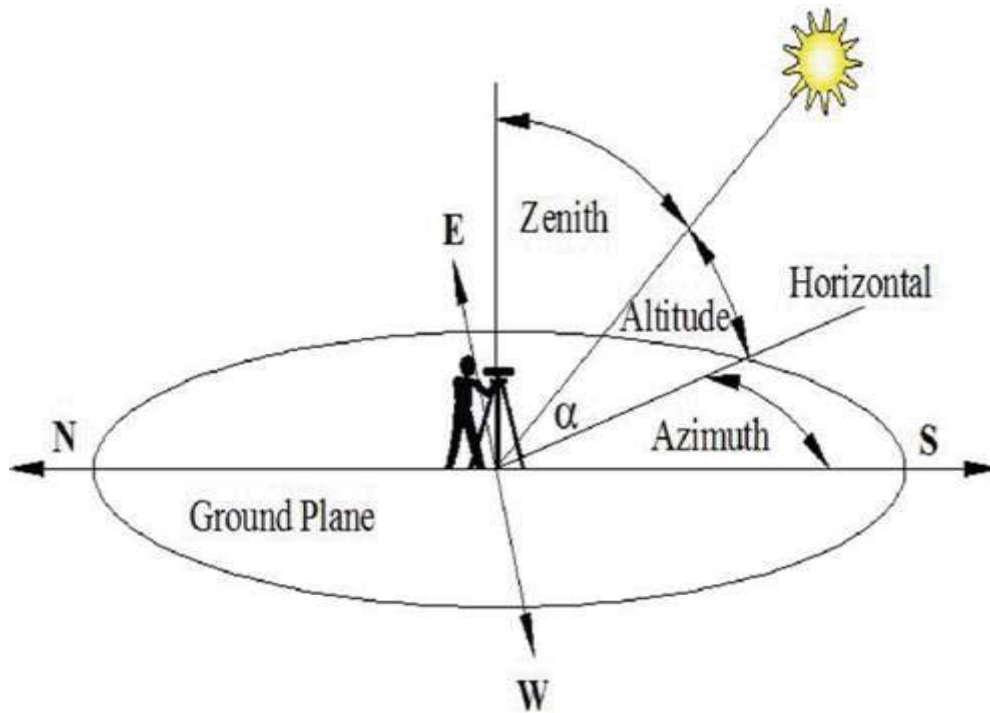
Calculating the equation of time is imperative to obtain the  $AST$ , and is denoted by  $EoT$ . It is calculated using the following equation:

$$EoT = 9.87 \sin(2B) - 7.53 \cos(B) - 1.5 \sin(B) \quad (2.6)$$

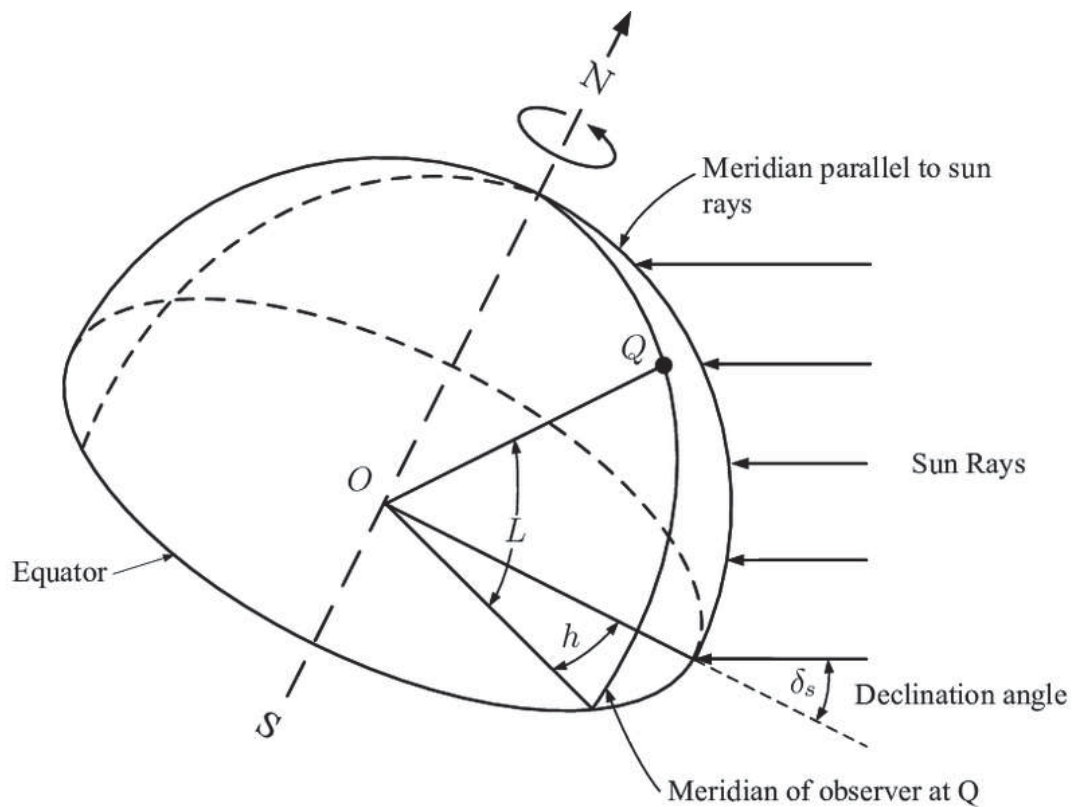
$$\text{Where } B = \frac{360(n-81)}{364} \quad (2.7)$$

Where  $h$  is the hour angle,  $L$  is the latitude angle,  $EoT$  is the equation of time,  $AST$  is the apparent solar time,  $SL$  is the standard time meridian and  $LL$  is the local time meridian.

$$a_s = \sin^{-1} \left( \frac{\sin \delta \cos h}{\cos \alpha} \right) \quad (2.8)$$



**Figure 2.12:** Coordinate system earth surface showing solar altitude angle, azimuth angle and zenith angle. Adopted from Terzioglu *et al.* (2015)



**Figure 2.13:** Fundamental sun angles. Adopted from Padilla (2011)



### 2.2.5.2 Incident Angle

The angle between the normal surface and the beam radiation is regarded as the incident angle. For a horizontal plane, the incident angle is established as the same as the zenith angle. The equation for the incident angle is a function of the normal surface and the slope, as shown in Equations 2.9 and 2.10.

For the incident angle on the normal surface:

$$\cos \theta_z = \cos L \cos \delta_s \sin h + \sin L \sin \delta_s \quad (2.9)$$

For the incident angle on a slope:

$$\cos(\theta) = \sin(L + \beta) \sin(\delta_s) + \cos(L + \beta) \cos(\delta_s) \cos(h) \quad (2.10)$$

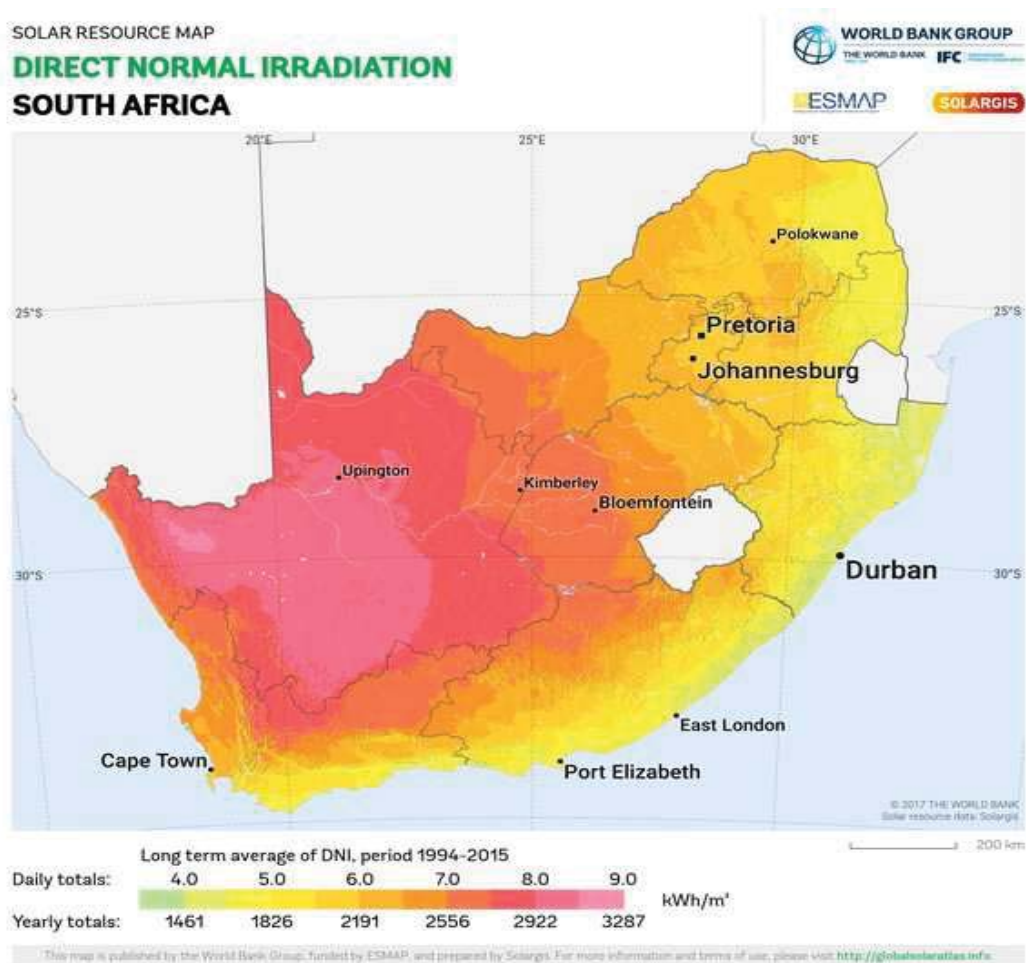
### 2.2.5.3 Solar energy potentials in South Africa

The potentials from solar energy vary per geographical location due to the earth-sun distance. Among countries in Africa, South Africa (SA) is one of the leading countries that have tapped into solar energy for various applications ranging from electrical power generation to water heating, air-conditioning and refrigeration, pool heating, and so on. South Africa's sunshine per day is at an average of 8-10 hours, having nationwide sunshine averaging 2 500 hours per year. The solar radiation level in SA varies between 4.5 to 6.6 kWh/m<sup>2</sup>, making SA among the world's top three countries in terms of sunshine average (Jain and Jain, 2017). The areas where there are solar energy potentials are shown in **Figure 2.14**, while the level of solar radiation is shown in **Figure 2.15**. The huge solar energy potential in SA is one of the reasons or justifications for the current research.





**Figure 2.14:** Provincial distribution of renewable energy resources in South Africa. Adopted from Department-of-Energy (2015)



**Figure 2.15:** Solar energy potentials of South Africa. Adopted from SolarGIS (2019)

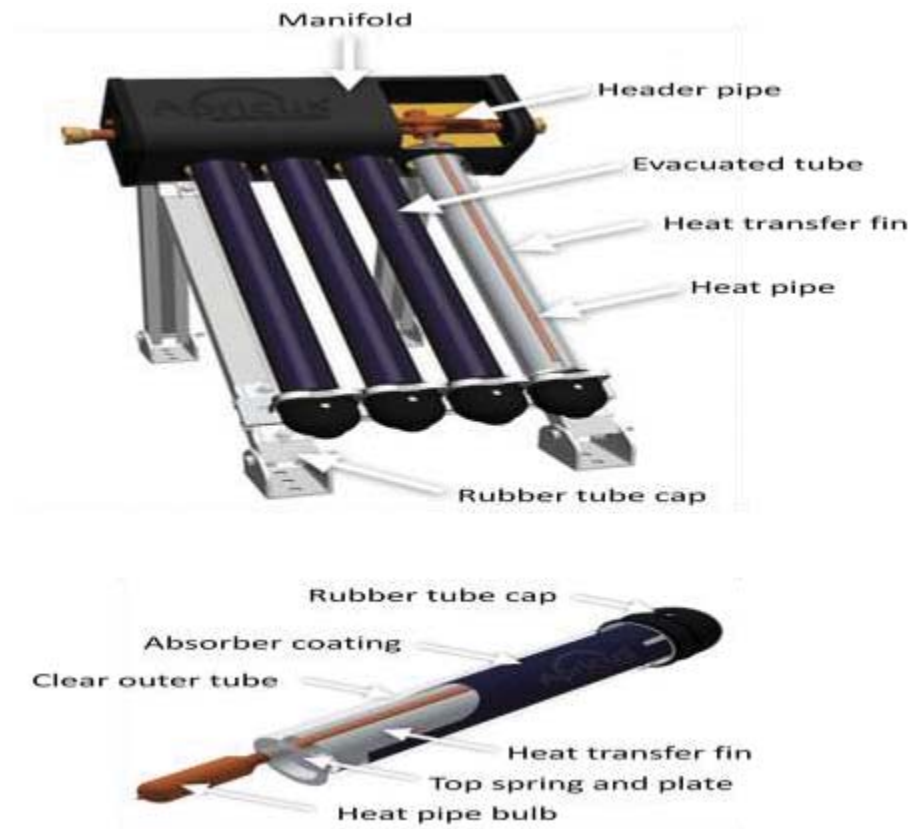
## **2.3 Solar Energy Collectors for Household Water Heating**

The steady growth in global energy consumption in the past decades of which, fossil fuels contributed to more than 80%, has been responsible for various studies into other energy sources (Zou *et al.*, 2016). The escalating price increase of energy, the increasing energy demand and the hazardous impact of CO<sub>2</sub> emission from carbon-based energy generation like coal have intensified the shift to alternative renewable and sustainable energy globally. One of the most common renewable and sustainable energy sources is solar radiation. The energy from the sun can be harvested through various means. The use of solar collector to harvest solar energy is one of the practical approaches already in use. A solar collector is a form of heat exchanger that operates by transferring the heat of the sun unto an absorber to heat the liquids (e.g. water) passing through the absorber. The flat plate collector design by Hottel and Whillier in the 1950s is widely considered as the most popular design for the solar water heater (SWH) (Wikipedia). The SWH efficiency depends significantly on the effectiveness of the solar collector and this has prompted numerous researchers to focus on ways to potentially improve the collectors' performance (Shukla *et al.*, 2013).

### **2.3.1 Evacuated tube solar collector**

The evacuated tube solar collector (ETSC) has been commercially in supply for more than 25 years. Studies have shown its improved performance when compared to the flat plate solar collector (FPSC) due to the higher temperature being achieved. However, the cost of the ETSC is higher than the FPSC when both prices are compared. The ETSC comprises of the following components: evacuated tube, aluminium casing, absorber coating, heat transfer fin and copper pipe (see **Figure 2.16**). The glass-evacuated tubes are usually common in present times due to low heat loss and low heat extraction when compared with flat plate collectors. The designs

have been modified by various researchers to improve the performance of the collector (Kim and Seo, 2007, Liang *et al.*, 2011). Glassed semi-cylindrical ETSC was reported to have absorbed 16% more energy than ETSC with a flat plate-shaped absorber tube (Perez *et al.*, 1995).



**Figure 2.16:** Schematic diagram of evacuated solar tube collector. Source (Apricus.)

### 2.3.2 Flat plate collectors

The flat plate collectors (FPCs) are the major components of a solar water heating system and it is widely used in most parts of the world like China, Brazil, India, South Africa, etc. The FPC consists of a dark flat-plate absorber, heat-insulating backing and a transparent cover (which could be polycarbonate or glass) to decrease the rate of heat loss and ensure the components are protected from moisture and dust as shown in **Figure 2.17** (Shukla *et al.*, 2013).

The arrangement of the collectors has been reported by many researchers to be one of the major decisive factors depicting the thermal performance of the entire system (Matrawy and Farkas, 1997). Parallel tube collector method of design is the prominent method used, in which the tubes and the absorber plates are integrated as a single plate structure. The drawback with this kind of system is the non-uniform distribution of temperature over the surface of the absorber plate, and the irregular working fluid circulation through the tubes (Shukla *et al.*, 2013).



**Figure 2.17:** Schematic diagram of a glazed flat plate solar collector. Source (Apricus.)

### 2.3.3 Glazed and unglazed solar collector

The solar collector can either be unglazed or glazed. Glazing primarily reduces the rate of heat loss through convection by constraining air movement. Furthermore, glazing simply protects the absorber from environmental factors (such as wind, ice, dust, etc.). This is also important when the glazing is made with low-iron content, which helps to reduce radiative heat losses by reflecting the thermal radiation emitted by the absorber. A high transmittance is the most important property required of glazing

materials for perfect solar radiation because a slight loss in transmittance will result in a direct decrease in the collector's efficiency (Smyth *et al.*, 2006).

## **2.4 Solar Water Heating for Electrical Power Generation**

Among the different sources of renewable energy (geothermal, wind, biomass, hydro, etc.), solar energy is the most explored renewable resource across the globe based on available literature. The popularity of this energy source has led to various designs to harness, convert and store the energy. From a study by Manikandan *et al.* (2019), several collector designs have been fabricated and tested for various temperature ranges:

- (i) High temperature (heliostat field collector and parabolic dish reflector of temperature between 150-2000 °C and 100-1500 °C respectively)
- (ii) Medium temperature (parabolic trough, cylindrical trough and linear Fresnel reflector of temperatures of between 60-400 °C, 60-300 °C and 60-250 °C respectively)
- (iii) Low temperature (compound parabolic collector, evacuated tube, and a flat plate of temperatures of between 60-240 °C, 50-200 °C and 30-80 °C, respectively).

The design geometry and many other factors determine the performance and applicability of a collector (Manikandan *et al.*, 2019, Razmmand *et al.*, 2019, Azzouzi *et al.*, 2018). Various mathematical models have also been used to predict the performance of various solar concentrators (Salgado Conrado *et al.*, 2017, Li *et al.*, 2018, Cheng *et al.*, 2018). The most common designs for solar collectors are listed and explained in the following subsections.

### 2.4.1 Linear Fresnel reflector

In the last two decades, different companies in domains, e.g., thermal power plants, have commercialized solar collector technology involving Linear Fresnel Collector (LFC) for various applications. This was initially proposed as a substitute for tower systems that have heliostat fields (Dicanio *et al.*, 1979). Previously, the most used technology for solar concentration was the parabolic trough collectors (PTCs). The continuous development in terms of research and innovation (RnI) has led to the development of alternative concentrations. LFC technology has been widely developed by companies from Germany (Novatec Solar, MAN/Solar Power Group, and Industrial Solar). Other notable companies are Areva Solar from France and the USA, Fera from Italy and CNIM from France. Several other designs of LFC and locations in terms of countries were also highlighted by Grena and Tarquini (2011). From a design perspective by various companies, Morin *et al.* (2012) reported that the followings should be taken into consideration:

- i. The primary mirror field: Number of mirrors, spacing, and width of the mirror's parallel rows and the tracking design of the mirror.
- ii. In-depth receiver design: This could be in the numbers of tube receivers or a single tube receiver that has a secondary concentrator placed above the tube, air receiver or vacuum technology, operating pressures and temperatures, dimensions and materials.
- iii. Receiver height above the primary mirror field.
- iv. Heat transfer fluid used and the highest operating temperature level of the system.

In attaining the same solar radiation while tracking the sun, the mirrors have to be arranged in an orderly manner, having different tracking angles in order to achieve a

common focal point for the absorber positioning. Multiple motors are required due to different tracking angles. This leads to the high-cost of the design when compared to an equal solar radiation area of PTCs, which has been in existence since the first solar water-heating device was commercialized in 1891 (Islam *et al.*, 2013). Geometrically, LFC is more complex than PTC, due to the increasing number of mirrors and dimension. Therefore, it requires a more precise arrangement in order to achieve optimum performance of the system, as shown in **Figure 2.18**. The performance of the system is directly influenced by the optical material in use, the tracking accuracy and mounting, degradation, receiver design and dirt formation on the surface of the mirrors (Morin *et al.*, 2012). Some similarities in the mode of application exist, which include: the use of a working fluid, solar tracking, concentration and secondary concentration (Montes *et al.*, 2014). In a study that was conducted by Gharbi *et al.* (2011), PTC and LFC having the same capacity unit in MW gave different results in terms of concentration, peak solar efficiency, annual solar efficiency and output temperature. The only similarity was the capacity solar factor, as shown in



**Table 2.6.** From the Table, it is evident that PTC exhibits better efficiency and output temperature than LFC at the same unit capacity.



**Figure 2.18:** Linear Fresnel solar power concentrated (a) and Saudi Arabia linear Fresnel solar power concentrated (b). Adopted from (Fineartamerica.com) and (helioscsp.com)



**Table 2.6:** Comparison of linear Fresnel collector with a parabolic trough collector.  
Adapted from Gharbi et al. (2011)

Collector type	Unit capacity (MW)	Concentration	Peak solar efficiency (%)	Annual solar efficiency (%)	Output temperature (°C)	Capacity solar factor (%)
Linear						
Fresnel collector	10 – 200	25 – 100	20	9 – 11	250 – 500	25 – 70
Parabolic						
trough collector	10 – 200	70 – 80	21	17 – 18	300 – 550	25 – 70

Similar, research was conducted by Giostri et al. (2013) to validate the assertion that PTC performs better than LFC. From their results, it was observed that parabolic trough technology had an optical efficiency and electrical efficiency of 75% and 23.6%, respectively when compared to the Fresnel technology with 67% and 19.25%, respectively. The amount of the sun-to-electric was equally, calculated on an annual average efficiency basis and a value of 10.2% was achieved for the Fresnel plant based on a 38.8% average optical efficiency. While the parabolic trough achieved a 16% plant efficiency as a result of a 52.7% optical efficiency. Lastly, from the economic assessment, it was shown that the cost of investment for the linear Fresnel collectors needs to be reduced by at least 45% to match-up with the parabolic trough collector for the same electricity cost.

In a separate study titled “Comparison of Medium-size Concentrating Solar Power Plants based on Parabolic Trough and Linear Fresnel Collectors”, Cau and Cocco (2014) used the same thermal oil for PTC and LFC solar power plants, as heat transfer

fluid and the storage medium was a two-tank direct thermal storage system. The authors reported that due to superior optical efficiency, the parabolic trough solar collector performed better in terms of energy production per unit area in comparison to the Fresnel collector. The energy productions per unit area were 180–190 kWh/m<sup>2</sup> and 130–140 kWh/m<sup>2</sup> for PTC and LFC respectively. The performance evaluation between PTC and LFC, are presented in **Table 2.7**. From the table, PTC required lesser solar field collecting area for approximately similar net power output for LFC, but with a better conversion efficiency of 13.97% and 12.35%, respectively. Research has shown that with similar parameters, especially the collector area, PTC performs better than LFC. Furthermore, the design cost, installation and maintenance of PTC is considerably cheaper than LFC, making PTC a better choice for solar thermal power plants or solar water heating (Morin *et al.*, 2012).

**Table 2.7:** Performance evaluation of CSP\* plants based on PTC and LFC. Adapted from Cau and Cocco (2014).

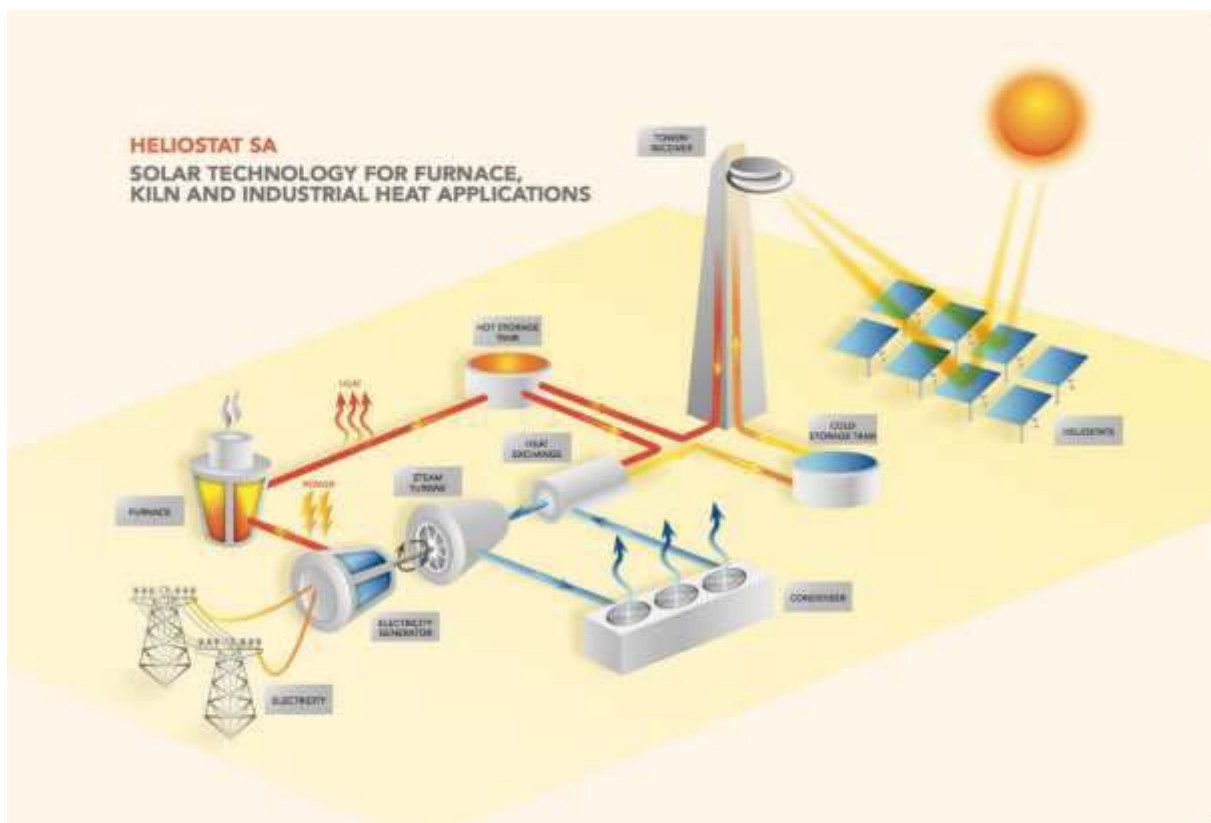
Parameters	Linear Fresnel Collector	Parabolic Trough Collector
Solar field collecting area (m <sup>2</sup> )	8501.30	7515.10
Solar field thermal power output (kW)	4043.00	4043.00
Thermal oil mass flow (kg/s)	16.01	16.01
Solar field conversion efficiency (%)	59.45	67.25
ORC <sup>a</sup> thermal power input (kW)	4043.00	4043.00
ORC <sup>a</sup> gross power output (kW)	931.30	931.30
ORC <sup>a</sup> gross efficiency (%)	23.03	23.03
CSP overall power consumption (kW)	91.40	102.20
CSP net power output (kW)	839.90	840.10
Required land area/collecting area	1.30	3.00
CSP net conversion efficiency (%)	12.35	13.97

\*Concentrating Solar Power; <sup>a</sup>Organic Rankine Cycle

#### 2.4.2 Heliostat field solar collector

Heliostat is a combination of two words, viz: “helios”, a Greek word meaning sun, and “stat”, for stationary. Heliostat is a device that includes a mirror (usually a plane mirror), which turns to continuously reflect sunlight towards a predetermined target, thereby compensating for the sun's apparent motions in the sky. The target may be a physical object, distant from the heliostat, or a direction in space. To achieve this, the reflective surface of the mirror, is kept perpendicular to the bisector of the angle between the directions of the sun and the target, as seen from the mirror. In most cases, the target

is stationary and relative to the heliostat, so that the light is reflected in a fixed direction, as shown in **Figure 2.19**. A heliostat field collector layout comprises of many reflecting plane mirrors and a tower that has a central receiver, from where the molten salt flows. This then facilitates the absorption of the heat, which is reflected by the collector. The wide field layout of mirrors focuses the incident rays of the sun onto a single receiver at the top of the tower to heat the molten salt. The molten salt is then allowed to travel through a heat exchanger where the heat is then transferred to the water in the tower/receiver to produce high-temperature superheated steam. The high-temperature steam is further expanded in a steam turbine that runs the generator to produce electrical energy.



**Figure 2.19:** Working principle of a heliostat solar thermal plant. Adopted from (Heliostat\_South\_Australia)

The performance of the system can be improved by increasing the height of the tower, and this directly increases the overall cost of installation. The arrangement of the

heliostats contributes to the effectiveness of the system. When the heliostats are arranged too close to each other, the solar flux could become blocked, thus reducing the amount of solar irradiation concentrating on the tower. To determine accurately the positioning for the field layouts, Lipps and Vant-Hull (1978) developed a mathematical model to determine the spacing and the average field density for the field layouts, as shown in **Figure 2.20**. Equations 2.11-2.14 can be used to determine correctly the exact field layout. Dellin *et al.* (1981) reported that high reflectance could be achieved for a heliostat based on the arrangement shown in **Figure 2.20b**. From the working principle and the improvement made to the heliostat, the system is best used for the steam power plant to generate electrical power rather than just water heating for domestic or industrial usage in buildings. The reason for this is the high installation and maintenance costs for the complete heliostat system.

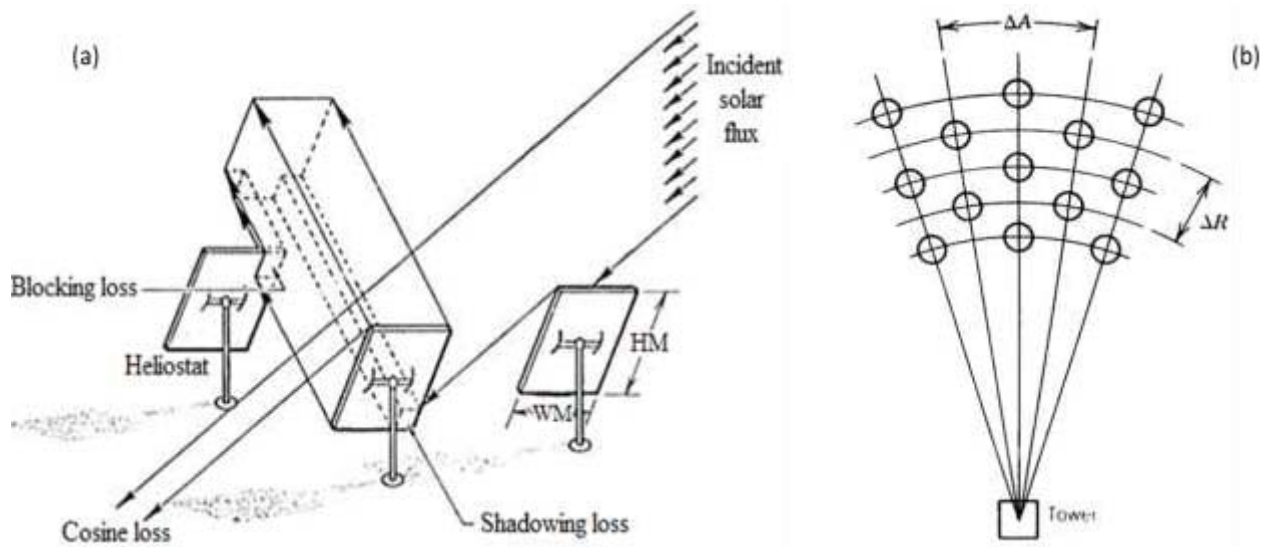
$$\Delta R = HM(1.44 \cot \theta_L - 1.094 + 3.068 \theta_L - 1.1256 \theta_L^2) \quad (2.11)$$

$$\Delta A = WM(1.749 + 0.6396 \theta_L) + \frac{0.2873}{\theta_L - 0.04902} \quad (2.12)$$

$$\theta_L = \tan^{-1} \left( \frac{1}{r} \right) \quad (2.13)$$

$$\rho_F = \frac{2DM*WH*HM}{\Delta R*\Delta A} \quad (2.14)$$

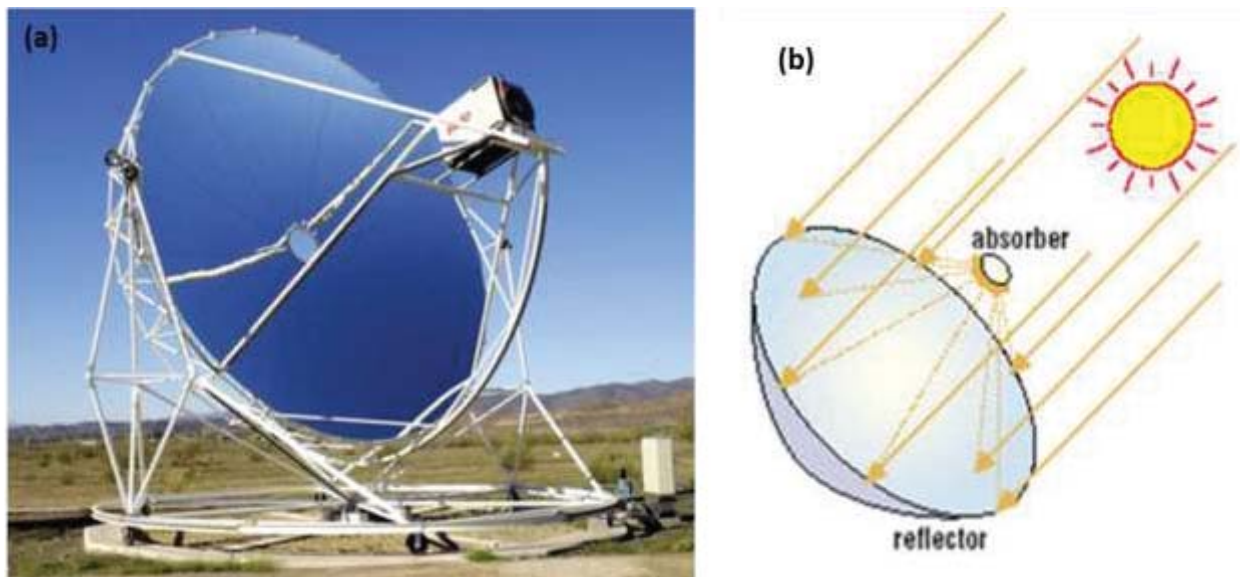
where  $\Delta R$  is the radial spacing (m),  $\Delta A$  is the azimuthal spacing (m),  $HM$  is the height of the heliostat (m),  $WM$  is the width of the heliostat (m),  $\theta_L$  is the altitude angle to the receiver from the heliostat location of interest (degree),  $\rho_F$  is the ratio of the mirror area to that of the land area, at a specific point in the field (local field density),  $DM$  is the ratio of the mirror area to the overall heliostat area (mirror density) and  $r$  is the normalised distance between the tower and the heliostat location (m).



**Figure 2.20:** Shading and blocking the loss of solar flux (a) and radial stagger heliostat layout (b). Adapted from (Lipps and Vant-Hull, 1978, Dellin *et al.*, 1981)

### 2.4.3 Parabolic dish solar collector

Parabolic dish collector (PDC) is regarded as a system of point-focus in which the paraboloid geometry is achieved by the revolution of half the parabola around its axis (Orosz and Dicks, 2017). With this type of solar collector design, the heat receiver (absorber) is located at the dish focal point. The parallel rays of the sun, which land on the surface of the dish, are concentrated on the point-focus, based on the geometric design of the solar collector. Considering the nature of the collector, dual-axis tracking is recommended for improved performance. The drawback of this type of technology is the inability to link several systems together like other forms of solar concentrators. A single PDC is known to be limited in its surface area, which can affect the system performance and, therefore, limits its applications (Zheng, 2017a). **Figure 2.21** shows a typical parabolic dish collector working principle. Among the areas of applications of PDC, desalination is one of the most common technology, due to its high flux density distribution and the high concentration ratio (Zheng, 2017b).



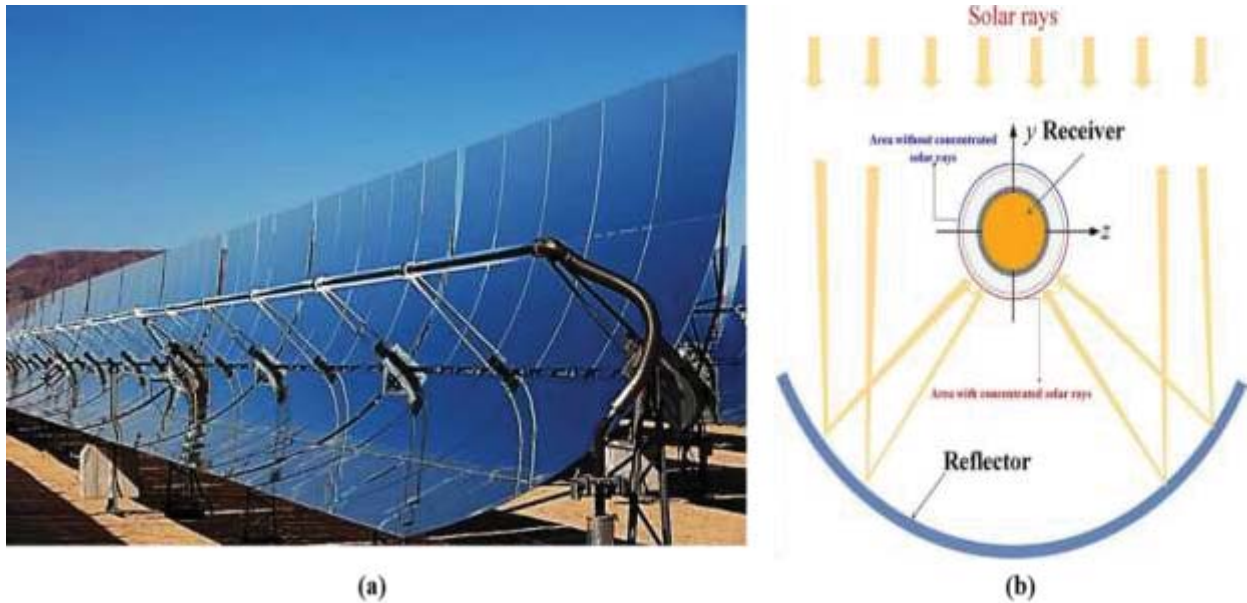
**Figure 2.21:** Parabolic dish collector: (a) typical PDC and (b) working principle of PDC. Adopted from (Energy., Heba, 2014)

#### 2.4.4 Parabolic trough solar collector

Parabolic trough collector (PTC) is known to be the most developed and frequently used solar concentrating technology and is often used for various thermal applications. PTC is used to concentrate incident solar radiation on a large collecting surface area and concentrates it on another surface with a smaller surface area, known as the receiver. The solar radiant energy received is then, converted into thermal energy. This, in turn, is used for a variety of applications. Among the four major solar concentrators, PTC is the most commonly used with over 85% installed total capacity globally, for all concentrating solar power-based plant technologies (Tagle-Salazar et al., 2018, Binotti et al., 2013). Due to the temperature range of PTC, the technology is categorized as a low-to-medium temperature system, operating between 50 and 400 °C (Kalogirou, 2004, Kalogirou, 2014). The wide operating temperature range makes it possible for the PTC technology to be widely used in various thermal operations, such as seawater desalination (Kalogirou, 1998, Alaydi, 2014), solar industrial process heating (Kalogirou, 2003), solar refrigeration and air-conditioning



(Cabrera *et al.*, 2013, Abu-Hamdeh *et al.*, 2013). **Figure 2.22** shows a typical parabolic trough collector.



**Figure 2.22:** Real-world installed PTC (a) and schematic diagram of the working principle of PTC (b). Adopted from (Gong *et al.*, 2017, Ivan, 2018)

The performance of the PTC over the years has been largely improved upon and this has been published in the literature (Li *et al.*, 2019, Wang *et al.*, 2019). A list of possible ways to enhance the performance of PTCs is listed in **Table 2.8**. Another method of improving PTC performance, other than the content in **Table 2.8**, is the use of insert in the absorber pipe. Jaramillo *et al.* (2016) analysed the effect of twisted tape insert on the performance of PTC. They reported that the heat exchange between the surfaces of the absorber tube and the thermal fluid was enhanced because of the twisted tape inserts that generated a swirling flow. Pressure drop was observed to have increased throughout the entire length of the tube. An increase in the volumetric flow due to the inserts led to an increase in thermal efficiency.

Similarly, Bellos *et al.* (2018), studied the effect of multiple cylindrical inserts for PTC. They reported that having more inserts led to better performance, in terms: of exergy,



thermal and overall efficiency of the parabolic trough collector. Among the cases that were considered, four inserts showed optimum performance of ~0.656% increase in thermal efficiency, ~5.63% decrease in thermal losses, and ~26.88% increase in the heat transfer coefficient. Parabolic trough collectors identified from literature, possess several merits, viz: high efficiency, high power density, versatility, modularity, long lifetime span, durable against moisture effects, and the parts can easily be manufactured by local manufacturers (Hafez *et al.*, 2018). Despite all the good qualities of PTCs, there are a few drawbacks, in the totality of the system, arising from the movable parts, tracking system mechanism, choice of an absorber and receiver. These factors all lead to high maintenance cost.

**Table 2.8:** Performance improvement analysis of parabolic trough collector

<b>Method of improvement</b>	<b>Parameter</b>	<b>Discussion of finding</b>	<b>Remark</b>	<b>Reference</b>
Design	Parabolic ribs	Designs for parabolic collectors have a common geometry e.g. rim angle, focal length, height, and width. The reflective surface of PTC should exhibit a stable and accurate profile. Murtuza et al designed PTC with mild steel putting in mind manufacturing constraints, optical error tolerance, material availability, and cost. They finalised the stainless steel substrate with an aluminized silver sheet. The choice of material and design showed good mechanical strength but led to an increase in the weight of the collector.	<ul style="list-style-type: none"> <li>• The geometry of PTC has similar design parameters.</li> <li>• The choice of material has a great influence on the overall weight of PTC.</li> </ul>	(Shigley and Mischke, 2005, Murtuza <i>et al.</i> , 2017)
	Wooden support	A wooden base was used to form a PTC shape, having a steel sheet as the reflective material. Heat pipe made of copper pipe was installed having ethanol as the heat transfer fluid. The system was fitted with a tracking mechanism for better performance.	<ul style="list-style-type: none"> <li>• System performance is not only dependent on the geometry but other parameters</li> <li>• The support frame and the reflective material can be made from different materials</li> </ul>	(Jafari Mosleh <i>et al.</i> , 2015)

<b>Method of improvement</b>	<b>Parameter</b>	<b>Discussion of finding</b>	<b>Remark</b>	<b>Reference</b>
			and, therefore, influence the design geometry in terms of length and width of the PTC.	
Flow rate	Flow	Among other criteria, flow rate is a determining factor when it comes to PTC performance as explained by Rehan and his colleagues. In their research study, two different working fluids were studied and the effect of flow rate was considered for both fluids. The system efficiency fluctuates with the flow rate, which is due to the changes in temperature as the time on the day changes.	<ul style="list-style-type: none"> <li>• The desired flow rate depends on the properties of the HTF and the amount of solar radiation per time.</li> <li>• The flow rate should not be constant throughout the hours of the day due to changes in solar radiation.</li> </ul>	(Rehan <i>et al.</i> , 2018)
Solar tracking	Two-axis tracking	The reflector by itself cannot follow the sun, potentially limiting the performance of the PTC. Tracking is made possible with the combination of software and sensors. The dual-axis tracking system was observed to perform ~46.46% better than the fixed surface in terms of efficiency. The tracking process can be incorporated into other forms of solar thermal applications. A photoresistor was used to capture the position of the sun.	<ul style="list-style-type: none"> <li>• Ability to follow the position of the sun can increase the PTC efficiency.</li> <li>• Tracking the sun from east to west and the altitude of the sun in the sky is made possible by the dual-axis tracking mechanism.</li> </ul>	(Bakos, 2006)

Method of improvement	Parameter	Discussion of finding	Remark	Reference
			<ul style="list-style-type: none"> <li>• Light sensor (photoresistors) is required for tracking. The solar cell can also be used in place of a light sensor.</li> </ul>	
	Rotatable axis tracking	<p>The research was based on a solar PTC North-South and rotatable axis tracking. The system was designed in such a way that it can automatically change the collector surface azimuth angle, to reduce the solar incidence angle and thus, reduce the cosine loss.</p> <p>A two-pattern system was adopted: during summer, tracking is done from the North-South axis due to smaller solar incidence angle and in winter, a larger solar incidence angle is observed leading to serious cosine loss. However, the use of rotatable axis tracking will enable more solar radiation to be harvested.</p>	<ul style="list-style-type: none"> <li>• System performance is greatly improved by tracking.</li> <li>• Complete system automation can limit energy losses for a PTC.</li> <li>• Optimal performance is achievable all year round with PTC irrespective of the position and trail of the sun in the sky.</li> </ul>	(Qu <i>et al.</i> , 2017)
Reflector material	Mirror and anodized aluminium	The research study involved the design of a compound parabolic collector. The reflector materials namely mirror and anodized aluminium	<ul style="list-style-type: none"> <li>• System performance depends on the nature and properties of the reflector.</li> </ul>	(Salve <i>et al.</i> , 2018)

Method of improvement	Parameter	Discussion of finding	Remark	Reference
	(MIRO-SUN) reflectors	(MIRO-SUN) were compared. The experiment was conducted for seven days between the hours of 11:00 and 13:00 daily. At a solar radiation intensity of 775 w/m <sup>2</sup> , the surface temperature was 58 °C and 68 °C respectively for the mirror reflector and the anodized aluminium (MIRO-SUN). The desired temperature was achieved at a shorter time for the anodized aluminium reflector due to higher reflectivity and its long life. All these factors contributed to the better performance shown by the anodized aluminium (MIRO-SUN).	<ul style="list-style-type: none"> <li>• The solar radiation intensity influences the working conditions of the PTC.</li> </ul>	
	Stainless steel reflector (SSR) and aluminium mirror reflector (AMR)	The research study focused on testing the thermal and optical performance of SSR and AMR at varying reflector view angles of 35, 40, and 45°. The effect of the reflector material on temperature was equally examined. At the end of the experiment and the simulation, it was reported that the reflector view angle of 45° showed optimal performance based on the angles that were considered. The AMR material	<ul style="list-style-type: none"> <li>• The reflector material view angle contributes to the performance of the system.</li> <li>• The type of reflector material is a major factor for the thermal and optical performance of solar collectors.</li> </ul>	(Imtiaz Hussain <i>et al.</i> , 2017)

Method of improvement	Parameter	Discussion of finding	Remark	Reference
		performed better than the SSR material for the three angular positions that were considered.		
Working fluid	Al <sub>2</sub> O <sub>3</sub> -water nanofluid	Simulation and experimental approaches were used where the error margin was recorded to be <1% for the outlet temperature and about 10-15% for the system efficiency. The receiver was not coated with anti-reflectance and the tube was not evacuated. The wind speed was assumed to 2 m/s and the flow rate was fixed at 0.475 kg/s. The outlet temperature was a function of the inlet and ambient temperature and amount of solar irradiance.	<ul style="list-style-type: none"> <li>• At a constant inlet and ambient temperature, an increase in solar irradiance will lead to an increase in outlet temperature for a PTC.</li> <li>• Nanofluids as HTF influence the performance of solar collectors positively.</li> <li>• The weight percent of nanoparticle in HTF affects the heat transfer rate of the working fluid.</li> </ul>	(Tagle-Salazar <i>et al.</i> , 2018)
	Al <sub>2</sub> O <sub>3</sub> /H <sub>2</sub> O and Fe <sub>2</sub> O <sub>3</sub> /H <sub>2</sub> O nanofluid	Two different nanofluids were considered, varying the particle concentration from 0.20, 0.25 to 0.30%, while the flow rate was equally varied, thus: 0.017, 0.025, and 0.033 kg/s. Al <sub>2</sub> O <sub>3</sub> performed better than Fe <sub>2</sub> O <sub>3</sub> , this was based on the good metallic properties of aluminium	<ul style="list-style-type: none"> <li>• The system performance of a PTC depends on the nature, weight percent, and properties of the nanoparticle in the HTF.</li> </ul>	(Rehan <i>et al.</i> , 2018, Chaudhari <i>et al.</i> , 2015)

Method of improvement	Parameter	Discussion of finding	Remark	Reference
		<p>particle. An increase in particle concentration showed an increase in temperature difference in the absorber tube while an increase in the flow rate led to a decrease in the temperature difference. This was pronounced at a very high flow rate. Based on the result of the research work, the optimum performance was observed when the flow rate was 0.033 kg/s (2 L/min).</p>	<ul style="list-style-type: none"> <li>• High flow affects the temperature difference of the PTC system.</li> <li>• Performance depends on various parameters.</li> </ul>	

Several models have been developed in order to predict the performance of parabolic trough collectors. Some of the models help in terms of cost-saving and the avoidance of trial and error methods, which are often, used when it comes to such designs and performance testing of the system. Error limits for an experiment should be within  $\pm 5\%$  for the model validation to be considered acceptable. If the condition is true, the model can be adopted for other solar collectors operating at different conditions. An example is shown in Lamrani et al. (2018), where the authors employed the numerical model to predict the thermal performance of the PTC system.

## **2.5 Importance of Solar Water Heating Systems**

The major areas of energy consumption in buildings are building-heating, ventilation and air-conditioning (HVAC) systems, lighting sector and major appliances such as freezers and dryers; accounting for 36, 11, and 18% respectively in the United States (DOE, 2014). Most research on energy consumption has mainly focused on these areas. However, recent researches have shown that water heating contributes enormously to the total energy demand for both residential and commercial buildings and this has been underestimated in the past (Pang and O'Neill, 2018).

In the case of South Africa, geyser (water heater) usage is responsible for approximately 40% of the total cost of electricity consumption in most homes (Claire, 2015). With an increasing population coupled with infrastructural development in most parts of the country, electricity utilization increased between 10-12%, especially in major cities like Johannesburg, Pretoria, among others (City of Johannesburg, A.T., 2014). The increasing consumption of fossil fuel-based power generation due to increasing demand will have a ripple effect on the degradation of the environment and adverse effects on the general wellbeing of people. Solar radiation energy is



renewable and readily available throughout the year in South Africa. The most known application of solar technology has been solar water heating (Kalogirou, 2013), which was first commercialized in 1891 (Islam *et al.*, 2013). The radiation of the sun can be utilise to heat water, thereby, aiding a reduction in the demand placed on the national power grid.

Several works have been done in utilizing solar radiation for domestic and commercial purposes (Mauthner and Weiss, 2013, Hossain *et al.*, 2011, Tang *et al.*, 2011, He, 2016). According to the method of solar radiation collection and hot water supply, the SWHSs for residential buildings are categorized into three basic classifications namely: decentralized collection and decentralized supply, centralized collection and decentralized supply, centralized collection, and centralized supply (He, 2016). In a case where the SWHS is for industries or large buildings, the centralized collection and decentralized supply (decentralized storage tank) system are the most applicable. This approach has been developed for high rise buildings in Japan (He, 2016). This method is considered to have the following attributes (He, 2016):

- a) Building integration—The solar collectors are installed in a location with the optimal solar radiation for optimum performance of the SWHS.
- b) Balanced benefits—The entire residents of the building enjoy equal benefits of the installed solar collectors on the rooftop irrespective of the floor they are situated,
- c) Reliability and safety—There is little or no risk attached because the solar collectors are mostly installed on the rooftops of the building instead of the individual installation found on most balconies.

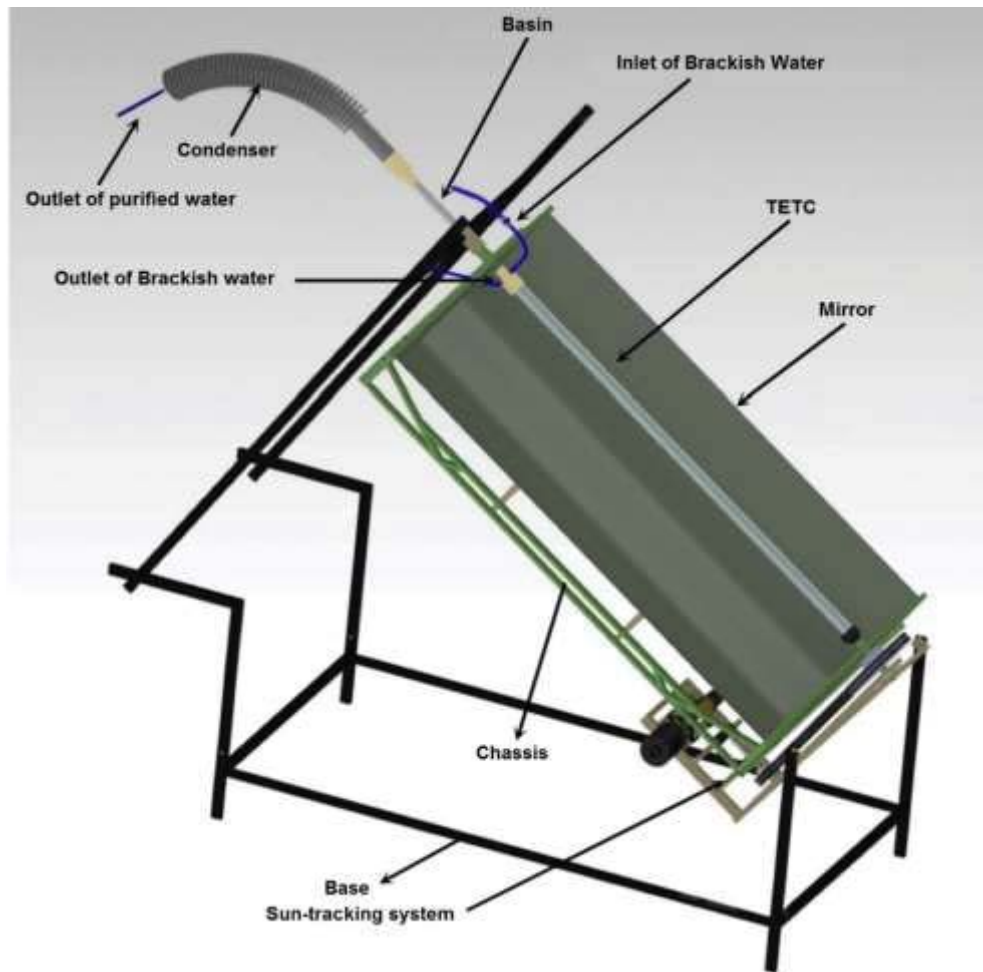
- d) Management convenience—The circulating pumps, solar collectors, and every other necessary equipment is installed on public property (or common property), making it easier to maintain and manage the SWHSs.
- e) Economical—The users will jointly contribute toward the installation and servicing cost for the facility and share the cost of power for the circulating pump.

The efficiency of the SWHS depends on several factors ranging from the type of collector to the geographical location, the intensity of the solar radiation, the material used, mode of design, government policy, etc. In Brazil, well over 300 000 low-income families have benefited from the incorporation of solar water heating systems in their public policies (Giglio and Lamberts, 2016). Furthermore, Giglio and Lamberts reported that the efficiency of the solar heater depends on the occupants of the building. In a study by Gram-Hanssen, it was reported that users having identical houses had varied energy consumption (Gram-Hanssen, 2010). The use of SWHSs by low-income earners can prevent possible system expansion of the country's utility, saving massive cost and also reduce the demand on the national power grid, leading to optimal performance of the facilities (Naspolini and Rüther, 2011). The utility can then transfer the energy saved from low-income consumers to other needy consumers at a higher price.

In a study by Naser and Abaas (2016), it was reported that the efficiency of the SWHSs depends on the water flow rate and the solar radiation intensity. The latter was equally reported by other researchers to affect the overall system performance (Papaeftimiou *et al.*, 2006, Reddy *et al.*, 2008, Zhai *et al.*, 2009). The weather condition is another factor that determines how efficient the system will be in terms of the degree of hotness of the water produced. If the skies are clear (bright and sunny sky), the collector

performs better reaching an optimum temperature but when the sky is cloudy, the performance of the SWHSs is very low. Also, the design of the collector affects operational performance, which has been reported in the literature (Mosleh *et al.*, 2015, Li and Wang, 2006).

The work of Mosleh *et al.* (2015), showed that the linear parabolic trough solar collectors can be utilised for desalination of water (removal of salt from water), which applies the same principle for SWHS as shown in **Figure 2.23**. They further explained that the system efficiency was enhanced by 22.1% when conducting foils made from aluminium was used between the twin-glass evacuated tube collector and the heat pipe to transfer heat to the pipe. The geographical location was reported to have contributed to the number of evacuated tubes or glazed flat plate collectors that may be required for an effective SWHS, while evacuated tubes proved to be more effective. Also, both types of collectors showed good financial and fuel savings, but evacuated tubes performed better with an improved reduction in the CO<sub>2</sub> emission, which is beneficial to the environment (Abd-ur-Rehman and Al-Sulaiman, 2016). The benefit of these collectors is mostly noticed over a long period, especially for a single housing unit with one or two occupant(s).

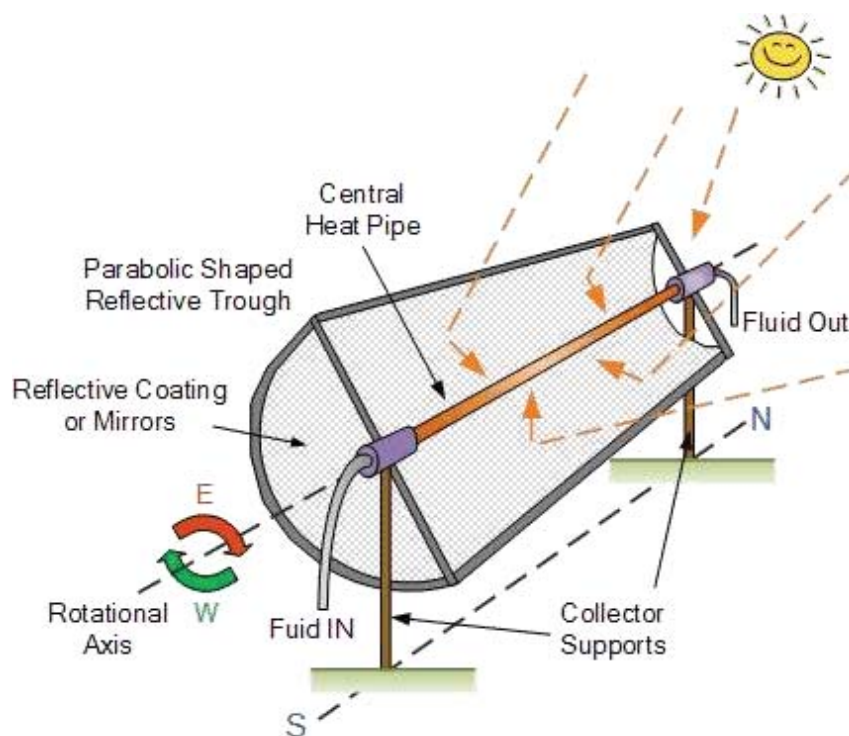


**Figure 2.23:** Schematic diagram of the linear parabolic solar collector. Mosleh *et al.* (2015)

The SWHSs have three major important components namely: the reflective surface (concentrator), the collector and the working fluid. Other important components, which are attached to the SWHSs is the tracking system and storage facility. Gautam *et al.* (2017) classified the solar water heating system components into two, which include the solar collector and the storage tank. Many researchers have conducted numerous studies regarding solar heating and cooling, but there are still drawbacks, which include system performance (solar collector), hot water storage and cost (Rassamakin *et al.*, 2013, Zou *et al.*, 2016, Abd-ur-Rehman and Al-Sulaiman, 2016).

### 2.5.1 Improvement of solar water collector

The performance of the SWHSs can be enhanced in several ways, some of which have been explained by many researchers (Wang *et al.*, 2016, Jebasingh and Herbert, 2016, Shukla *et al.*, 2013). The use of parabolic collectors is one of the ways to increase the thermal performance of the solar collector. The solar radiation from the sun is concentrated at a point for effectiveness, thereby increasing the intensity as shown in **Figure 2.24**. This approach has shown promising outcomes. Li and Wang (2006), explained that attaining solar radiation intensity of  $500 \text{ W/m}^2$  is equivalent to a temperature between  $60$  and  $90^\circ\text{C}$  and further intensity between  $900\text{--}1000 \text{ W/m}^2$  will cause the water to boil (i.e.  $100^\circ\text{C}$ ). The parabolic collector helps to concentrate the several thermal radiations onto a point, leading to the higher intensity required to heat the water and eventually boil the water.



**Figure 2.24:** Schematic diagram of a parabolic solar collector. Adopted from (Alternative\_Energy\_Tutorials)

Another factor, which determines the efficiency of the system, is the mass flow rate (MFR). In an experiment by Li and Wang (2006), it was concluded that if the MFR of water is 0.02 kg/s and the effective solar radiation period is 8 hours, the total mass of water through the solar collector will be approximately 576 kg for each day. The MFR can still be optimised to further improve the system's efficiency. They further verified the trough concentrating performance based on two different evacuated tubes having varying parameters as indicated in their study. The observed effect of increasing and decreasing MFR are presented in **Table 2.9** and **Table 2.10** respectively. The water output temperature through the evacuated tube was observed to decrease from 104 to 39.5 °C as the MFR increased from 0.0046 to 0.032 kg/s. Furthermore, an increase of 0.684 to 0.760 was reported for the heating efficiency, considering the same change in the mass flow rate of the system.

The use of reflectors is another important way of increasing the efficiency of the solar water collector. The reflector increases the solar radiation incident on the surface of the absorber for the SWHSs. The reflector design can be curved or flat, asymmetrical or symmetrical, line-focus or line-axis reflectors. The line-focus can be parabolic, circular, or compound parabolic. The absorbing surface temperature is increased by increasing the ratio of incident thermal energy to heat loss temperatures (Smyth et al., 2006).

**Table 2.9:** Performance evaluation of solar trough concentrating system by using water as working fluid in an evacuated tube with increasing flow rate. Adopted from Li and Wang (2006)

Water flow rate $\dot{m}$ (kg/s)	$c_p$ (kJ/kg °C)	$T_{out}$ (°C)	$T_{in}$ (°C)	Solar intensity $I_b$ (W/m <sup>2</sup> )	Effective receiver area, $A_{eff}$ (m <sup>2</sup> )	Mirror reflectivity $\rho$	Sensible heat increase, $Q$ (kW)	Solar concentrating system efficiency, $\eta$
0.0046	4.186	104	27	1040	2.084	0.910	1.483	0.684
0.008	4.186	75	28	1053	2.084	0.910	1.574	0.717
0.0115	4.186	61	28	1051	2.084	0.910	1.589	0.725
0.0152	4.186	56	31	1062	2.084	0.910	1.591	0.719
0.0189	4.186	51	31	1053	2.084	0.910	1.582	0.721
0.0227	4.186	48	31	1045	2.084	0.910	1.615	0.742
0.0267	4.186	43.5	29	1043	2.084	0.910	1.621	0.746
0.031	4.186	41.5	29	1040	2.084	0.910	1.622	0.748
0.0342	4.186	39.5	28	1040	2.084	0.910	1.646	0.760

**Table 2.10:** Performance evaluation of solar trough concentrating system by using water as working fluid in an evacuated tube with decreasing flow rate. Adopted from Li and Wang (2006)

Water flow	$C_p$	$T_{out}$	$T_{in}$	Solar intensity	Effective receiver	Mirror	Sensible heat	Solar concentrating
rate in (kg/s)	(kJ/kg °C)	(°C)	(°C)	$I_b$ (W/m <sup>2</sup> )	area $A_{eff}$ (m <sup>2</sup> )	reflectivity $\rho$	increase $Q$ (kW)	system efficiency $\eta$
0.0024	1.06	320	26.6	904	2.023	0.91	0.734	0.402
0.0023	1.06	358	27.2	916	2.023	0.91	0.821	0.443
0.0019	1.06	364	27.6	916	2.023	0.91	0.691	0.373
0.0017	1.06	401	29	910	2.023	0.91	0.653	0.355
0.0014	1.06	425	29	946	2.023	0.91	0.593	0.310
0.0012	1.06	463	29	950	2.023	0.91	0.539	0.280



## 2.6 Hailstones Damages as a Result of Heavy Rainfall

Hailstones are associated with thunderstorms and are a destructive phenomenon that is common in many parts of the world. The hailstone phenomenon occurs more frequently than the records of tornadoes reported (Allen *et al.*, 2020). Hailstone is known to be produced by all forms of deep convective storms that occur generally for a short period in most places globally. Hailstorms have also been listed as natural disasters according to Sun *et al.* (2015). Hailstones do many damages to buildings and other properties as shown in **Figure 2.25**. Property owners often give an account of the magnitude of damages inflicted on their properties, building roof coverings and facades, causing ingress of water into the buildings (Paterson and Sankaran, 1994). These damages could be in the form of breakages, indentations, or cracks into the surface of the roofing materials, windows and panelling of buildings, vehicle windows and panelling. Hailstones also damage farms and crops (Brown *et al.*, 2015). The level of damage is a result of the force generated due to the drop height of the hailstone.

### 2.6.1 Hailstones damages in South Africa

In a report by the *Express News*, the account of Mr. Kevin Pieterse—a former cricketer player, was shared on how he found hailstones shockingly as huge as the size of a Tennis ball (Mowat, 2017). This incident happened when a heavy storm hit the City of Durban in South Africa. **Figure 2.26** shows the pictorial comparison of hailstones with a Tennis ball. In 2013, heavy downpour and hail were reported in most parts of Pretoria in South Africa where mostly windows, panelling and roofs of houses, vehicle windscreens and other properties were damaged. The estimate of the damage was in millions of South African rand. The worst-hit areas were Ga-Rankuwa, Hammanskraal, Karen Park, Nellmapius, Orchards, Soshanguve and some suburbs such as Mamelodi in the east of the city (IOL\_News, 2013).

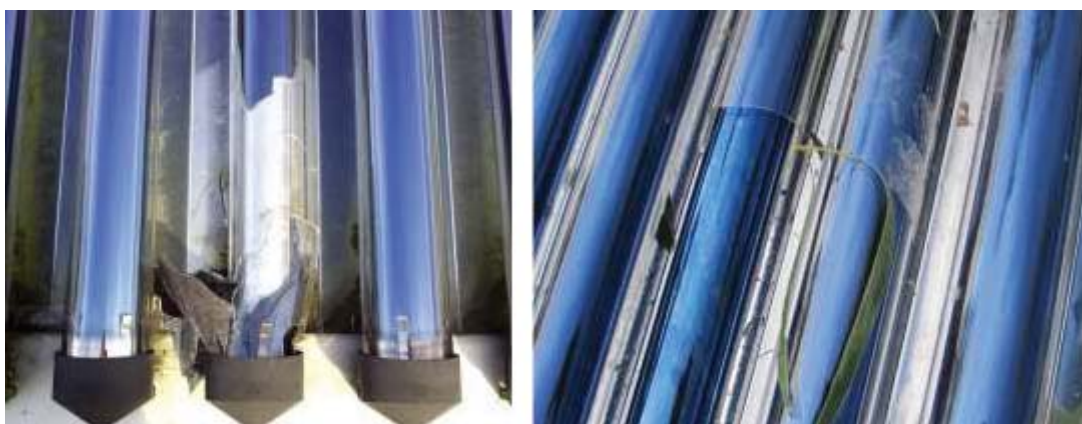


**Figure 2.25:** Photo of buildings and cars damaged due to hailstones. Adopted from (<https://stormandsky.com>); Lynch (2014)



**Figure 2.26:** Photo of hailstones as big as a tennis ball. Adopted from Mowat (2017)

Mr. Jacob Mamabolo who was the MEC at the time, the Gauteng Department of Human Settlements and Cooperative Governance and Traditional Affairs jointly visited the areas that were damaged by the hailstorm in the City of Tshwane. Approximately 71 000 houses were damaged by the hailstorm and almost 29 000 were seriously damaged ([www.gov.za](http://www.gov.za), 2014). Evacuated glass tubes were also damaged during the hailstorm as shown in **Figure 2.27**. Evacuated tubes are made with glass and they are for solar water heating. Direct exposure to hailstones could result in potential damage to the glass, rendering the evacuated glass tubes useless. Hence, the need to protect the evacuated glass tube, which is one of the reasons for the research study.



**Figure 2.27:** Damages caused by hailstones to evacuated glass tubes. Adopted from (*SolarHotWaterParts*) and ([www.solarrepairs.co.uk/](http://www.solarrepairs.co.uk/))

## **2.7 Sun Chaser**

The intensity of solar radiation can be fully utilised by tracking the maximum peak power for each day. Mosleh et al. (2015) explained that proper orientation is crucial for a solar collector to prevent shaded zones, and this can be accomplished through a comprehensive/thorough identification of the sun's trail in the sky. To achieve all these, the following parameters must be known: the tilt angle of the collector, the latitude of the location, incident angle, declination angle and the acceptance angle of the system. The current research seeks to optimize the existing maximum power point tracker (MPPT) for efficient solar water heating using a parabolic trough collector.

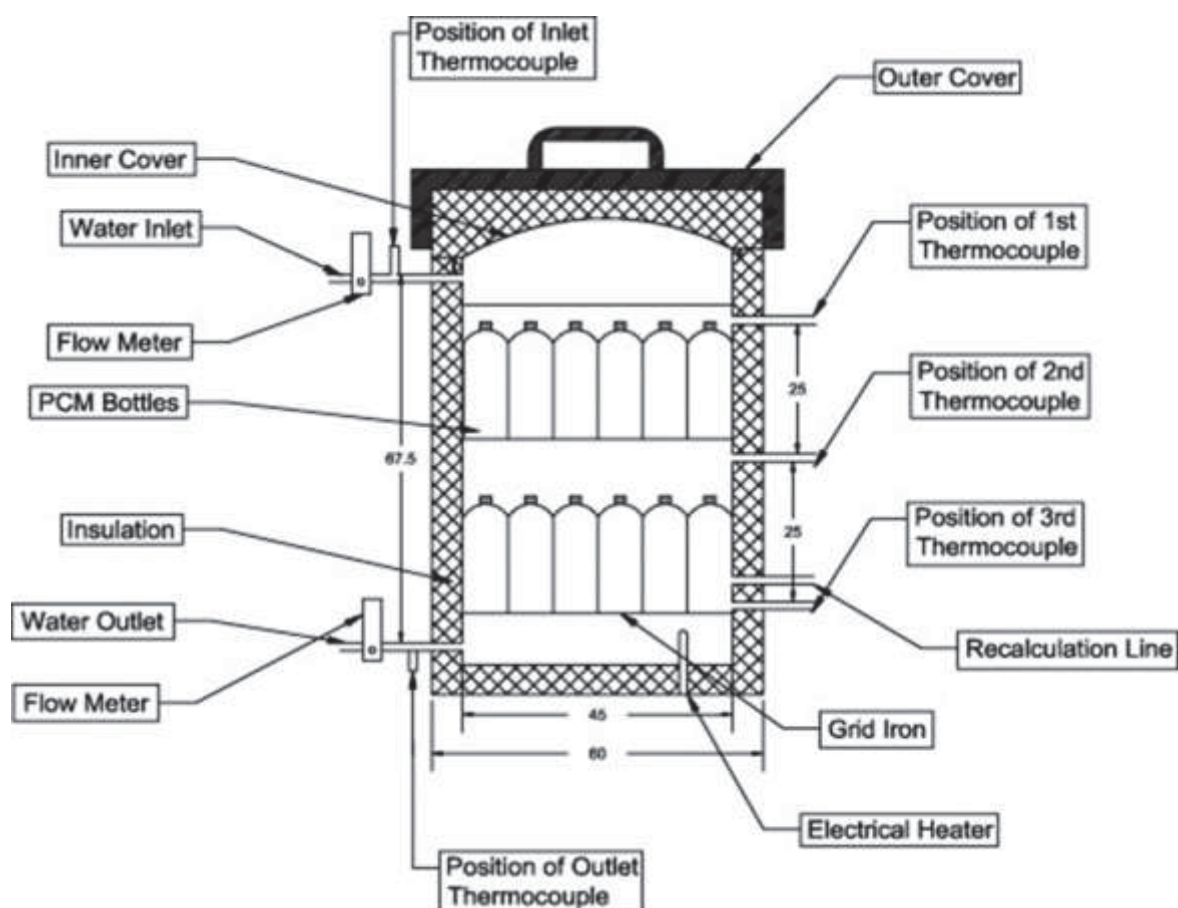
## **2.8 Hot Water Storage Tank**

The storage tank is an important aspect when it comes to solar water heating systems. The tank is either, incorporated or located separately from the SWH collector and it is used to store the water that was heated using the harnessed solar radiation of the sun. The choice of materials used plays a vital role in the effectiveness of the storage tank. The storage tank comprises of an inner part, which has low thermal conductivity to prevent heat loss by conduction, the insulated portion between the inner and the outer compartment of the storage tank and the external portion, which helps to mitigate heat loss. The design and specification of the tank may vary from country to country depending on the local climate, market demand, local regulations and/or manufactural norms.

Several studies (Smyth *et al.*, 2005, Burns *et al.*, 1985), have been conducted on the choice of shape design for the storage tank. Among the two major designs (rectangular and cylindrical), the cylindrical tank showed an increased heat transfer rate (Kaushik *et al.*, 1994, Gautam *et al.*, 2017). Hot water storage tank (HWST) can be made from materials such as plastic, concrete, steel, glass fibre and other suitable materials with

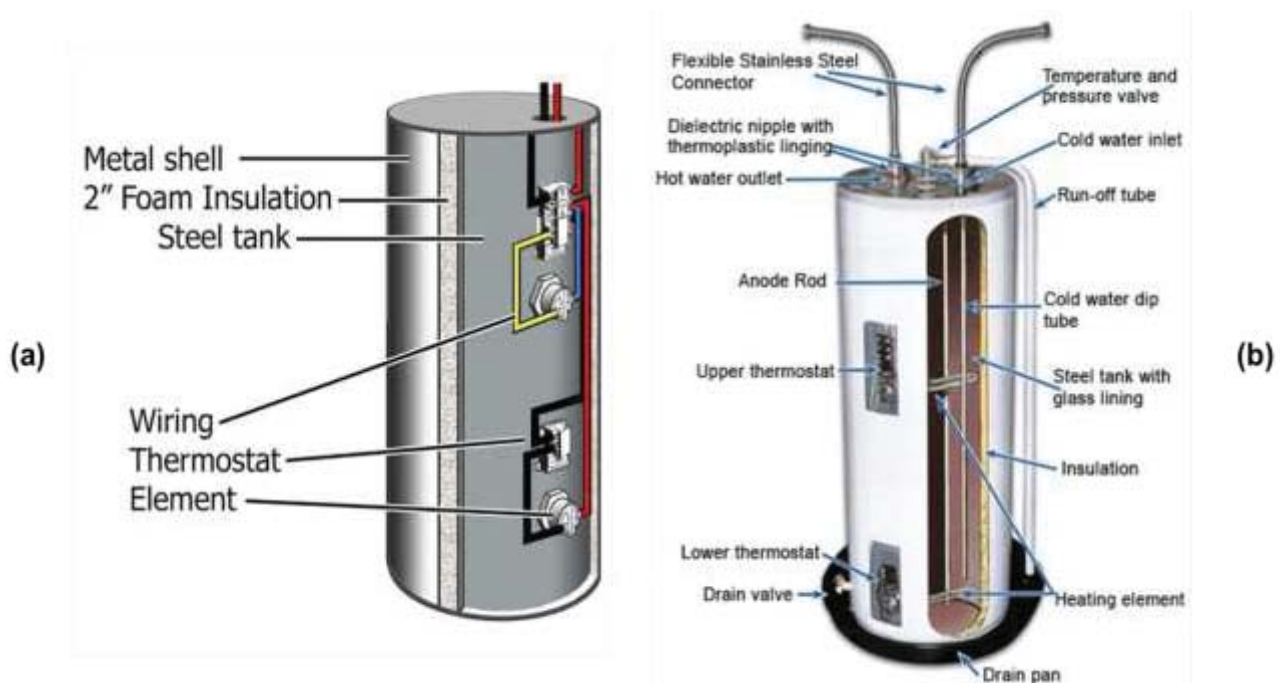


the potential to store heat (Gautam *et al.*, 2017). The major problems of storage tanks arise from heat loss due to the mixing of inlet cold fluid and hot fluid. One way to reduce heat loss is by a process known as stratification, which was reported by Rhee *et al.* (2010) and Devore *et al.* (2013). In separate research, the use of phase change material (PCM) was reported by Al-Hinti *et al.* (2010). The PCM was paraffin wax, which was placed inside small cylindrical aluminium containers as shown in



**Figure 2.28:** Schematic cross-sectional view of a hot water storage tank with PCM containers insert. Adopted from Al-Hinti *et al.* (2010)

The conventional hot water storage tank inners are often made from steel or steel with glass lining as shown in **Figure 2.29**. The storage tanks with direct steel inner are prone to rust and leakages, hence, the need for alternative materials. Weight is another factor limiting both the steel- and steel with glass lining-based hot water storage tanks. The weight is due to the tank been made from steel, which is a heavy material. Conventional tanks comprise of three major layers, which are the inner layer (steel or steel with glass lining), insulation layer and an outer layer (metal shell). This can be modified for better performance.



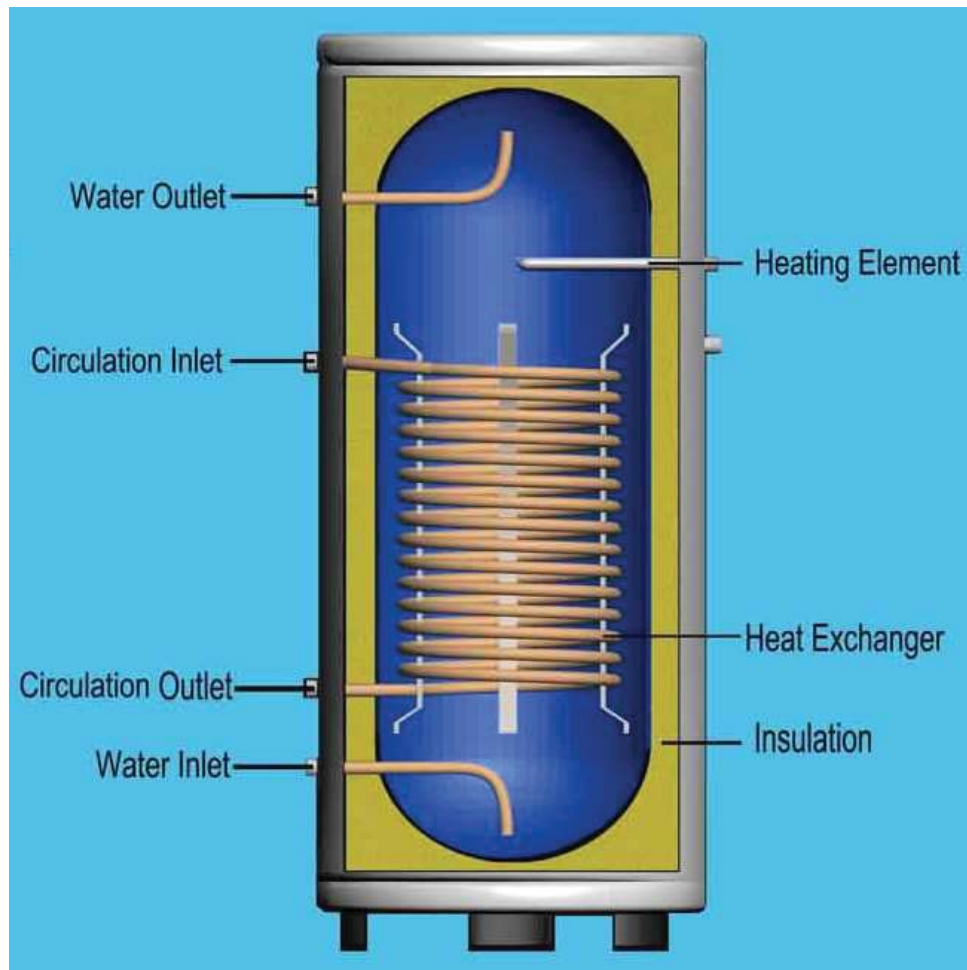
**Figure 2.29:** Conventional hot water storage tank showing the cross-sectional layers: (a) steel tank and (b) steel tank with glass lining. Adopted from ([Waterheatertimer.org](http://Waterheatertimer.org), [PlumbingSupply.com](http://PlumbingSupply.com))

Other possible ways to enhance the performance of the HWST will be by using insulating materials with low-heat transfer rate and/or introducing heat storage materials that can store the heat energy and then release it later when it is needed. The latter method is already being used in human body therapy for pain relief (SoWell, 2018) and it involves the use of salt. The salt is usually heated up in an oven at a

temperature of 175 °C for 10-15 minutes and then placed on the portion where the pain is felt. This technology can be adopted by incorporating salt bags between the layers of the hot water storage tank due to the ability of salt to store heat energy for later usage.

## 2.9 Insulation

Insulating the hot water storage tank is a highly significant factor to ensure effective retention of the temperature of the water and to avoid heat loss to the surrounding environment through conduction and convection. The rate of heat loss depends on the kind of materials used for the tank and the insulated portion. The effect of insulating the storage tank was not considered important by the early Japanese and US solar water heater manufacturers (Smyth *et al.*, 2006). It was further explained by Smyth *et al.* (2006), that Baer was the first to investigate the effect of insulation on the performance of the SWH storage tank by changing the insulator thickness, which was achieved through a series of experiments. The modifications made on the storage tank resulted in a higher percentage of heat retained. This was a significant improvement for the solar water heater manufacturers. Several modifications have since, been made to further improve on the existing technologies. Heating elements have been incorporated into the storage tank to complement for the periods in which the available solar radiation is insufficient to heat the water, especially during winter or cloudy weather. **Figure 2.30** shows a typical example of an insulated storage tank with an optional heating element and heat exchanger.



**Figure 2.30:** Schematic diagram of a hot water storage tank with heat exchanger and heating element. Adapted from Commonpraise (2017)

## 2.10 Conclusion

The depletion of fossil fuel and environmental concerns have led researchers to, deeply engage in studies that are focused on other sources of energy generation and utilisation. Renewable and sustainable energy have shown great merit, of which solar energy is among the leading forms of energy, which have been greatly researched on. The energy of the sun has been harnessed for various applications such as solar panels, steam boilers, solar water heating, etc. The emphasis of this study is on solar water heating systems (SWHSs). The efficiency of the SWHSs depends on numerous factors such as the choice of material, ability to track the sun path, solar collector design, fluid flow rate and hot water storage tank. Despite the achievement so far,



there are still needs for improvement. Hence, more researches lean towards this area (solar energy). The rapid population growth and the environmental issues surrounding CO<sub>2</sub> emission is also one of the major contributing factors to seeking alternative renewable and sustainable energy. In this case, the SWHS is being considered because it is eco-friendly and readily available. In addition, damages caused by hailstones to evacuated glass tubes is another reason for the research. Heavy rainfall with hail often wreaks major havoc to buildings and cars, as well as glass tubes. Evacuated glass tubes are used to harness solar energy for water heating and electric power generation. Therefore, the proposed research seeks to optimise the existing solar collectors and maximum power point tracker (MPPT) for efficient solar water heating using a parabolic trough collector. In addition, a new and improved hot water storage tank (layered composite materials) is proposed.

## CHAPTER THREE

### 3.0 MODELLING AND SIMULATION

#### 3.1 Introduction

The chapter presents the modelling and simulation aspect of the research. The entire system was simulated with due consideration for all fixed and changing variables. The chapter also presents relevant mathematical equations for the system. The system was subdivided into three parts namely the collector, the absorber and the storage tank. The amount of solar radiation reaching the collector surface was evaluated. Similarly, the quantity of heat energy received by the absorber pipe, which was then, transferred to the fluid in the pipe was evaluated. The temperature/heat energy of the fluid exiting the absorber pipe to the storage tank was evaluated. Lastly, the water storage tank temperature was model, by so doing, the overall system behaviour was analysed for effectiveness and performance.

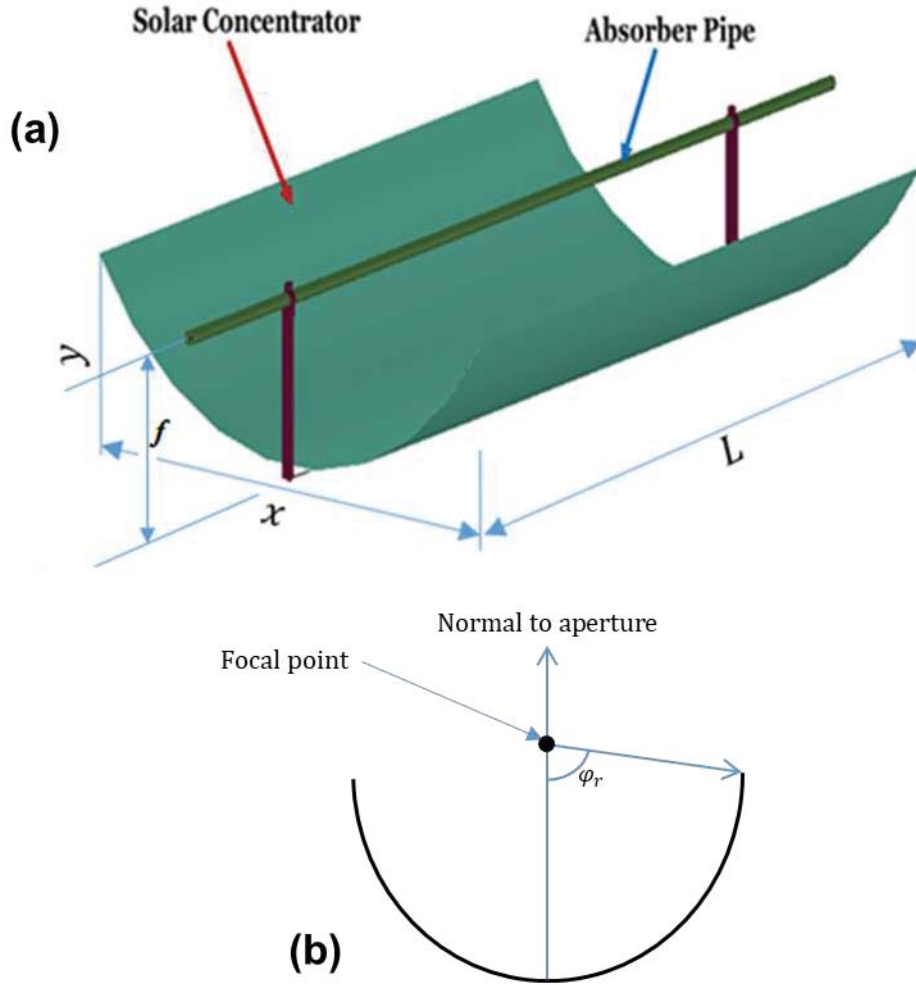
#### 3.2 Mathematical Modelling of Parabolic Trough Solar Collector Geometry

The geometry of the parabolic trough solar collector (PTSC) plays a significant role in achieving optimum performance of the system. Therefore, careful attention was taken to ensure the geometry is perfect. The PTSC shape was determined using Equation 3.1 and the schematic diagram is shown in **Figure 3.1**.

$$y = \frac{x^2}{4*f} \quad (3.1)$$

Where  $y$  the height of the parabola,  $f$  is the focal distance and  $x$  is the aperture width. Therefore, the rim angle ( $\varphi_r$ ) can be evaluated using Equation 3.2.

$$\varphi_r = \arctan \left[ \frac{8 \frac{f}{x}}{16 * \left( \frac{f}{x} \right)^2 - 1} \right] \quad (3.2)$$



**Figure 3.1:** Schematic design of: (a) a parabolic trough solar collector and (b) rim angle evaluation

The overall collector aperture area ( $A_a$ ) was calculated by finding the product of the collector length ( $L$ ) and the width ( $x$ ) as shown in Equation 3.3.

$$A_a = L * x \quad (3.3)$$

Concentration ratio ( $C$ ) of the geometry is defined as the ratio of the collector aperture area to the absorber area ( $A_{ao}$ ) (that is the outer area of the absorber tube).

$$C = \frac{A_a}{A_{ao}} \quad (3.4)$$

The absorber outer surface area can be computed using the absorber outer diameter and the length of the glass-evacuated tube. The same formula can be used to determine the absorber inner area, in this case, the inner diameter of the absorber will be used for computation.

$$A_{ao} = \pi D_{ao} * L \quad (3.5)$$

Where,  $A_{ao}$  is the absorber total surface area,  $D_{ao}$  is the absorber outer diameter and  $L$  is the length of the evacuated tube.

### 3.3 Heat Production, Transferred and Losses by the PTSC to the Glass Cover

The quantity of PTSC's useful heat production is a function of the specific heat capacity of the fluid, the beam solar irradiation and the aperture surface area. The heat production can be calculated by using the energy balance on the fluid volume as shown in Equation 3.6 (Bellos and Tzivanidis, 2019).

$$\dot{Q}_c = \dot{m} * c_p * (T_{out} - T_{in}) \quad (3.6)$$

Where  $\dot{Q}_c$  is the rate of heat flow,  $\dot{m}$  is the mass flow rate of the fluid,  $c_p$  is the specific heat of the fluid,  $T_{in}$  and  $T_{out}$  are respectively the inlet and outlet temperature of the absorber.

An alternative method for determining  $\dot{Q}_c$  is shown in Equation 3.7 provided the heat transfer coefficient ( $h$ ), absorber outer area ( $A_{ao}$ ), absorber external diameter ( $D_{ai}$ ), thermal conductivity ( $k$ ) and absorber temperature ( $T_a$ ) are known, given the Nusselt number ( $Nu$ ).

$$\dot{Q}_c = A_{ao} * h * (T_a - T_{fm}) \quad (3.7)$$

$$h = \frac{Nu * k}{D_{ai}} \quad (3.8)$$

$$T_{fm} = \frac{T_{in} - T_{out}}{2} \quad (3.9)$$

The available solar irradiation ( $\dot{Q}_s$ ) received on the collector aperture can be calculated by evaluating the product of the direct beam irradiation ( $G_b$ ) and the outer aperture ( $A_a$ ) of the collector.

$$\dot{Q}_s = A_a * G_b \quad (3.10)$$

Based on the output of Equations 3.6, 3.7 and 3.10, the solar collector thermal efficiency can be calculated by computing the ratio of the useful heat production and the available direct solar beam irradiation as shown in Equation 3.11.

$$\eta_{th} = \frac{Q_c}{Q_s} \quad (3.11)$$

The thermal efficiency of the solar collector is affected due to thermal losses. These losses can be evaluated by using Equation 3.12. The evaluation can be achieved by using the mean absorber temperature ( $T_{ao}$ ), thermal loss coefficient ( $U_L$ ) and absorber outer surface area ( $A_{ao}$ ).

$$\dot{Q}_{loss} = A_{ao} * U_L * (T_{ao} - T_{am}) \quad (3.12)$$

Where,  $T_{am}$  is the ambient temperature.

Other thermal losses are from the absorber pipe to the glass cover. These are essentially the thermal radiation and convection losses from the absorber pipe to the glass cover. This observation was reported by Bellos *et al.* (2018).

$$\dot{Q}_{loss}^a = \left\{ A_{ao} * \sigma * \frac{T_{ao}^4 - T_{gi}^4}{\frac{1}{\varepsilon_{ao}} + \frac{1 - \varepsilon_{gi}}{\varepsilon_{gi}} * \frac{A_{ai}}{A_{go}}} \right\} + \{ A_{go} * h_{in} * (T_{gi} - T_{am}) \} \quad (3.13)$$

For the case of an evacuated tube, convection thermal losses do not exist. This is because the inner heat transfer coefficient ( $h_{in}$ ) is zero, then Equation 3.13 can be reduced to Equation 3.14.

$$\dot{Q}_{loss}^a = A_{ao} * \sigma * \frac{T_{ao}^4 - T_{gi}^4}{\frac{1}{\varepsilon_{ao}} + \frac{1 - \varepsilon_{gi}}{\varepsilon_{gi}} * \frac{A_{ai}}{A_{go}}} \quad (3.14)$$

When the system is not an evacuated tube, the inner heat transfer coefficient ( $h_{in}$ ) has a value which can be evaluated by using the following Equations 3.15–3.18, according to Raithby and Hollands (1975).

$$h_{in} = \frac{2 * k_{eff}}{D_{ao} * \ln \frac{D_{go}}{D_{ao}}} \quad (3.15)$$

The effective thermal conductivity,  $k_{eff}$  can be evaluated by using Equation 3.16. Where  $Pr$  is the Prandtl number,  $Ra$  is Rayleigh number,  $k_{air}$  is the thermal conductivity of air existing between the absorber and the glass cover.

$$k_{eff} = k_{air} * 0.386 * \left( \frac{Pr_{air}}{Pr_{air} + 0.861} \right)^{0.25} * F_g^{0.25} * Ra_{air}^{0.25} \quad (3.16)$$

According to Raithby and Hollands (1975), the geometric parameter,  $F_g$  can be evaluated using Equation 3.17.

$$F_g = \frac{[\ln(D_{gi}) - \ln(D_{ao})]^4}{\left( \frac{D_{gi} + D_{ao}}{2} \right)^3 * (D_{gi}^{-0.6} + D_{ao}^{-0.6})^5} \quad (3.17)$$

According to a study by Forristall (2003), the emittance of the cermet coating can be evaluated by Equation 3.18.

$$\varepsilon_r = 0.06282 + 10208 * 10^{-4} * T_a + 1.907 * 10^{-7} * T_a^2 \quad (3.18)$$

Where  $\sigma$  is the Stefan-Boltzmann constant (equivalent to  $5.67 * 10^{-8} W/m^2 K^4$ ),  $\varepsilon_{ao}$  and  $\varepsilon_{gi}$  respectively are the absorber emittance and the cover emittance for the materials,  $D_{ao}$  and  $D_{gi}$  respectively are the diameters of the absorber outer surface and the glass cover inner,  $T_{ao}$  and  $T_{gi}$  are the temperature of the absorber outer surface and the glass cover inner.

### 3.4 Heat Losses from the Glass Cover to the Environment

The thermal losses from the absorber pipe to the glass cover is the same with the amount of heat loss from the glass cover to the environment provided the system is in a steady-state condition. Equations 3.19–3.21 show the mathematical evaluations for determining heat losses to the environment. The units of the temperatures are in Kelvin. The coefficient of heat transfer ( $h_{out}$ ) from the glass cover to the ambient is shown in Equation 3.21 as explained by Qiu *et al.* (2017).

$$\dot{Q}_{loss} = \{A_{go} * \sigma * \varepsilon_{gi} * (T_{gi} - T_{sky})\} + \{A_{go} * h_{out} * (T_{gi} - T_{am})\} \quad (3.19)$$

$$T_{sky} = 0.0553 * T_{am}^{1.5} \quad (3.20)$$

$$h_{out} = 4 * V_{wind}^{0.58} * D_{go}^{-0.48} \quad (3.21)$$

Where  $V$  is the velocity of wind,  $T_{am}$  is the ambient temperature and  $T_{sky}$  is the sky temperature.

### 3.5 Effective Solar Energy Absorbed

Determining the energy balance is the most important aspect of the research. One of the most significant equations for modelling the system performance is the solar energy absorbed ( $\dot{Q}_{abs}$ ) as a function of the useful heat and the system thermal losses.

$$\dot{Q}_{abs} = \dot{Q}_{loss} + \dot{Q}_u \quad (3.22)$$

In a situation where the optical efficiency ( $\eta_{opt}$ ) is known, alongside with the available solar radiation energy on the collector aperture, the  $\dot{Q}_{abs}$  can be calculated as shown in Equation 3.23.

$$\dot{Q}_{abs} = \eta_{opt} \dot{Q}_s \quad (3.23)$$

### 3.6 Solar Absorber Tube (Amount of Heat Transferred to the Fluid and Heat Loss)

#### 3.6.1 Heat transfer by convection from the receiver pipe internal wall to the heat transfer fluid (HTF)

According to Newton's law of cooling, the convection heat transfer from the surface of the internal absorber tube to the heat transfer fluid is given by  $hA(T_{sky} - T_\infty)$ .

$$\dot{Q}_{conv,f-ai} = \pi h_f D_{ai} (T_{ai} - T_f) \quad (3.24)$$

$$h_f = Nu_f \frac{k_f}{D_{ai}} \quad (3.25)$$

$$Nu_f = \frac{\frac{f_{ai}}{8(Re_f - 1000)Pr_f}}{1 + 12.7 \sqrt{\frac{f_{ai}}{8}} (Pr_f^{2/3} - 1)} \left( \frac{Pr_f}{Pr_{ai}} \right) \quad (3.26)$$

$$f_{ai} = [1.82 \log(Re_f) - 1.65]^{-2} \quad (3.27)$$



where,  $h_f$  is the convection heat transfer coefficient at the pipe internal diameter,  $D_{ai}$  is the diameter of the absorber inner in mm,  $T_{ai}$  and  $T_f$  are the temperature of the absorber inner and the HTF respectively in °C,  $Nu_f$  is the Nusselt number of working fluid in the absorber,  $k_f$  is the thermal conductivity of the working fluid,  $f_{ai}$  is the frictional factor for the inner surface of the absorber pipe,  $Re_f$  is the Reynolds number of the working fluid,  $Pr_f$  is the Prandtl number based on the working fluid temperature,  $Pr_{ai}$  is the Prandtl number based on the absorber inner surface temperature.

### 3.6.2 Heat transfer by conduction through the absorber pipe

The heat transferred by conduction from the absorber pipe inner to outer can be evaluated as follows:

$$\dot{Q}_{cond,ai-ao} = \frac{2\pi k_a(T_{ai} - T_{ao})}{\ln\left(\frac{D_{ao}}{D_{ai}}\right)} \quad (3.28)$$

Where  $D_{ai}$  and  $D_{ao}$  are the diameter of the absorber inner and absorber outer respectively in mm.  $T_{ai}$  and  $T_{ao}$  are the temperature of the absorber inner and absorber outer respectively °C.  $k_a$  is the thermal conductivity of the absorber pipe  $[(T_{ai} + T_{ao})/2]$  in W/m °C.

## 3.7 Heat Transfer from the Absorber to the Glass Cover

### 3.7.1 Heat transfer by convection

During heat transfer via convection from the absorber pipe to the glass envelope, there are two mechanisms of heat transfer that can be considered, namely: free-molecular and natural convection (Kalogirou, 2012). The mechanisms are dependent on the annulus pressure, which can be examined in two different ways:

- i. **Vacuum in annulus:** The convection heat transfer between the absorber pipe and the glass cover will occur by free-molecular convection. When the annulus region is under vacuum, the annulus pressure will be reduced (pressure <0.013 Pa). The expression was presented by (Kalogirou, 2012, Lu *et al.*, 2013, Cheng *et al.*, 2015, Ratzel *et al.*, 1979).

$$\dot{Q}_{conv,ao-gi} = \pi h_{ao-gi} D_{ao} (T_{ao} - T_{gi}) \quad (3.29)$$

$$h_{ao-gi} = \frac{k_{an}}{\frac{D_{ao}}{2 \ln \left( \frac{D_{gi}}{D_{ao}} \right)} + b \lambda \left( \frac{D_{ao}}{D_{gi}} + 1 \right)} \quad (3.30)$$

$$b = \frac{(2-a)(9\gamma-5)}{2a(\gamma+1)} \quad (3.31)$$

$$\lambda = \frac{2.331 \times 10^{-20} (T_{ao-gi} + 273)}{(P_{an} \delta^2)} \quad (3.32)$$

where  $h_{ao-gi}$  is the convection heat transfer coefficient,  $T_{ao}$  and  $T_{gi}$  are the temperature of the absorber outer and glass cover inner respectively in °C,  $T_{ao-gi}$  is the average temperature of the annular gas °C,  $D_{ao}$  and  $D_{gi}$  in mm are the diameter of the absorber outer and glass cover inner respectively,  $k_{an}$  is the thermal conductivity of the annulus gas at standard temperature and pressure,  $b$  is the interaction coefficient = 1.571 according to Marshal (1976),  $\gamma$  is the ratio of specific heat for the annular gas = 1.39 according to Marshal (1976),  $a$  is the accommodation coefficient,  $P_{an}$  is the annular gas pressure, and  $\delta$  is the molecular diameter of the annular gas. According to Marshal (1976),  $\delta$  is  $3.55 \times 10^{-8}$  cm.

- ii. **Pressure in annulus:** The convection heat transfer between the absorber pipe and the glass cover will occur by natural convection when the absorber annulus region loses its vacuum or when the absorber is partially or filled with ambient

air, the annulus pressure will increase (pressure >0.013 Pa). The expression is represented by (Cengel, 2006, Kalogirou, 2012, Silva et al., 2013).

$$\dot{Q}_{conv,ao-gi} = \frac{2\pi k_{eff}}{\ln\left(\frac{D_{gi}}{D_{ao}}\right)} (T_{gi} - T_{ao}) \quad (3.33)$$

### 3.8 Heat Transfer from the Glass Cover to the Environment

#### 3.8.1 Heat transfer by convection

The heat transfer by convection is determined by knowing the Nusselt number, which is dependent on whether the heat transfer convection is, forced (wind influence) or natural (no wind). When there is the influence of wind, the heat transfer convection from the glass cover to the environment/sky presents a larger heat loss. Newton's law of cooling can be used for estimation.

$$\dot{Q}_{conv,go-s} = \pi h_{go-s} D_{go} (T_{go} - T_{am}) \quad (3.34)$$

$$h_{go-s} = \frac{k_{air}}{D_{go}} Nu_{D_{go}} \quad (3.35)$$

Where  $h_{go-s}$  is the convection heat transfer coefficient for ambient air at  $(T_{go} - T_{am})/2$ ,  $D_{go}$  is the outer diameter of the glass cover,  $Nu_{D_{go}}$  is the average Nusselt number based on the glass cover outer diameter,  $T_{go}$  and  $T_{am}$  are the temperatures of the glass cover outer and the sky in °C.

The glass cover can either be subjected to wind disturbance or no wind at all. This affects the convection heat transfer from the glass cover to the environment. These conditions will determine how the Nusselt number is evaluated.

- i. **No wind:** Whenever there is no influence by wind, the heat transfer convection from the glass cover to the sky/environment will occur naturally (i.e. natural

convection). The Nusselt number is then estimated or computed using the correlation established/developed by Churchill and Chu (Cengel, 2006).

$$Nu_{D_{go}} = \left[ 0.06 + \frac{0.387 Ra_{D_{go}}^{1/6}}{\left[ 1 + \left( 0.559 / Pr_{go-s} \right)^{9/16} \right]^{8/27}} \right]^2 \quad (3.36)$$

$$10^5 < Ra_{D_{go-s}} < 10^{12}$$

$$Ra_{D_{go}} = \frac{g\beta(T_{go} - T_s)D_{go}^3}{v_{go-s}^2} Pr_{go-s} \quad (3.37)$$

$$\beta = \frac{1}{T_{go-s}} \quad (3.38)$$

$$Pr_{go-s} = \frac{v_{go-s}}{\mu_{go-a}} \quad (3.39)$$

Where  $Ra_{D_{go}}$  is the Rayleigh number for air which is based on the glass cover outer diameter,  $D_{go}$  is the outer diameter of the glass cover,  $Pr_{go-s}$  is the Prandtl number for air at  $T_{go-s}$ ,  $v_{go-s}$  is the air kinematic viscosity at  $T_{go-s}$  and  $\mu_{go-a}$  is the air thermal diffusivity at  $T_{go-s}$ .

- ii. **Wind:** Whenever there is wind influence, the heat transfer convection from the glass cover to the environment/sky will occur by forced convection. The Nusselt number is then computed using the correlation developed by Zhukauskas for external forced convection flow (Bergman *et al.*, 2011). The properties of all fluids are evaluated at the sky temperature ( $T_{sky}$ ), except for  $Pr_{go}$ , which is evaluated at the outer surface wall temperature of the glass cover.

$$Nu_{D_{go}} = C Re_{D_{go}}^m Pr_s^n \left( \frac{Pr_s}{Pr_{go}} \right)^{\frac{1}{4}} \quad (3.40)$$

$$0.7 < Pr_s < 500$$

$$1 < Re_{D_{go}} < 10^6$$

Where  $Re$  is the Raynolds number based on the glass cover outer diameter,  $n$  is a constant (equal to 0.37 when  $Pr_s \leq 10$  and equal to 0.36 when  $Pr_s > 10$ ),  $C$  and  $m$  are both constants. These respective values, in correlation with the Reynolds number, are shown in **Table 3.1**.

**Table 3.1:** Constant for computing Nusselt number with wind influence (Kalogirou, 2012)

Reynolds number	$C$	$m$
1–40	0.75	0.4
40–1000	0.51	0.5
1000–200000	0.26	0.6
200000–1000000	0.076	0.7

### 3.8.2 Heat transfer by radiation

The radiation heat transfer from the glass cover to the environment/sky can be evaluated as follows:

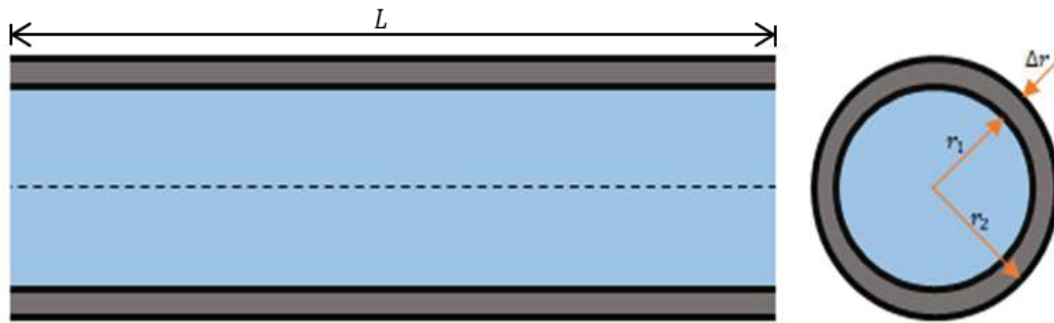
$$\dot{Q}_{rad,go-s} = \pi \sigma D_{ao} (T_{go}^4 - T_{sky}^4) \quad (3.41)$$

$$T_{sky} = 0.0552 * T_{am}^{1.5} \quad (3.42)$$

where,  $T_s$  is the effective temperature of the sky.

### 3.9 Heat Exchanger Chamber (Heat Transfer Rate and Amount of Heat Transferred)

In a cylindrical geometry, the steady temperature profile is logarithmic in the radial coordinate under a similar situation. Below is a model of steady conduction for radial direction through a pipe wall that is cylindrical when the outer and inner surfaces are kept at two different temperatures. **Figure 3.2** shows the schematic diagram of a cylindrical pipe.



**Figure 3.2:** Schematic diagram of the heat exchanger pipe

Area of a cylinder,  $A = 2\pi rL$ , where  $L$  is the total length of the cylindrical pipe. Heat flow rate,  $\dot{Q}$  can be evaluated when the cylinder area,  $A$  and the heat flux in the radial direction are known.

$$\dot{Q} = q_r A \quad (3.43)$$

From the Fourier's Law,

$$q_r = -k \frac{dT}{dr} \quad (3.44)$$

$$\therefore \dot{Q} = -2\pi rLk \frac{dT}{dr} \quad (3.45)$$

Where  $2\pi rLk$  is a constant, the temperature distribution resulted in a linear differential equation.

$$r \frac{dT}{dr} = C_1 \quad (3.46)$$

Where  $C_1$  is a constant.

$$\frac{dT}{dr} = \frac{C_1}{r} \quad (3.47)$$

$$dT = \frac{C_1}{r} dr \quad (3.48)$$

By integrating both sides, this gives the temperature profile.

$$T = C_1 \ln r + C_2 \quad (3.49)$$

where,  $C_2$  is another constant of integration. In order to determine both constants, the boundary conditions for the temperature distribution, that is, the temperature at the outer and inner wall of the pipe surfaces must be evaluated.

$$T(r_1) = T_1$$

$$T(r_2) = T_2$$

Substituting, the boundary conditions will give two separate equations that can be used to determine  $C_1$  and  $C_2$ .

$$T_1 = C_1 \ln r_1 + C_2 \quad (3.50)$$

$$T_2 = C_1 \ln r_2 + C_2 \quad (3.51)$$

Solving the two linear equation will help solve the values for  $C_1$  and  $C_2$ .

$$C_1 = \frac{T_1 - T_2}{\ln(r_1/r_2)} \quad (3.52)$$

$$C_2 = T_1 - \left[ \frac{T_1 - T_2}{\ln(r_1/r_2)} \right] * \ln r_1 \quad (3.53)$$

By substituting the expression for  $C_1$  and  $C_2$  in the temperature profile, the temperature distribution in the wall of the pipe can be evaluated after a rearrangement of the equation.

$$\frac{T_1 - T}{T_1 - T_2} = \frac{\ln(r/r_1)}{\ln(r_2/r_1)} \quad (3.54)$$

$$\text{Since, } \frac{dT}{dr} = \frac{C_1}{r}$$

$$\dot{Q} = (-kC_1)2\pi L \quad (3.55)$$

$$\dot{Q} = -2\pi L \frac{T_1 - T_2}{\ln(r_1/r_2)} = 2\pi L \frac{T_1 - T_2}{\ln(r_2/r_1)} \quad (3.56)$$

### 3.10 Numerical Model Summary for the Entire System

The purpose of this section is to present a summary of the numerical model of the complete system. To essentially allow the representation of the dynamic evolution according to real meteorological conditions. **Figure 3.3** shows the main algorithm for the entire system. The model needs to have the following characteristics:

- Precise enough to facilitate the correct sizing of future installations.
- Simple enough to be used over long periods (simulating a period of between 1 to 5 years) within a reasonable time.



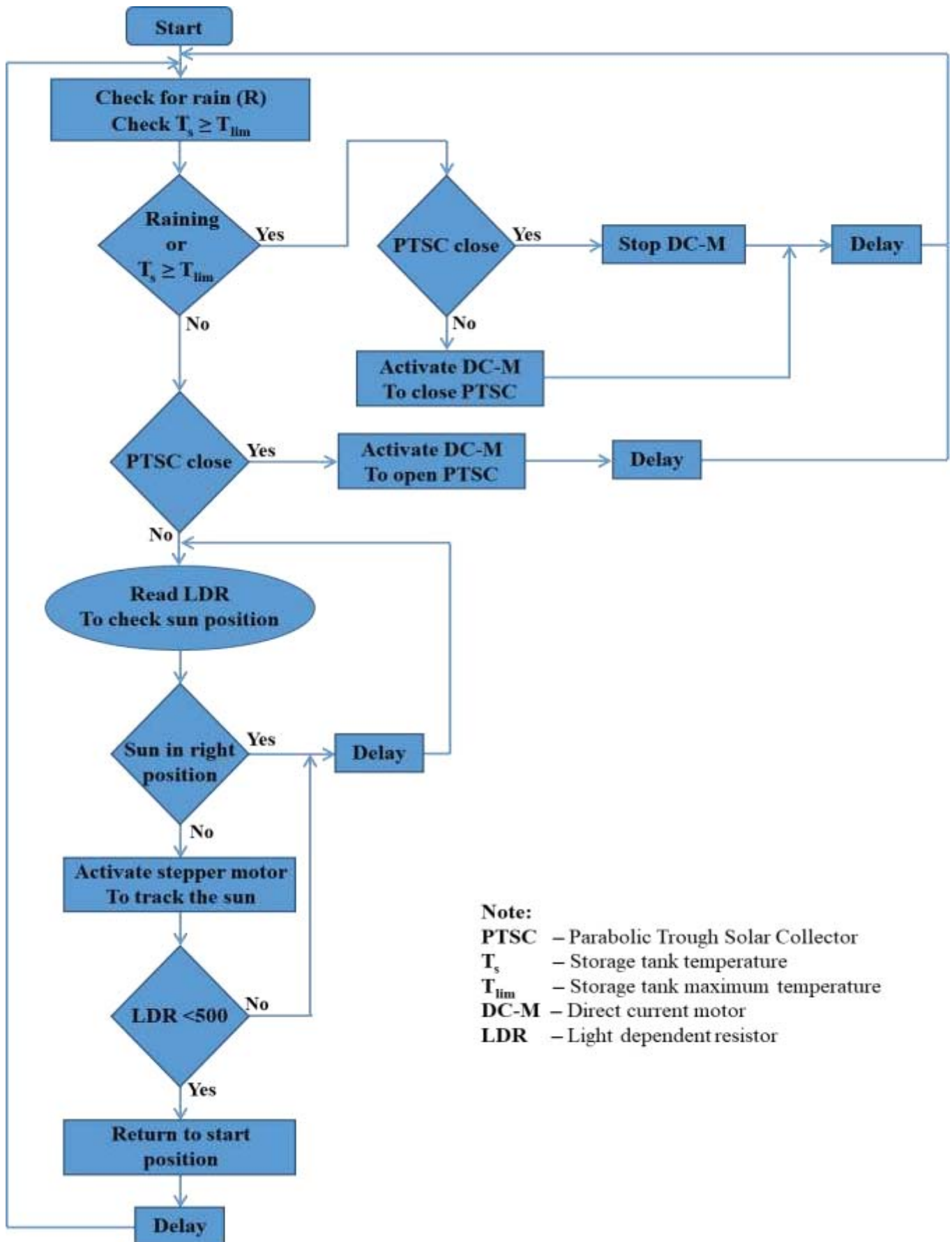


Figure 3.3: Main algorithm for the entire system.

In order to satisfy these two characteristics, a certain number of simplifications were made. In addition, by analysing the various components of the system, a set, which was made up of elements exhibiting quite different dynamic behaviours, was addressed. The response time of an absorber was very different from that of storage. In order to consider these differences, a careful choice of the time steps, which effectively facilitated the simulation of the entire system was made. The rest of this report shows how to manage this problem, knowing that the meteorological data used were collected on an hourly step.

### 3.10.1 Thermal storage model

In general, the thermal balance of the domestic hot water storage can be expressed quite simply in the following manner:

$$Mc_p \frac{dT_s}{dt} = W_c^{in} - W_c^{out} \quad (3.57)$$

where  $M$  represents the mass of the storage (in this case, equivalent to the mass of water),  $c_p$  is the specific heat capacity of water,  $T_s$  is the average temperature of the storage and the two flows,  $W_c^{in}$  and  $W_c^{out}$  represent the respective contributions coming from the absorber to the storage (in this case the exchanger coming from the solar collector) and the losses from the same storage, which consist of the losses of the storage and that, coming from the volumes of the withdrawn hot water. Therefore, these two flows can be expressed as follows:

$$W_c^{in} = \dot{m}c_{p_w}(T_f^{in} - T_f^{out}) \quad (3.58)$$

where,  $\dot{m}$  is the mass flow coming from the solar collector and  $T_f^{in}$  and  $T_f^{out}$ , are the respective inlet and outlet temperatures of the heat transfer fluid at the outlet of the

exchanger located in the repository. This quantity can also be expressed in the following simplified manner:

$$W_c^{in} = KS \left( \frac{T_f^{in} + T_f^{out}}{2} - T_s \right) \quad (3.59)$$

Where  $K$  represents the surface of the heat exchange coefficient and  $S$  the surface area of the exchanger (the value of  $K$  is obtained from the following:  $K = \lambda_{cu}/PT_{cu}$ , where  $PT_{cu}$  is the thickness of the exchanger pipe). Therefore, this equation can be used to evaluate  $T_f^{out}$ , which is the outlet temperature of the heat transfer fluid in the exchanger. This can take two different values and can be expressed as follows:

$$T_f^{out} = \frac{T_f^{in} \times (2\dot{m}c_p - KS) + 2KST_s}{KS + 2\dot{m}c_p} \quad (3.60)$$

$$\text{If } T_f^{out} > T_s$$

Or

$$T_f^{out} = T_s, \text{ in the second case.}$$

The second case means that the storage has been able to absorb all the energy available in the heat transfer fluid before the latter passes through the entire exchanger. Therefore, Equation (3.59) is modified simply, by replacing  $T_f^{out}$  with  $T_s$ , which gives:

$$W_c^{in} = KS \left( \frac{T_f^{in} - T_s}{2} \right) \quad (3.61)$$

It is important to note that this equation gives an idea with regards to the size of the exchanger as a function of the mass flow delivered by the heating system of the

storage system. When the product of the surface by the area exchange coefficient is close to twice the mass flow and is multiplied by the specific heat of the heat transfer fluid, an almost perfect exchange exists. This assertion is certainly a simplification of the physical processes in the measurement. For example, where  $T_s$  is considered to be homogeneous and constant over the exchange period. Furthermore, the quantity  $W_c^{out}$  was represented in two distinct simplified equations:

- i. The first represents the general storage losses by the direct exchanges at ambient environment. In order to simplify the equation as much as possible, an overall exchange coefficient was fixed, depending only on the storage volume and the external exchange temperature  $T_{ext}$ . This simplification can easily be justified if it is considered that the storage is either, installed underground or placed inside a building, whose temperature is regulated. The equation will, therefore, take the following form:

$$W_c^{out1} = G V_s (T_s - T_{ext}) \quad (3.62)$$

where  $G$  represents the volume exchange coefficient, expressed in  $W/Km^3$  and  $V_s$  represents the equivalent volume of the repository.

- iii. The second represents the losses caused by the domestic hot water drawn. This is simply considered as the mass flow rate. Thus, the withdrawn is simply replaced by its equivalent, the temperature of which is also equal to the outside temperature. To increase its accuracy to a real scenario, it can be considered that this flow  $\dot{m}_s(t)$  is a function of the time of the day that was considered. Therefore, the following will be obtained:

$$W_c^{out2} = \dot{m}_s(t) c_p \times (T_s - T_{ext}) \quad (3.63)$$

### 3.10.2 Dynamic model of a concentrated solar absorber

By describing the thermal equilibrium of the absorber only, the system can be summarized as the evolution of the temperature of the fluid circulating in the absorber being enough. Since the system is a closed circuit, the thermal equilibrium of this system can be written, thus, considering the flow through it. Therefore, a global expression exists, thus:

$$TI_{abs} \frac{dT_{abs}}{dt} = W_{abs}^{in} - W_{abs}^{out} \quad (3.64)$$

Where  $TI_{abs}$  represents the thermal inertia of the absorber,  $T_{abs}$  represents the temperature of the absorber fluid,  $W_{abs}^{in}$  represents the energy flow supplying the absorber and in heating the heat transfer fluid,  $W_{abs}^{out}$  represents the flow of energy dissipated by this same fluid.

In order to be as simple as possible, it was proposed for all these values, a certain number of simplifications, which considered some constraints linked to the functioning of the system, such as the overheating of the heat transfer fluid and that of the storage. In order to represent the situation in a simplified way, it was considered that the incoming flux is simply proportional to the direct solar flux measured in  $W/m^2$ . The proportionality coefficient is represented by the interception (and concentration) area of the absorber in  $m^2$ . Therefore:

$$W_{abs}^{in} = A_{eq} \times DS_r(t) \quad (3.65)$$

where  $A_{eq}$  is the equivalent surface area in  $m^2$  and  $DS_r(t)$  is the direct solar radiation data in  $W/m^2$ .

Concerning the outgoing flow, several elements must be considered. To simplify the model, two types of outgoing flows were considered, namely:

- i. Radiation losses at the active part of the absorber.
- ii. Transfer through the exchanger in the storage.

Therefore, the conduction and/or convection losses that exist along with the connections between the different elements of the absorber loop were considered negligible. Hence, the following equation:

$$W_{abs}^{out} = \{\sigma \times \alpha_s \times A_{eq} \times (T_{abs}^4 - T_{ext}^4)\} + \{\dot{m}c_p(T_{abs} - T_f^{out})\} \quad (3.66)$$

Where,  $\sigma$  is the Stefan - Boltzmann constant,  $\alpha_s$  is the emissivity of the absorber,  $T_{ext}$  is the outdoor temperature data in Kelvin and  $\dot{m}$  is the mass flow in the condenser. Note that the second term of the sum is the value of  $W_c^{in}$ , as it appears in Equation 3.57.

The choice to use only the outside temperature to calculate the radiation losses and not the temperature of the sky can be justified by the design of the absorber, which is automatically obscured when direct sunlight disappears or is insufficient. Indeed, the presence of a term in power 4, in the formulation of the radiation losses, can cause significant differences if the length of the absorber is relatively long. One way of limiting errors could be by decomposing the useful part of the absorber into a reduced length section, to better account for this type of loss.

This type of modelling, which is similar in some ways to the resolution of a partial derivative system, is also dependent on the length of the absorber and time. This has also been considered and programmed. In this case, a system of  $n$  related equations is developed, which can be expressed as follows:

$$T_{abs}(i + 1) = T_{abs}(i) + \Delta T_{abs}(i) \quad (3.67)$$

Where  $i$  represents the portion of the absorber considered and  $\Delta T_{abs}(i)$  represents the temperature of the absorber fluid. Based on the portion considered and as per Equation 3.64, the following equation is obtained:

$$\frac{TI_{abs}}{n} \times \frac{d}{dt} \Delta T_{abs}(i) = \left\{ \left( \frac{A_{eq}}{n} \times DS_r(t) \right) - \left( \sigma \times \alpha_s \times A_{eq} \times (T_{abs}^4(i) - T_{ext}^4) \right) \right\} \quad (3.68)$$

Where  $n$  represents the number of unit elements representing the active part of the absorber.

It is possible to consider this equation as an ordinary differential equation and solve it as such. Finally, to represent the thermal inertia of the system  $TI_{abs}$ , it is pertinent to focus on the absorber itself (copper pipe and volume of stagnant fluid) as a first approximation.

$$TI_{abs} = (V_{Cu} \times \rho_{Cu} \times c_{p_{Cu}}) + (V_{wabs} \times \rho_w \times c_p) \quad (3.69)$$

Where  $V_{Cu}$  and  $V_{wabs}$  are the volume of copper in the absorber pipe and the volume of standing water contained in the absorber respectively.

### 3.10.3 Weather history

Most of the works in the literature use typical days or typical months. The study posits this as insufficient and hence, this work used weather history to evaluate the real cost of additional electricity. Furthermore, the weather history used has a one-hour period and the time series analysis proposed to have this period reduced to 15 minutes. This approach increased the computation time but has the potential to improve the economic value of the design.

### 3.10.4 Control systems

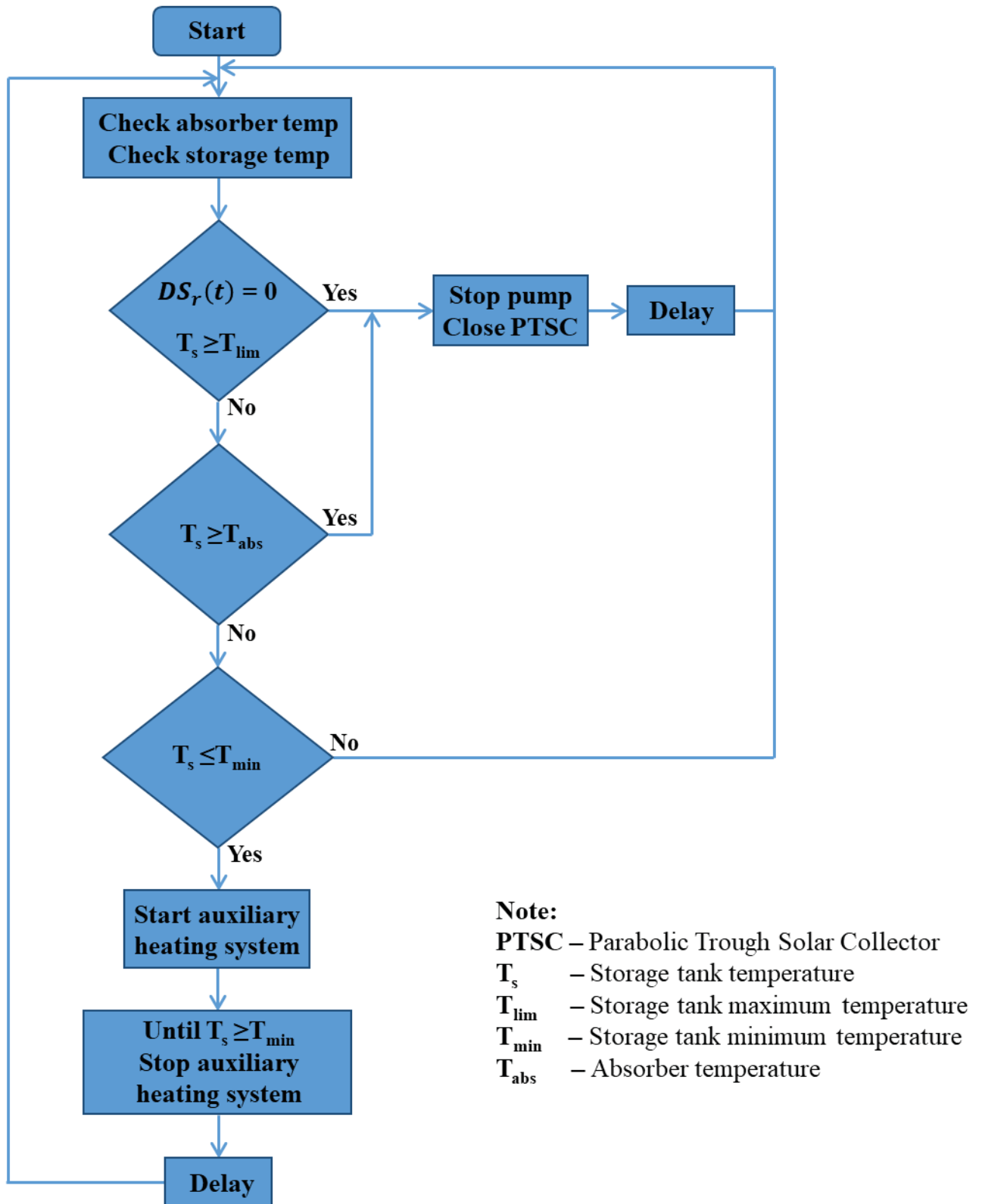
The overall envisaged system presents a certain number of control mechanisms intended to guarantee the harmonious functioning of the whole system. Some of these systems are, solely related to the operation of the absorber, while others are, intended to minimize storage losses and maintain the needed temperature level. The control elements affecting the absorber could potentially obscure the exchanger, thus, forcing the value of  $DS_r(t)$  to 0. At the same time, the circulation pump will be stopped and the mass flow  $\dot{m}(t)$  will also be forced to 0. The conditions considered, are the following and shown in **Figure 3.4**:

- $DS_r(t) = 0$ : The sun is covered by the clouds or it is night-time.
- $T_{abs} \geq T_{lim}$ : The temperature of the absorber exceeds a limit temperature; in this case, the circulation pump may be left in operation.

In cases where storage is involved, the following cases were accounted for:

- $T_s \geq T_{lims}$ : The storage temperature exceeds its safety limit: the circulation pump is stopped and the absorber covered.
- $T_s \geq T_{abs}$ : The storage temperature exceeds the temperature of the absorber: the circulation pump is stopped.
- $T_s \leq T_{min}$ : The storage temperature drops below a minimum temperature: an auxiliary heating system is commenced to bring the storage temperature above the minimum threshold.





**Figure 3.4:** Solar heating and auxiliary heating system algorithm.

### **3.10.5 Considering the different response times of the various parts of the system**

As it was noted in the preamble, the system considered will have significantly different response times, whether at the level of these main components:

- Absorber
- Storage

Also at the level of control systems.

- Shading of the absorber
- Stop-start of the circulation pump
- Stop-start of the auxiliary heating system.

In order to constitute a set of data presenting a time step that is suitable for all these systems, the study used a linear interpolation of the real data in steps of 5 and 10 minutes. This interpolation, therefore, generates time series for direct solar radiation and the ambient temperature in order to achieve stable simulations. In addition, a time delay is set up to prevent the control systems from being triggered abruptly.

### **3.10.6 A scenario for the use of domestic hot water**

With regards to a possible scenario of domestic hot water circulation, 3 time periods were defined. These were of variable duration and flow, but also accounts for the volume that was set, i.e. close to 500 l/day. A plausible breakdown could be as follows:

- i. 6 a.m.–8 a.m. use of the shower and morning ablutions 80 l/hr
- ii. 11 a.m.–1 p.m. various domestic uses 50 l/hr
- iii. 5 p.m.–8 p.m. various domestic uses and night ablutions 80 l/hr

The distribution of these three-time slots as well as the proposed values can also be modified according to the day of the week or according to the time of the year when necessary.

### **3.11 Conclusion**

The chapter has shown the mathematical model that was used to model the parabolic trough solar collector (PTSC) design. This was done to ensure that the geometry of the PTSC is perfect and to ensure the positioning of the focal line is correct. Thus, maximizing the performance of the solar collector. The mathematical models that are required for the modelling the amount of heat energy received by the solar collector and the amount of energy that was received by the absorber tube was presented. The various equations for analysing the heat losses due to conduction, convection and radiation was equally presented. The flow chart diagram for the processes involved in the overall system was presented. The different factors (such as solar intensity, temperature upper and lower limits) that determine the behaviour of the system was highlighted in this chapter.

## CHAPTER FOUR

### 4.0 DESIGN METHODOLOGY

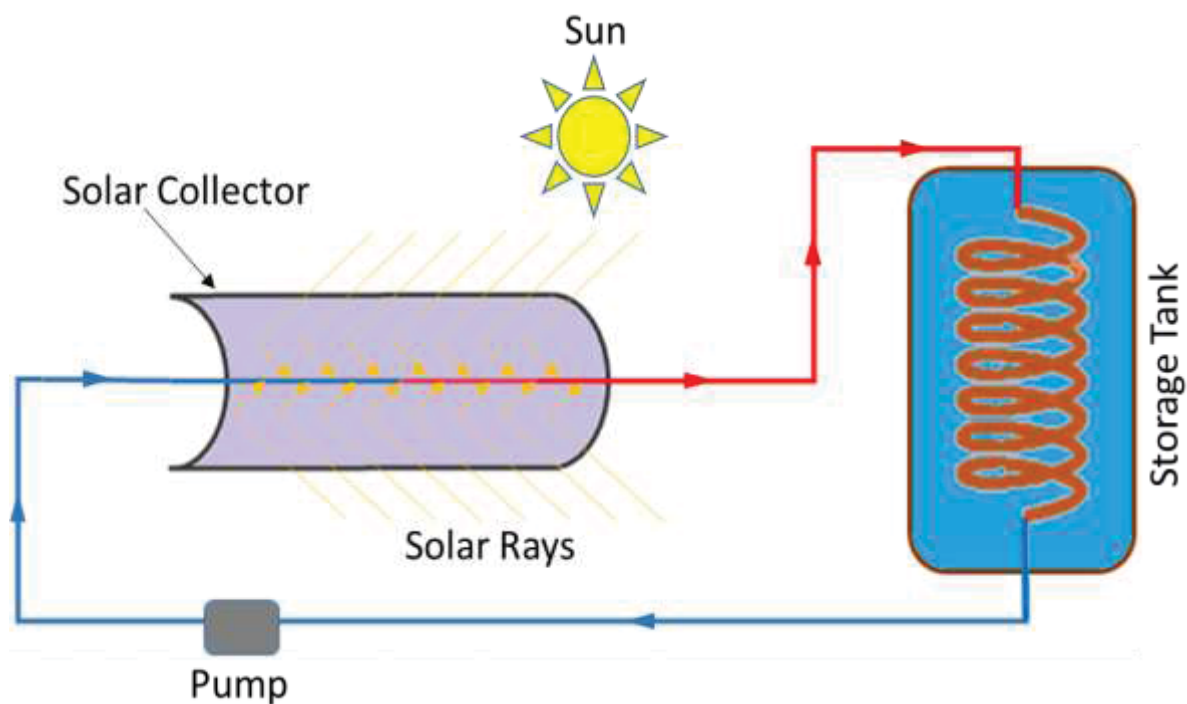
#### 4.1 Introduction

The construction of a parabolic trough solar collector (PTSC) depends majorly on three key factors, namely: the torsional resistance, the parabolic shape of the collector, and the absorber/reflector materials. The collector's weight and other external factors such as wind speed, rain, dust, humidity, etc. can lead to high moments at the rotating part of the system and the thermal performance of the solar collector. Overall system performance and efficiency is a function of the design. Therefore, significant and careful considerations were made in the choice of materials and geometry of the PTSC. The main components of the PTSC used for this research are the concentrator (flexible mirror), absorber pipe, support structure, tracking system, heat transfer fluid and other accessories (bolt and nut, insulator, etc.). The flexible plastic mirrors should be carefully mounted on the supporting structure made from mild steel to help reflect and concentrate the solar radiation of the sun unto the focal line of the parabolic trough where the absorber is placed. This process helped to achieve the required temperature. The design process for the entire system is sub-divided into three distinct categories, namely: (i) the parabolic trough design (ii) the solar tracking mechanism and (iii) hot water storage tank. Each of these design procedures is succinctly discussed in the following sub-sections. A schematic representation of the system is presented in **Figure 4.1**.

#### 4.2 Design of Parabolic Trough Solar Collector

The parabolic trough design depends on several parameters ranging from the concentrator reflector material to the solar distribution, parabolic trough concentrator

diameter, aperture area of the concentrator and the parabolic trough focal length. Other equally important parameters are the diameter of the absorber pipe, receiver/absorber aperture area, concentration ratio, orientation and rim angle. The PTSC can be positioned in the North-South axis direction while the tracking of the sun should be from East-West direction. For the case of a solar power plant, PTSCs are split into many modules. These modules are positioned linearly in series. Subsequently, these series are connected in a parallel arrangement. The whole system arrangement is regarded as a solar field. For the study, only a single solar collector was considered because the intended application is for household water heating and not for solar thermal plants as in the case of electrical power generation.



**Figure 4.1:** Schematic representation of the entire solar water heating system

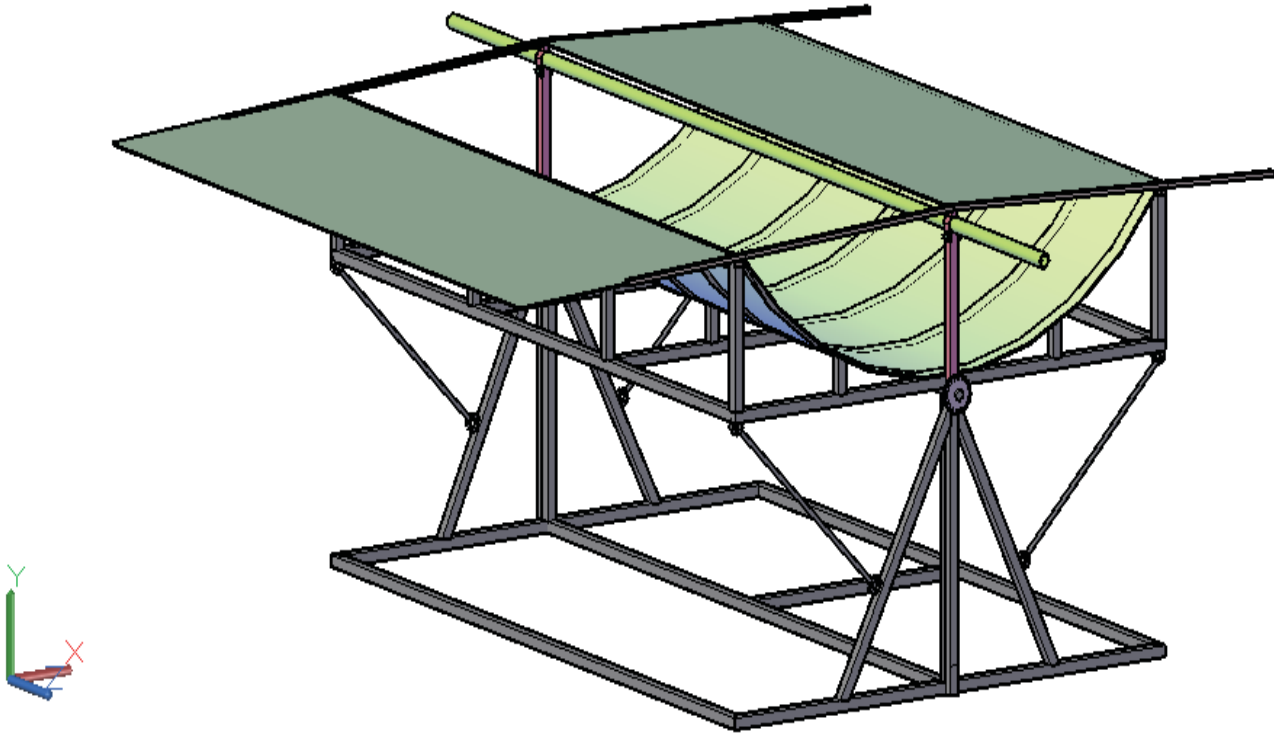
An evacuated glass tube should be used as the receiver for the PTSC. It should have a copper pipe as the inner tube acting as the absorber pipe while the glass tube acts as the cover. The evacuated glass tube was suggested in order to eliminate the absorber thermal losses due to convection. This is achievable due to the vacuum

between the absorber pipe and the glass cover (Bellos and Tzivanidis, 2019). According to a study by Price *et al.* (2002), the pressure was reported to be generally low with an approximate value of 0.013 Pa. The absorber outer surface is, usually coated with a certain coating to minimize the rate of thermal losses to the immediate environment. According to Kennedy and Price (2005), the most widely used coating for PTSC is Cermet coating. An example of coating is Luz Cermet coating having varying emittance at different temperature ranges as shown in **Table 4.1**, while the absorbance is about 0.938.

The designing of the PTSC was done using AutoCAD and SolidWorks® as shown in **Figure 4.2**. Some analyses were done on the structure to verify the structural rigidity/integrity of the support frame. The analysis includes finite element analysis (FEA), shear force, bending moment, and deflection. The findings are discussed in detail in Chapter 5 of this thesis. The CAD orthographic drawings are also shown in **Appendix 1**. All necessary workshop safety rules should be, strictly followed during the marking-out, cutting, welding, grinding and painting.

**Table 4.1:** Luz Cermet coating emittance at various temperatures. Adapted from Kennedy and Price (2005)

Temperature	Emittance value
25 °C	0.061
400 °C	0.146
500 °C	0.179



**Figure 4.2:** Schematic 3D model of a modify parabolic trough solar collector

#### 4.2.1 Materials

The materials used for the development of the parabolic trough structure and the flexible mirror can be sourced and supplied locally, in South Africa. The supporting structure was made from square tubing mild steel for structural rigidity and flat bars to form the parabolic shape that the flexible mirror was placed in. The dimensions of the square tubing are respectively 38mm x 1.6mm x 6.0m and 25mm x 1.6mm x 6.0m for the base and the movable structure (where the mirror was placed). The dimension for the flat bar is 25mm x 3mm x 3m. The mechanical properties of the square tubing are shown in **Table 4.2**. These materials can be supplied by Builders®, South Africa. The flexible plastic mirror (Acrylic XT Mirror sheet 3 mm) is manufactured and supplied by Maizey Plastics, PO Box 19502, Pretoria West, 0117, South Africa.

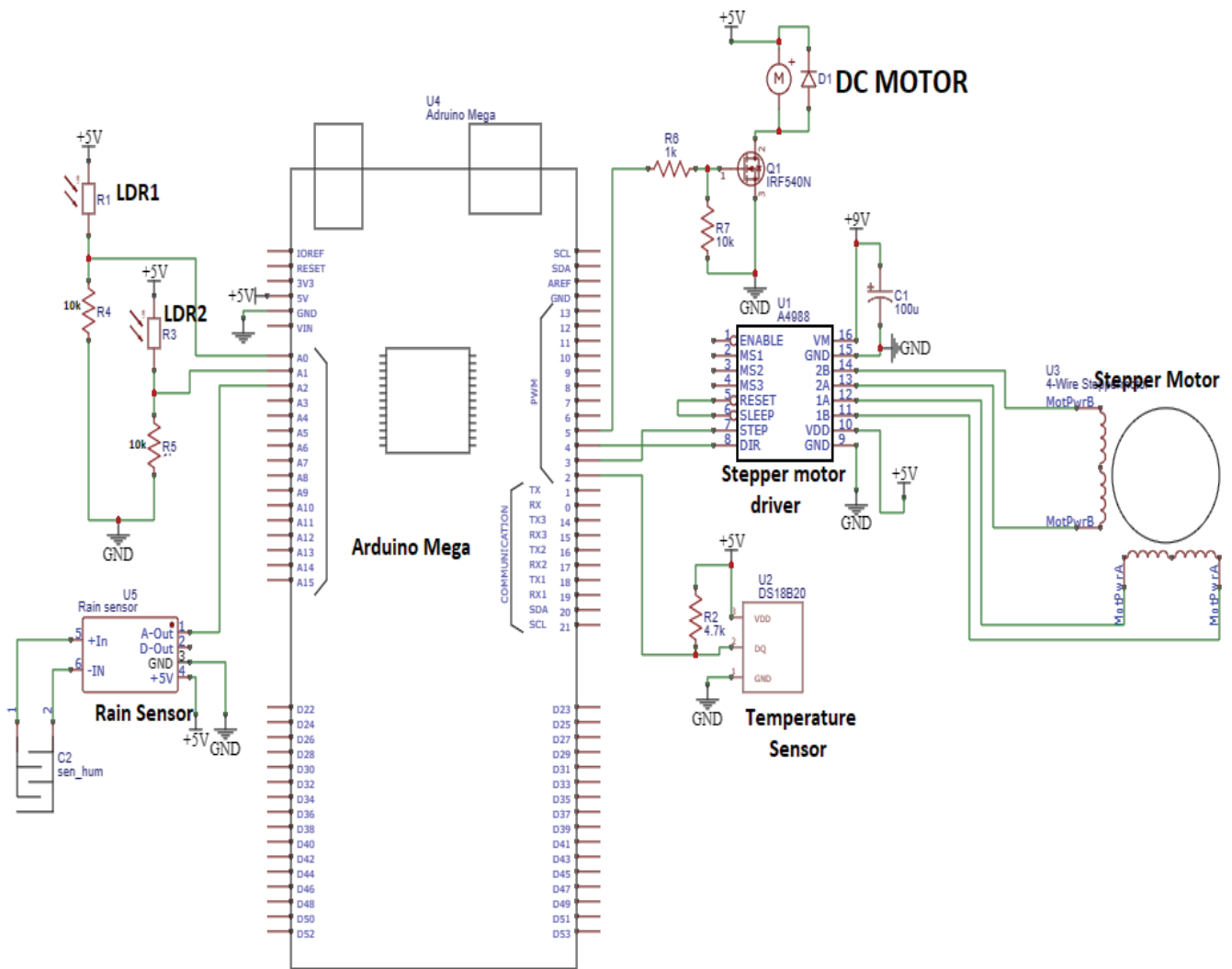
**Table 4.2:** Mechanical properties of the square tubing

Property analysed	Value/description	Unit
Material type	Mild steel	–
Model type	Linear Elastic Isotropic	–
Default failure criterion	Max von Mises Stress	–
Yield strength	3.51571e+08	N/m <sup>2</sup>
Tensile strength	4.20507e+08	N/m <sup>2</sup>
Elastic modulus	2e+11	N/m <sup>2</sup>
Poisson's ratio	0.29	–
Mass density:	7,900	kg/m <sup>3</sup>
Shear modulus:	7.7e+10	N/m <sup>2</sup>
Thermal expansion coefficient:	1.5e-05	Per kelvin

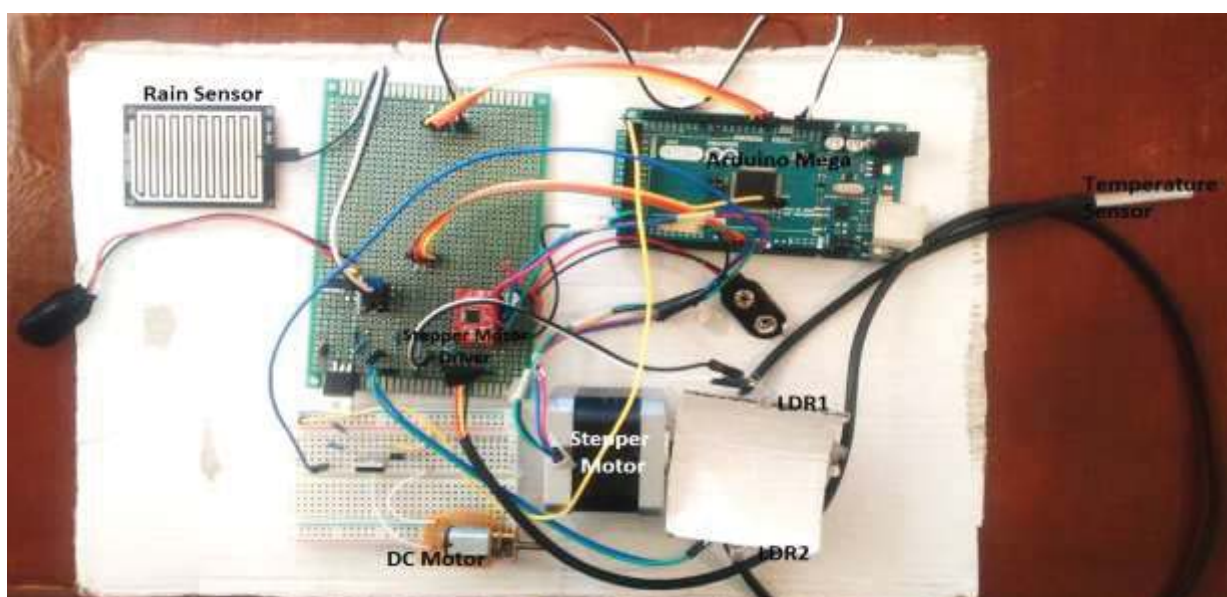
### 4.3 Solar Tracking Development and Calibration

The stepper motor controls the movement of the parabolic trough. The stepper motor changes the position of the collector facing the sun until the difference in the light dependent resistor (LDR) readings are low, which indicates that the system is facing the sun. The DC motor controls the covering of the parabolic trough. The DC motor is triggered to close whenever there are rain droplets and/or the temperature in the storage tank exceed 383 K. The circuit diagram for the entire system is shown in **Figure 4.3**, while the mini prototype is shown in **Figure 4.4**. The mini prototype was done to confirm if the system works perfectly and to calibrate each component (rain sensor, temperature sensor, DC motor, stepper motor and LDR). Each of these components is briefly explained in sub-session 4.2.1 – 4.2.3.





**Figure 4.3:** Schematic circuit diagram for the control system



**Figure 4.4:** Pictorial view of the mini prototype

#### 4.3.1 Rain sensor installation and calibration

A rain sensor is a switching device that is activated whenever rain droplets are detected on the rain sensor panel surface. It is also known as a rain switch. Most of the modern rain sensors in the market are based on the principle known as the total internal reflection. This is a process where infrared light is beamed at a 45° angle into the windshield from the interior. If the glass is dry, the critical angle for total internal refraction is around 42°. This value is obtained with the total internal refraction formula according to Snell's Law (Rivera-Ortega *et al.*, 2019).

$$n_1 \sin \theta_1 = n_2 \sin \theta_2 \quad (4.1)$$

$$\text{At critical angle, } \theta_2 = 90^\circ \quad (4.2)$$

At total internal reflection, the angle of incidence is the same as the critical angle.

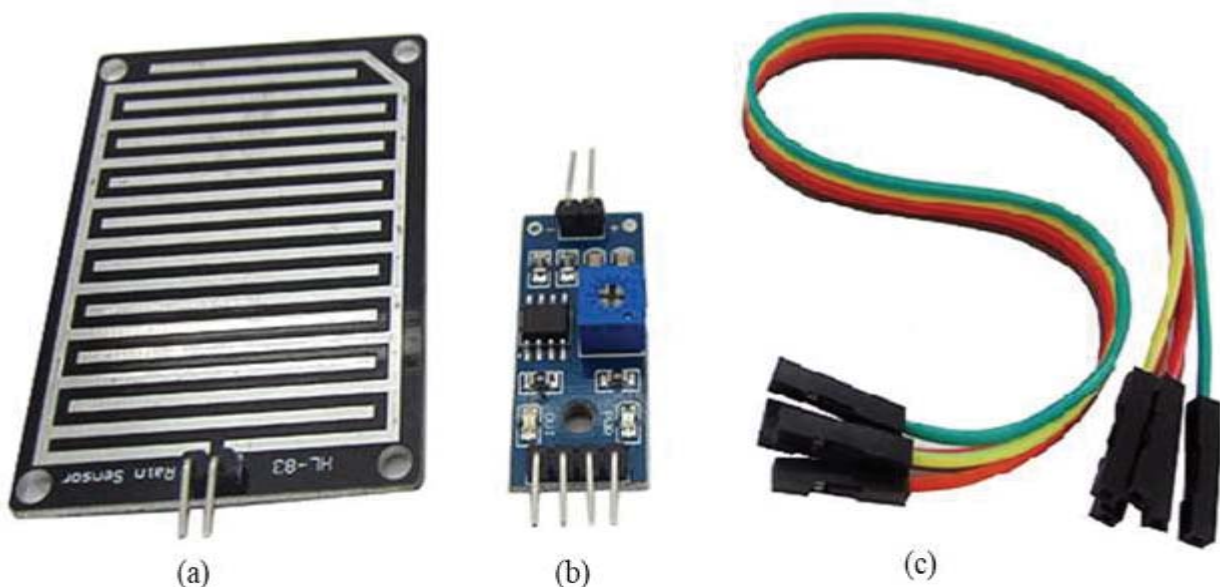
$$\theta_1 = \theta_c \quad (4.3)$$

$$\therefore n_1 \sin \theta_c = n_2 \sin 90^\circ \quad (4.4)$$

Where  $n_1$  is the first media refractive index,  $n_2$  is the second media refractive index,  $\theta_c$  is the incidence angle and  $\theta_2$  is the angle of refraction.

The highest analog value for rain sensor is 1023 when rain is not detected. This value can be viewed on the serial monitor `[Serial.begin(9600)]` on the Arduino software. Therefore, when water droplets drop on the sensor, the analog value begins to decrease. As the water droplets increase, the analog value reduces. This helps in determining the range of values the sensor sensed. This signal goes to the microcontroller due to the output value been used by the microcontroller to send a new signal to the DC motor to perform a task. The essence of the rain sensor is to alert the system on the current weather condition (i.e. it is raining). Sometimes, the rain may

come with hailstones and this could potentially damage the evacuated glass tube. When rain is detected (that is “*rainfall*”), a signal is sent to the microcontroller to activate the sliding cover (“*Close*”) for the parabolic trough solar collector. When the surface of the rain sensor is dry (that is “*no rainfall*”), a different message is sent to the controller to open the cover (“*Open*”). This enables the parabolic trough solar collector to reposition itself to face the sun and continue tracking if the tracking cycle for that particular day is not yet completed. For the sake of the research work, the detection rate is set at <400 (that is the “*sensorReading*”) on the Arduino code. **Figure 4.5** shows the basic components of the rain sensor module, sensor board and connecting wires. The rain sensor components mentioned above were supplied by Communica®, South Africa. The calibration was done by dipping the rain sensor board in water to determine the lowest appropriate analog value suitable for the current research work. The surface of the sensor board was wiped dried and the process was repeated four additional times to establish the required value to code into the Arduino UNO microcontroller.



**Figure 4.5:** Pictorial images of (a) water-drop sensor board, (b) rain sensor module and (c) connecting cables

#### 4.3.2 Temperature sensor installation and calibration

A DS18B20 temperature sensor unit was used, which is sealed (i.e. waterproofed) and pre-wired with a digital temperature probe. The DS18B20 consists of a temperature sensor and a memory unit used to store the value of the temperature. The conversion of the analog value to a 12-bit value is performed in the DS18B20. The 12-bit value is communicated to the Arduino UNO microcontroller over a one-wire bus. The Arduino acts as a master device and uses various commands to request information from the temperature sensor. The Arduino UNO converts the 12-bit value to a temperature value with an accuracy operation range between -55 °C and 125 °C. The temperature of the water is updated every 15 seconds. When a temperature above 80 °C in the storage tank is recorded, the DC motors will be triggered to cover the parabolic trough. This process is to prevent over-heating, which can lead to excessive temperature and pressure within the storage tank. High temperature and pressure could cause the storage tank to explode. The pictorial image of the temperature sensor is shown in **Figure 4.6**. The sensor at a temperature range between -10 °C to 85 °C has the optimum accuracy of  $\pm 0.5$  °C. The only shortcoming associated with the DS18B20 temperature sensor unit is the usage of the Dallas 1-Wire protocol which has some level of complexity and requires some coding to parse the communication. A 4.7k resistor is attached to the sensing pin when used with a microcontroller. This is an important requirement as a pull-up to the Vdd line from the Data. The datasheet showing the comprehensive detail for the temperature sensor is included in **Appendix 2**.



**Figure 4.6:** Pictorial image of a temperature sensor with cable labelling

### 4.3.3 Light dependent resistor sensor installation and calibration

Light dependent resistors (LDRs) also known as photoresistors were used for the tracking system. One end of the LDR is connected to a pull-up resistor and the other end is connected to the ground. The node consisting of the pull-up resistor and the LDR is connected to an analog pin on the Arduino UNO board. The analog value is converted to a digital value that represents the intensity of the sun. Two LDRs are placed on either side of the solar collector as shown in **Figure 4.4**. The direction of movement of the system is determined by the LDR that gives the higher reading, which in turn triggers the direction of movement of the stepper motor.

10 k-Ohm resistors are used as the pull-up resistors. For calibration, flashlights of equal intensity were shone on each LDR, and the 10k potentiometer was adjusted until the digital reading of each LDR was the same. The *analogRead* function of the

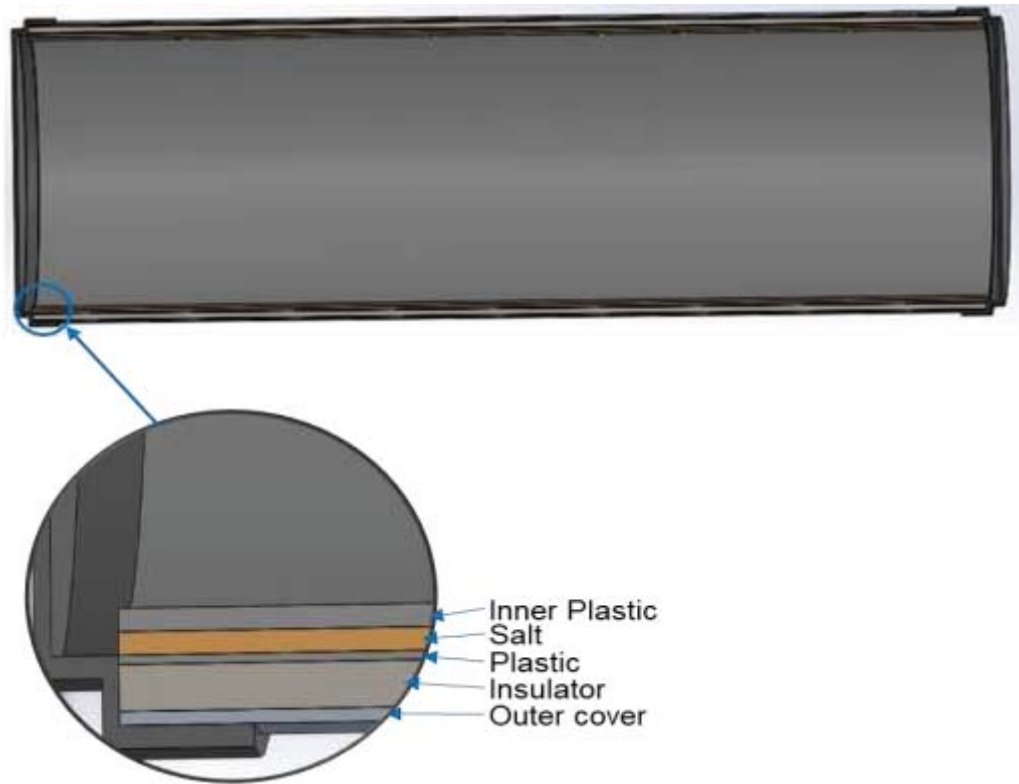
Arduino is used to determine the digital value of each LDR and the *serial.println* function is used to view the digital value of the intensity on the LDR. Samples of the LDR used are shown in **Figure 4.7**.



**Figure 4.7:** Light dependent resistor

#### **4.4 Design of the Hot Water Storage Tank**

The storage tank is an important component of the whole system in a household. The capacity of the tank in terms of volume and performance depends on several parameters ranging from the collector size to the solar intensity, heating method and the material of the tank to the number of household users. The heat retention capacity of the storage tank is a function of the rate of thermal losses of the materials used. Improving the performance of the system can reduce the demand for hot water heating. According to Celador *et al.* (2011) and Chandra and Matuska (2020), the storage tank model has an important effect on the annual savings based on the decisions made during the design phase of the entire system. Based on these assumptions and other factors such as tank orientation (Assari *et al.*, 2018), dual tank (Banister and Collins, 2015), and so on as reported in the literature, the current research focused on using polymeric composite materials in laminate form for the storage tank. The schematic image of the proposed hot water storage tank (HWST) is shown in **Figure 4.8**.



**Figure 4.8:** Schematic image of a hot water storage tank in layers

The HWST is in five layers starting from the inner part, which is made from polypropylene having a thickness of 5 mm. The second layer from the inner layer is salt with a wall thickness of 5 mm, while the third layer is another polypropylene with a thickness of 2 mm. The fourth and fifth layers can be made from polyurethane and aluminium with respective thicknesses of 50 and 2 mm. The justification for proposing each of these materials are presented in **Table 4.3**.



**Table 4.3:** Justification for selected materials

Material	Thickness (mm)	Justification
Polypropylene (PP)	5 and 2	<ul style="list-style-type: none"> <li>▪ Polypropylene has good resistance to chemicals such as acids, alkalis, greases, oil, alcohols, ketones, etc.</li> <li>▪ Good mechanical properties (<i>Wei et al., 2020, Gou et al., 2020</i>).</li> <li>▪ Density of about 0.9 g/cm<sup>3</sup> and Water absorption - equilibrium of 0.03% (<i>Pérez et al., 2019</i>).</li> <li>▪ Coefficient of thermal expansion 100–180 x10<sup>-6</sup> K<sup>-1</sup>.</li> <li>▪ Thermal conductivity ranges from 0.1–0.22 Wm<sup>-1</sup>K<sup>-1</sup> at a temperature of 23 °C (<i>GoodFellow, 2020, Chen et al., 2017, Patti and Domenico, 2019</i>).</li> </ul>
Salt	5	<ul style="list-style-type: none"> <li>▪ An increase in temperature will lead to a decrease in density. At a temperature of 25 °C and standard atmospheric pressure, NaCl has a density of 2 170 kg/m<sup>3</sup>.</li> <li>▪ Melting point and the boiling point stands at 800.7 and 1465 °C respectively (<a href="http://www.aqua-calc.com">www.aqua-calc.com</a>).</li> <li>▪ The thermal conductivity of NaCl varies from 0.5932–0.6279 Wm<sup>-1</sup>K<sup>-1</sup> depending on temperature and molarity (<i>Ramires et al., 1994, Ozbek et al., 1980</i>).</li> </ul>
Polyurethane (PU)	50	<ul style="list-style-type: none"> <li>▪ Polyurethane (PU) is flexible and soft or rigid and hard depending on the application. The most commonly available form is PU foams which can be low-density rigid foams or low-density flexible foams (<i>Szycher,</i></li> </ul>



1999). Rigid PU possesses low heat conduction, low density, low moisture absorption, and high mechanical strength (Reghunadhan and Thomas, 2017).

- PU has a variable density ranging from as low as 14 to as high as 961 kg/m<sup>3</sup> (Hwang et al., 2020, Demirel and Tuna, 2019).
- Nanoparticle-based rigid PU foams have good thermal stability and flame retardance (Atagür *et al.*, 2017).
- PU is recyclable, which makes it a sustainable and environmentally-friendly material (Simón et al., 2018).
- Thermal conductivity is ~0.0306 Wm<sup>-1</sup>K<sup>-1</sup> (Sair *et al.*, 2018).

Aluminium (Al)

2

- Al is a lightweight material, having good mechanical properties and is easy to shape.
  - The density of aluminium is about 2,710 kg/m<sup>3</sup> (thyssenkrupp-Materials, 2018).
  - Al can be recycled 100%, which makes it environmentally-friendly (Baffari *et al.*, 2019).
  - Thermal conductivity of Al is ~250 Wm<sup>-1</sup>K<sup>-1</sup> (farm.net).
- 

#### 4.5 Storage Tank Sizing

Among natural resources, water is disputably the most significant and a key component of any geographical location and contributes to the growth of the community (Gajda *et al.*, 2018). The rapidly growing population and rate of

urbanisation: especially in large cities and other dense residential areas constitute the main consumers of the global water resources. Therefore, water distribution and consumption play a major role in water management considering the water shortages faced by many countries globally (Gain and Wada, 2014, Fan *et al.*, 2014). The increasing water consumption levels have necessitated the development of probabilistic models and forecasts for water demand as shown in many studies (Pacchin *et al.*, 2019, Gharabaghi *et al.*, 2019, Lee and Derrible, 2020, Muhammad *et al.*, 2019). Therefore, this exacerbates the need for the development and sizing of water storage containers.

#### **4.5.1 General water demand estimation**

A household with good water conservation behaviour normally uses an average of 95 to 189 litres of water per person daily (Krishna *et al.*, 2005). To estimate the volume of water used per person per day, the population serviced by the Municipality can divide the total volume of water distributed from the Municipality. This assumption does not give the true reflection of water usage due to leakages along the water distribution network between the water source and the end-users. Another valid method to calculate water usage is to check the installed water meter or the water bill, which the Municipality supplies every month, in the case of South Africa. For this study, the daily usage is estimated by dividing the monthly total by the total number of people living within the household and the number of days in that month. Notably, water demand depends on the ages of the members of the household, seasons of the year, and the behaviour of the household members.

#### 4.5.2 Estimating the indoor water demand

The total water demand, ( $\psi$ ) can be evaluated by using Equation 4.5. The water demand is a function of the number of occupants, the number of usages per day, and the size/type of the plumbing fixtures.

$$\psi = \sum_i^n [(\vartheta^i * \varphi^i) * \omega] \quad (4.5)$$

Where  $\vartheta$  is the required volume of water usage per plumbing fixture per time,  $\omega$  is the number of person per household,  $\varphi$  is the number of usages of a plumbing fixture per day,  $n$  is the possible number of plumbing fixtures in a house and  $i$  is a single plumbing fixture in a house.

#### 4.5.3 Estimating the hot water storage tank size

The actual hot water storage tank volume ( $\nabla$ ) can be calculated by using Equation 4.6. The tank size evaluation is similar to the general indoor water demand estimation. The singular difference is that plumbing fixtures that have to do with hot water alone are considered. In addition, a factor of uncertainty ( $\alpha$ ) was introduced into the equation.

$$\nabla = \psi + \alpha \quad (4.6)$$

$$\alpha = 0.05 * \psi \quad (4.7)$$

Therefore, the expanded equation for the total storage tank size can be evaluated using Equation 4.8, considering all relevant constraints, where  $\alpha$  is the extra volume of water for uncertainties.

$$\nabla = \sum_i^n [(\vartheta^i * \varphi^i) * \omega] + \alpha \quad (4.8)$$

The plumbing fixtures considered for the storage tank are fixtures that have to do with hot water. Therefore, plumbing fixtures such as water closet (WC), urinary bowl, etc.

are not considered. The fixtures have different usage per day, which is accounted for during the evaluation of the total storage tank size. **Table 4.4** shows the basic usage according to *WaterWise* by Rand Water of South African. This was adopted and modified for the hot water storage tank design.

**Table 4.4:** Indoor daily hot water estimation per single-family household. Generated from (Rand\_Water-South\_Africa, 2020)

Plumbing fixture	Water consumption (litre)	Number of usages	Number of household users	Total (litre)
Bath	150	1	1	150
Shower	110	2	1	220
Wash hand basin	2	5	1	10
Kitchen basin	20	3	1	60
Washing machine	21	1	1	21

## 4.6 Conclusion

The chapter presented the new improved design for the parabolic trough solar collector. Furthermore, the various materials needed for the solar tracking system were also highlighted and the working procedures for each of the components were explained. The material properties and the design arrangement for the layers of the proposed hot water storage tank were succinctly explained. Lastly, the amount of water usage per individual in a household was analysed and quantified.

## CHAPTER FIVE

### 5.0 RESULTS AND DISCUSSION

#### 5.1 Introduction

The design analysis of the parabolic trough solar collector (PTSC) and the thermal performance of the entire system are discussed in detail in this chapter. The design analysis was done using Solidworks®, while the system thermal performance analysis was modelled and simulated using Matlab Simulink®. Based on the mathematical models in Chapter 3, the real-time data, which was obtained from the weather station at the University of Pretoria, was fed into the model. **Table 5.1** shows the weather data station information. The following are the key parameters that were used to evaluate the system performance: solar irradiation, solar collector area (aperture area), ambient and absorber input temperature, the mass flow rate of the working fluid and the solar position (solar tracking). The influence of these factors on the output of the system is discussed in the following sub-sections.

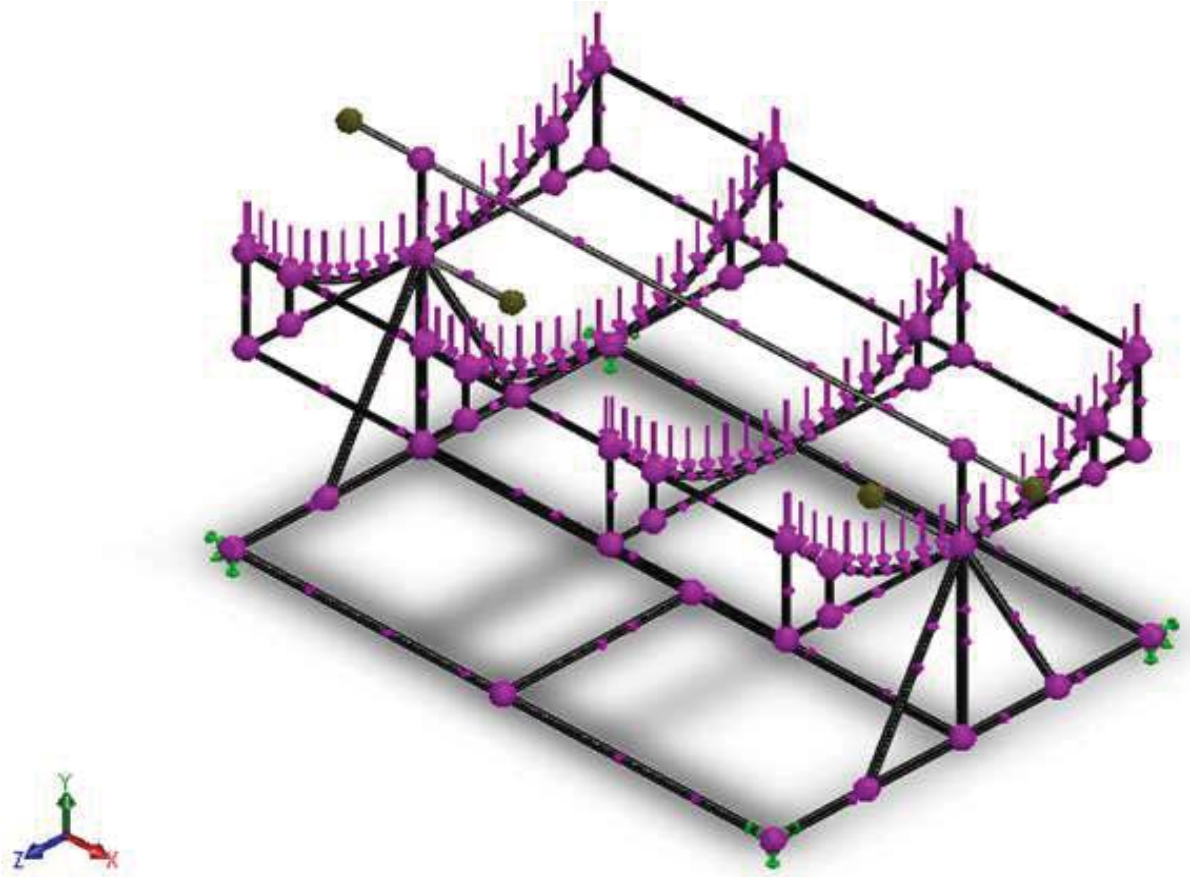
**Table 5.1:** Weather station data source. <https://sauran.ac.za/>.

Location	Latitude (degree)	Longitude (degree)	Elevation (m)	Topography
Pretoria, South Africa	-25.75308037	28.22859001	1410	Roof of university building

#### 5.2 Collector Supporting Frame Design Analysis

The structural analysis of the supporting frame for the parabolic trough solar collector (PTSC) was done to determine the structural integrity of the solar collector. **Figure 5.1** shows the fixed geometry and force loading. The applied force was a static force since the base of the frame was bolted to the ground using a foundation bolt. **Tables 5.2** and **5.3** show the resultant forces (reaction forces and reaction moments) for the system and the properties of the material properties respectively. The analysis was

conducted to assess the total load, which the structure can withstand before structural failure occurs. The meshing lasted for 10 seconds with a total of 429 and 335 nodes and elements respectively. The meshing was possible because there were no overlapping elements. The total applied force was 667.18 N, which is equivalent to the total approximate weight the supporting frame will experience on a constant base. **Appendices 3, 4, and 5** show the beam information, beam forces, and beam stresses respectively. In **Appendix 3**, each of the structural member being analysed is shown in colour blue while every other member is shown in colour black.



**Figure 5.1:** Structural force loading and nodes of the supporting frame

**Table 5.2:** Overall resultant forces for the supporting frame

Selection set	Units	Sum X	Sum Y	Sum Z	Resultant
<b>Reaction Forces</b>					
Entire Model	N	-2.9802x10 <sup>-6</sup>	4,198.52	-3.0518x10 <sup>-5</sup>	4,198.52
<b>Reaction Moments</b>					
Entire Model	Nm	-29.7275	0.1808	1.3373	29.7581

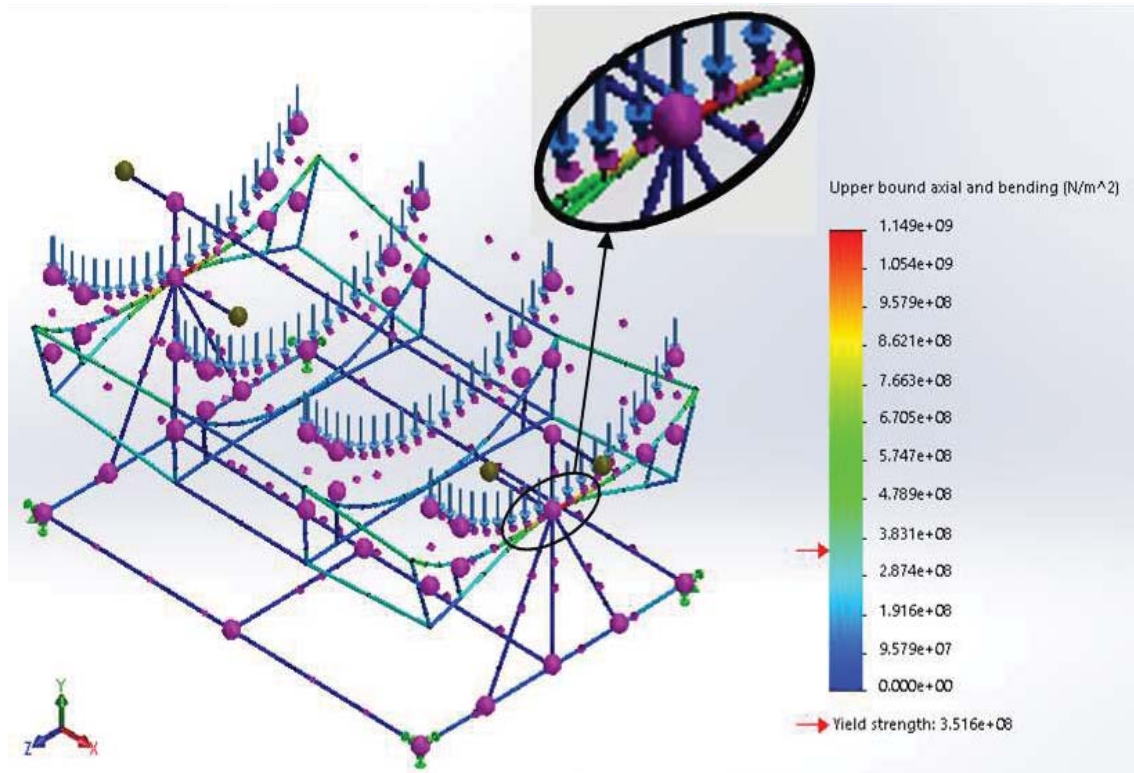
**Table 5.3:** Square-tubing properties from Solidworks® analysis

Property	Magnitude	Unit
Yield strength	3.51571x10 <sup>8</sup>	N/m <sup>2</sup>
Tensile strength	4.20507 x10 <sup>8</sup>	N/m <sup>2</sup>
Elastic modulus	2 x10 <sup>11</sup>	N/m <sup>2</sup>
Poisson's ratio	0.29	-
Mass density	7,900	kg/m <sup>3</sup>
Shear modulus	7.7x10 <sup>10</sup>	N/m <sup>2</sup>
Thermal expansion coefficient	1.5x10 <sup>-5</sup>	Kelvin

The material stress level is very important in order to ascertain the amount of load the material can withstand before failure. Therefore, the stress analysis was conducted on the supporting frame of the solar collector. To analyse the stresses on the frame made from mild steel, the finite element analysis (FEA) was used. The FEA was done using Solidworks®. **Figure 5.2** shows numerically, the maximum stress acting on the material. From the figure, it was observed that the material's yield stress or elastic limit is at a value of 3.516x10<sup>8</sup> N/m<sup>2</sup>. Based on the enlarged portion in **Figure 5.2**, the frame is likely to fail at the point shown. To prevent structural failure, the frame should be

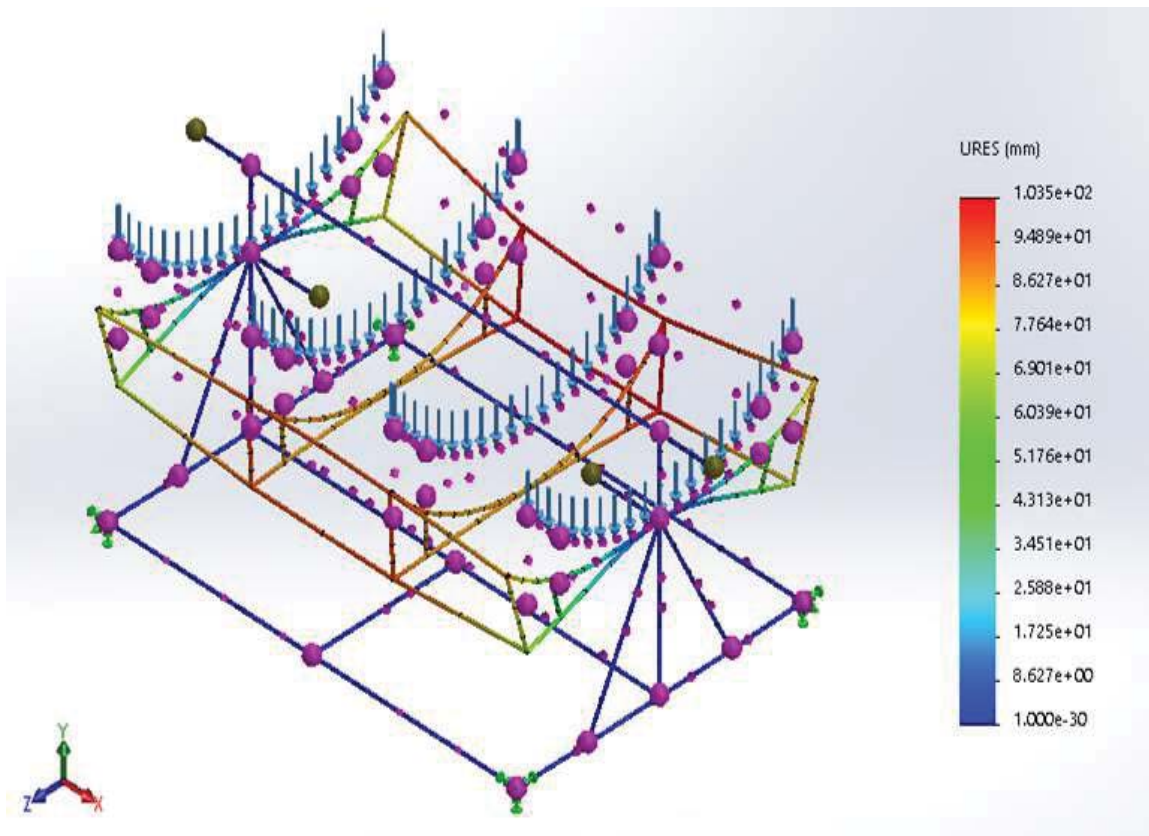
reinforced at the point of the highest possible failure in order to increase the strength of the structural frame. The displacement resultant (URES) analysis is shown in **Figure 5.3**. From the figure, it was observed that the points farther from the diagonal support frame displaced more than any other part. This was due to the load acting on the body of the frame. These points showing higher displacement values are due to the top portion of the collector frame acting as a cantilever. For a cantilever, the farther a component is away from the fixed point or support, the more displacement it will experience. The URES can be calculated manually if the x, y, and z components are known using Equation 5.1. The simulation used the magnitude of the vector in terms of  $\hat{i}$ ,  $\hat{j}$  and  $\hat{k}$ . These values for each node can be obtained from the Solidworks® simulation software.

$$URES = |\vec{U}| = \sqrt{(U_x)^2 + (U_y)^2 + (U_z)^2} \quad (5.1)$$



**Figure 5.2:** Stress analysis of the solar collector-supporting frame



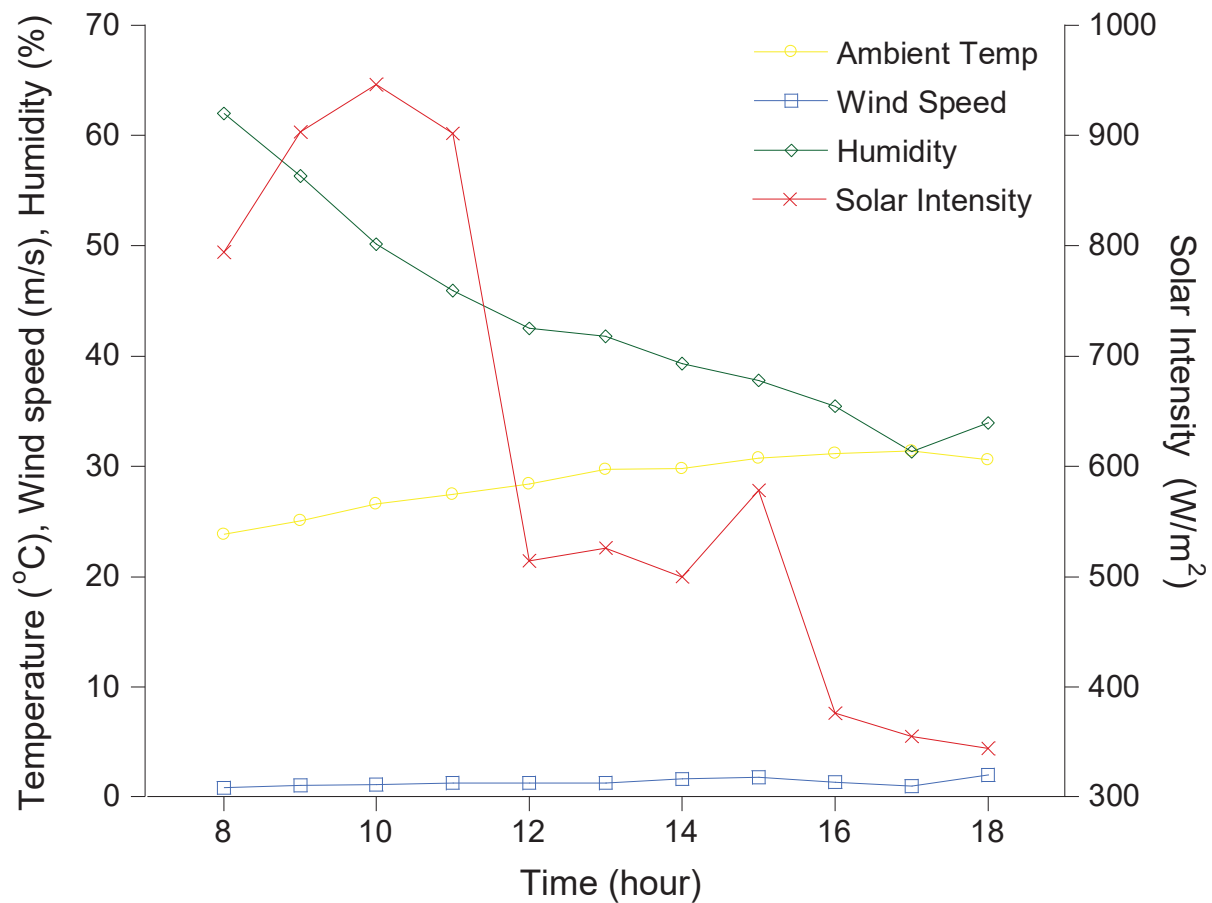


**Figure 5.3:** Typical static displacement resultant

### 5.3 Weather Data Analysis

Weather data variation for the first day of the year being 1<sup>st</sup> January 2017 was examined to determine the influence of various parameters such as solar intensity, ambient, wind speed and humidity exhibit on each other and the effect on the system as shown in **Figure 5.4**. Based on the chosen day of the year, the ambient temperature varied between 23.8 and 31.41 °C as shown in **Table 5.4**. The change in direct solar intensity with time of the day is shown in **Figure 5.5**. From the figures, an extreme fall in solar intensity was observed at about 11:00 a.m. This significant change could be due to the prevailing cloud conditions. The peak solar intensity of  $\sim 946 \text{ W/m}^2$  was experienced at about 10:00 a.m., while the minimum solar intensity of  $\sim 344 \text{ W/m}^2$  was observed at 18:00, despite the ambient temperature still increasing as the day

progressed. The average relative humidity and wind speed for the day are respectively 43.36% and 1.33 m/s.

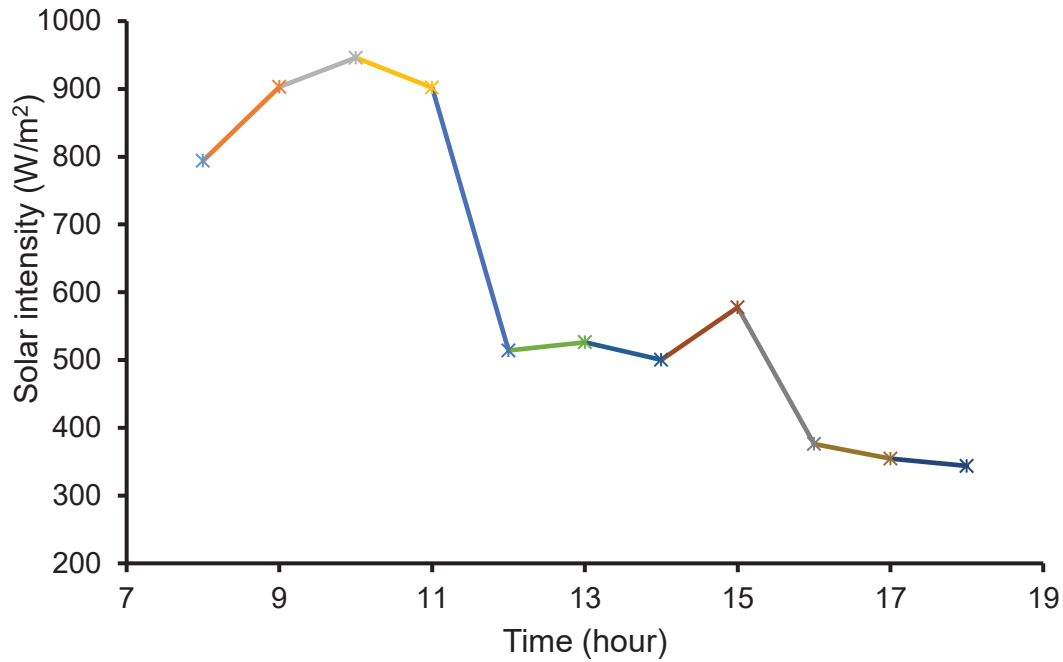


**Figure 5.4:** Change in wind speed, humidity and ambient temperature with a corresponding change in time

All these parameters have a combined direct impact on the performance of the system. The relative humidity was observed to progressively decrease as the ambient temperature increased. This is because the air becomes dry as the day warms up. Based on the wind speed shown in **Table 5.4**, there is little or no observed effect on the system due to the level of insulation for the piping network.

**Table 5.4:** Daily weather data for 01, January 2017

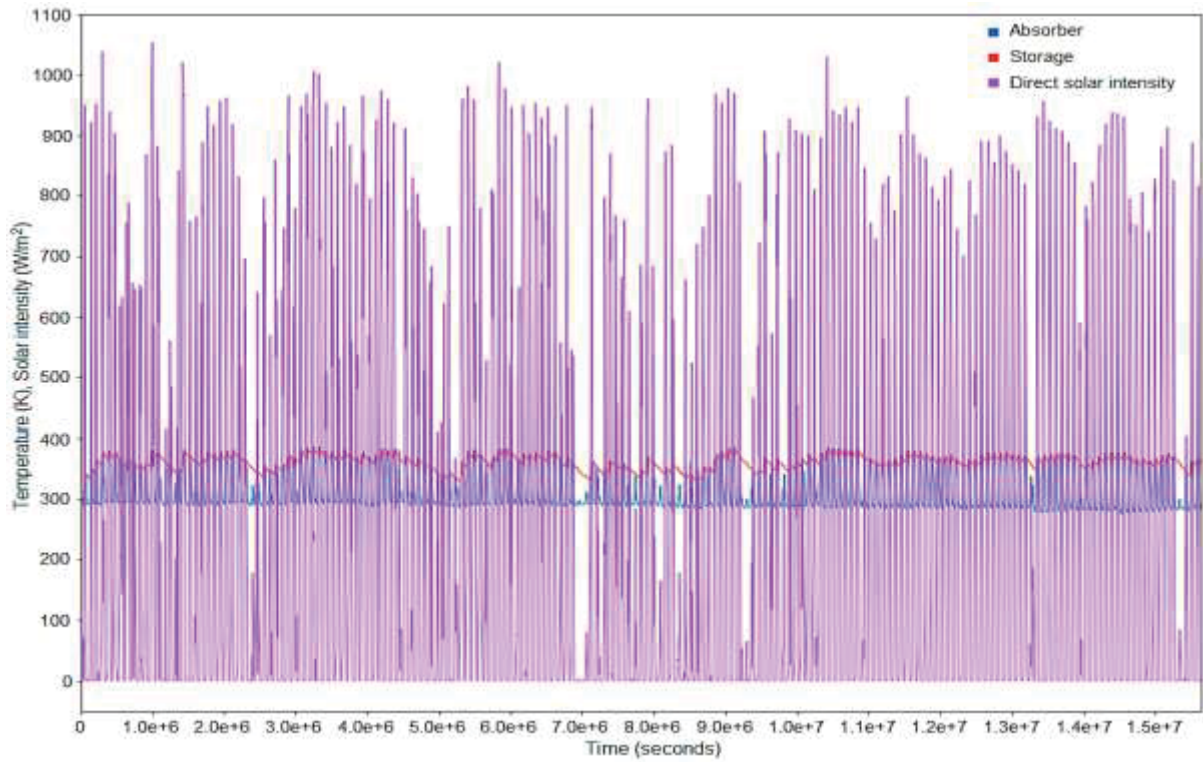
<b>Time (hour)</b>	<b>Ambient Temperature (°C)</b>	<b>Wind Speed (m/s)</b>	<b>Humidity (%)</b>	<b>Solar intensity (W/m<sup>2</sup>)</b>
8:00	23.8	0.867	62	793.9783
9:00	25.08	1.028	56.31	903.0069
10:00	26.58	1.124	50.17	946.0573
11:00	27.43	1.306	45.9	901.878
12:00	28.44	1.287	42.5	514.106
13:00	29.74	1.243	41.81	526.147
14:00	29.76	1.641	39.31	500.2254
15:00	30.7	1.794	37.78	577.7843
16:00	31.16	1.378	35.44	376.0946
17:00	31.41	1.007	31.32	354.5276
18:00	30.61	2.007	33.89	343.7509



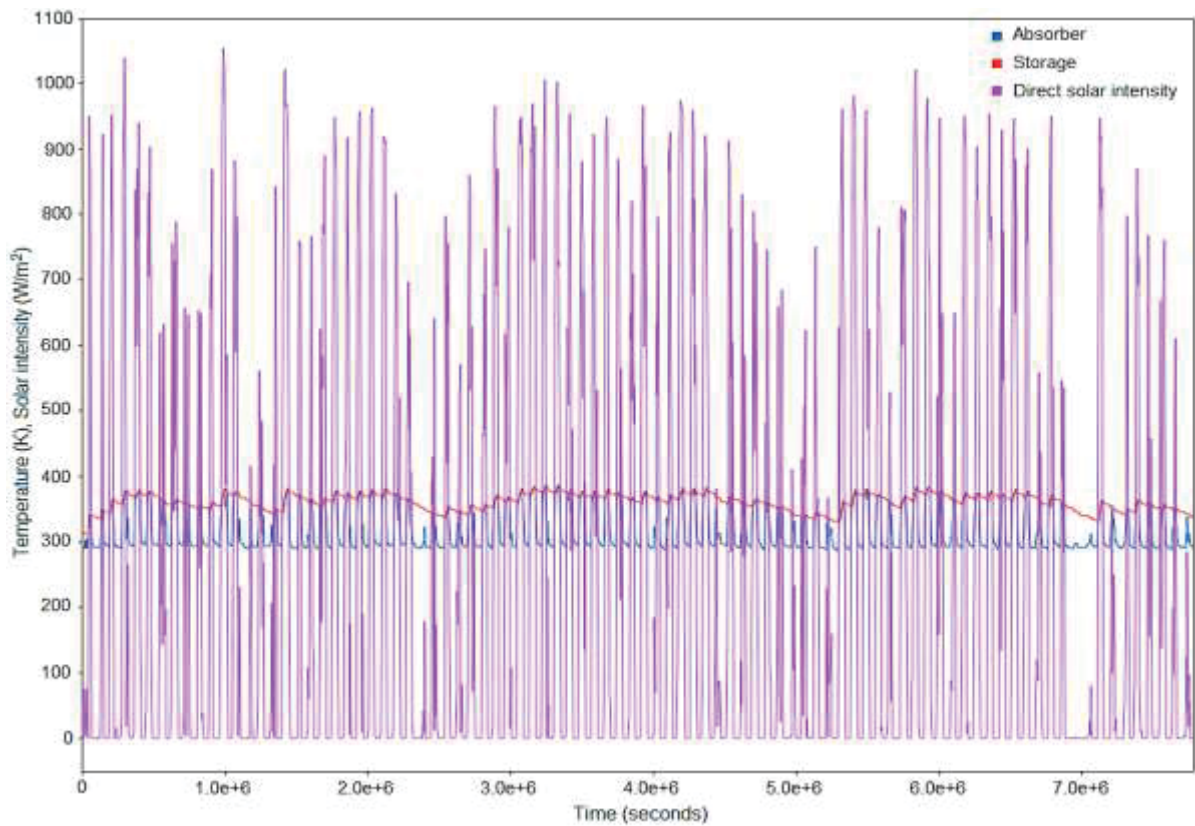
**Figure 5.5:** Solar intensity variation with time of the day

#### 5.4 Performance Evaluation of the Model

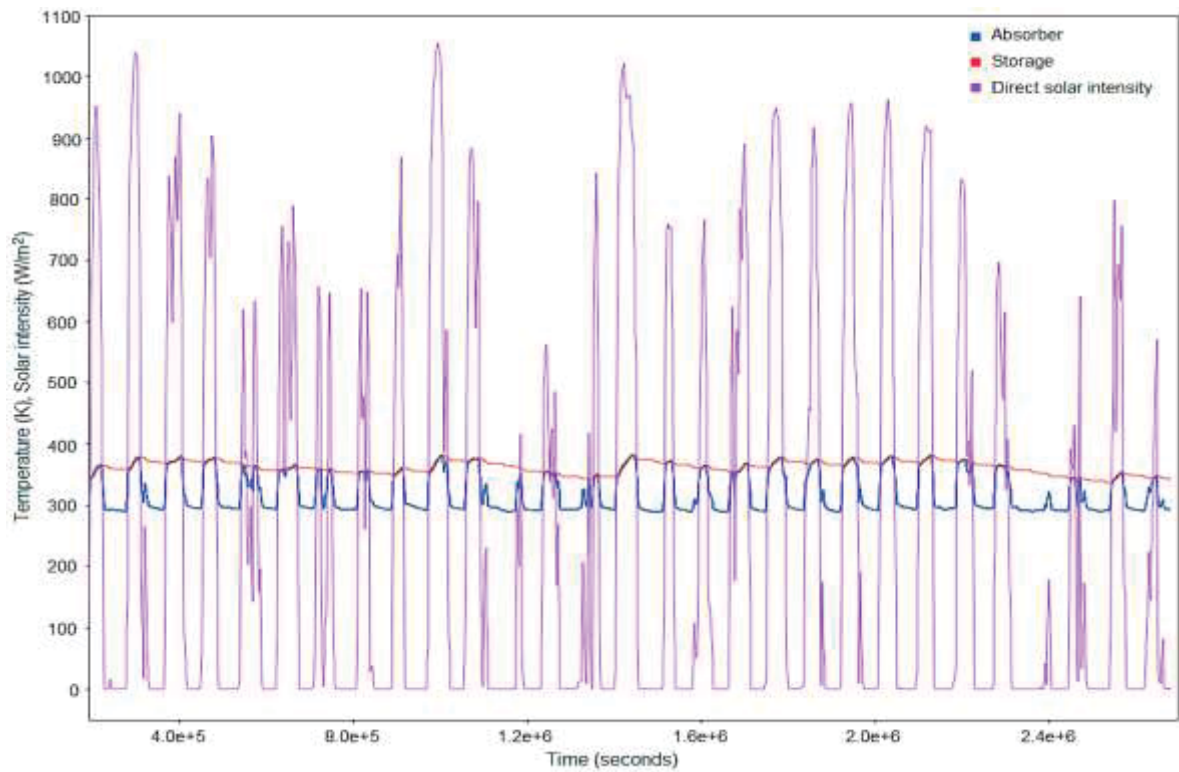
The absorber output temperature and the storage tank temperature based on the solar intensity received by the solar collector is shown in **Figures 5.6 – 5.8**. These figures are for six months, three months, and one month respectively. From the figures, it was observed that as the solar intensity increased, there was a corresponding increase in the absorber and storage tank temperature. The final model was an improvement of several models. The model is representative of all the variables, which are present in the system. This was done to see how the variables affect the global behaviour of the system. As shown in **Figures 5.6 – 5.8**, the global system time response is responding rapidly. Data with smaller timestamps than 1 hour can be used. However, this will result in increased computation time. The corresponding changes in the absorber and storage tank temperature are proof that the model performs excellently well based on the weather data that was fed into the model.



**Figure 5.6:** Influence of solar intensity on the absorber and storage temperature for six months (January–June 2015)

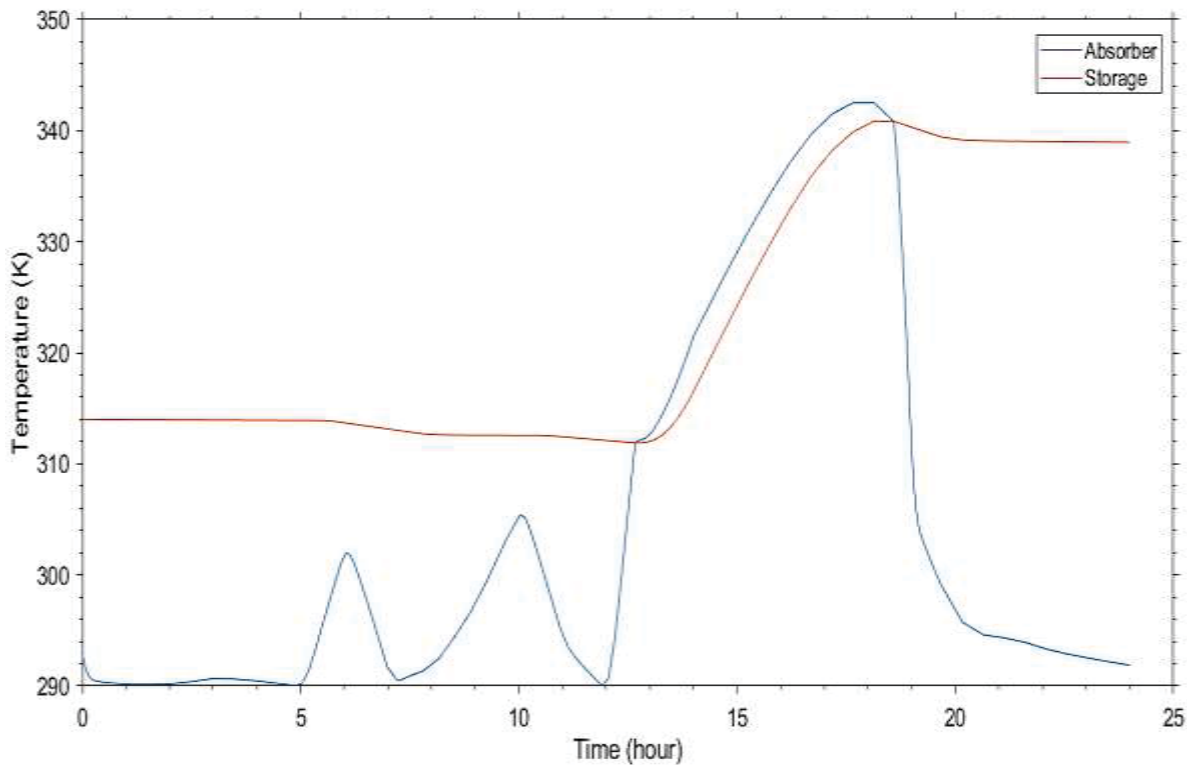


**Figure 5.7:** Influence of solar intensity on the absorber and storage temperature for three months (January–March 2015)



**Figure 5.8:** Impact of solar intensity on the absorber and storage temperature for one month (January 2015)

To facilitate a clearer understanding of the effect, which the changes in solar intensity have on absorber and storage temperature, a one-day simulation was made as shown in **Figure 5.9**. Furthermore, the influence of direct solar intensity and ambient temperature on the absorber and storage tank temperature for each month in 2019 are shown in **Appendix 6**. From the figures in **Appendix 6**, it was observed that the values of the absorber and storage tank temperature vary per month based on the amount of direct solar intensity received. The changes in the weather season were also observed to have an impact on the outcome of the overall system temperatures. These results were anticipated because each weather season is characterised by different factors such as rain, cloud, sunshine, wind, and humidity. The influence of various seasons on the absorber and storage tank temperature is discussed in detail in section 5.4.



**Figure 5.9:** Impact of solar intensity on the absorber and storage temperature for one day (1 January 2015)

Weather data for five years, three years and one year were fed into the model to observe the response of the system over extended periods. **Appendices 7–9** show the influence of the weather data which were fed into the model on the absorber and storage temperature for five years, three years and one year, respectively. Thus, **Table 5.5** shows the minimum, mean and maximum temperature for the absorber and storage tank for the five-year, three-year, and one-year durations, which were considered. This result shows that the system will keep performing well provided all the necessary parameters are functioning optimally. The factors which could affect the performance of the system are cloud sky, shadow, dust and dirt covering or settling on the surface of the collector (mirror). The challenge of dust and dirt settling on the surface of the collector can be resolved simply by washing the surface periodically. On the other hand, the casting of shadows on the parabolic solar collector can be prevented by installing the system at a location void of obstructions between the sun



and the parabolic trough solar collector. In order to avoid shadows, most solar power plants using solar concentration technology have the solar field in an open land far from buildings and any other forms of obstruction.

**Table 5.5:** Statistical data for absorber outlet temperature and storage tank temperature for a period of 5, 3 and 1 year(s)

Measured variable	Absorber Temperature (K)	Storage temperature (K)
<b>Five years' data (2015-2019)</b>		
Minimum	275.46 (2.46)	311.93 (38.93)
Maximum	397.04 (124.04)	396.25 (123.25)
Mean	329.45 (56.45)	362.36 (89.36)
Standard deviation	32.00	13.20
<b>Three years' data (2015-2017)</b>		
Minimum	276.68 (3.68)	311.93 (38.93)
Maximum	397.04 (124.04)	396.25 (123.25)
Mean	329.10 (56.10)	361.59 (88.59)
Standard deviation	31.61	13.14
<b>One year's data (2015)</b>		
Minimum	276.68 (3.68)	311.93 (38.93)
Maximum	394.46 (121.46)	393.76 (120.76)
Mean	329.54 (56.54)	362.63 (89.63)
Standard deviation	31.60	11.83

The values in parentheses are the temperature in °C

## 5.5 System Performance During the Four Weather Seasons in South Africa

South Africa as a country in Africa is characterized by four different weather seasons, unlike most African countries. **Table 5.6** shows the various weather seasons (summer,



autumn, winter, and spring) and their duration for the year. The parabolic trough solar collector performance for the various weather seasons was analysed in order to verify the impact of seasonal changes on the performance of the system. Each of the weather seasons comes with unique challenges. These challenges range from thunderstorms, cloudiness and sunshine to snow. Therefore, the performance of the system depends significantly on the weather conditions. The impact of the various weather seasons is discussed in the following sub-sections. The weather data used were obtained from the weather station at the University of Pretoria, South Africa (see the link to different weather stations in South Africa and some neighbouring countries: <https://sauran.ac.za/>).

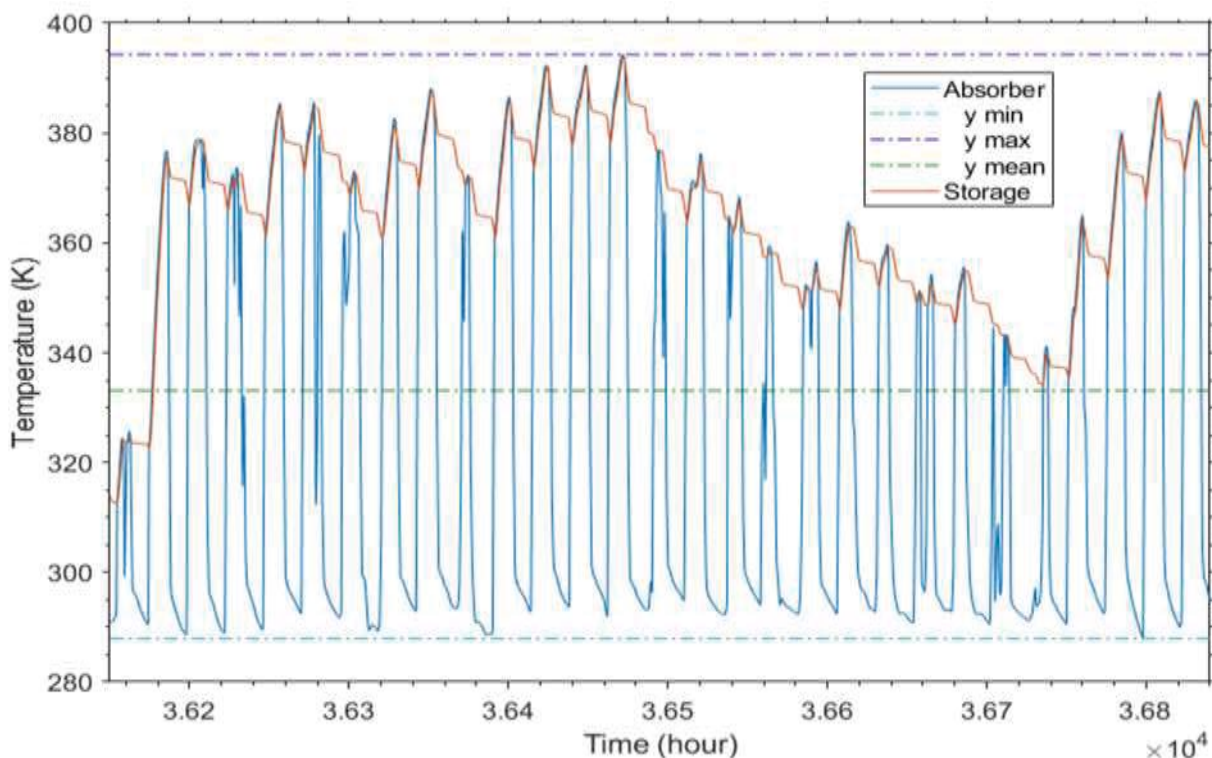
**Table 5.6:** Periods of various weather seasons in South Africa.

([www.photodestination.co.za/](http://www.photodestination.co.za/))

Season	Duration	Comment
Autumn	Mid-February to April	Slight rainfalls are experienced over the entire country with warm weather.
Winter	May to July	Characterised by higher-lying areas with sunny, dry, chilly days and frosty nights.
Spring	August to mid-October	The plains are covered with plants in an iridescent mat of flowers.
Summer	Mid-October to mid-February	This period is characterized by hot and sunny weather; frequently with afternoon rainstorms, leaving a warm and uniquely African scent in the air.

### 5.5.1 Autumn

The first season being discussed is autumn which occurs from mid-February to April. In order to understand how the season affects the performance of the system, the full duration of the season was analysed and presented in **Figure 5.10**. Based on the period under consideration and the solar collector design, the observed minimum, maximum and mean temperatures for the absorber are 287.96, 394.31 and 333.08 K respectively, with a standard deviation of 15.83. The corresponding minimum, maximum and mean temperatures of the storage tank are 312.68, 393.90 and 362.96 K respectively, with a standard deviation of 8.78. As winter approached, both the temperature of the absorber and the storage tank gradually reduced. This shows that the direct solar irradiation is lower, hence, the decrease in the temperature of the system. **Appendix 10** shows the relationship between solar intensity and temperature.



**Figure 5.10:** Absorber and storage tank temperature during autumn. Note: y min, y max and y mean represent the minimum, maximum and mean temperatures respectively

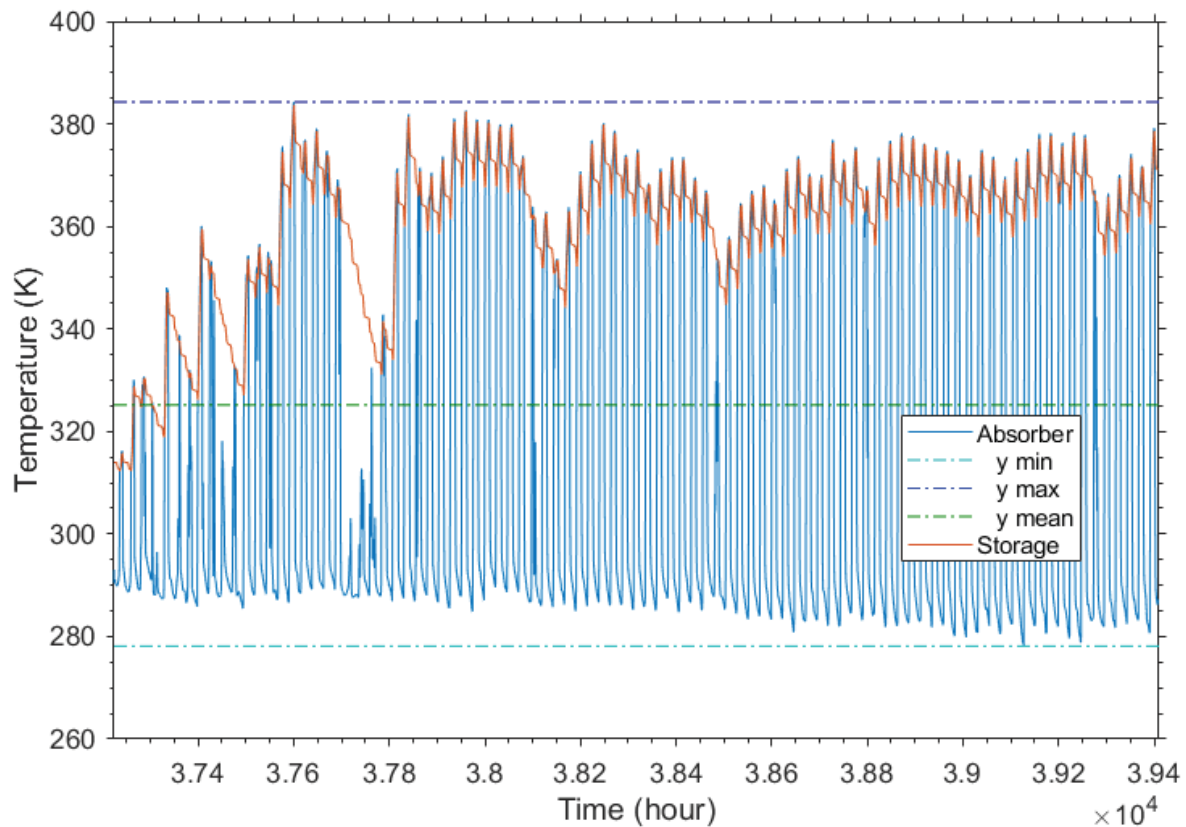
### 5.5.2 Winter

Winter is the coldest season of the year and it is characterised by higher-lying areas with sunny, dry, crisp days and cold nights. According to [www.photodestination.co.za/](http://www.photodestination.co.za/), winter occurs from May to July each year in South Africa. Since the parabolic trough solar collector is to be used throughout the entire year, there is a need to examine the performance in the winter season. The peak of the winter season is usually in May and occasionally in June. Thus, the season showed much impact on the system's performance. The system performance for the entire duration of winter is presented in **Figure 5.11** while the relationship between solar intensity and various temperatures is shown in **Appendix 11**. Based on the data presented in **Table 5.7**, it was observed that the minimum, maximum and mean temperatures of the absorber and the storage tank decreased. The decrease in temperature was due to the decrease in direct solar intensity, which is an expected result for the system. In order to ensure the availability of hot water through the winter season, an auxiliary heating element can be introduced inside the hot water storage tank. In the subsequent section of the thesis, the possible cost incurred on electricity is discussed.

**Table 5.7:** Statistical data for absorber outlet temperature and storage temperature during winter.

Measured variable	Absorber Temperature (K)	Storage temperature (K)
Minimum	278.12 (5.12)	312.25 (39.25)
Maximum	384.27 (111.27)	383.72 (110.72)
Mean	325.18 (52.18)	360.00 (87.00)
Standard deviation	16.37	7.31

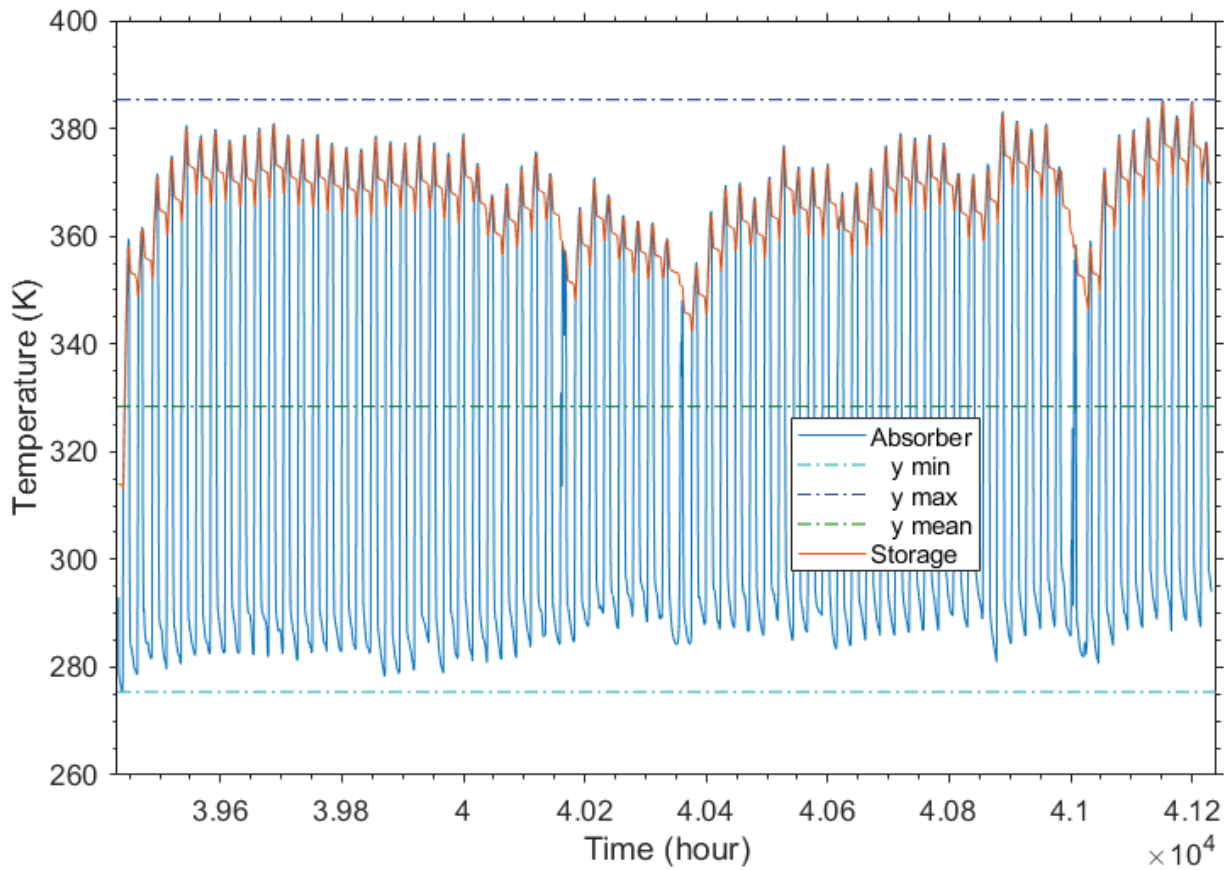
The values in parentheses are the temperature in °C



**Figure 5.11:** Absorber and storage tank temperature during winter. Note: y min, y max and y mean represent the minimum, maximum and mean temperatures respectively

### 5.5.3 Spring

Spring is another weather season in South Africa, which occurs from August to mid-October annually. This season is characterised by plains covered with plants in a colourful mat of flowers. Based on the period been considered and the solar collector design, the observed minimum, mean and maximum temperatures for the absorber are 275.42, 328.40 and 385.34 K, respectively, with a standard deviation of 17.20 as shown in **Figure 5.12** and **Appendix 12**. The corresponding minimum, mean and maximum temperatures of the storage tank are 313.02, 365.64 and 384.94 K respectively, with a standard deviation of 4.84. Observing the mean temperature for the spring season, there is a good possibility of getting the required hot water throughout the season. This ascertains that the system is performing significantly well.



**Figure 5.12:** Absorber and storage tank temperature during spring. Note: y min, y max and y mean represent the minimum, maximum and mean temperatures respectively

#### 5.5.4 Summer

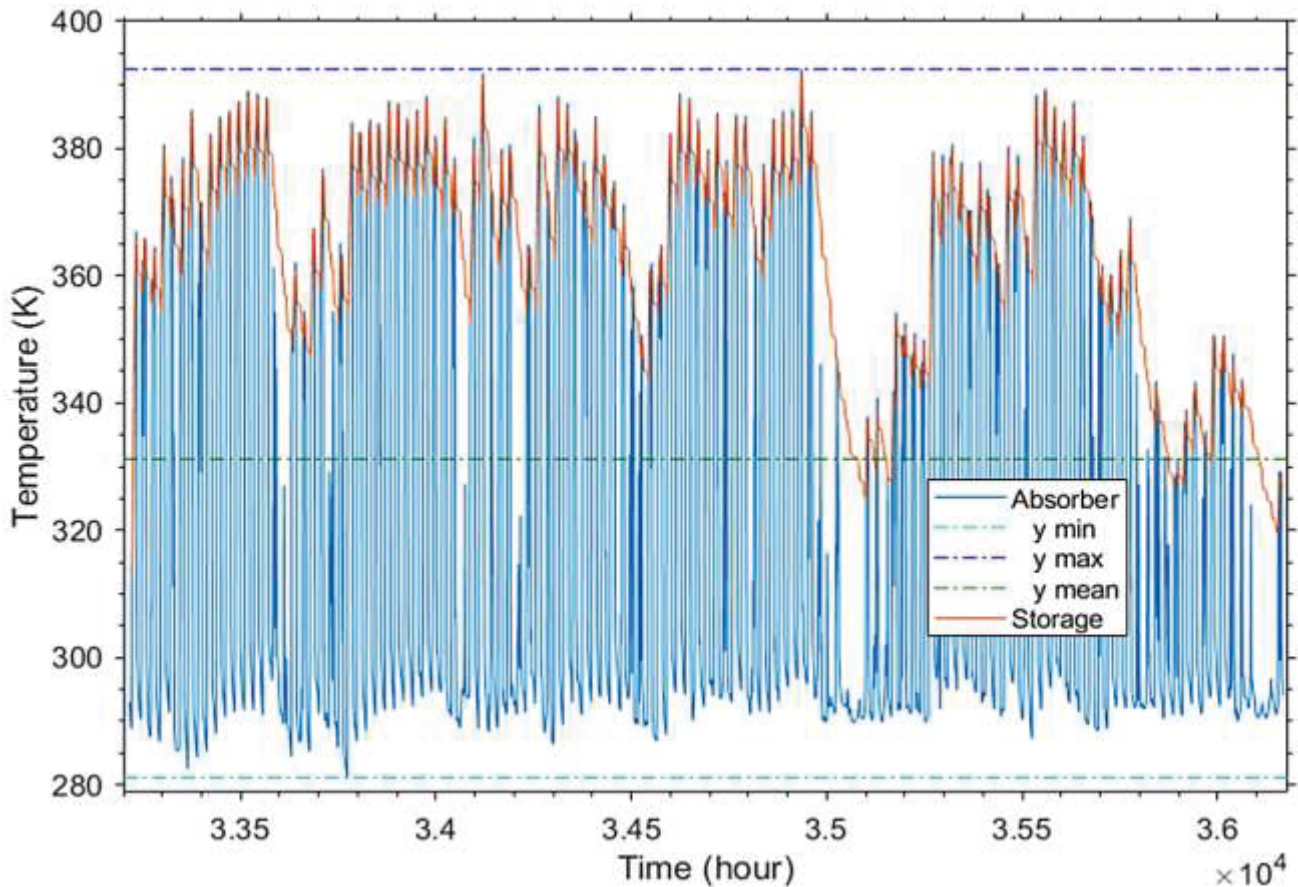
Summer is the hottest season of the year and it is characterised by sunny weather with frequent afternoon thunderstorms, leaving a warm and uniquely African scent in the air. The period of summer is between mid-October of the previous year to mid-February of the following year. Based on the weather data history, which was considered, the data for the year 2018/2019 was fed into the model to evaluate the performance of the system for a complete summer season. The system performance for the entire duration of summer is shown in **Figure 5.13**, while the relationship between the solar intensity and the various temperatures is shown in **Appendix 13**. Based on the data presented in **Table 5.8**, it was observed that the minimum, mean

and maximum temperatures of the absorber and the storage tank during spring and summer are significantly identical with a maximum difference of 6.78 °C. This closeness in temperature values could be due to the similarity in weather season. This result is expected based on the similarities in the solar intensity characteristics of both seasons.

**Table 5.8:** Statistical data for absorber outlet temperature and storage temperature during summer

Measured variable	Absorber Temperature (K)	Storage temperature (K)
Minimum	281.16 (8.16)	313.63 (40.63)
Mean	331.19 (58.19)	363.71 (90.71)
Maximum	392.51 (119.51)	391.72 (118.72)
Standard deviation	15.79	7.94

The values in parentheses are the temperature in °C



**Figure 5.13:** Absorber and storage tank temperature during summer. Note: y min, y max and y mean represent the minimum, maximum and mean temperatures respectively

## 5.6 Effect of Solar Radiation on Absorber Outlet Temperature and Storage Tank Temperature

The findings have established that the overall system performance of the parabolic trough solar concentrator is a direct reflection of the amount of solar radiation it can receive. The absorber output temperature and storage tank temperature vary based on the amount of direct solar intensity captured by the solar collector per time. To verify the influence of solar intensity, parameters such as fluid mass flow rate, inlet fluid temperature, collector aperture area, and absorber tube diameter were maintained at constant values. For an effective solar collector aperture area of  $6 \text{ m}^2$ , a flow rate of  $0.02 \text{ kg/s}$  and varying solar intensity values, the corresponding absorber output temperature and storage temperature are shown in **Table 5.9**.

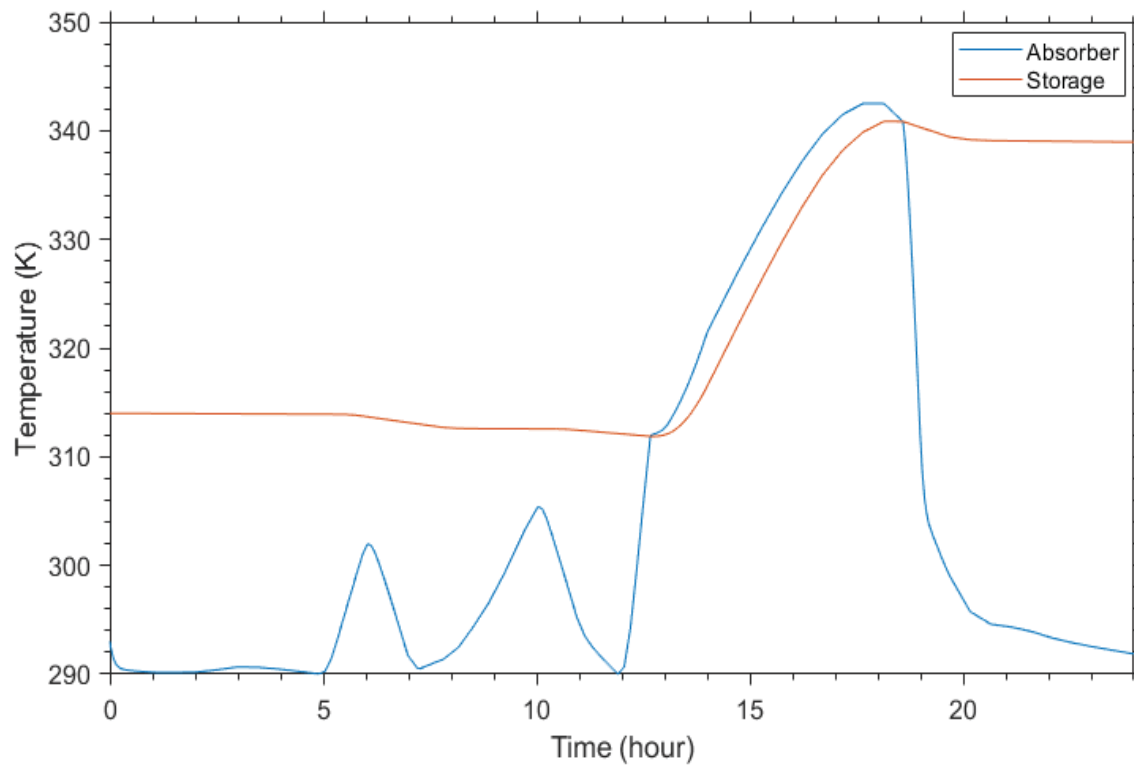
**Table 5.9:** Effect of solar intensity on absorber outlet temperature and storage tank temperature

Time (hour)	Solar intensity (W/m <sup>2</sup> )	Absorber temperature (K)	Storage temperature (K)
8:00	9.06	292.0	313.0
9:00	36.57	298.0	313.0
10:00	77.69	305.5	313.0
11:00	4.84	294.5	312.5
12:00	0.70	291.0	312.0
13:00	198.82	313.0	312.0
14:00	924.80	321.0	316.0
15:00	956.80	329.0	324.0
16:00	936.52	336.0	331.0
17:00	842.90	341.0	337.0
18:00	647.16	342.5	341.0
19:00	43.85	312.0	340.5

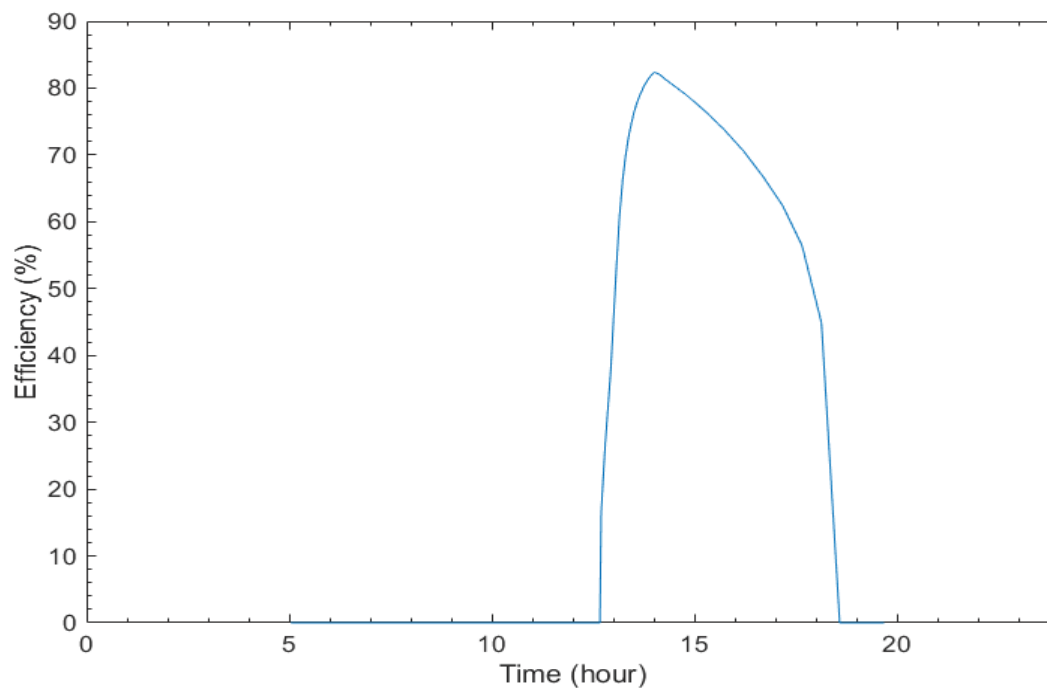
Based on the observed influence of solar intensity, the water passing through the absorber pipe starts to warm up when the solar intensity is between 100 and 300 W/m<sup>2</sup>. For water temperature difference between 60 and 90 °C, the solar intensity was between 500 and 900 W/m<sup>2</sup>. With due consideration to the selected collector size, a solar intensity above 950 W/m<sup>2</sup> will cause the water to boil and evaporate if exposed directly to the atmosphere. **Figure 5.14** shows the impact of solar intensity on absorber outlet temperature and storage tank temperature, while **Figure 5.15** shows the system efficiency for the solar absorber. The efficiency of the absorber tube is good for the



nature and choice of application of the system. The maximum absorber efficiency is approximately 82%.



**Figure 5.14:** Influence of solar intensity on absorber output and storage tank temperature



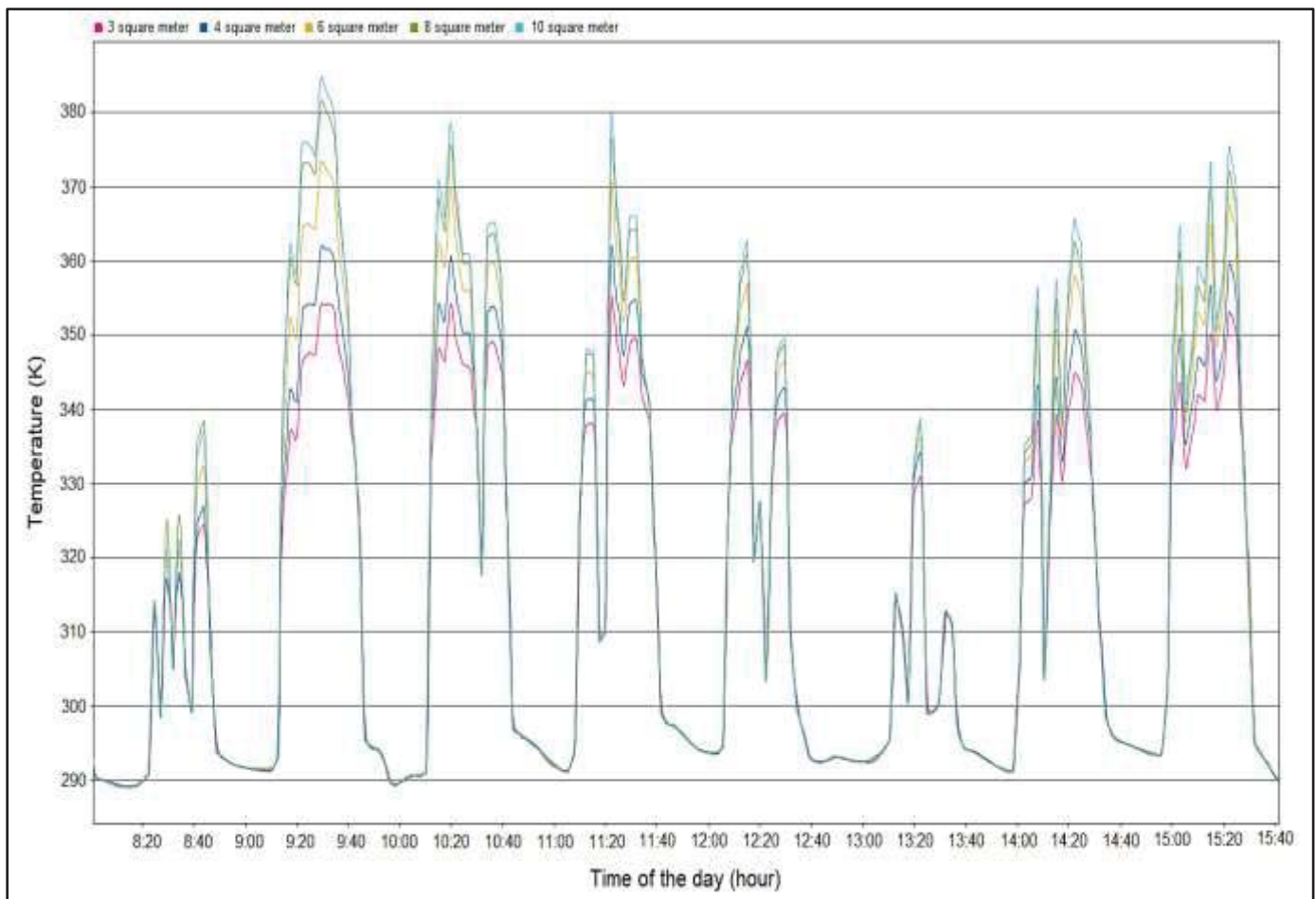
**Figure 5.15:** Influence of solar intensity on absorber efficiency

## 5.7 Collector Aperture Area

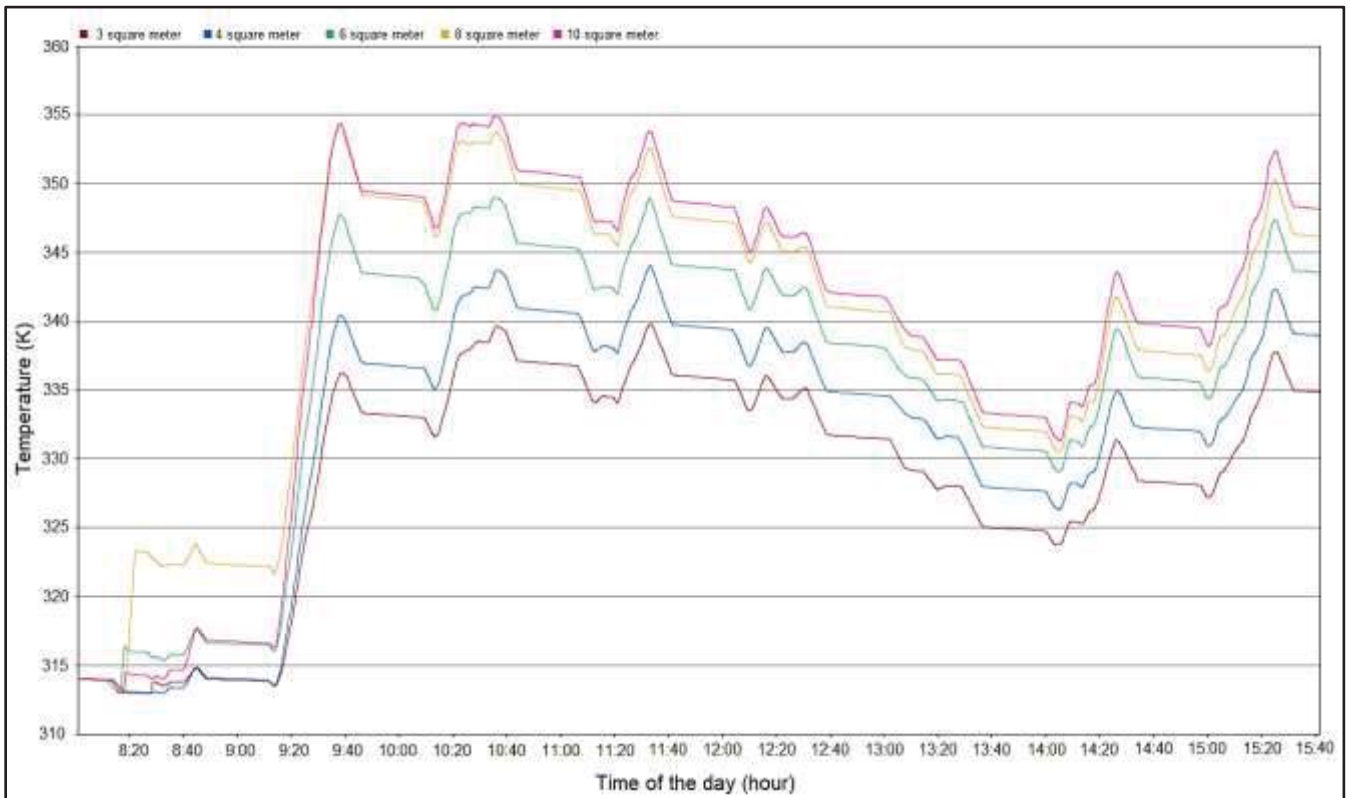
The collector aperture area (also known as the solar concentrating area) was proven to have much effect on the absorber outlet temperature and ultimately on the storage tank temperature. Increasing or decreasing the area has a direct impact on the system's outlet temperature. To verify the impact of the collector aperture area in this research study, the solar collector aperture area was varied from 3, 4, 6, 8 to 10 m<sup>2</sup>, and it is operated as a single trough solar collector. **Table 5.10** shows the parameters that were imputed into the model. The model was made to run between the hours of 8:00 and 16:00. The effect of the solar collector aperture areas is shown in **Figures 5.16 and 5.17**. From the Figures, it is visible that increasing the collector aperture area led to an increase in the outlet temperature of the absorber and storage tank temperature. For the aperture area range, the outlet temperature between the smallest and largest area is approximately 30 °C. Increasing the collector aperture area above 6 m<sup>2</sup> will cause the water in the evacuated tube to evaporate if exposed to the atmosphere. A similar observation was reported by Li and Wang (2006). Based on the mass flow rate, solar collector aperture area, solar intensity and the effective solar irradiation, the total volume of water per day through the absorber tube is approximately 490 litres. **Figure 5.18** shows the interaction between the ambient temperature, absorber temperature and storage temperature based on the 6 m<sup>2</sup> aperture area. From the figure, the ambient, absorber and storage temperatures are observed to have a direct relationship. In other words, an increase in one will lead to an increase in the other.

**Table 5.10:** Input data for modelling the influence of increasing solar concentration area

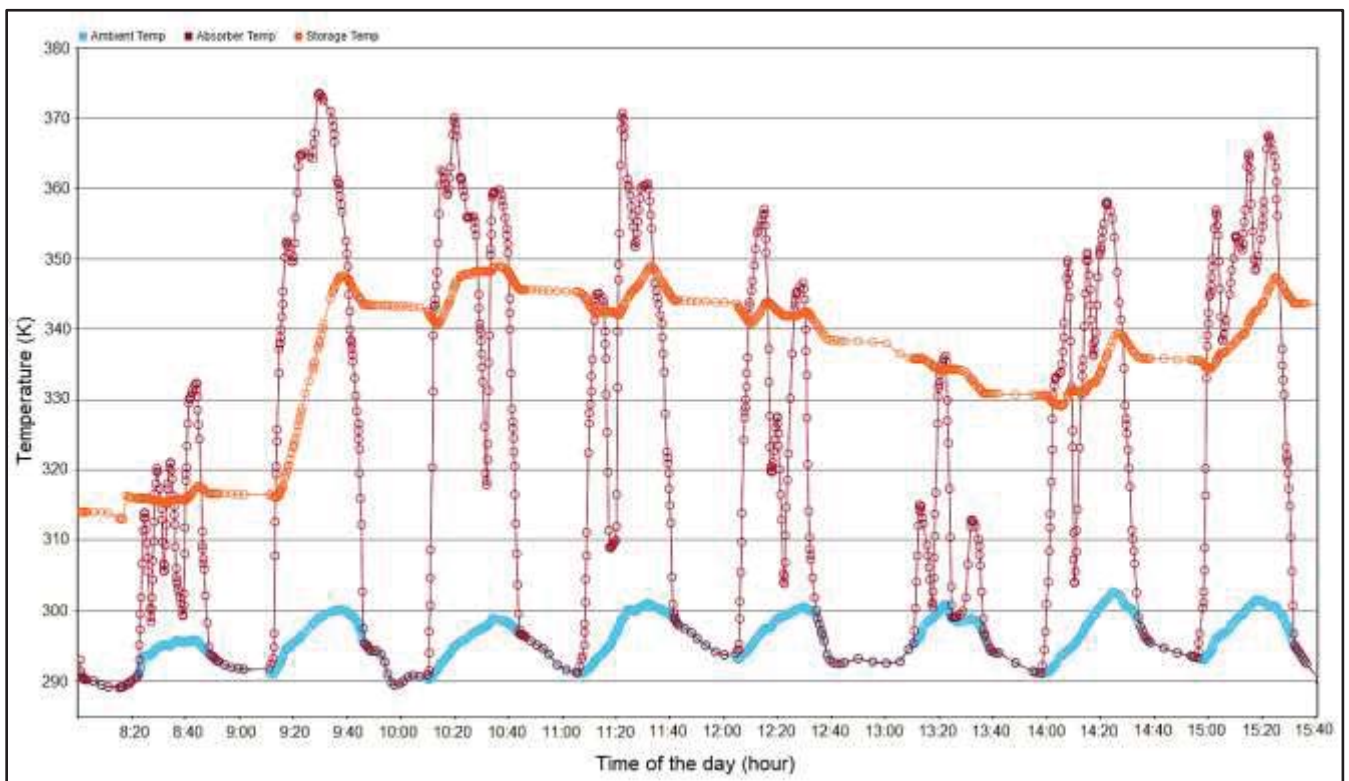
Mass flow rate (kg/s)	Solar intensity (W/m <sup>2</sup> )	collector aperture area (m <sup>2</sup> )	Input temperature of fluid (K)
0.02	900	3.0	293.0
0.017	900	4.0	293.0
0.017	900	6.0	293.0
0.017	900	8.0	293.0
0.017	900	10.0	293.0



**Figure 5.16:** Effect of increasing collector aperture area on absorber outlet temperature



**Figure 5.17:** Effect of increasing collector aperture area on storage tank temperature



**Figure 5.18:** Interaction between the ambient, absorber and storage temperature for an aperture area of 6 m<sup>2</sup>

## 5.8 System Evaluation of Additional Cost of Electricity for Heating During Low Solar Intensity

The evaluation of additional cost on electricity for the global system was carried out for five years. The five years were selected in order to determine how much additional cost will be spent on electricity for the developed model period, which is five years. To achieve this, the electricity tariff from the City of Tshwane (CoT), South Africa was obtained. Furthermore, the peak, standard, and off-peak period tariff rates were obtained. According to the CoT, the tariff used for the study took effect from 7<sup>th</sup> August 2019 in accordance with the National Energy Regulator of South Africa (NERSA). The used tariffs are based on the period of the day and the season of the year as shown in **Table 5.11**. From the table, it was observed that the period in which an additional heating element may be required is during the period with the lowest electricity tariff. This is because the historical weather data that was used started from 00:00 hour of the day. Therefore, the additional cost of electricity will be minimal because, during the day, there is enough solar intensity to heat the water.

**Table 5.11:** Varying electricity tariffs showing the effective periods. Adapted from (City-of-Tshwane, 2019/20)

Tariff type	Days of the week	Period	Cost (c/kWh)
Peak	Weekdays	06:00-09:00 and 17:00-19:00	158.74
	Saturday	None	–
	Sunday	None	–
Standard	Weekdays	09:00-17:00 and 19:00-22:00	99.97
	Saturday	7:00-12:00 and 18:00-20:00	99.97
	Sunday	None	–
Off-peak	Weekdays	22:00-06:00	70.79
	Saturday	12:00-18:00 and 20:00-07:00	70.79
	Sunday	00:00-24:00	70.79

The total additional electricity cost was evaluated by feeding the CoT approved tariffs and the rate as per the periods of the day into the model. The robustness of the model made it easy to determine when exactly additional power will be required and the amount of electrical power required. Based on the aperture area, tracking mechanism, flow rate, storage tank size, dimension of the absorber and the initial conditions, the system only requires electrical energy for the initial operation of the system. Thereafter, the system is self-sufficient for the remainder of the 5 years. The total time duration required to raise the temperature to a minimum of 50 °C is approximately 14 hours 25 minutes. From the system analysis, the total amount that will be spent on electricity for 5 years is ZAR14.21 provided the system remains in good working condition. There is a possibility that the system may have been over-designed. Therefore, the aperture area was varied to determine the impact it has on the use of additional electric power. The results of these findings are presented in **Table 5.12**. Based on the obtained results, it was observed that the size of the solar collector had minimal impact on the additional electrical power used.

**Table 5.12:** Impact of aperture area on additional cost of electricity

Aperture area	Heating time*	Additional cost of electricity
(m <sup>2</sup> )	(hour)	(ZAR)
3.0	14.94	14.93
4.0	14.94	14.89
6.0	14.42	14.21
8.0	14.31	14.13
10.0	14.10	14.00

\*Time duration to reach the minimum storage tank temperature

## **5.9 Conclusion**

Solar energy appears to have great promises and is the most widely researched renewable energy resources. The results that were discussed in this chapter highlight the merits of using solar energy as a means of heating water for domestic applications. This process also protects the environment through the reduction of carbon dioxide emission into the atmosphere. The results of the model were discussed extensively in this chapter. Based on the discussion, the collector aperture area proved to be adequate to capture the required solar intensity to heat and maintain the temperature of the storage tank at the desired temperature. The model performs excellently well based on the weather data that was available for Pretoria in South Africa. The behaviour of the system was observed to vary per month and season due to the changing direct solar intensity. The model behaviour for the four weather seasons in South Africa was analysed. This was done to determine the performance of the system during these seasons. The additional cost on electricity needed for the period where there is no adequate solar irradiation was evaluated for five years.

## CHAPTER SIX

### 6.0 CONCLUSION AND RECOMMENDATIONS

#### 6.1 Summary

Various energy sources, methods, and techniques have been used for many years to heat water in domestic and commercial buildings. The known sources for water heating include electrical energy and solar irradiation energy in the urban regions or the burning of wood in rural areas. The methods/techniques can either be the electrical heating element, solar concentrators, flat plate collector, evacuated tube collector, etc. The purpose of the study was to determine further ways of improving the system performance by using solar energy and solar concentrator techniques for heating water. Furthermore, the study proposed an alternative material for the hot water storage tank.

The solar collector's supporting frame was designed and analysed using Solidworks®. The forces acting on the structural members were simulated to determine the capacity of the frame to sustain the load and the possible regions in which a structural failure in the supporting frame could occur during operation.

The system performance was modelled using Matlab Simulink®, where five years of historical weather data for Pretoria, South Africa was fed into the model. The historical weather data was obtained from the weather station at the University of Pretoria, South Africa. Based on the weather data input, the absorber outlet temperature and the storage tank temperature were obtained and discussed. Other things that were studied were the influence of collector size, the system behaviour during the different weather seasons in South Africa and the additional cost of electricity for the periods where there is no adequate solar intensity.



## 6.2 Conclusion

The research was conducted with the aim of using a parabolic trough solar collector to heat water and to identify possible improvements to the performance of the system. Based on the review of the literature performed as explained in Chapter 2 of this report, there is a growing demand for alternative energy sources due to global increasing population and the environmental impact caused by a large dependence on fossil fuel-based energy generation. Solar energy appears to have the greatest promise and is the most researched alternative energy source.

It was discovered that evacuated glass tubes have been used for solar water heating. These evacuated glass tubes can be damaged during thunderstorms with hailstone leading to high maintenance costs. Furthermore, limited research has been reported regarding system modelling using historical weather to analyse the performance of parabolic trough solar collectors for water heating in domestic and commercial buildings. The study sought to address this gap.

The obtained results from this study highlight the merits of using solar energy as a means of heating water for domestic applications. On one hand, the environment is preserved through the reduction of carbon dioxide (CO<sub>2</sub>) emission, which is a product of fossil fuel. On the other hand, the system behaviour in terms of performance, and the cost implication due to the use of alternative heat sources were analysed and improved. Based on the results obtained, the following conclusions were made:

- i. The designed structural frame can withstand the weight of the solar collector. Based on the finite element analysis, the yield strength, tensile strength, elastic modulus, and thermal expansion coefficient of the material were  $3.5157 \times 10^8 \text{ N/m}^2$ ,  $4.2051 \times 10^8 \text{ N/m}^2$ ,  $2 \times 10^{11} \text{ N/m}^2$ , and  $1.5 \times 10^{-5} \text{ K}^{-1}$  respectively. The total aperture area of the collector was  $6 \text{ m}^2$ , which was

adequate to produce the required volume of hot water needed daily. The collector aperture area proved to be adequate to capture the required solar intensity to heat and maintain the temperature of the storage tank at the desired temperature. The number of occupants in the building, the quantity of solar irradiation per time and the geographical location has a direct influence on the collector sizing.

- ii. A mini prototype controller system comprising of a rain sensor, temperature sensor, and solar tracker (also known as maximum peak power tracking (MPPT)) was developed using Arduino Uno as a microcontroller. The rain sensor detects rain droplets and sends a signal to the controller to close the collector. This protects the absorber (evacuated glass tube) from being damaged during thunderstorms with hailstones. The temperature sensor ensures the temperature of the storage tank is maintained. When the set temperature limit is reached, a signal is instantly sent to the controller to stop the pump from circulating the fluid flowing through the absorber and to also close the absorber cover. Lastly, the solar tracker helped to ensure that the solar concentrator is constantly facing the sun. This enables it to receive the highest power from the sun, which is required to heat the water.
- iii. The model responded rapidly based on the global system time and data that were fed to it. The corresponding changes in the absorber outlet temperature and storage tank temperature are proof that the model performs excellently well based on the weather data that was fed into the model. The behaviour of the system was observed to vary per month and season due to the changing direct solar intensity. From the model analysis for the year 2019, January has the highest direct solar intensity while May

2019, has the least solar intensity. Thus, the observed temperature difference for the absorber outlet temperature and storage tank temperature for both months.

South Africa as a country in Africa is characterised by four different seasons. From the obtained results, it was observed that the various weather seasons have varying impacts on the absorber outlet temperature and storage tank temperature. The average outlet temperature of the absorber in the order of magnitude was 333, 332, 328 and 325 K during the autumn, summer, spring and winter seasons respectively. Similarly, the average storage tank temperature in the order of magnitude was 366, 364, 363 and 360 K in spring, summer, autumn and winter, respectively.

In a view that the solar irradiation may not be adequate to provide the required hot water for the whole year, this means that additional heating sources may be required. Therefore, the study accounted for this and incorporated it into the designing of the model. From the observed results, using the City of Tshwane's Municipality electricity tariffs per billing system daily, the maximum additional cost on electricity is approximately ZAR15.00. Therefore, the system is self-sufficient for the evaluated five-year period provided the system remains in good working condition as a result of periodical system maintenance.

- iv. The use of polypropylene alongside other materials such as polyurethane, salt, and aluminium was suggested for a hot water storage tank. This was based on their inherent properties, which include good resistance to chemicals, good mechanical properties, lightweight properties, low thermal conductivity, recyclability and cost-effectiveness.

Based on the results originating from this research, the summary of conventional systems/models as against improvement made are shown in **Table 6.1**.

**Table 6.1:** Conventional systems/models and improvements made.

System	Conventional system/model	Improvement made
Parabolic collector system	<ul style="list-style-type: none"> <li>The evacuated glass tube is exposed to potential damages resulting from thunderstorms with hailstone.</li> <li>The hot water storage tank sometimes overheats due to excess or high temperature in the system.</li> </ul>	<ul style="list-style-type: none"> <li>Introduced a sliding cover to the parabolic collector.</li> <li>This cover is activated to close whenever there is rain and when the temperature in the storage tank goes above the set temperature for the system.</li> </ul>
Control system	<ul style="list-style-type: none"> <li>The existing models are designed to analyse weather data for typical days or months.</li> <li>Most of the existing models can only handle short-term simulation.</li> </ul>	<ul style="list-style-type: none"> <li>The model was designed for historical weather data.</li> <li>The model can be used to analyse historical weather data for a longer period.</li> </ul>
Storage system	<ul style="list-style-type: none"> <li>Hot water tank inner is made from either steel, aluminium, or glass.</li> <li>They don't have heat retaining and releasing mechanism.</li> </ul>	<ul style="list-style-type: none"> <li>Proposed the use of polymeric composite due to the good properties.</li> <li>Introduction of heat retaining and releasing material within the layers of the storage container.</li> </ul>
Integrated system	<ul style="list-style-type: none"> <li>Existing work focused on individual systems alone, either a solar collector or storage tank.</li> </ul>	<ul style="list-style-type: none"> <li>Overall system design and analysis were done to show how they depend on each other</li> <li>Making necessary improvements and adjustments needed for the system design and optimization is made possible.</li> </ul>

### **6.3 Contribution to the Body of Knowledge**

The current study contributed to the broader body of scientific knowledge in the following areas:

- ❖ New improved design for parabolic trough solar collector with the ability to protect the evacuated glass tube and regulate the temperature within the hot water storage tank.
- ❖ Proposed design of a laminated polymeric hybrid composite, which can serve as the hot water storage container.
- ❖ Development of a model that can accommodate and analyse five years of historical weather data rather than the usual typical days or months.
- ❖ Improved system-based analysis for an additional cost on electricity for five years, using the current Municipality electricity tariff.
- ❖ Systematic analysis of the behaviour of a combined integrated solar collector and hot water storage tank.

### **6.4 Recommendations for Future Work**

Extending the present research findings in this thesis will further improve the designs for solar concentrator technologies and solar water heating systems. Therefore, the following suggestions and recommendations are made to improve the overall system design, analysis and performance:

- ❖ The full additional electrical energy required to run the pump and the control system needs to be evaluated. This will give a clear view of the total possible running cost for the overall system.
- ❖ Life cycle analysis of the entire system based on the working conditions of the solar collector and the hot water storage tank.

- ❖ Design Engineers should try to optimise the system by varying the different variables in the model to know the optimum performance of the overall system.
- ❖ Building and testing a physical model based on the finding of this research to investigate the performance with respect to the model's predictions.

## REFERENCES

- Alternative Energy Tutorials. online: <http://www.alternative-energy-tutorials.com/solar-hot-water/parabolic-trough-reflector.html>. Accessed: 11/01/2017.
- ABD-UR-REHMAN, H. M. & AL-SULAIMAN, F. A. 2016. Optimum selection of solar water heating (SWH) systems based on their comparative techno-economic feasibility study for the domestic sector of Saudi Arabia. *Renewable and Sustainable Energy Reviews*, 62, 336-349.
- ABU-HAMDEH, N. H., ALNEFAIE, K. A. & ALMITANI, K. H. 2013. Design and performance characteristics of solar adsorption refrigeration system using parabolic trough collector: experimental and statistical optimization technique. *Energy conversion and management*, 74, 162-170.
- AHMAD, N. & DERRIBLE, S. 2018. An information theory based robustness analysis of energy mix in US States. *Energy Policy*, 120, 167-174.
- AL-HINTI, I., AL-GHANDOOR, A., MAALY, A., NAQEERA, I. A., AL-KHATEEB, Z. & AL-SHEIKH, O. 2010. Experimental investigation on the use of water-phase change material storage in conventional solar water heating systems. *Energy Conversion and Management*, 51, 1735-1740.
- ALAYDI, J. Y. 2014. Design of a parabolic solar collector system for seawater desalination in Gaza. *Desalination and Water Treatment*, 52, 2502-2511.
- ALLEN, J. T., GIAMMANCO, I. M., KUMJIAN, M. R., JURGEN PUNGE, H., ZHANG, Q., GROENEMEIJER, P., KUNZ, M. & ORTEGA, K. 2020. Understanding hail in the earth system. *Reviews of Geophysics*, 58, 1-49.
- ALOTAIBI, S., ALOTAIBI, F. & IBRAHIM, O. M. 2020. Solar-assisted steam power plant retrofitted with regenerative system using Parabolic Trough Solar Collectors. *Energy Reports*, 6, 124-133.

- ALTERNATIVE\_ENERGY\_TUTORIALS. *Alternative Energy Tutorials*. online: <http://www.alternative-energy-tutorials.com/solar-hot-water/parabolic-trough-reflector.html>. (Accessed date: 11/01/2017) [Online]. [Accessed].
- APRICUS. 2017. Apricus solar hot water. Online: [http://www.apricus.com/html/solar\\_collector.htm#.WHOYAn22qkl](http://www.apricus.com/html/solar_collector.htm#.WHOYAn22qkl). (Accessed date: 09/01/2017).
- ARAÚJO, A. & SILVA, R. 2020. Energy modeling of solar water heating systems with on-off control and thermally stratified storage using a fast computation algorithm. *Renewable Energy*, 150, 891-906.
- ASHFAQ, A. & IANAKIEV, A. 2018. Features of fully integrated renewable energy atlas for Pakistan; wind, solar and cooling. *Renewable and Sustainable Energy Reviews*, 97, 14-27.
- ASSARI, M. R., BASIRAT TABRIZI, H. & SAVADKOHY, M. 2018. Numerical and experimental study of inlet-outlet locations effect in horizontal storage tank of solar water heater. *Sustainable Energy Technologies and Assessments*, 25, 181-190.
- ASSIGNMENTPOINT. *Solar Radiation*. <https://www.assignmentpoint.com/other/assignment-on-solar-radiation.html>. Accessed online: 21/05/2019 [Online]. [Accessed].
- ATAGÜR, M., DEMIROĞLU, S. & SEYDIBEYOĞLU, M. Ö. 2017. Chapter 17 - Flame Retardancy of Composites and Nanocomposites Based on PU Polymers. In: THOMAS, S., DATTA, J., HAPONIUK, J. T. & REGHUNADHAN, A. (eds.) *Polyurethane Polymers*. Amsterdam: Elsevier.



- AZZOUZI, D., BOURORGA, H. E., BELAININE, K. A. & BOUMEDDANE, B. 2018. Experimental study of a designed solar parabolic trough with large rim angle. *Renewable Energy*, 125, 495-500.
- BAFFARI, D., BUFFA, G., INGARAO, G., MASNATA, A. & FRATINI, L. 2019. Aluminium sheet metal scrap recycling through friction consolidation. *Procedia Manufacturing*, 29, 560-566.
- BAKOS, G. C. 2006. Design and construction of a two-axis Sun tracking system for parabolic trough collector (PTC) efficiency improvement. *Renewable Energy*, 31, 2411-2421.
- BANISTER, C. J. & COLLINS, M. R. J. A. E. 2015. Development and performance of a dual tank solar-assisted heat pump system. 149, 125-132.
- BELLOS, E., DANIIL, I. & TZIVANIDIS, C. 2018. Multiple cylindrical inserts for parabolic trough solar collector. *Applied Thermal Engineering*, 143, 80-89.
- BELLOS, E. & TZIVANIDIS, C. 2019. Alternative designs of parabolic trough solar collectors. *Progress in Energy and Combustion Science*, 71, 81-117.
- BERGMAN, T. L., INCROPERA, F. P., DEWITT, D. P. & LAVINE, A. S. 2011. *Fundamentals of heat and mass transfer*, John Wiley & Sons.
- BINOTTI, M., ZHU, G., GRAY, A., MANZOLINI, G. & SILVA, P. 2013. Geometric analysis of three-dimensional effects of parabolic trough collectors. *Solar Energy*, 88, 88-96.
- BOREL-SALADIN, J. M. & TUROK, I. N. 2013. The impact of the green economy on jobs in South Africa. *South African Journal of Science*, 109, 01-04.
- BREEZE, P. 2018a. Chapter 1 - An Introduction to Hydropower. In: BREEZE, P. (ed.) *Hydropower*. Academic Press.

- BREEZE, P. 2018b. Chapter 2 - The Hydropower Resource, Hydropower Sites and Types of Hydropower Plants. *In: BREEZE, P. (ed.) Hydropower. Academic Press.*
- BREEZE, P. 2018c. Chapter 6 - Small Hydropower. *In: BREEZE, P. (ed.) Hydropower. Academic Press.*
- BROWN, T. M., POGORZELSKI, W. H., GIAMMANCO, I. M. & SOCIETY 2015. Evaluating hail damage using property insurance claims data. *Weather and Climate Extremes*, 7, 197-210.
- BURNS, S., ZEENNI, E. & GUVEN, H. Stratification and performance of a solar breadbox water heater. Proceedings of the American solar energy conference, San Diego, CA, USA, 1985. 430-435.
- CABRERA, F., FERNÁNDEZ-GARCÍA, A., SILVA, R. & PÉREZ-GARCÍA, M. 2013. Use of parabolic trough solar collectors for solar refrigeration and air-conditioning applications. *Renewable and Sustainable Energy Reviews*, 20, 103-118.
- CAU, G. & COCCO, D. 2014. Comparison of Medium-size Concentrating Solar Power Plants based on Parabolic Trough and Linear Fresnel Collectors. *Energy Procedia*, 45, 101-110.
- CELADOR, A. C., ODRIOZOLA, M. & SALA, J. 2011. Implications of the modelling of stratified hot water storage tanks in the simulation of CHP plants. *Energy conversion management*, 52, 3018-3026.
- CENGEL, Y. A. 2006. *Heat and Mass Transfer: A Practical Approach*, McGraw-Hill.
- CHANDRA, Y. P. & MATUSKA, T. 2020. Numerical prediction of the stratification performance in domestic hot water storage tanks. *Renewable Energy*, 154, 1165-1179.

- CHAUDHARI, K., WALKE, P., WANKHEDE, U. & SHELKE, R. 2015. An experimental investigation of a nanofluid (Al<sub>2</sub>O<sub>3</sub>+ H<sub>2</sub>O) based parabolic trough solar collectors. *British Journal of Applied Science & Technology*, 9, 551-557.
- CHEN, L., XU, H.-F., HE, S.-J., DU, Y.-H., YU, N.-J., DU, X.-Z., LIN, J. & NAZARENKO, S. 2017. Thermal conductivity performance of polypropylene composites filled with polydopamine-functionalized hexagonal boron nitride. *PloS one*, 12, e0170523.
- CHENG, Z.-D., HE, Y.-L. & QIU, Y. 2015. A detailed nonuniform thermal model of a parabolic trough solar receiver with two halves and two inactive ends. *Renewable Energy*, 74, 139-147.
- CHENG, Z.-D., ZHAO, X.-R., HE, Y.-L. & QIU, Y. 2018. A novel optical optimization model for linear Fresnel reflector concentrators. *Renewable Energy*, 129, 486-499.
- CHOWDHURY, R., SADHUKHAN, J., TRAVERSO, M. & KEEN, P. L. 2018. Effects of residence time on life cycle assessment of bioenergy production from dairy manure. *Bioresource Technology Reports*, 4, 57-65.
- City of Johannesburg, A.T., 2014. .Available from: <http://www.joburg.org.za/images/stories/2014/June/2014-15%20approved%20tariffs.pdf>. [Accessed on 02/12/2016].
- CITY-OF-TSHWANE. 2019/20. *Promulgated-Tariffs: 2019-2020 Electricity Part I* [Online]. Available: <http://www.tshwane.gov.za/sites/Departments/Financial-Services/Financial-Documents/Approved%20MTREF/2019-20%20electricity%20tariff%20part%201%20-%20rectified%20schedule.pdf> [Accessed 29/07/2020].

- CLAIRE. 2015. *How to save Electricity and money from your geyser?* [Online]. Available: <https://powertime.co.za/online/how-to-save-electricity-geyser/> [Accessed 01/06/2020].
- COMMONPRAISE 2017. Stainless Steel Solar Water Tank. online: <http://www.solarproductcn.com/5-4-solar-water-tank.html>. Accessed: 10/01/2017.
- COOK, J. & BEYEA, J. 2000. Bioenergy in the United States: progress and possibilities<sup>1</sup>. *Biomass and bioenergy*, 18, 441-455.
- CULLEN, M. 2012. *Commercial Solar Water Heating Systems*. Waterford Institute of Technology.
- DELLIN, T., FISH, M. & YANG, C. 1981. User's manual for DELSOL2: a computer code for calculating the optical performance and optimal system design for solar-thermal central-receiver plants. Sandia National Labs., Albuquerque, NM (USA); Sandia National Labs ....
- DEMIREL, S. & TUNA, E. B. 2019. Evaluation of the cyclic fatigue performance of polyurethane foam in different density and category. *Polymer Testing*, 76, 146-153.
- DENG, M., LI, J., ZHANG, S., SHAN, M., BAUMGARTNER, J., CARTER, E. & YANG, X. 2019. Real-time combustion rate of wood charcoal in the heating fire basin: Direct measurement and its correlation to CO emissions. *Environmental Pollution*, 245, 38-45.
- DEPARTMENT-OF-ENERGY. 2015. [http://www.gov.za/sites/www.gov.za/files/State%20of%20Renewable%20Energy%20in%20South%20Africa\\_s.pdf](http://www.gov.za/sites/www.gov.za/files/State%20of%20Renewable%20Energy%20in%20South%20Africa_s.pdf). Accessed Online: 27/04/2017. [Online]. [Accessed].

- DEVI, L., PTASINSKI, K. J. & JANSSEN, F. J. 2003. A review of the primary measures for tar elimination in biomass gasification processes. *Biomass and bioenergy*, 24, 125-140.
- DEVORE, N., YIP, H. & RHEE, J. 2013. Domestic hot water storage tank: design and analysis for improving thermal stratification. *Journal of Solar Energy Engineering*, 135, 040905.
- DICANIO, D. G., TREYTL, W., JUR, F. & WATSON, C. 1979. Line focus solar thermal central receiver research study. *Final Report, 30 Apr. 1977-31 Mar. 1979 FMC Corp., Santa Clara, CA. Engineered Systems Division.*  
<https://www.osti.gov/biblio/5535434>.
- DINCER, I. & EZZAT, M. F. 2018. 3.6 Geothermal Energy Production. *In: DINCER, I. (ed.) Comprehensive Energy Systems*. Oxford: Elsevier. 252-303.
- DOE. 2014. *Annual Energy Review* [Online]. U.S. Energy Information Administration. Available: <http://www.eia.gov/forecasts/archive/aeo14/> [Accessed 18/04/2020].
- DUPONT, E., KOPPELAAR, R. & JEANMART, H. 2018. Global available wind energy with physical and energy return on investment constraints. *Applied Energy*, 209, 322-338.
- DYE, S. 2012. Geoneutrinos and the radioactive power of the Earth. *Reviews of Geophysics*, 50, 1-19.
- ELLABBAN, O., ABU-RUB, H. & BLAABJERG, F. 2014. Renewable energy resources: Current status, future prospects and their enabling technology. *Renewable and Sustainable Energy Reviews*, 39, 748-764.
- ENERGY. Parabolic Dish Collectors.  
[http://energy.kth.se/compedu/webcompedu/WebHelp/S9\\_Renewable\\_Energy/](http://energy.kth.se/compedu/webcompedu/WebHelp/S9_Renewable_Energy/)

[B5 Solar Energy/C3 Advanced Solar Thermal/ID107 files/Parabolic Dish Collectors.htm](#). Accessed online: 28/03/2019.

EREN. WATER HEATING:Energy-efficient strategies for supplying hot water in the home. Available: [https://www1.eere.energy.gov/buildings/publications/pdfs/building\\_america/26465.pdf](https://www1.eere.energy.gov/buildings/publications/pdfs/building_america/26465.pdf) [Accessed 18/04/2020].

FAN, L., LIU, G., WANG, F., RITSEMA, C. J. & GEISSEN, V. 2014. Domestic water consumption under intermittent and continuous modes of water supply. *Water resources management*, 28, 853-865.

FARM.NET. *Thermal Conductivity for some common Materials* [Online]. Available: [http://www.farm.net/~mason/materials/thermal\\_conductivity.html](http://www.farm.net/~mason/materials/thermal_conductivity.html) [Accessed 13/05/2020].

FINEARTAMERICA.COM <https://fineartamerica.com/featured/compact-linear-fresnel-reflector-us-department-of-energy.html?product=wood-print>. Accessed online: 12/01/2019.

FORRISTALL, R. 2003. Heat transfer analysis and modeling of a parabolic trough solar receiver implemented in engineering equation solver. National Renewable Energy Lab., Golden, CO.(US).

FRANÇOIS, B., HINGRAY, B., RAYNAUD, D., BORGA, M. & CREUTIN, J. D. 2016. Increasing climate-related-energy penetration by integrating run-of-the river hydropower to wind/solar mix. *Renewable Energy*, 87, 686-696.

GAI, C. & DONG, Y. 2012. Experimental study on non-woody biomass gasification in a downdraft gasifier. *International Journal of hydrogen energy*, 37, 4935-4944.

- GAIN, A. K. & WADA, Y. 2014. Assessment of future water scarcity at different spatial and temporal scales of the Brahmaputra River Basin. *Water resources management*, 28, 999-1012.
- GAJDA, J., BARTNICKI, G. & BURNECKI, K. 2018. Modeling of water usage by means of ARFIMA–GARCH processes. *Physica A: Statistical Mechanics and its Applications*, 512, 644-657.
- GANDO, A., GANDO, Y., ICHIMURA, K., IKEDA, H., INOUE, K., KIBE, Y., KISHIMOTO, Y., KOGA, M., MINEKAWA, Y. & MITSUI, T. 2011. Partial radiogenic heat model for Earth revealed by geoneutrino measurements. *Nature Geoscience*, 4, 647.
- GAUTAM, A., CHAMOLI, S., KUMAR, A. & SINGH, S. 2017. A review on technical improvements, economic feasibility and world scenario of solar water heating system. *Renewable and Sustainable Energy Reviews*, 68, 541-562.
- GHARABAGHI, S., STAHL, E. & BONAKDARI, H. 2019. Integrated nonlinear daily water demand forecast model (case study: City of Guelph, Canada). *Journal of Hydrology*, 579, 124182.
- GHARBI, N. E., DERBAL, H., BOUAICHAOU, S. & SAID, N. 2011. A comparative study between parabolic trough collector and linear Fresnel reflector technologies. *Energy Procedia*, 6, 565-572.
- GIGLIO, T. & LAMBERTS, R. 2016. Savings related to solar water heating system: A case study of low-income families in Brazil. *Energy and Buildings*, 130, 434-442.
- GIOSTRI, A., BINOTTI, M., SILVA, P., MACCHI, E. & MANZOLINI, G. 2013. Comparison of two linear collectors in solar thermal plants: parabolic trough versus Fresnel. *Journal of Solar Energy Engineering*, 135, 011001.

- GLASSLEY, W. E. 2010. *Geothermal energy: renewable energy and the environment*, CRC Press.
- Global Status Report 2007. Average annual growth rates of renewable energy capacity, 2002-2006. Source: Renewable 2007 Global Status Report.
- GONG, X., WANG, F., WANG, H., TAN, J., LAI, Q. & HAN, H. 2017. Heat transfer enhancement analysis of tube receiver for parabolic trough solar collector with pin fin arrays inserting. *Solar Energy*, 144, 185-202.
- GOODFELLOW. 2020. *Polypropylene (PP) Material Information* [Online]. Available: <http://www.goodfellow.com/E/Polypropylene.html> [Accessed 22/03/2020].
- GOSWAMI, D. Y., KREITH, F. & KREIDER, J. F. 2000. *Fundamentals of solar radiation*, Philadelphia, PA, CRC Press.
- GOU, J., ZHANG, L. & LI, C. 2020. A new method combining modification of montmorillonite and crystal regulation to enhance the mechanical properties of polypropylene. *Polymer Testing*, 82, 106236.
- GRAM-HANSSEN, K. 2010. Residential heat comfort practices: understanding users. *Building Research & Information*, 38, 175-186.
- GRENA, R. & TARQUINI, P. 2011. Solar linear Fresnel collector using molten nitrates as heat transfer fluid. *Energy*, 36, 1048-1056.
- GUEYMARD, C. A. 2004. The sun's total and spectral irradiance for solar energy applications and solar radiation models. *Solar Energy*, 76, 423-453.
- HAFEZ, A. Z., ATTIA, A. M., ELTWAB, H. S., ELKOUSY, A. O., AFIFI, A. A., ABDELHAMID, A. G., ABDELQADER, A. N., FATEEN, S. E. K., ELMETWALLY, K. A., SOLIMAN, A. & ISMAIL, I. M. 2018. Design analysis of solar parabolic trough thermal collectors. *Renewable and Sustainable Energy Reviews*, 82, 1215-1260.



- HE, Z. 2016. Solar Water Heating Systems Applied in High-rise Residential Buildings in China. *Energy Procedia*, 91, 408-414.
- HEBA, H. 2014. Dish Stirling for Dubai? <http://newenergyupdate.com/csp-today/markets/dish-stirling-dubai>. Accessed online: 28/03/2019.
- HELIOSCSP.COM <http://helioscsp.com/saudi-arabia-linear-fresnel-system-concentrated-solar-power-commissioned-successfully/>. Accessed online: 12/01/2019.
- HELIOSTAT\_SOUTH\_AUSTRALIA <https://heliostat.com.au/>. Accessed: 18/03/2019.
- HERNÁNDEZ-ESCOBEDO, Q., PEREA-MORENO, A.-J. & MANZANO-AGUGLIARO, F. 2018. Wind energy research in Mexico. *Renewable Energy*, 123, 719-729.
- HILLER, C. C. & JOHNSON, R. 2017. Hot-water use in hotels: Part 5-updated hotel hot-water system design techniques. *ASHRAE Transactions*, 123, 160.
- HOSSAIN, M., SAIDUR, R., FAYAZ, H., RAHIM, N., ISLAM, M., AHAMED, J. & RAHMAN, M. 2011. Review on solar water heater collector and thermal energy performance of circulating pipe. *Renewable and Sustainable Energy Reviews*, 15, 3801-3812.
- <HTTPS://STORMANDSKY.COM>. Available: <https://stormandsky.com/2014-6-3> [Accessed 01/07/2020].
- HWANG, B.-K., KIM, S.-K., KIM, J.-H., KIM, J.-D. & LEE, J.-M. 2020. Dynamic Compressive Behavior of Rigid Polyurethane Foam with Various Densities under Different Temperatures. *International Journal of Mechanical Sciences*, 105657.

- IMTIAZ HUSSAIN, M., LEE, G. H. & KIM, J.-T. 2017. Experimental validation of mathematical models of identical aluminum and stainless steel engineered conical solar collectors. *Renewable Energy*, 112, 44-52.
- INTERNATIONAL-ENERGY-AGENCY 2016.  
[http://www.iea.org/ciab/South\\_Africa\\_Role\\_Coal\\_Energy\\_Security.pdf](http://www.iea.org/ciab/South_Africa_Role_Coal_Energy_Security.pdf). Online.  
 Accessed: 27/04/2017.
- IOL\_NEWS. 2013. *Hailstorm wreaks havoc* [Online]. Available:  
<https://www.iol.co.za/news/south-africa/gauteng/hailstorm-wreaks-havoc-1614184> [Accessed 01/07/2020].
- ISLAM, M. R., SUMATHY, K. & KHAN, S. U. 2013. Solar water heating systems and their market trends. *Renewable and Sustainable Energy Reviews*, 17, 1-25.
- IVAN, S. 2018. US DOE awards USD 72m for CSP R&D programme.  
<https://renewablesnow.com/news/us-doe-awards-usd-72m-for-csp-rd-programme-612829/>. Accessed online: 25/03/2019.
- JAFARI MOSLEH, H., JAHANGIRI MAMOURI, S., SHAFII, M. B. & HAKIM SIMA, A. 2015. A new desalination system using a combination of heat pipe, evacuated tube and parabolic trough collector. *Energy Conversion and Management*, 99, 141-150.
- JAIN, S. & JAIN, P. K. 2017. The rise of Renewable Energy implementation in South Africa. *Energy Procedia*, 143, 721-726.
- JARAMILLO, O. A., BORUNDA, M., VELAZQUEZ-LUCHO, K. M. & ROBLES, M. 2016. Parabolic trough solar collector for low enthalpy processes: An analysis of the efficiency enhancement by using twisted tape inserts. *Renewable Energy*, 93, 125-141.

- JEBASINGH, V. & HERBERT, G. J. 2016. A review of solar parabolic trough collector. *Renewable and Sustainable Energy Reviews*, 54, 1085-1091.
- JIN, E. & SUTHERLAND, J. W. 2018. An integrated sustainability model for a bioenergy system: Forest residues for electricity generation. *Biomass and Bioenergy*, 119, 10-21.
- JOUBERT, E., HESS, S. & VAN NIEKERK, J. 2016. Large-scale solar water heating in South Africa: Status, barriers and recommendations. *Renewable Energy*, 97, 809-822.
- KALOGIROU, S. 1998. Use of parabolic trough solar energy collectors for sea-water desalination. *Applied Energy*, 60, 65-88.
- KALOGIROU, S. 2003. The potential of solar industrial process heat applications. *Applied Energy*, 76, 337-361.
- KALOGIROU, S. A. 2004. Solar thermal collectors and applications. *Progress in energy and combustion science*, 30, 231-295.
- KALOGIROU, S. A. 2012. A detailed thermal model of a parabolic trough collector receiver. *Energy*, 48, 298-306.
- KALOGIROU, S. A. 2013. *Solar energy engineering: processes and systems*, Academic Press.
- KALOGIROU, S. A. 2014. Chapter 3 - Solar Energy Collectors. *In: KALOGIROU, S. A. (ed.) Solar Energy Engineering (Second Edition)*. Boston: Academic Press.
- KAMEL, S., EL-SATTAR, H. A., VERA, D. & JURADO, F. 2018. Bioenergy potential from agriculture residues for energy generation in Egypt. *Renewable and Sustainable Energy Reviews*, 94, 28-37.

- KAUSHIK, S., KUMAR, R., GARG, H. & PRAKASH, J. 1994. Transient analysis of a triangular built-in-storage solar water heater under winter conditions. *Heat Recovery Systems and CHP*, 14, 337-341.
- KENNEDY, C. & PRICE, H. Progress in development of high-temperature solar-selective coating. ASME 2005 International Solar Energy Conference, 2005. American Society of Mechanical Engineers Digital Collection, 749-755.
- KIM, Y. & SEO, T. 2007. Thermal performances comparisons of the glass evacuated tube solar collectors with shapes of absorber tube. *Renewable Energy*, 32, 772-795.
- KRALOVA, I. & SJÖBLOM, J. 2010. Biofuels—renewable energy sources: a review. *Journal of Dispersion Science and Technology*, 31, 409-425.
- KRISHNA, H. J., BROWN, C., GERSTON, J. & COLLEY, S. 2005. *The Texas manual on rainwater harvesting*, Austin, Texas, United States of America, Texas Water Development Board.
- LAMRANI, B., KHOUYA, A., ZEGHMATI, B. & DRAOUI, A. 2018. Mathematical modeling and numerical simulation of a parabolic trough collector: A case study in thermal engineering. *Thermal Science and Engineering Progress*, 8, 47-54.
- LAY, T., HERNLUND, J. & BUFFETT, B. A. 2008. Core–mantle boundary heat flow. *Nature geoscience*, 1, 25-32.
- LEE, D. & DERRIBLE, S. 2020. Predicting Residential Water Demand with Machine-Based Statistical Learning. *Journal of Water Resources Planning and Management*, 146, 04019067.
- LI, C., ZHAI, R., LIU, H., YANG, Y. & WU, H. 2018. Optimization of a heliostat field layout using hybrid PSO-GA algorithm. *Applied Thermal Engineering*, 128, 33-41.

- LI, M. & WANG, L. 2006. Investigation of evacuated tube heated by solar trough concentrating system. *Energy Conversion and Management*, 47, 3591-3601.
- LI, X., CHANG, H., DUAN, C., ZHENG, Y. & SHU, S. 2019. Thermal performance analysis of a novel linear cavity receiver for parabolic trough solar collectors. *Applied Energy*, 237, 431-439.
- LIANG, R., MA, L., ZHANG, J. & ZHAO, D. 2011. Theoretical and experimental investigation of the filled-type evacuated tube solar collector with U tube. *Solar Energy*, 85, 1735-1744.
- LIPPS, F. & VANT-HULL, L. 1978. A cellwise method for the optimization of large central receiver systems. *Solar Energy*, 20, 505-516.
- LODHI, M. A. K., ABIDIN, A. Z. & YUSOF SULAIMAN, M. 1997. Pollutant emissions from fossil fuel use in Kuala Lumpur and environmental damage. *Energy Conversion and Management*, 38, 213-216.
- LU, J., DING, J., YANG, J. & YANG, X. 2013. Nonuniform heat transfer model and performance of parabolic trough solar receiver. *Energy*, 59, 666-675.
- LYNCH, E. D. W. 2014. *Astonishing Photos of Hail Damage in Blair, Nebraska* [Online]. Available: <https://laughingsquid.com/astonishing-photos-of-hail-damage-in-blair-nebraska/> [Accessed 01/07/2020].
- MANIKANDAN, G. K., INIYAN, S. & GOIC, R. 2019. Enhancing the optical and thermal efficiency of a parabolic trough collector – A review. *Applied Energy*, 235, 1524-1540.
- MARSHAL, N. 1976. *Gas encyclopedia*, New York, Elsevier.
- MATRAWY, K. & FARKAS, I. 1997. Comparison study for three types of solar collectors for water heating. *Energy conversion and management*, 38, 861-869.

- MAUTHNER, F. & WEISS, W. 2013. Solar heat worldwide-markets and contribution to the energy supply 2011. Solar Heating and Cooling Programme. *Paris: International Energy Agency (IEA)*. Available from: <http://www.aee-intec.at/Uploads/dateien932.pdf>.
- MICROSOFT® 2009. Definition of a dam. *Microsoft® Encarta®*.
- MONTES, M. J., RUBBIA, C., ABBAS, R. & MARTÍNEZ-VAL, J. M. 2014. A comparative analysis of configurations of linear Fresnel collectors for concentrating solar power. *Energy*, 73, 192-203.
- MORIN, G., DERSCH, J., PLATZER, W., ECK, M. & HÄBERLE, A. 2012. Comparison of Linear Fresnel and Parabolic Trough Collector power plants. *Solar Energy*, 86, 1-12.
- MOSLEH, H. J., MAMOURI, S. J., SHAFII, M. & SIMA, A. H. 2015. A new desalination system using a combination of heat pipe, evacuated tube and parabolic trough collector. *Energy Conversion and Management*, 99, 141-150.
- MOWAT, L. 2017. *Kevin Pietersen caught up in Durban storms with hail stones size of Tennis Balls* [Online]. Express.co.uk. Available: <https://www.express.co.uk/news/world/865217/Durban-weather-storms-South-Africa-Kevin-Pieterse-hail-stones> [Accessed 01/07/2020].
- MUHAMMAD, A. U., LI, X. & FENG, J. Artificial Intelligence Approaches for Urban Water Demand Forecasting: A Review. *International Conference on Machine Learning and Intelligent Communications*, 2019. Springer, 595-622.
- MURTUZA, S. A., BYREGOWDA, H. V., H, M. M. A. & IMRAN, M. 2017. Experimental and simulation studies of parabolic trough collector design for obtaining solar energy. *Resource-Efficient Technologies*, 3, 414-421.

- NASER, A.-S. H. & ABAAS, K. I. 2016. Solar Water Heating for Space Heating Purposes. *International Journal of Civil, Mechanical and Energy Science (IJCMES)* 2, 57-63.
- NASPOLINI, H. F. & RÜTHER, R. 2011. The impacts of solar water heating in low-income households on the distribution utility's active, reactive and apparent power demands. *Solar Energy*, 85, 2023-2032.
- OROSZ, M. & DICKES, R. 2017. 16 - Solar thermal powered Organic Rankine Cycles. *In: MACCHI, E. & ASTOLFI, M. (eds.) Organic Rankine Cycle (ORC) Power Systems*. Woodhead Publishing.
- OZBEK, H., PHILLIPS, S. L. J. J. O. C. & DATA, E. 1980. Thermal conductivity of aqueous sodium chloride solutions from 20 to 330. degree. C. 25, 263-267.
- OZONOH, M., ANIOKETE, T., OBOIRIEN, B. & DARAMOLA, M. 2018. Techno-economic analysis of electricity and heat production by co-gasification of coal, biomass and waste tyre in South Africa. *Journal of Cleaner Production*, 201, 192-206.
- PACCHIN, E., GAGLIARDI, F., ALVISI, S. & FRANCHINI, M. 2019. A comparison of short-term water demand forecasting models. *Water Resources Management*, 33, 1481-1497.
- PADILLA, R. V. 2011. *Simplified methodology for designing parabolic trough solar power plants*. Doctor of Philosophy, University of South Florida, USA.
- PAN, S.-Y., GAO, M., SHAH, K. J., ZHENG, J., PEI, S.-L. & CHIANG, P.-C. 2019. Establishment of enhanced geothermal energy utilization plans: Barriers and strategies. *Renewable Energy*, 132, 19-32.
- PANG, Z. & O'NEILL, Z. 2018. Uncertainty quantification and sensitivity analysis of the domestic hot water usage in hotels. *Applied Energy*, 232, 424-442.

- PANWAR, N. L., KAUSHIK, S. C. & KOTHARI, S. 2011. Role of renewable energy sources in environmental protection: A review. *Renewable and Sustainable Energy Reviews*, 15, 1513-1524.
- PAPAEFTHIMIOU, S., LEFTHERIOTIS, G., YIANOULIS, P., HYDE, T., EAMES, P., FANG, Y., PENNARUN, P.-Y. & JANNASCH, P. 2006. Development of electrochromic evacuated advanced glazing. *Energy and Buildings*, 38, 1455-1467.
- PAPILO, P., MARIMIN, HAMBALI, E. & SITANGGANG, I. S. 2018. Sustainability index assessment of palm oil-based bioenergy in Indonesia. *Journal of Cleaner Production*, 196, 808-820.
- PARIKKA, M. 2004. Global biomass fuel resources. *Biomass and bioenergy*, 27, 613-620.
- PATERSON, D. A. & SANKARAN, R. 1994. Hail impact on building envelopes. *Journal of Wind Engineering and Industrial Aerodynamics*, 53, 229-246.
- PATTI, A. & DOMENICO, A. 2019. Thermal Conductivity of Polypropylene-Based Materials. In: WEIYU, W. & YIMING, Z. (eds.) *Polypropylene - polymerization and characterization of mechanical and thermal properties*. IntechOpen.
- PÉREZ, N., QI, X.-L., NIE, S., ACUÑA, P., CHEN, M.-J. & WANG, D.-Y. 2019. Flame retardant polypropylene composites with low densities. *Materials*, 12, 152.
- PEREZ, R., SEALS, R., ANDERSON, J. & MENICUCCI, D. 1995. Calculating solar radiation received by tubular collectors. *Journal of solar energy engineering*, 117, 341-344.
- PLUMBINGSUPPLY.COM. *How To Replace a Water Heater Element* [Online]. Available: <https://www.plumbingsupply.com/element-installation-instructions.html> [Accessed 15/12/2020].



- PRICE, H., LU PFERT, E., KEARNEY, D., ZARZA, E., COHEN, G., GEE, R. & MAHONEY, R. 2002. Advances in parabolic trough solar power technology. *J. Sol. Energy Eng.*, 124, 109-125.
- QIU, Y., LI, M.-J., HE, Y.-L. & TAO, W.-Q. 2017. Thermal performance analysis of a parabolic trough solar collector using supercritical CO<sub>2</sub> as heat transfer fluid under non-uniform solar flux. *Applied Thermal Engineering*, 115, 1255-1265.
- QU, W., WANG, R., HONG, H., SUN, J. & JIN, H. 2017. Test of a solar parabolic trough collector with rotatable axis tracking. *Applied Energy*, 207, 7-17.
- RAITHBY, G. & HOLLANDS, K. 1975. A general method of obtaining approximate solutions to laminar and turbulent free convection problems. *Advances in heat transfer*. Elsevier.
- RAMIRES, M. L., NIETO DE CASTRO, C. A., FARELEIRA, J. M., WAKEHAM, W. A. J. J. O. C. & DATA, E. 1994. Thermal conductivity of aqueous sodium chloride solutions. 39, 186-190.
- RAMIREZ, A. D., RIVELA, B., BOERO, A. & MELENDRES, A. M. 2019. Lights and shadows of the environmental impacts of fossil-based electricity generation technologies: A contribution based on the Ecuadorian experience. *Energy Policy*, 125, 467-477.
- RAND\_WATER-SOUTH\_AFRICA. 2020. *calculator.waterwise* [Online]. Available: <http://calculator.waterwise.co.za:92/> [Accessed 22/04/2020].
- RASSAMAKIN, B., KHAIRNASOV, S., ZARIPOV, V., RASSAMAKIN, A. & ALFOROVA, O. 2013. Aluminum heat pipes applied in solar collectors. *Solar Energy*, 94, 145-154.

- RATZEL, A., HICKOX, C. & GARTLING, D. 1979. Techniques for reducing thermal conduction and natural convection heat losses in annular receiver geometries. *Journal of Heat Transfer*, 101, 108-113.
- RAZMMAND, F., MEHDIPOUR, R. & MOUSAVI, S. M. 2019. A numerical investigation on the effect of nanofluids on heat transfer of the solar parabolic trough collectors. *Applied Thermal Engineering*, 152, 624-633.
- REDDY, K., KUMAR, K. R. & SATYANARAYANA, G. 2008. Numerical investigation of energy-efficient receiver for solar parabolic trough concentrator. *Heat Transfer Engineering*, 29, 961-972.
- REGHUNADHAN, A. & THOMAS, S. 2017. Chapter 1 - Polyurethanes: Structure, Properties, Synthesis, Characterization, and Applications. *In*: THOMAS, S., DATTA, J., HAPONIUK, J. T. & REGHUNADHAN, A. (eds.) *Polyurethane Polymers*. Amsterdam: Elsevier.
- REHAN, M. A., ALI, M., SHEIKH, N. A., KHALIL, M. S., CHAUDHARY, G. Q., RASHID, T. U. & SHEHRYAR, M. 2018. Experimental performance analysis of low concentration ratio solar parabolic trough collectors with nanofluids in winter conditions. *Renewable Energy*, 118, 742-751.
- RHEE, J., CAMPBELL, A., MARIADASS, A. & MORHOUS, B. 2010. Temperature stratification from thermal diodes in solar hot water storage tank. *Solar Energy*, 84, 507-511.
- RIVERA-ORTEGA, U., HERNÁNDEZ-GÓMEZ, C. R., VEGA-TORRES, G. & LOPEZ-MEDINA, M. E. 2019. Simple apparatus to calculate the refractive index of liquids based on Snell's law. *Measurement*, 134, 658-661.
- SAHU, B. K. 2018. Wind energy developments and policies in China: A short review. *Renewable and Sustainable Energy Reviews*, 81, 1393-1405.

- SAIR, S., OUSHABI, A., KAMMOUNI, A., TANANE, O., ABBOUD, Y. & EL BOUARI, A. 2018. Mechanical and thermal conductivity properties of hemp fiber reinforced polyurethane composites. *Case Studies in Construction Materials*, 8, 203-212.
- SALGADO CONRADO, L., RODRIGUEZ-PULIDO, A. & CALDERÓN, G. 2017. Thermal performance of parabolic trough solar collectors. *Renewable and Sustainable Energy Reviews*, 67, 1345-1359.
- SALVE, A. R., MALWAD, D. S. & TUNGIKAR, V. B. 2018. Role of reflector material in performance of compound parabolic concentrator. *IOSR Journal of Engineering (IOSRJEN)*, 2278-8719.
- SÁNCHEZ HERRANZ, D. 2009. *DESIGN OF A SOLAR WATER HEATING SYSTEM IN A RESIDENTIAL BUILDING*. Master's Dissertation, University of Gävle.
- SHAHZAD, M., QU, Y., JAVED, S. A., ZAFAR, A. U. & REHMAN, S. U. 2020. Relation of environment sustainability to CSR and green innovation: A case of Pakistani manufacturing industry. *Journal of Cleaner Production*, 253, 119938.
- SHIGLEY, J. E. & MISCHKE, C. R. 2005. *Mechanical Engineering Design: In SI Units*, McGraw-Hill.
- SHUKLA, R., SUMATHY, K., ERICKSON, P. & GONG, J. 2013. Recent advances in the solar water heating systems: A review. *Renewable and Sustainable Energy Reviews*, 19, 173-190.
- SILVA, R., PÉREZ, M. & FERNÁNDEZ-GARCIA, A. 2013. Modeling and co-simulation of a parabolic trough solar plant for industrial process heat. *Applied energy*, 106, 287-300.

- SIMÓN, D., BORREGUERO, A. M., DE LUCAS, A. & RODRÍGUEZ, J. F. 2018. Recycling of polyurethanes from laboratory to industry, a journey towards the sustainability. *Waste Management*, 76, 147-171.
- SLADE, R., SAUNDERS, R., GROSS, R. & BAUEN, A. 2011. Energy from biomass: the size of the global resource. Accessed online (02/10/2018). [https://spiral.imperial.ac.uk/bitstream/10044/1/12650/4/GlobalBiomassReport\\_LOLO.pdf](https://spiral.imperial.ac.uk/bitstream/10044/1/12650/4/GlobalBiomassReport_LOLO.pdf).
- SMYTH, M., EAMES, P. & NORTON, B. 2006. Integrated collector storage solar water heaters. *Renewable and Sustainable Energy Reviews*, 10, 503-538.
- SMYTH, M., MCGARRIGLE, P., EAMES, P. & NORTON, B. 2005. Experimental comparison of alternative convection suppression arrangements for concentrating integral collector storage solar water heaters. *Solar energy*, 78, 223-233.
- SOLARGIS. 2019. <https://solargis.com/maps-and-gis-data/download/south-africa>. Accessed online: 22/05/2019. [Online]. [Accessed].
- SOLARHOTWATERPARTS. *Replacement broken hills evacuated tubes* [Online]. Available: [https://www.solarhotwaterparts.com.au/replacement-broken-hills-evacuated-tubes/Replacement\\_Broken\\_Hills\\_evacuated\\_tubes](https://www.solarhotwaterparts.com.au/replacement-broken-hills-evacuated-tubes/Replacement_Broken_Hills_evacuated_tubes) [Accessed 01/07/2020].
- SOWELL. 2018. Salt Therapy Pillows. <http://www.natural-salt-lamps.com/natural-pain-relief-therapy.html> Online (Accessed date: 16/05/2019).
- STATHOPOULOS, T., ALRAWASHDEH, H., AL-QURAAN, A., BLOCKEN, B., DILIMULATI, A., PARASCHIVOIU, M. & PILAY, P. 2018. Urban wind energy: Some views on potential and challenges. *Journal of Wind Engineering and Industrial Aerodynamics*, 179, 146-157.

- SUN, J., LAM, N., ZHANG, L., RUAN, D. & GAD, E. 2015. Contact forces generated by hailstone impact. *International Journal of Impact Engineering*, 84, 145-158.
- SZYCHER, M. 1999. *Szycher's handbook of polyurethanes*, CRC press.
- TAGLE-SALAZAR, P. D., NIGAM, K. & RIVERA-SOLORIO, C. I. 2018. Heat transfer model for thermal performance analysis of parabolic trough solar collectors using nanofluids. *Renewable energy*, 125, 334-343.
- TANG, R., YANG, Y. & GAO, W. 2011. Comparative studies on thermal performance of water-in-glass evacuated tube solar water heaters with different collector tilt-angles. *Solar Energy*, 85, 1381-1389.
- TERZIOGLU, H., KAZAN, F. A. & SUNGUR, C. The Irrigation System Fed from Biaxial PV Panels. 2015 2nd International Conference on Information Science and Control Engineering, 2015. IEEE, 981-987.
- THYSSENKRUPP-MATERIALS. 2018. *Density of Aluminium* [Online]. Available: <https://www.thyssenkrupp-materials.co.uk/density-of-aluminium.html> [Accessed 13/05/2020].
- TOWNSEND, T. J., SPARKES, D. L., RAMSDEN, S. J., GLITHERO, N. J. & WILSON, P. 2018. Wheat straw availability for bioenergy in England. *Energy Policy*, 122, 349-357.
- VARELA, M., LECHON, Y. & SAEZ, R. 1999. Environmental and socioeconomic aspects in the strategic analysis of a biomass power plant integration. *Biomass and Bioenergy*, 17, 405-413.
- WANG, Q., HU, M., YANG, H., CAO, J., LI, J., SU, Y. & PEI, G. 2019. Performance evaluation and analyses of novel parabolic trough evacuated collector tubes with spectrum-selective glass envelope. *Renewable Energy*, 138, 793-804.

WANG, Y., JI, J., SUN, W., YUAN, W., CAI, J., GUO, C. & HE, W. 2016. Experiment and simulation study on the optimization of the PV direct-coupled solar water heating system. *Energy*, 100, 154-166.

WATERHEATERTIMER.ORG. *How electric water heater works: Installation* [Online].

Available: <http://waterheatertimer.org/How-it-works.html> [Accessed 15/12/2020].

WEI, S., LI, X., SHEN, Y., ZHANG, L. & WU, X. 2020. Study on microscopic mechanism of nano-silicon dioxide for improving mechanical properties of polypropylene. *Molecular Simulation*, 46, 468-475.

WEISS, W. & MAUTHNER, F. 2010. Solar heat worldwide. *IEA Solar Heating and Cooling Programme*.

WIKIPEDIA

[https://en.wikipedia.org/wiki/Solar\\_thermal\\_collector#Flat\\_plate\\_collectors](https://en.wikipedia.org/wiki/Solar_thermal_collector#Flat_plate_collectors).

Accessed: 10/01/2017.

WORLD\_BIOENERGY\_ASSOCIATION 2017. WBA Global Bioenergy Statistics. *World Bioenergy Association: Stockholm, Sweden*.

WORLD\_HEALTH\_ORGANIZATION\_(WHO)

<http://www.who.int/mediacentre/factsheets/fs292/en/>. Online (Accessed: 17/07/2017).

WWW.AQUA-CALC.COM. *Density of Salt (NaCl)* [Online]. Available: <https://www.aqua-calc.com/page/density-table/substance/salt> [Accessed 13/05/2020].

WWW.GOV.ZA. 2014. *MEC Mamabolo visit hailstorm victims in Soshanguve and Mamelodi* [Online]. Gauteng: Government of South Africa. Available:

<https://www.gov.za/mec-mamabolo-visit-hailstorm-victims-soshanguve-and-mamelodi> [Accessed 01/07/2020].

[WWW.PHOTODESTINATION.CO.ZA/](http://www.photodestination.co.za/). *South Africa's Weather* [Online]. Available: <http://www.photodestination.co.za/south-africa-weather.html> [Accessed 14/07/2020].

[WWW.SOLARREPAIRS.CO.UK/](http://www.solarrepairs.co.uk/). *Broken glass on evacuated tube* [Online]. The Solar Repair Service. Available: <https://www.solarrepairs.co.uk/solar-repairs/solar-heating-repairs/solar-flat-panels-and-solar-tubes/attachment/broken-glass-evacuated-tube/> [Accessed 01/07/2020].

XIE, M., SHEN, G., HOLDER, A. L., HAYS, M. D. & JETTER, J. J. 2018. Light absorption of organic carbon emitted from burning wood, charcoal, and kerosene in household cookstoves. *Environmental Pollution*, 240, 60-67.

ZAIMI, M., EL ACHOUBY, H., IBRAL, A. & ASSAID, E. M. 2019. Determining combined effects of solar radiation and panel junction temperature on all model-parameters to forecast peak power and photovoltaic yield of solar panel under non-standard conditions. *Solar Energy*, 191, 341-359.

ZHAI, H., DAI, Y., WU, J. & WANG, R. 2009. Study on Trough Receiver for Linear Concentrating Solar Collector. In: GOSWAMI, D. Y. & ZHAO, Y. (eds.) *Proceedings of ISES World Congress 2007 (Vol. I – Vol. V): Solar Energy and Human Settlement*. Berlin, Heidelberg: Springer Berlin Heidelberg.

ZHENG, B., XU, J., NI, T. & LI, M. 2015. Geothermal energy utilization trends from a technological paradigm perspective. *Renewable Energy*, 77, 430-441.

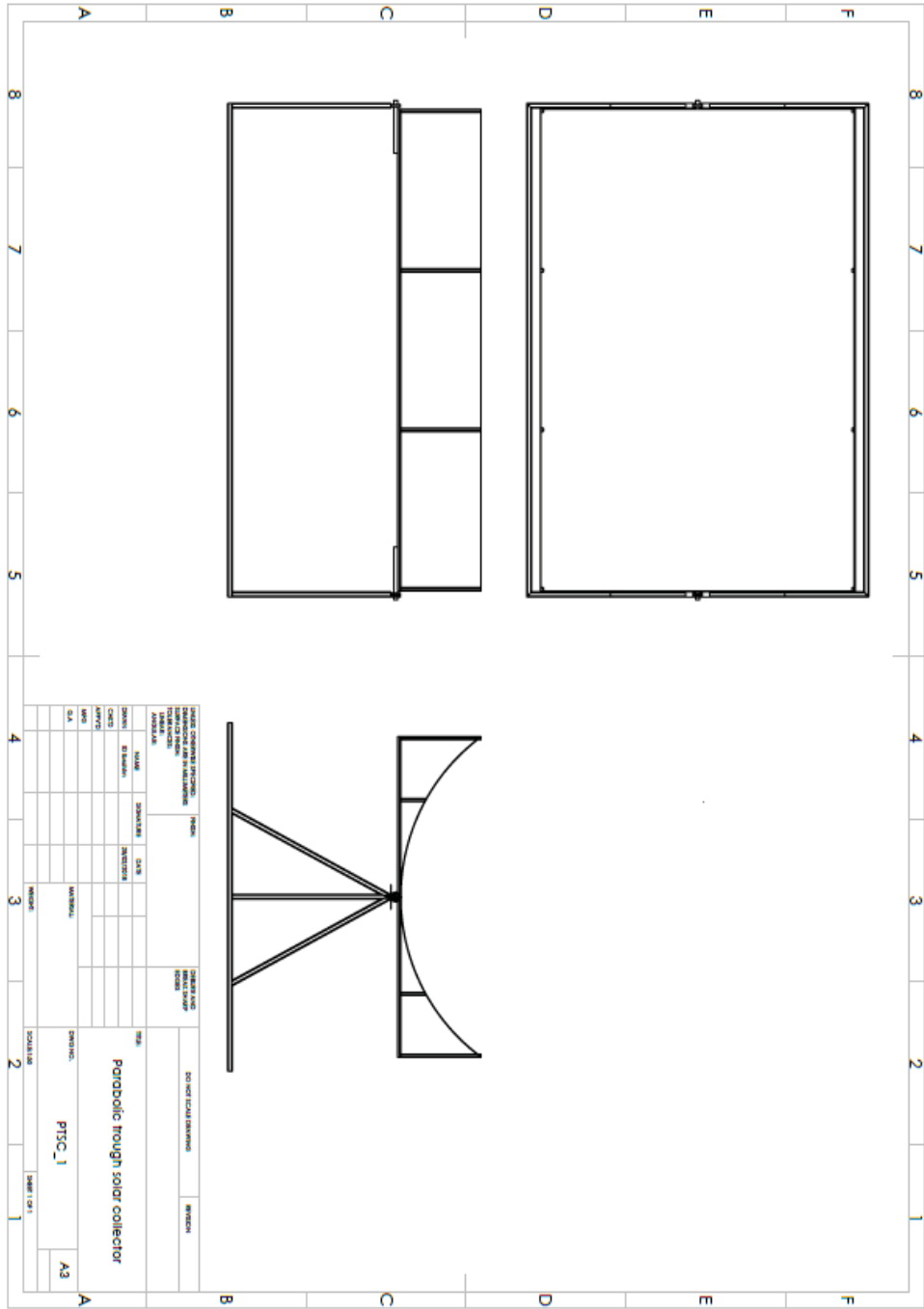
ZHENG, C.-W., XIAO, Z.-N., PENG, Y.-H., LI, C.-Y. & DU, Z.-B. 2018. Rezoning global offshore wind energy resources. *Renewable Energy*, 129, 1-11.

- ZHENG, H. 2017a. Chapter 4 - Traditional Solar Desalination Units. *In: ZHENG, H. (ed.) Solar Energy Desalination Technology*. Amsterdam: Elsevier.
- ZHENG, H. 2017b. Chapter 9 - Solar Concentrating Directly to Drive Desalination Technologies. *In: ZHENG, H. (ed.) Solar Energy Desalination Technology*. Amsterdam: Elsevier.
- ZHU, J. & PAN, X. 2010. Woody biomass pretreatment for cellulosic ethanol production: technology and energy consumption evaluation. *Bioresource technology*, 101, 4992-5002.
- ZOU, B., DONG, J., YAO, Y. & JIANG, Y. 2016. An experimental investigation on a small-sized parabolic trough solar collector for water heating in cold areas. *Applied Energy*, 163, 396-407.



APPENDICES

Appendix 1: CAD Orthographic Drawing of Parabolic Trough Solar Collector



# DS18B20 Temperature Sensor **GAIMC**

## GTS200



### DESCRIPTION

The probe adopts the new original imported DS18B20 temperature sensor chip. Each pin of the chip is separated by heat-shrinkable tube to prevent short circuit, internal sealing, waterproof and moisture proof. The high quality stainless steel tube package is waterproof, moisture proof and rust proof. The DS18B20 digital temperature sensor from Dallas Semiconductor of the United States is encapsulated with a highly thermally conductive sealant to ensure high sensitivity of the temperature sensor and minimal temperature delay. The temperature sensor supports a "one-wire bus" interface (1-Wire) with a temperature range of -55°C to +125°C and an accuracy of  $\pm 0.5^{\circ}\text{C}$  in the range of -10 to +85°C. The on-site temperature is directly transmitted in the digital way of "one-line bus", which greatly improves the anti-interference of the system. Suitable for on-site temperature measurement in harsh environments. The DS18B20 digital temperature sensor has a unique number, and the temperature acquisition device identifies the corresponding temperature sensor by number.

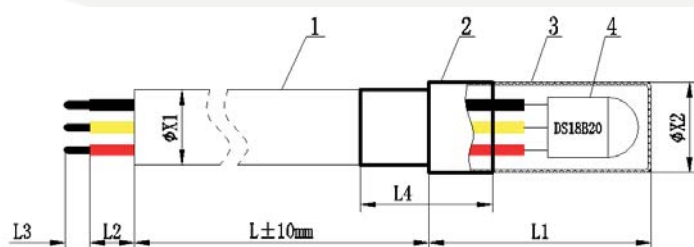
### FEATURES

- Power supply range: 3.0V to 5.5V
- Operating temperature range: -55 ° C to + 125 ° C (-67 ° F to + 257 ° F)
- Storage temperature range: -55°C to + 125°C (-67F to + 257F)
- Accuracy in the range of -10 ° C to + 85 ° C:  $\pm 0.5^{\circ}\text{C}$
- Waterproof stainless steel sheath
- Sheath size: 6 \* 50mm or custom

### APPLICATION

DS18B20 temperature sensor is mainly used in refrigerator temperature monitoring, pharmaceutical factory GMP monitoring system, telecommunication room monitoring, beer production, building automation, warehouse temperature monitoring, environmental monitoring, process temperature monitoring, air conditioning monitoring, incubation temperature control, aquaculture temperature measurement, greenhouse temperature monitoring.

## DIMENSIONS



1	Cable length, wire diameter OD	PVC cable*3P	OD5.0mm
2	Heat shrinkable tube size	Heat shrinkable tube	OD6*30mm
3	Probe size	Stainless steel probe	OD6*30mm
4	DS18B20 sensor		Red VDD is the external power supply input The yellow DQ is a digital signal input / output terminal Black GND is the power ground

## PARAMETERS

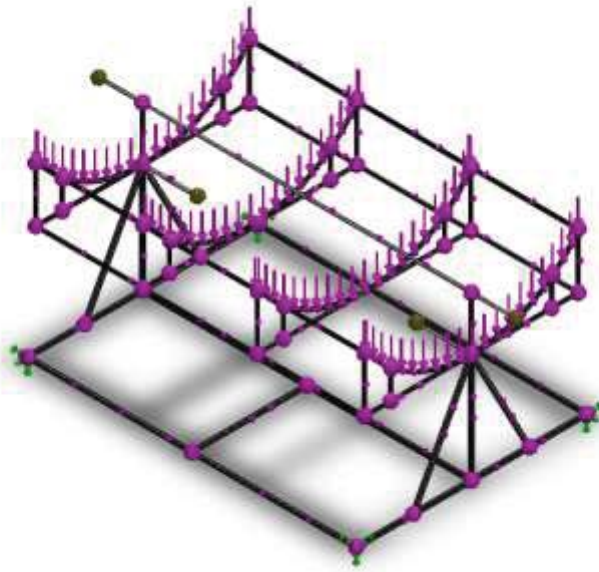
Digital chip	1DS18B20
Probe size	Φ 8mm, Φ6mm (inside), length = 30mm or custom
Insulation Materials	Glass fiber, PVC, Teflon, silicone rubber or custom made
Wire material	FRP, PVC, Teflon, silicone rubber, stainless steel braided
Shell material	Stainless steel · nickel plated copper, brass, plastic
Wire Connector	UL Series(such as UL1007), Supply wire number, using temperature range, outside diameter and material requirements.
Special requirements	Molex, JST, DuPont, CWB, CJT, SM, TJC3, PH, EH, 5264, U-type etc.
Wiring	Waterproof, acid proof, antiseptic
	Black: GND Yellow: DATA Red: VDD+

## ORDER INSTRUCTION

When you placing order, please inform us the following parameters:

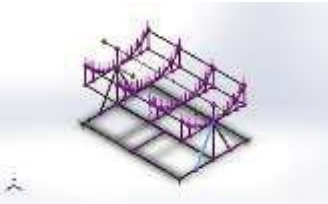
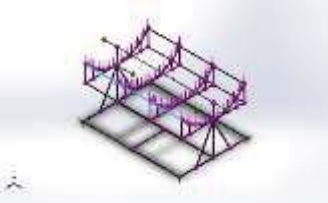
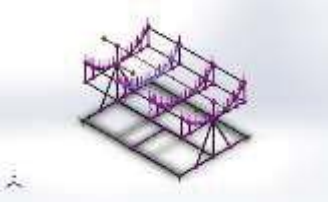
1. Application and working environment (whether to be waterproof, acid or alkali and others)
2. Shell diameter D and length L (commonly size: 6 \* 30mm, 6 \* 50mm, other can be customized)?
3. How many lines of output? (Commonly used 2-wire/ 3-wire, choose one) ?
4. Wire material and length (commonly wire PVC, Silicone, Teflon wire)?
5. Temperature range (temperature range cannot exceed -50 to +125 °C )?
6. How to deal with the cable end (hanging tin or with connector)?

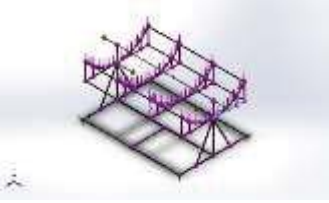

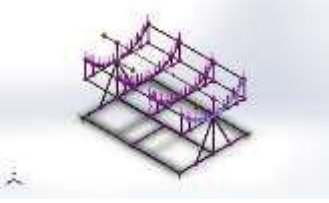
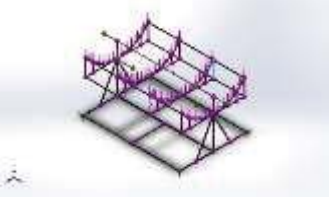
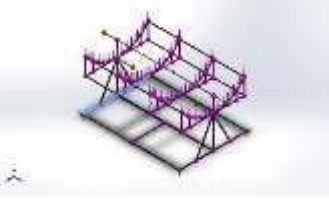
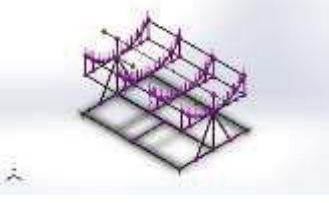
### Appendix 3: Solar collector beam body information

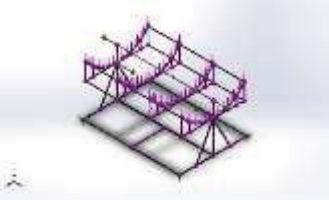
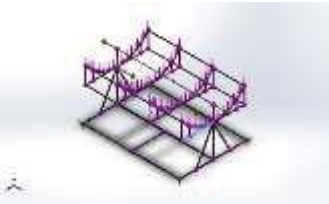
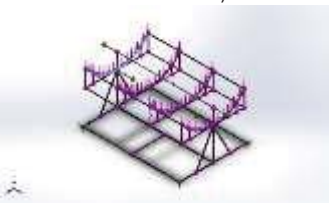

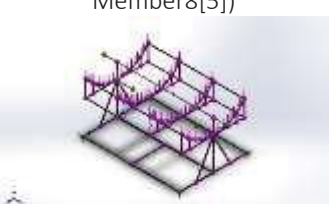


Model name: Solar Water Heater  
Current Configuration: Default<As Machined>

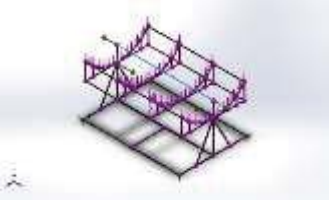

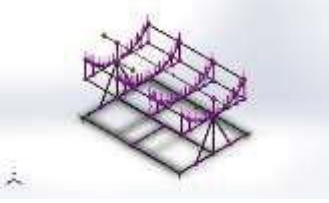
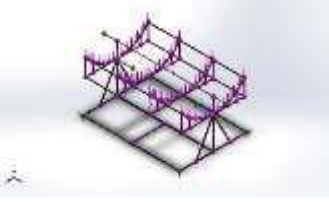
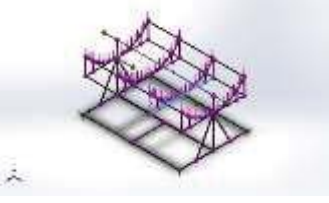
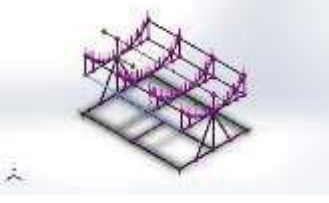
#### Beam Bodies:

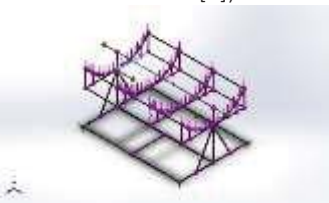



Document Name and Reference	Formulation	Properties	Document Path/Date Modified
Beam-1(Structural Member5[1]) 	Beam – Uniform C/S	Section Standard-iso/square tube/30 x 30 x 2.6 Section Area: 0.000267551m <sup>2</sup> Length:1,127.35mm Volume:0.000301624m <sup>3</sup> Mass Density:7,900kg/m <sup>3</sup> Mass:2.38283kg Weight:23.3517N	E:\Solar Water Heater.SLDPRT Mar 3 20:00:48 2020
Beam-2(Structural Member9[1]) 	Beam – Uniform C/S	Section Standard-iso/square tube/20 x 20 x 2 Section Area: 0.000133699m <sup>2</sup> Length:3,000mm Volume:0.000401097m <sup>3</sup> Mass Density:7,900kg/m <sup>3</sup> Mass:3.16867kg Weight:31.053N	E:\Solar Water Heater.SLDPRT Mar 3 20:00:48 2020
Beam-3(Structural Member12) 	Beam – Uniform C/S	Section Standard-iso/angle iron/20 x 20 x 3 Section Area: 0.000109766m <sup>2</sup> Length:2,263.69mm Volume:0.00024857m <sup>3</sup> Mass Density:7,900kg/m <sup>3</sup> Mass:1.9637kg Weight:19.2443N	E:\Solar Water Heater.SLDPRT Mar 3 20:00:48 2020

<p>Beam-4(Structural Member7[3])</p> 	Beam – Uniform C/S	<p>Section Standard-iso/square tube/20 x 20 x 2</p> <p>Section Area: 0.000133699m<sup>2</sup></p> <p>Length:975mm</p> <p>Volume:0.000130359m<sup>3</sup></p> <p>Mass Density:7,900kg/m<sup>3</sup></p> <p>Mass:1.02983kg</p> <p>Weight:10.0924N</p>	E:\Solar Water Heater.SLDPRT Mar 3 20:00:48 2020
<p>Beam-5(Structural Member8[6])</p> 	Beam – Uniform C/S	<p>Section Standard-iso/square tube/20 x 20 x 2</p> <p>Section Area: 0.000133699m<sup>2</sup></p> <p>Length:251.27mm</p> <p>Volume:3.35945e-05m<sup>3</sup></p> <p>Mass Density:7,900kg/m<sup>3</sup></p> <p>Mass:0.265397kg</p> <p>Weight:2.60089N</p>	E:\Solar Water Heater.SLDPRT Mar 3 20:00:48 2020
<p>Beam-6(Structural Member15)</p> 	Beam – Uniform C/S	<p>Section Standard-iso/angle iron/20 x 20 x 3</p> <p>Section Area: 0.000109766m<sup>2</sup></p> <p>Length:2,263.69mm</p> <p>Volume:0.00024857m<sup>3</sup></p> <p>Mass Density:7,900kg/m<sup>3</sup></p> <p>Mass:1.9637kg</p> <p>Weight:19.2443N</p>	E:\Solar Water Heater.SLDPRT Mar 3 20:00:48 2020
<p>Beam-7(Structural Member8[10])</p> 	Beam – Uniform C/S	<p>Section Standard-iso/square tube/20 x 20 x 2</p> <p>Section Area: 0.000133699m<sup>2</sup></p> <p>Length:500mm</p> <p>Volume:6.68496e-05m<sup>3</sup></p> <p>Mass Density:7,900kg/m<sup>3</sup></p> <p>Mass:0.528111kg</p> <p>Weight:5.17549N</p>	E:\Solar Water Heater.SLDPRT Mar 3 20:00:48 2020
<p>Beam-8(Structural Member1[1])</p> 	Beam – Uniform C/S	<p>Section Standard-iso/square tube/30 x 30 x 2.6</p> <p>Section Area: 0.000267551m<sup>2</sup></p> <p>Length:2,100mm</p> <p>Volume:0.000561868m<sup>3</sup></p> <p>Mass Density:7,900kg/m<sup>3</sup></p> <p>Mass:4.43875kg</p> <p>Weight:43.4998N</p>	E:\Solar Water Heater.SLDPRT Mar 3 20:00:48 2020
<p>Beam-9(Structural Member8[14])</p> 	Beam – Uniform C/S	<p>Section Standard-iso/square tube/20 x 20 x 2</p> <p>Section Area: 0.000133699m<sup>2</sup></p> <p>Length:251.27mm</p> <p>Volume:3.35945e-05m<sup>3</sup></p> <p>Mass Density:7,900kg/m<sup>3</sup></p> <p>Mass:0.265397kg</p> <p>Weight:2.60089N</p>	E:\Solar Water Heater.SLDPRT Mar 3 20:00:48 2020

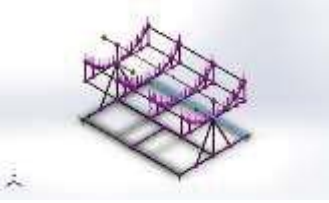

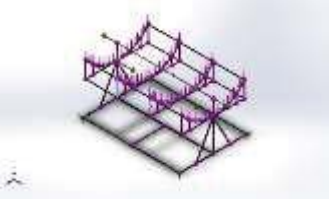
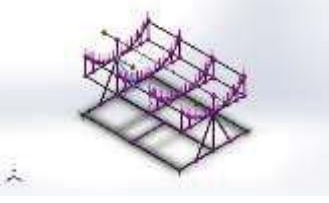
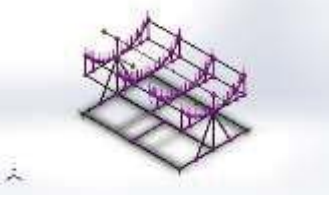
<p>Beam-10(Structural Member8[1])</p> 	Beam – Uniform C/S	<p>Section Standard-iso/square tube/20 x 20 x 2  Section Area: 0.000133699m<sup>2</sup>  Length:500mm  Volume:6.68496e-05m<sup>3</sup>  Mass Density:7,900kg/m<sup>3</sup>  Mass:0.528111kg  Weight:5.17549N</p>	<p>E:\Solar Water Heater.SLDPRT  Mar 3 20:00:48 2020</p>
<p>Beam-11(Structural Member7[4])</p> 	Beam – Uniform C/S	<p>Section Standard-iso/square tube/20 x 20 x 2  Section Area: 0.000133699m<sup>2</sup>  Length:975mm  Volume:0.000130357m<sup>3</sup>  Mass Density:7,900kg/m<sup>3</sup>  Mass:1.02982kg  Weight:10.0922N</p>	<p>E:\Solar Water Heater.SLDPRT  Mar 3 20:00:48 2020</p>
<p>Beam-12(Structural Member11)</p> 	Beam – Uniform C/S	<p>Section Standard-iso/angle iron/20 x 20 x 3  Section Area: 0.000109766m<sup>2</sup>  Length:2,263.69mm  Volume:0.00024857m<sup>3</sup>  Mass Density:7,900kg/m<sup>3</sup>  Mass:1.9637kg  Weight:19.2443N</p>	<p>E:\Solar Water Heater.SLDPRT  Mar 3 20:00:48 2020</p>
<p>Beam-13(Structural Member5[2])</p> 	Beam – Uniform C/S	<p>Section Standard-iso/square tube/30 x 30 x 2.6  Section Area: 0.000267551m<sup>2</sup>  Length:1,127.35mm  Volume:0.00030163m<sup>3</sup>  Mass Density:7,900kg/m<sup>3</sup>  Mass:2.38287kg  Weight:23.3522N</p>	<p>E:\Solar Water Heater.SLDPRT  Mar 3 20:00:48 2020</p>
<p>Beam-14(Structural Member8[18])</p> 	Beam – Uniform C/S	<p>Section Standard-iso/square tube/20 x 20 x 2  Section Area: 0.000133699m<sup>2</sup>  Length:487.5mm  Volume:6.51783e-05m<sup>3</sup>  Mass Density:7,900kg/m<sup>3</sup>  Mass:0.514909kg  Weight:5.04611N</p>	<p>E:\Solar Water Heater.SLDPRT  Mar 3 20:00:48 2020</p>
<p>Beam-15(Structural Member8[5])</p> 	Beam – Uniform C/S	<p>Section Standard-iso/square tube/20 x 20 x 2  Section Area: 0.000133699m<sup>2</sup>  Length:251.27mm  Volume:3.35945e-05m<sup>3</sup>  Mass Density:7,900kg/m<sup>3</sup>  Mass:0.265397kg  Weight:2.60089N</p>	<p>E:\Solar Water Heater.SLDPRT  Mar 3 20:00:48 2020</p>

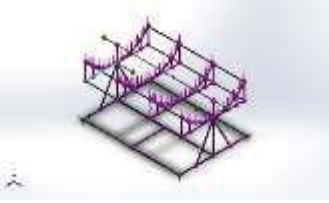
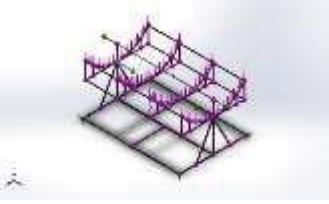

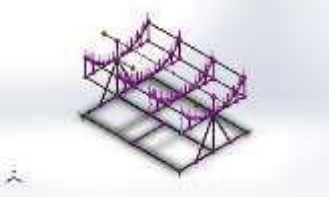
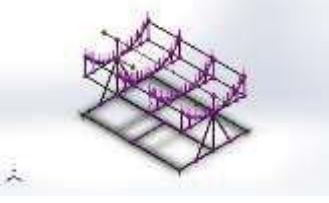
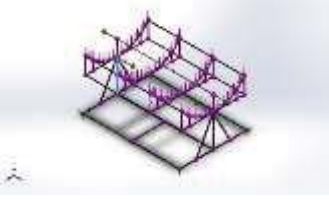


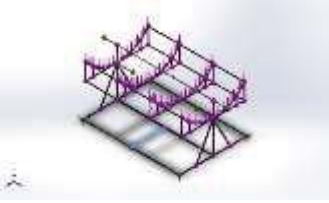
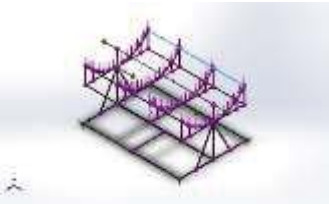



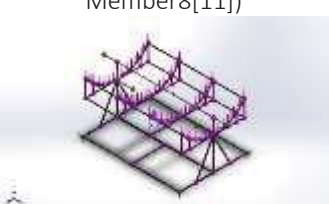
<p>Beam-16(Structural Member18[2])</p> 	Beam – Uniform C/S	<p>Section Standard-iso/pipe/21.3 x 2.3  Section Area: 0.000137288m<sup>2</sup>  Length:3,000mm  Volume:0.000411863m<sup>3</sup>  Mass Density:7,900kg/m<sup>3</sup>  Mass:3.25372kg  Weight:31.8864N</p>	<p>E:\Solar Water Heater.SLDPRT  Mar 3 20:00:48 2020</p>
<p>Beam-17(Structural Member1[4])</p> 	Beam – Uniform C/S	<p>Section Standard-iso/square tube/30 x 30 x 2.6  Section Area: 0.000267551m<sup>2</sup>  Length:3,000mm  Volume:0.000802668m<sup>3</sup>  Mass Density:7,900kg/m<sup>3</sup>  Mass:6.34108kg  Weight:62.1426N</p>	<p>E:\Solar Water Heater.SLDPRT  Mar 3 20:00:48 2020</p>
<p>Beam-18(Structural Member8[9])</p> 	Beam – Uniform C/S	<p>Section Standard-iso/square tube/20 x 20 x 2  Section Area: 0.000133699m<sup>2</sup>  Length:251.27mm  Volume:3.35945e-05m<sup>3</sup>  Mass Density:7,900kg/m<sup>3</sup>  Mass:0.265397kg  Weight:2.60089N</p>	<p>E:\Solar Water Heater.SLDPRT  Mar 3 20:00:48 2020</p>
<p>Beam-19(Structural Member16[1])</p> 	Beam – Uniform C/S	<p>Section Standard-iso/pipe/26.9 x 3.2  Section Area: 0.000238258m<sup>2</sup>  Length:500mm  Volume:0.000119129m<sup>3</sup>  Mass Density:7,900kg/m<sup>3</sup>  Mass:0.941121kg  Weight:9.22298N</p>	<p>E:\Solar Water Heater.SLDPRT  Mar 3 20:00:48 2020</p>
<p>Beam-20(Structural Member10[2])</p> 	Beam – Uniform C/S	<p>Section Standard-iso/square tube/20 x 20 x 2  Section Area: 0.000133699m<sup>2</sup>  Length:1,950mm  Volume:0.000260713m<sup>3</sup>  Mass Density:7,900kg/m<sup>3</sup>  Mass:2.05963kg  Weight:20.1844N</p>	<p>E:\Solar Water Heater.SLDPRT  Mar 3 20:00:48 2020</p>
<p>Beam-21(Structural Member7[5])</p> 	Beam – Uniform C/S	<p>Section Standard-iso/square tube/20 x 20 x 2  Section Area: 0.000133699m<sup>2</sup>  Length:3,000mm  Volume:0.000401105m<sup>3</sup>  Mass Density:7,900kg/m<sup>3</sup>  Mass:3.16873kg  Weight:31.0535N</p>	<p>E:\Solar Water Heater.SLDPRT  Mar 3 20:00:48 2020</p>

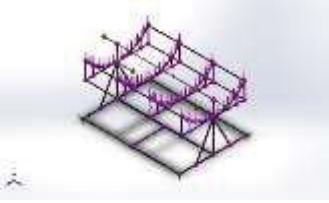


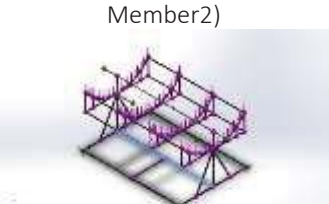
<p>Beam-22(Structural Member8[13])</p> 	Beam – Uniform C/S	<p>Section Standard-iso/square tube/20 x 20 x 2</p> <p>Section Area: 0.000133699m<sup>2</sup></p> <p>Length:500mm</p> <p>Volume:6.68496e-05m<sup>3</sup></p> <p>Mass Density:7,900kg/m<sup>3</sup></p> <p>Mass:0.528111kg</p> <p>Weight:5.17549N</p>	<p>E:\Solar Water Heater.SLDPRT</p> <p>Mar 3 20:00:48 2020</p>
<p>Beam-23(Structural Member4[1])</p> 	Beam – Uniform C/S	<p>Section Standard-iso/square tube/30 x 30 x 2.6</p> <p>Section Area: 0.000267551m<sup>2</sup></p> <p>Length:1,127.35mm</p> <p>Volume:0.000301624m<sup>3</sup></p> <p>Mass Density:7,900kg/m<sup>3</sup></p> <p>Mass:2.38283kg</p> <p>Weight:23.3517N</p>	<p>E:\Solar Water Heater.SLDPRT</p> <p>Mar 3 20:00:48 2020</p>
<p>Beam-24(Structural Member7[1])</p> 	Beam – Uniform C/S	<p>Section Standard-iso/square tube/20 x 20 x 2</p> <p>Section Area: 0.000133699m<sup>2</sup></p> <p>Length:975mm</p> <p>Volume:0.000130357m<sup>3</sup></p> <p>Mass Density:7,900kg/m<sup>3</sup></p> <p>Mass:1.02982kg</p> <p>Weight:10.0922N</p>	<p>E:\Solar Water Heater.SLDPRT</p> <p>Mar 3 20:00:48 2020</p>
<p>Beam-25(Structural Member18[1])</p> 	Beam – Uniform C/S	<p>Section Standard-iso/pipe/21.3 x 2.3</p> <p>Section Area: 0.000137288m<sup>2</sup></p> <p>Length:400mm</p> <p>Volume:5.4915e-05m<sup>3</sup></p> <p>Mass Density:7,900kg/m<sup>3</sup></p> <p>Mass:0.433829kg</p> <p>Weight:4.25152N</p>	<p>E:\Solar Water Heater.SLDPRT</p> <p>Mar 3 20:00:48 2020</p>
<p>Beam-26(Structural Member8[17])</p> 	Beam – Uniform C/S	<p>Section Standard-iso/square tube/20 x 20 x 2</p> <p>Section Area: 0.000133699m<sup>2</sup></p> <p>Length:487.5mm</p> <p>Volume:6.51783e-05m<sup>3</sup></p> <p>Mass Density:7,900kg/m<sup>3</sup></p> <p>Mass:0.514909kg</p> <p>Weight:5.04611N</p>	<p>E:\Solar Water Heater.SLDPRT</p> <p>Mar 3 20:00:48 2020</p>
<p>Beam-27(Structural Member8[4])</p> 	Beam – Uniform C/S	<p>Section Standard-iso/square tube/20 x 20 x 2</p> <p>Section Area: 0.000133699m<sup>2</sup></p> <p>Length:500mm</p> <p>Volume:6.68496e-05m<sup>3</sup></p> <p>Mass Density:7,900kg/m<sup>3</sup></p> <p>Mass:0.528111kg</p> <p>Weight:5.17549N</p>	<p>E:\Solar Water Heater.SLDPRT</p> <p>Mar 3 20:00:48 2020</p>



<p>Beam-28(Structural Member1[2])</p> 	Beam – Uniform C/S	<p>Section Standard-iso/square tube/30 x 30 x 2.6</p> <p>Section Area: 0.000267551m<sup>2</sup></p> <p>Length:3,000mm</p> <p>Volume:0.000802668m<sup>3</sup></p> <p>Mass Density:7,900kg/m<sup>3</sup></p> <p>Mass:6.34108kg</p> <p>Weight:62.1426N</p>	E:\Solar Water Heater.SLDPRT Mar 3 20:00:48 2020
<p>Beam-29(Structural Member10[1])</p> 	Beam – Uniform C/S	<p>Section Standard-iso/square tube/20 x 20 x 2</p> <p>Section Area: 0.000133699m<sup>2</sup></p> <p>Length:1,950mm</p> <p>Volume:0.000260713m<sup>3</sup></p> <p>Mass Density:7,900kg/m<sup>3</sup></p> <p>Mass:2.05963kg</p> <p>Weight:20.1844N</p>	E:\Solar Water Heater.SLDPRT Mar 3 20:00:48 2020
<p>Beam-30(Structural Member8[8])</p> 	Beam – Uniform C/S	<p>Section Standard-iso/square tube/20 x 20 x 2</p> <p>Section Area: 0.000133699m<sup>2</sup></p> <p>Length:500mm</p> <p>Volume:6.68496e-05m<sup>3</sup></p> <p>Mass Density:7,900kg/m<sup>3</sup></p> <p>Mass:0.528111kg</p> <p>Weight:5.17549N</p>	E:\Solar Water Heater.SLDPRT Mar 3 20:00:48 2020
<p>Beam-31(Structural Member6[2])</p> 	Beam – Uniform C/S	<p>Section Standard-iso/square tube/30 x 30 x 2.6</p> <p>Section Area: 0.000267551m<sup>2</sup></p> <p>Length:995mm</p> <p>Volume:0.000266214m<sup>3</sup></p> <p>Mass Density:7,900kg/m<sup>3</sup></p> <p>Mass:2.10309kg</p> <p>Weight:20.6103N</p>	E:\Solar Water Heater.SLDPRT Mar 3 20:00:48 2020
<p>Beam-32(Structural Member4[2])</p> 	Beam – Uniform C/S	<p>Section Standard-iso/square tube/30 x 30 x 2.6</p> <p>Section Area: 0.000267551m<sup>2</sup></p> <p>Length:1,127.35mm</p> <p>Volume:0.00030163m<sup>3</sup></p> <p>Mass Density:7,900kg/m<sup>3</sup></p> <p>Mass:2.38287kg</p> <p>Weight:23.3522N</p>	E:\Solar Water Heater.SLDPRT Mar 3 20:00:48 2020
<p>Beam-33(Structural Member8[12])</p> 	Beam – Uniform C/S	<p>Section Standard-iso/square tube/20 x 20 x 2</p> <p>Section Area: 0.000133699m<sup>2</sup></p> <p>Length:500mm</p> <p>Volume:6.68496e-05m<sup>3</sup></p> <p>Mass Density:7,900kg/m<sup>3</sup></p> <p>Mass:0.528111kg</p> <p>Weight:5.17549N</p>	E:\Solar Water Heater.SLDPRT Mar 3 20:00:48 2020

<p>Beam-34(Structural Member7[6])</p> 	Beam – Uniform C/S	<p>Section Standard-iso/square tube/20 x 20 x 2</p> <p>Section Area: 0.000133699m<sup>2</sup></p> <p>Length:975mm</p> <p>Volume:0.000130359m<sup>3</sup></p> <p>Mass Density:7,900kg/m<sup>3</sup></p> <p>Mass:1.02983kg</p> <p>Weight:10.0924N</p>	E:\Solar Water Heater.SLDPRT Mar 3 20:00:48 2020
<p>Beam-35(Structural Member16[2])</p> 	Beam – Uniform C/S	<p>Section Standard-iso/pipe/26.9 x 3.2</p> <p>Section Area: 0.000238258m<sup>2</sup></p> <p>Length:500mm</p> <p>Volume:0.000119129m<sup>3</sup></p> <p>Mass Density:7,900kg/m<sup>3</sup></p> <p>Mass:0.941121kg</p> <p>Weight:9.22298N</p>	E:\Solar Water Heater.SLDPRT Mar 3 20:00:48 2020
<p>Beam-36(Structural Member1[3])</p> 	Beam – Uniform C/S	<p>Section Standard-iso/square tube/30 x 30 x 2.6</p> <p>Section Area: 0.000267551m<sup>2</sup></p> <p>Length:2,100mm</p> <p>Volume:0.000561868m<sup>3</sup></p> <p>Mass Density:7,900kg/m<sup>3</sup></p> <p>Mass:4.43875kg</p> <p>Weight:43.4998N</p>	E:\Solar Water Heater.SLDPRT Mar 3 20:00:48 2020
<p>Beam-37(Structural Member8[16])</p> 	Beam – Uniform C/S	<p>Section Standard-iso/square tube/20 x 20 x 2</p> <p>Section Area: 0.000133699m<sup>2</sup></p> <p>Length:500mm</p> <p>Volume:6.68496e-05m<sup>3</sup></p> <p>Mass Density:7,900kg/m<sup>3</sup></p> <p>Mass:0.528111kg</p> <p>Weight:5.17549N</p>	E:\Solar Water Heater.SLDPRT Mar 3 20:00:48 2020
<p>Beam-38(Structural Member8[3])</p> 	Beam – Uniform C/S	<p>Section Standard-iso/square tube/20 x 20 x 2</p> <p>Section Area: 0.000133699m<sup>2</sup></p> <p>Length:251.27mm</p> <p>Volume:3.35945e-05m<sup>3</sup></p> <p>Mass Density:7,900kg/m<sup>3</sup></p> <p>Mass:0.265397kg</p> <p>Weight:2.60089N</p>	E:\Solar Water Heater.SLDPRT Mar 3 20:00:48 2020
<p>Beam-39(Structural Member6[1])</p> 	Beam – Uniform C/S	<p>Section Standard-iso/square tube/30 x 30 x 2.6</p> <p>Section Area: 0.000267551m<sup>2</sup></p> <p>Length:995mm</p> <p>Volume:0.000266214m<sup>3</sup></p> <p>Mass Density:7,900kg/m<sup>3</sup></p> <p>Mass:2.10309kg</p> <p>Weight:20.6103N</p>	E:\Solar Water Heater.SLDPRT Mar 3 20:00:48 2020

<p>Beam-40(Structural Member3)</p> 	Beam – Uniform C/S	<p>Section Standard-iso/square tube/30 x 30 x 2.6  Section Area: 0.000267551m<sup>2</sup>  Length:1,050mm  Volume:0.000280929m<sup>3</sup>  Mass Density:7,900kg/m<sup>3</sup>  Mass:2.21934kg  Weight:21.7495N</p>	<p>E:\Solar Water Heater.SLDPR  Mar 3 20:00:48 2020</p>
<p>Beam-41(Structural Member9[2])</p> 	Beam – Uniform C/S	<p>Section Standard-iso/square tube/20 x 20 x 2  Section Area: 0.000133699m<sup>2</sup>  Length:3,000mm  Volume:0.000401097m<sup>3</sup>  Mass Density:7,900kg/m<sup>3</sup>  Mass:3.16867kg  Weight:31.053N</p>	<p>E:\Solar Water Heater.SLDPR  Mar 3 20:00:48 2020</p>
<p>Beam-42(Structural Member8[7])</p> 	Beam – Uniform C/S	<p>Section Standard-iso/square tube/20 x 20 x 2  Section Area: 0.000133699m<sup>2</sup>  Length:500mm  Volume:6.68496e-05m<sup>3</sup>  Mass Density:7,900kg/m<sup>3</sup>  Mass:0.528111kg  Weight:5.17549N</p>	<p>E:\Solar Water Heater.SLDPR  Mar 3 20:00:48 2020</p>
<p>Beam-43(Structural Member7[2])</p> 	Beam – Uniform C/S	<p>Section Standard-iso/square tube/20 x 20 x 2  Section Area: 0.000133699m<sup>2</sup>  Length:3,000mm  Volume:0.000401105m<sup>3</sup>  Mass Density:7,900kg/m<sup>3</sup>  Mass:3.16873kg  Weight:31.0535N</p>	<p>E:\Solar Water Heater.SLDPR  Mar 3 20:00:48 2020</p>
<p>Beam-44(Structural Member14)</p> 	Beam – Uniform C/S	<p>Section Standard-iso/angle iron/20 x 20 x 3  Section Area: 0.000109766m<sup>2</sup>  Length:2,263.69mm  Volume:0.00024857m<sup>3</sup>  Mass Density:7,900kg/m<sup>3</sup>  Mass:1.9637kg  Weight:19.2443N</p>	<p>E:\Solar Water Heater.SLDPR  Mar 3 20:00:48 2020</p>
<p>Beam-45(Structural Member8[11])</p> 	Beam – Uniform C/S	<p>Section Standard-iso/square tube/20 x 20 x 2  Section Area: 0.000133699m<sup>2</sup>  Length:251.27mm  Volume:3.35945e-05m<sup>3</sup>  Mass Density:7,900kg/m<sup>3</sup>  Mass:0.265397kg  Weight:2.60089N</p>	<p>E:\Solar Water Heater.SLDPR  Mar 3 20:00:48 2020</p>

<p>Beam-46(Structural Member8[15])</p> 	Beam – Uniform C/S	<p>Section Standard-iso/square tube/20 x 20 x 2  Section Area: 0.000133699m<sup>2</sup>  Length:251.27mm  Volume:3.35945e-05m<sup>3</sup>  Mass Density:7,900kg/m<sup>3</sup>  Mass:0.265397kg  Weight:2.60089N</p>	<p>E:\Solar Water Heater.SLDPRT  Mar 3 20:00:48 2020</p>
<p>Beam-47(Structural Member8[2])</p> 	Beam – Uniform C/S	<p>Section Standard-iso/square tube/20 x 20 x 2  Section Area: 0.000133699m<sup>2</sup>  Length:251.27mm  Volume:3.35945e-05m<sup>3</sup>  Mass Density:7,900kg/m<sup>3</sup>  Mass:0.265397kg  Weight:2.60089N</p>	<p>E:\Solar Water Heater.SLDPRT  Mar 3 20:00:48 2020</p>
<p>Beam-48(Structural Member18[3])</p> 	Beam – Uniform C/S	<p>Section Standard-iso/pipe/21.3 x 2.3  Section Area: 0.000137288m<sup>2</sup>  Length:400mm  Volume:5.4915e-05m<sup>3</sup>  Mass Density:7,900kg/m<sup>3</sup>  Mass:0.433829kg  Weight:4.25152N</p>	<p>E:\Solar Water Heater.SLDPRT  Mar 3 20:00:48 2020</p>
<p>Beam-49(Structural Member2)</p> 	Beam – Uniform C/S	<p>Section Standard-iso/square tube/30 x 30 x 2.6  Section Area: 0.000267551m<sup>2</sup>  Length:3,000mm  Volume:0.000802654m<sup>3</sup>  Mass Density:7,900kg/m<sup>3</sup>  Mass:6.34097kg  Weight:62.1415N</p>	<p>E:\Solar Water Heater.SLDPRT  Mar 3 20:00:48 2020</p>

#### Appendix 4: Solar collector beam forces

Beam Name	Joints	Axial(N)	Shear1(N)	Shear2(N)	Moment1(N.m)	Moment2(N.m)	Torque(N.m)
Beam-1 (Structural Member5[1])	1	1,663.12	5.86913	116.173	-51.6744	6.06508	0.0387353
	2	-1,663.12	-5.86896	-116.173	-79.2937	0.551381	-0.0387364
Beam-2 (Structural Member9[1])	1	-1,081.49	-3.38346	-116.916	-5.46245	-46.7237	2.42704
	2	571.984	-198.067	-395.207	154.164	-82.7758	-55.6736
	3	-574.284	-194.57	-393.469	-154.353	82.4478	-57.7142
	4	-571.984	198.067	175.321	123.72	-110.166	55.6736
Beam-3 (Structural Member12)	1	-568.056	11.9415	-139.619	54.9129	23.9518	-3.39288
	2	489.362	-41.7732	139.619	-7.41104	-14.163	-2.32432
	3	572.163	18.085	-142.549	-55.8341	-25.1073	-3.42468
	4	275.673	-30.4526	-0.220882	-1.80471	6.84902	-1.06029
Beam-4 (Structural Member7[3])	1	803.863	124.466	810.701	-470.011	39.9522	-6.43564
	2	-228.533	-148.941	232.701	-13.3414	-32.7185	40.7219
	3	228.533	148.941	-232.701	-42.507	-3.02739	-40.7219
Beam-5 (Structural Member8[6])	1	-89.1171	-142.106	143.846	-25.5995	-5.44275	-0.137581
	2	89.1164	142.106	-143.847	-10.5448	-30.2642	0.137522
Beam-6 (Structural Member15)	1	526.524	296.191	116.46	71.0014	-186.939	10.1178
	2	594.151	-27.6662	145.489	-63.084	0.0900778	4.05914
	3	-644.568	216.094	-145.489	13.765	-40.8815	2.6033
	4	-585.896	-28.6267	146.718	63.3391	0.825183	4.04298
	5	281.777	-199.733	-63.3448	-11.4332	44.0159	2.84072
Beam-7 (Structural Member8[10])	1	-403.598	-396.23	-236.684	-54.1943	100.418	26.8612
	2	403.598	396.23	236.684	-64.1475	97.6967	-26.8612
Beam-8 (Structural Member1[1])	1	-451.351	2.91259	1,009.32	303.29	-0.830921	-0.552747
	2	451.351	-2.91259	-1,009.32	221.557	-0.683627	0.552747
	3	451.684	-0.674163	1,075.7	-322.583	-0.10595	-0.0840134
	4	-451.684	0.674163	-1,075.7	-236.781	-0.244615	0.0840134
	5	457.696	3.2222	447.323	73.8951	-0.969317	1.31022
Beam-9 (Structural Member8[14])	1	-578.001	-273.42	-1,032.39	-139.195	47.1591	18.8119
	2	0	0	0	0	0	0
Beam-10 (Structural Member8[1])	1	-87.8333	-439.887	-147.096	50.705	-113.802	39.3539
	2	87.8333	439.887	147.096	22.8429	-106.141	-39.3539
Beam-11 (Structural Member7[4])	1	-652.844	117.955	751.742	437.683	-36.5696	-6.13982
	2	-234.624	143.995	-201.349	39.6517	2.93096	-39.3814
	3	234.624	-143.995	201.349	8.67208	31.6279	39.3814
Beam-12 (Structural Member11)	1	606.013	-37.4936	-156.994	60.3551	-2.91816	-4.21932
	2	-599.827	-38.3245	-159.523	-61.0323	3.71492	-4.19918
	3	-654.367	227.981	156.994	-7.07943	-41.5653	-2.84124
	4	538.408	292.053	-113.337	-71.7815	-185.993	-10.1333
	5	285.462	-200.037	61.0855	10.2174	43.905	-2.84641
Beam-13 (Structural Member5[2])	1	-1,782.66	2.2245	86.6724	23.8113	-2.54389	1.30859
	2	1,782.66	-2.22485	-86.6723	73.8995	0.0358	-1.30859
Beam-14 (Structural Member8[18])	1	-0.088228	-10.0152	0.0090219	-0.00265585	4.44007	-0.124285
	2	0.088228	10.0152	-0.0090217	0.00705398	0.442334	0.124289
Beam-15 (Structural Member8[5])	1	-111.891	-140.061	-141.583	25.2326	-5.46666	-0.618184
	2	111.891	140.061	141.583	10.3429	-29.7264	0.618184



Beam Name	Joints	Axial(N)	Shear1(N)	Shear2(N)	Moment1(N.m)	Moment2(N.m)	Torque(N.m)
Beam-16(Structural Member18[2])	1	10.0152	0.008938	0.0882259	-0.442334	0.124288	0.00705032
	2	-10.0152	0.00893402	-0.0882299	0.17765	-0.0974804	-0.00705015
Beam-17(Structural Member1[4])	1	-0.008325	0.137468	8.45182	-6.3341	0.104618	4.63282
	2	-0.008325	0.14956	8.41384	6.31514	-0.110653	4.63282
	3	0.0083248	-0.137468	-8.45182	-6.34363	0.101584	-4.63282
Beam-18(Structural Member8[9])	1	101.283	-135.588	-66.0479	-4.03657	31.3509	0.965116
	2	-101.284	135.588	66.0474	-12.5592	2.71835	-0.965048
Beam-19(Structural Member16[1])	1	4.99474e-13	1.60262e-11	8.23406e-13	1.89529e-11	2.66529e-11	-8.06123e-11
	2	5.41324e-14	2.94728e-12	2.6765e-13	-2.07149e-12	-2.64939e-12	8.95749e-12
Beam-20(Structural Member10[2])	1	-321.648	135.377	-103.441	9.01213	-23.3744	-31.3078
	2	321.648	-135.377	103.441	-33.8381	-9.11615	31.3078
	3	324.661	132.927	-122.17	-7.67536	23.1408	-30.5259
	4	-324.661	-132.927	122.17	36.9961	8.76163	30.5259
Beam-21(Structural Member7[5])	1	-570.49	85.1855	-288.864	141.778	44.3479	-62.1002
	2	570.49	-85.1855	288.864	141.308	39.1338	62.1002
	3	572.947	88.5144	-285.839	-139.997	-46.667	-60.4065
	4	1,080.23	-0.415668	1.63681	16.9277	-10.4559	-0.799159
Beam-22(Structural Member8[13])	1	69.1436	-447.9	143	20.0233	107.448	41.4684
	2	-69.1436	447.9	-143	51.4769	116.502	-41.4684
Beam-23(Structural Member4[1])	1	-1,654.97	5.58224	-115.119	-78.7492	0.131198	0.386616
	2	1,654.97	-5.58207	115.12	-51.0311	-6.42428	-0.386615
Beam-24(Structural Member7[1])	1	236.834	-161.59	-209.714	-37.784	8.0987	39.7134
	2	802.985	-120.105	808.414	-466.23	-36.0718	5.07539
	3	-236.834	161.59	209.714	-12.5474	30.6828	-39.7134
Beam-25(Structural Member18[1])	1	-2.9425e-12	-3.63757e-12	5.34676e-12	-2.71543e-12	1.31308e-12	-8.72207e-12
	2	1.16405e-11	-8.70826e-12	-4.19936e-11	4.00295e-11	-1.26687e-11	7.84937e-11
Beam-26(Structural Member8[17])	1	0.088228	10.0152	-0.00902191	0.00265359	-4.70475	0.0974753
	2	-0.088228	-10.0152	0.0090217	-0.00705172	-0.17765	-0.0974808
Beam-27(Structural Member8[4])	1	-104.654	-417.291	152.606	-51.2308	-107.034	-39.1843
	2	104.654	417.291	-152.606	-25.0722	-101.611	39.1843
Beam-28(Structural Member1[2])	1	0	0	0	0	0	0
	2	0	0	0	0	0	0
Beam-29(Structural Member10[1])	1	239.093	142.468	91.3189	-39.5385	9.73122	-30.3909
	2	-241.355	139.7	109.689	42.5742	-9.50537	-29.5997
	3	241.355	-139.7	-109.689	-16.2489	-24.0227	29.5997
	4	-239.093	-142.468	-91.3189	17.6219	24.4611	30.3909
Beam-30(Structural Member8[8])	1	397.164	-367.582	-152.425	32.8539	-90.1932	-26.5103
	2	-397.164	367.582	152.425	43.3585	-93.5978	26.5103
Beam-31(Structural Member6[2])	1	-841.126	1.19256	30.3642	-19.5442	4.01772	-0.815202
	2	841.126	-1.19256	-30.3652	-10.6686	-2.83112	0.815198

Beam Name	Joints	Axial(N)	Shear1(N)	Shear2(N)	Moment1(N.m)	Moment2(N.m)	Torque(N.m)
Beam-32(Structural Member4[2])	1	1,771.74	2.54778	-86.6019	73.595	-0.620304	1.44413
	2	-1,771.74	-2.54812	86.6019	24.0363	3.49265	-1.44413
Beam-33(Structural Member8[12])	1	409.396	376.813	-239.891	64.7217	92.8497	26.8813
	2	-409.396	-376.813	239.891	55.224	95.5568	-26.8813
Beam-34(Structural Member7[6])	1	-657.694	-114.674	751.675	435.318	33.5759	5.04491
	2	-241.12	-155.657	-181.185	35.3343	-7.4827	38.3854
	3	241.12	155.657	181.185	8.15007	-29.8749	-38.3854
Beam-35(Structural Member16[2])	1	2.280e-11	-7.339e-13	4.6903e-11	3.41905e-11	-1.55662e-11	-7.83368e-11
	2	2.421e-11	1.6165e-13	-1.2059e-12	-4.66987e-12	1.73462e-12	8.70598e-12
Beam-36(Structural Member1[3])	1	454.054	3.26249	-1,014.45	222.682	0.731472	-1.25909
	2	-454.007	-1.04071	-1,082.18	-238.207	0.382507	-0.696045
	3	-454.054	-3.26249	1,014.45	304.829	0.965025	1.25909
	4	454.007	1.04071	1,082.18	-324.529	0.158662	0.696045
	5	0	0	0	0	0	0
Beam-37(Structural Member8[16])	1	-87.5146	426.495	149.438	-52.2707	110.851	41.417
	2	87.5146	-426.495	-149.438	-22.4485	102.397	-41.417
Beam-38(Structural Member8[3])	1	570.49	-270.331	-898.814	100.531	-24.4956	-20.8346
	2	-570.49	270.331	898.814	125.314	-43.4303	20.8346
Beam-39(Structural Member6[1])	1	835.81	1.15558	-29.5302	-10.3967	3.69854	-0.678608
	2	-835.81	-1.15558	29.5292	-18.9854	-4.84834	0.678613
Beam-40(Structural Member3)	1	-0.287029	-0.0166495	16.8657	9.26564	0.0121033	-0.0380093
	2	0.287029	0.0166495	-16.8657	8.4433	0.00537867	0.0380093
Beam-41(Structural Member9[2])	1	-1,126.46	3.0219	-116.655	-4.46845	46.7272	-2.58408
	2	594.618	198.623	-407.708	160.055	83.0142	55.7469
	3	-594.618	-198.623	187.39	129.796	110.469	-55.7469
	4	-599.411	195.585	-405.959	-159.25	-81.8543	57.9492
Beam-42(Structural Member8[7])	1	390.555	-384.503	148.787	-32.0646	-94.5698	26.3492
	2	-390.555	384.503	-148.787	-42.3288	-97.6818	-26.3492
Beam-43(Structural Member7[2])	1	-596.841	-85.5321	-301.845	148.17	-44.4958	62.5304
	2	596.841	85.5321	301.845	147.639	-39.3257	-62.5304
	3	601.477	-89.7383	-297.547	-145.855	47.4526	60.6268
	4	1,128.45	0.567922	1.6887	17.6689	10.3193	0.676067
Beam-44(Structural Member14)	1	-639.004	-56.5257	132.688	-47.1122	-15.2079	2.95659
	2	641.477	-50.7189	135.616	48.1708	14.7335	3.00266
	3	283.326	-36.2432	0.0141594	-0.631076	9.45868	-0.272403
	4	571.939	12.1007	-132.688	1.96065	4.1948	1.97184
Beam-45(Structural Member8[11])	1	124.328	-132.716	63.0358	4.0229	30.4829	-1.01046
	2	0	0	0	0	0	0
Beam-46(Structural Member8[15])	1	550.393	261.95	-887.468	99.474	20.2988	18.4993
	2	-550.393	-261.95	887.468	123.52	45.5212	-18.4993
Beam-47(Structural Member8[2])	1	598.698	-281.682	1,039.82	-120.773	-25.9909	21.5223
	2	-598.703	281.682	-1,039.82	-140.503	-44.7871	-21.5223

Beam Name	Joints	Axial(N)	Shear1(N)	Shear2(N)	Moment1(N.m)	Moment2(N.m)	Torque(N.m)
Beam-48(Structural Member18[3])	1	-1.103e-11	2.4346e-12	5.01336e-12	-3.38017e-11	1.26238e-11	8.04559e-11
	2	1.200e-11	3.2815e-13	7.17496e-14	4.34211e-12	-1.36225e-12	-8.93797e-12
Beam-49(Structural Member2)	1	-7.04755	-0.133426	-8.74356	5.85904	-0.161021	4.22621
	2	7.0642	-0.153601	-8.12209	-4.96484	0.196663	4.21709
	3	7.04755	0.133426	8.74356	7.25631	-0.0391189	-4.22621



## Appendix 5: Solar collector beam stresses.

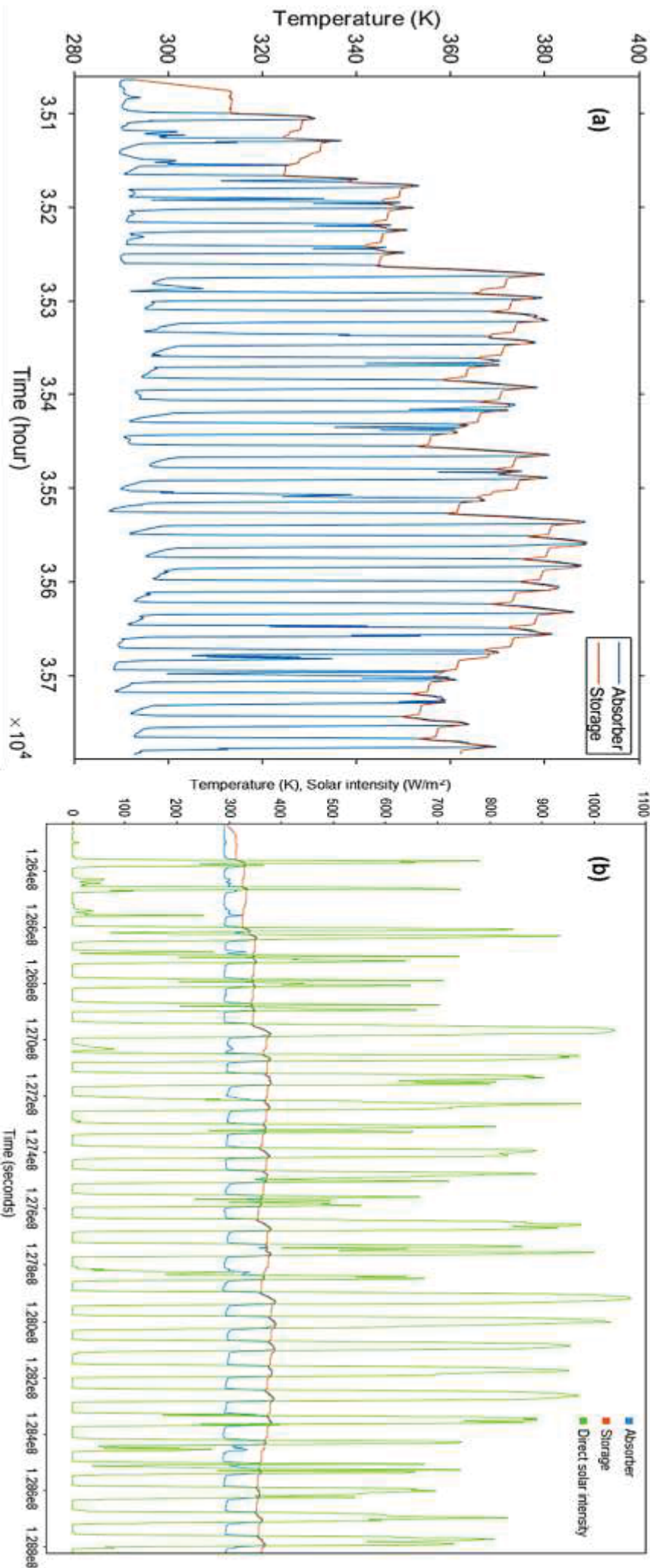
Beam Name	Joints	Axial(N/m <sup>2</sup> )	Bending Dir1(N/m <sup>2</sup> )	Bending Dir2(N/m <sup>2</sup> )	Torsional (N/m <sup>2</sup> )	Upper bound axial and bending(N/m <sup>2</sup> )
Beam-1(Structural Member5[1])	1	-6.21607e+06	2.39811e+07	2.81468e+06	13,288.7	3.30118e+07
	2	-6.21607e+06	-3.67986e+07	-255,885	-13,289.1	4.32706e+07
Beam-2(Structural Member9[1])	1	-8.08895e+06	-7.89182e+06	6.75036e+07	2.50134e+06	8.34843e+07
	2	-4.27815e+06	-2.22726e+08	-1.19589e+08	-5.73779e+07	3.46594e+08
	3	-4.29535e+06	-2.22999e+08	-1.19116e+08	-5.9481e+07	3.4641e+08
	4	-4.27815e+06	1.78743e+08	1.59162e+08	5.73779e+07	3.42183e+08
Beam-3(Structural Member12)	1	5.17515e+06	-2.38669e+08	-4.70657e+07	-1.69167e+08	2.90909e+08
	2	4.45822e+06	4.94921e+06	5.73637e+07	-1.15889e+08	6.67711e+07
	3	5.21257e+06	-2.4011e+08	-4.34622e+07	-1.70752e+08	2.88785e+08
	4	2.51146e+06	-3.38043e+07	-4.60595e+07	-5.28653e+07	8.23752e+07
Beam-4(Structural Member7[3])	1	-6.01248e+06	6.79043e+08	5.77205e+07	-6.63265e+06	7.42776e+08
	2	1.70931e+06	1.92748e+07	-4.72698e+07	4.19685e+07	6.82538e+07
	3	1.70931e+06	-6.14116e+07	4.37379e+06	-4.19685e+07	6.74947e+07
Beam-5(Structural Member8[6])	1	666,550	3.69846e+07	-7.86335e+06	-141,793	4.55145e+07
	2	666,545	-1.52344e+07	4.37238e+07	141,732	5.96248e+07
Beam-6(Structural Member15)	1	4.79679e+06	-2.21649e+08	8.48318e+08	5.04363e+08	1.07476e+09
	2	-5.41288e+06	3.67421e+08	-2.13939e+08	2.02345e+08	5.86773e+08
	3	-5.8722e+06	-5.87443e+07	1.91509e+08	1.29773e+08	2.56125e+08
	4	-5.33768e+06	3.7202e+08	-2.20142e+08	2.0154e+08	5.97499e+08
	5	2.56707e+06	8.29929e+07	-2.17707e+08	1.41608e+08	3.03267e+08
Beam-7(Structural Member8[10])	1	-3.0187e+06	-7.82966e+07	-1.45078e+08	2.76835e+07	2.26393e+08
	2	-3.0187e+06	9.26765e+07	1.41146e+08	-2.76835e+07	2.36841e+08
Beam-8(Structural Member1[1])	1	-1.68697e+06	1.40751e+08	385,614	-189,627	1.42823e+08
	2	-1.68697e+06	-1.0282e+08	-317,258	189,627	1.04824e+08
	3	-1.68821e+06	1.49704e+08	-49,169.2	-28,822	1.51442e+08
	4	-1.68821e+06	-1.09885e+08	113,521	28,822	1.11687e+08
	5	1.71069e+06	3.42932e+07	449,840	449,491	3.64537e+07
Beam-9(Structural Member8[14])	1	-4.32315e+06	-2.011e+08	-6.81327e+07	1.93878e+07	2.73556e+08
	2	0	0	0	0	0
Beam-10(Structural Member8[1])	1	656,947	-7.32555e+07	-1.64415e+08	4.05586e+07	2.38327e+08
	2	656,947	3.3002e+07	1.53346e+08	-4.05586e+07	1.87005e+08
Beam-11(Structural Member7[4])	1	-4.88293e+06	6.32337e+08	5.28336e+07	-6.32777e+06	6.90054e+08
	2	1.75487e+06	-5.72863e+07	4.23447e+06	-4.0587e+07	6.32756e+07
	3	1.75487e+06	1.25289e+07	-4.5694e+07	4.0587e+07	5.99778e+07
Beam-12(Structural Member11)	1	-5.52096e+06	-3.61741e+08	-2.22197e+08	-2.10373e+08	5.89459e+08
	2	-5.46459e+06	-3.68397e+08	-2.29144e+08	-2.09368e+08	6.03006e+08
	3	-5.96147e+06	1.00041e+08	2.18223e+08	-1.41662e+08	3.24225e+08
	4	4.90505e+06	2.13885e+08	8.40151e+08	-5.05239e+08	1.05894e+09
	5	2.60064e+06	-8.97031e+07	-2.21194e+08	-1.4192e+08	3.13498e+08
Beam-13(Structural Member5[2])	1	-6.66288e+06	1.10503e+07	1.18057e+06	448,930	1.88938e+07
	2	-6.66288e+06	-3.42952e+07	16,614	-448,930	4.09747e+07
Beam-14(Structural Member8[18])	1	-659.899	-3,837.01	-6.41474e+06	-128,089	6.41923e+06
	2	-659.899	-10,191.2	639,057	128,094	649,908
	1	836,886	-3.64545e+07	-7.8979e+06	-637,108	4.51893e+07

Beam Name	Joints	Axial(N/m <sup>2</sup> )	Bending Dir1(N/m <sup>2</sup> )	Bending Dir2(N/m <sup>2</sup> )	Torsional (N/m <sup>2</sup> )	Upper bound axial and bending(N/m <sup>2</sup> )
Beam-15(Structural Member8[5])	2	836,886	1.49428e+07	4.29468e+07	637,108	5.87266e+07
Beam-16(Structural Member18[2])	1	-72,950.4	749,434	210,578	5,972.58	851,407
	2	-72,950.4	300,988	165,158	-5,972.44	416,274
Beam-17(Structural Member1[4])	1	31.1146	2.93953e+06	48,551.2	1.58935e+06	2.98811e+06
	2	-31.1146	2.93073e+06	51,352	1.58935e+06	2.98211e+06
	3	31.1146	-2.94395e+06	-47,143.1	-1.58935e+06	2.99112e+06
Beam-18(Structural Member8[9])	1	757,548	-5.8318e+06	-4.52939e+07	994,660	5.18832e+07
	2	757,550	1.81448e+07	3.92731e+06	-994,590	2.28296e+07
Beam-19(Structural Member16[1])	1	2.09636e-09	1.49657e-05	-2.10458e-05	-3.18268e-05	2.58265e-05
	2	-2.272e-10	1.6357e-06	-2.09202e-06	3.53653e-06	2.6558e-06
Beam-20(Structural Member10[2])	1	-2.40576e+06	1.30202e+07	3.37699e+07	-3.22662e+07	4.91959e+07
	2	-2.40576e+06	4.88872e+07	-1.31705e+07	3.22662e+07	6.44634e+07
	3	-2.4283e+06	1.10889e+07	3.34324e+07	-3.14604e+07	4.69496e+07
	4	-2.4283e+06	5.34497e+07	-1.26583e+07	3.14604e+07	6.85363e+07
Beam-21(Structural Member7[5])	1	4.26697e+06	-2.04832e+08	6.40712e+07	-6.39997e+07	2.73171e+08
	2	4.26697e+06	2.04154e+08	-5.65382e+07	6.39997e+07	2.64959e+08
	3	4.28535e+06	-2.02259e+08	6.74217e+07	-6.22542e+07	2.73966e+08
	4	8.07956e+06	2.44561e+07	1.5106e+07	-823,604	4.76417e+07
Beam-22(Structural Member8[13])	1	517,158	2.89285e+07	-1.55234e+08	4.27378e+07	1.8468e+08
	2	517,158	-7.43707e+07	1.68316e+08	-4.27378e+07	2.43203e+08
Beam-23(Structural Member4[1])	1	-6.18561e+06	-3.65459e+07	-60,886.3	132,634	4.27924e+07
	2	-6.18561e+06	2.36825e+07	-2.98138e+06	-132,634	3.28495e+07
Beam-24(Structural Member7[1])	1	1.7714e+06	-5.4588e+07	-1.17005e+07	4.09282e+07	6.80599e+07
	2	-6.00591e+06	6.7358e+08	-5.21144e+07	5.23064e+06	7.31701e+08
	3	1.7714e+06	1.81278e+07	4.43287e+07	-4.09282e+07	6.42279e+07
Beam-25(Structural Member18[1])	1	-2.14331e-08	-4.60068e-06	-2.22471e-06	-7.38878e-06	5.13177e-06
	2	-8.47894e-08	-6.78208e-05	-2.14642e-05	6.64948e-05	7.12211e-05
Beam-26(Structural Member8[17])	1	659.899	3,833.75	6.79714e+06	100,459	6.80163e+06
	2	659.899	10,187.9	-256,658	-100,465	267,506
Beam-27(Structural Member8[4])	1	782,756	7.40152e+07	-1.54636e+08	-4.03839e+07	2.29434e+08
	2	782,756	-3.62227e+07	1.46802e+08	4.03839e+07	1.83808e+08
Beam-28(Structural Member1[2])	1	0	0	0	0	0
	2	0	0	0	0	0
Beam-29(Structural Member10[1])	1	-1.78829e+06	5.71228e+07	1.40591e+07	-3.13213e+07	7.29702e+07
	2	-1.80521e+06	6.15086e+07	1.37328e+07	-3.05058e+07	7.70466e+07
	3	-1.80521e+06	2.34754e+07	-3.47065e+07	3.05058e+07	5.99871e+07
	4	-1.78829e+06	2.54591e+07	-3.534e+07	3.13213e+07	6.25873e+07
Beam-30(Structural Member8[8])	1	-2.97058e+06	-4.74654e+07	-1.30306e+08	-2.73218e+07	1.80742e+08
	2	-2.97058e+06	6.26417e+07	1.35224e+08	2.73218e+07	2.00837e+08
Beam-31(Structural Member6[2])	1	3.14379e+06	9.07008e+06	1.86454e+06	-279,666	1.40784e+07
	2	3.14379e+06	-4.9511e+06	1.31387e+06	279,665	9.40876e+06
	1	-6.62207e+06	-3.41539e+07	-287,870	495,428	4.10639e+07

Beam Name	Joints	Axial(N/m <sup>2</sup> )	Bending Dir1(N/m <sup>2</sup> )	Bending Dir2(N/m <sup>2</sup> )	Torsional (N/m <sup>2</sup> )	Upper bound axial and bending(N/m <sup>2</sup> )
Beam-32(Structural Member4[2])	2	-6.62207e+06	1.11548e+07	-1.62087e+06	-495,428	1.93977e+07
Beam-33(Structural Member8[12])	1	-3.06207e+06	-9.35061e+07	1.34144e+08	2.77042e+07	2.30712e+08
	2	-3.06207e+06	7.97843e+07	-1.38055e+08	-2.77042e+07	2.20901e+08
Beam-34(Structural Member7[6])	1	-4.91921e+06	6.28921e+08	-4.85084e+07	5.19923e+06	6.82348e+08
	2	1.80346e+06	-5.10489e+07	-1.08106e+07	3.95595e+07	6.36629e+07
	3	1.80346e+06	1.17747e+07	4.31614e+07	-3.95595e+07	5.67396e+07
Beam-35(Structural Member16[2])	1	-9.57082e-08	-2.69977e-05	-1.22915e-05	-3.09284e-05	2.97597e-05
	2	1.01594e-07	-3.68745e-06	-1.3697e-06	3.43723e-06	4.03521e-06
Beam-36(Structural Member1[3])	1	-1.69707e+06	-1.03342e+08	339,461	-431,948	1.05379e+08
	2	-1.6969e+06	-1.10547e+08	-177,514	-238,788	1.12421e+08
	3	-1.69707e+06	1.41465e+08	-447,849	431,948	1.4361e+08
	4	-1.6969e+06	1.50607e+08	73,632.1	238,788	1.52378e+08
	5	0	0	0	0	0
Beam-37(Structural Member8[16])	1	654,564	7.55175e+07	1.6015e+08	4.26848e+07	2.36323e+08
	2	654,564	-3.24323e+07	-1.47936e+08	-4.26848e+07	1.81023e+08
Beam-38(Structural Member8[3])	1	-4.26697e+06	-1.45241e+08	-3.53897e+07	-2.14724e+07	1.84898e+08
	2	-4.26697e+06	1.81046e+08	6.27454e+07	2.14724e+07	2.48058e+08
Beam-39(Structural Member6[1])	1	3.12392e+06	-4.8249e+06	-1.71642e+06	-232,806	9.66523e+06
	2	3.12392e+06	8.81074e+06	-2.25002e+06	232,808	1.41847e+07
Beam-40(Structural Member3)	1	-1,072.8	4.3e+06	-5,616.89	-13,039.6	4.30669e+06
	2	-1,072.8	-3.91836e+06	2,496.13	13,039.6	3.92193e+06
Beam-41(Structural Member9[2])	1	-8.42536e+06	-6.45574e+06	-6.75086e+07	-2.66319e+06	8.23897e+07
	2	-4.44743e+06	-2.31237e+08	1.19934e+08	5.74535e+07	3.55619e+08
	3	-4.44743e+06	1.87521e+08	-1.596e+08	-5.74535e+07	3.51568e+08
	4	-4.48328e+06	-2.30075e+08	1.18258e+08	5.97231e+07	3.52817e+08
Beam-42(Structural Member8[7])	1	-2.92115e+06	4.6325e+07	-1.36629e+08	2.71558e+07	1.85875e+08
	2	-2.92115e+06	-6.11541e+07	1.41125e+08	-2.71558e+07	2.052e+08
Beam-43(Structural Member7[2])	1	4.46406e+06	-2.14066e+08	-6.42848e+07	6.44446e+07	2.82815e+08
	2	4.46406e+06	2.13299e+08	5.68154e+07	-6.44446e+07	2.74579e+08
	3	4.49874e+06	-2.10722e+08	-6.85566e+07	6.24828e+07	2.83777e+08
	4	8.44021e+06	2.5527e+07	-1.49087e+07	696,763	4.88759e+07
Beam-44(Structural Member14)	1	5.82151e+06	2.22923e+08	7.1516e+07	1.47413e+08	3.00261e+08
	2	5.84404e+06	2.30707e+08	7.78799e+07	1.49711e+08	3.14431e+08
	3	2.58118e+06	-3.58349e+07	-5.72817e+07	-1.35819e+07	9.56978e+07
	4	5.21052e+06	-2.83191e+06	-1.77866e+07	9.83146e+07	2.58291e+07
Beam-45(Structural Member8[11])	1	929,906	5.81205e+06	-4.40399e+07	-1.04139e+06	5.07818e+07
	2	0	0	0	0	0
Beam-46(Structural Member8[15])	1	-4.11665e+06	-1.43714e+08	2.93265e+07	1.90656e+07	1.77157e+08
	2	-4.11665e+06	1.78454e+08	-6.57663e+07	-1.90656e+07	2.48337e+08
Beam-47(Structural Member8[2])	1	-4.47795e+06	1.74486e+08	-3.75501e+07	2.21812e+07	2.16514e+08
	2	-4.47799e+06	-2.0299e+08	6.47057e+07	-2.21812e+07	2.72174e+08
	1	-8.03738e-08	-5.72693e-05	-2.13882e-05	6.81571e-05	6.12132e-05

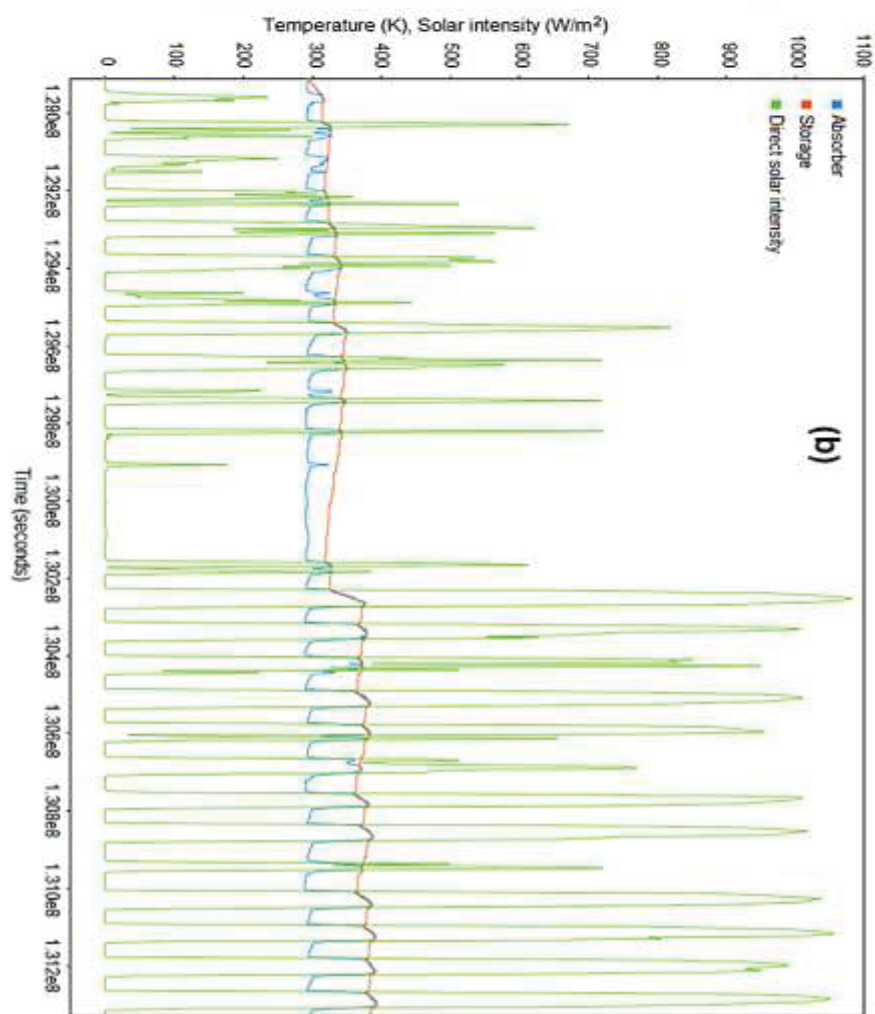
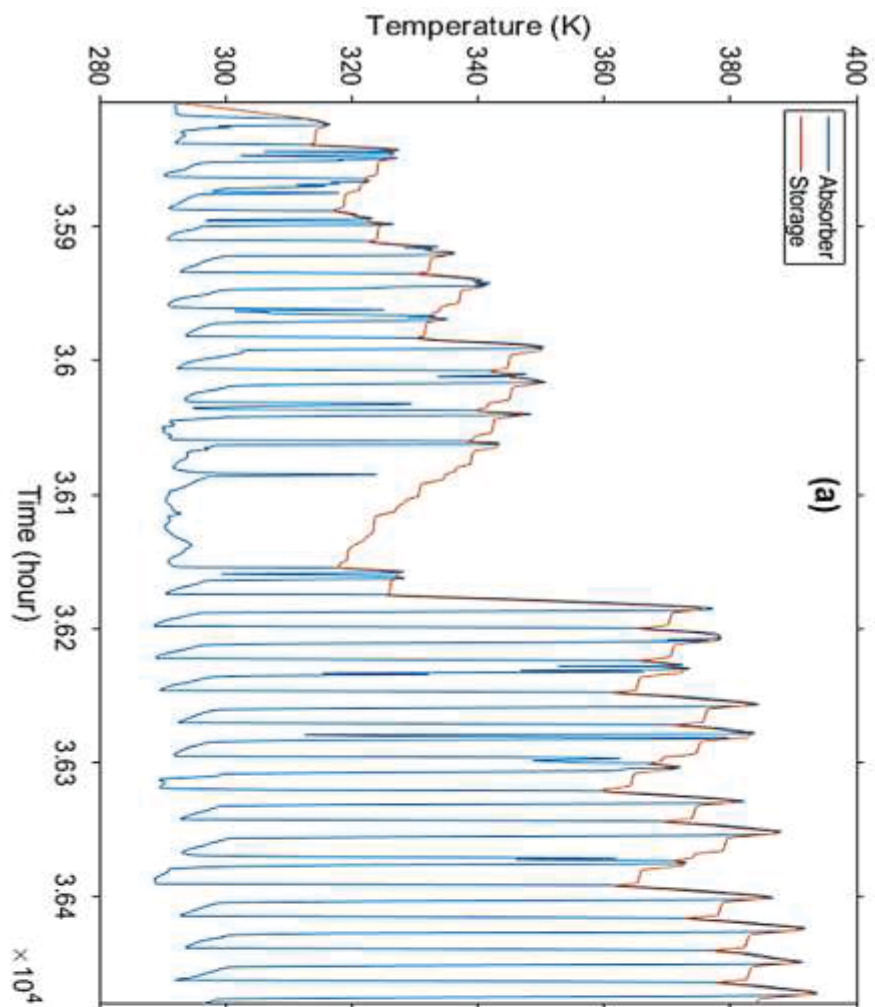
Beam Name	Joints	Axial(N/m <sup>2</sup> )	Bending Dir1(N/m <sup>2</sup> )	Bending Dir2(N/m <sup>2</sup> )	Torsional (N/m <sup>2</sup> )	Upper bound axial and bending(N/m <sup>2</sup> )
Beam-48(Structural Member18[3])	2	-8.74111e-08	-7.35672e-06	-2.30802e-06	-7.57168e-06	7.79768e-06
Beam-49(Structural Member2)	1	26,340.9	-2.71906e+06	-74,726.5	1.44986e+06	2.82013e+06
	2	26,403.1	-2.30408e+06	-91,267.4	1.44673e+06	2.42175e+06
	3	26,340.9	3.36751e+06	18,154.3	-1.44986e+06	3.412e+06

**Appendix 6:** Impact of solar intensity on the absorber and storage temperature for each month in year 2019.

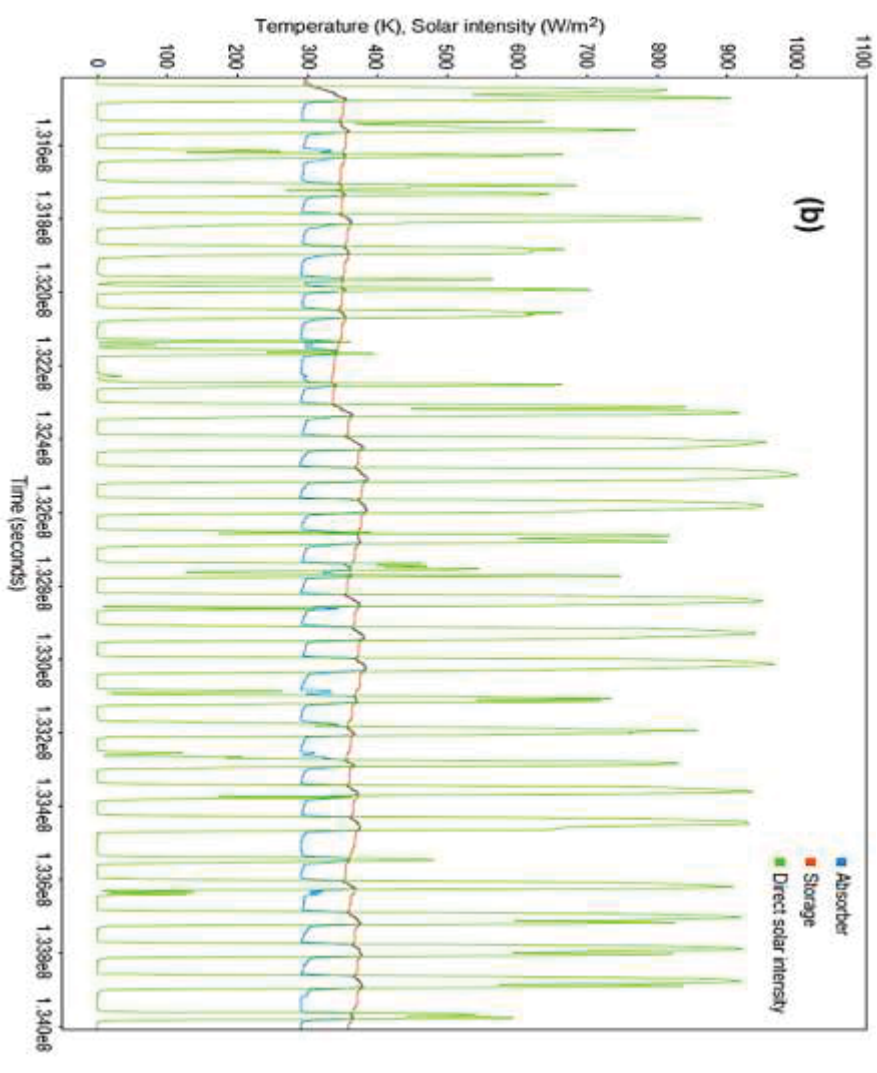
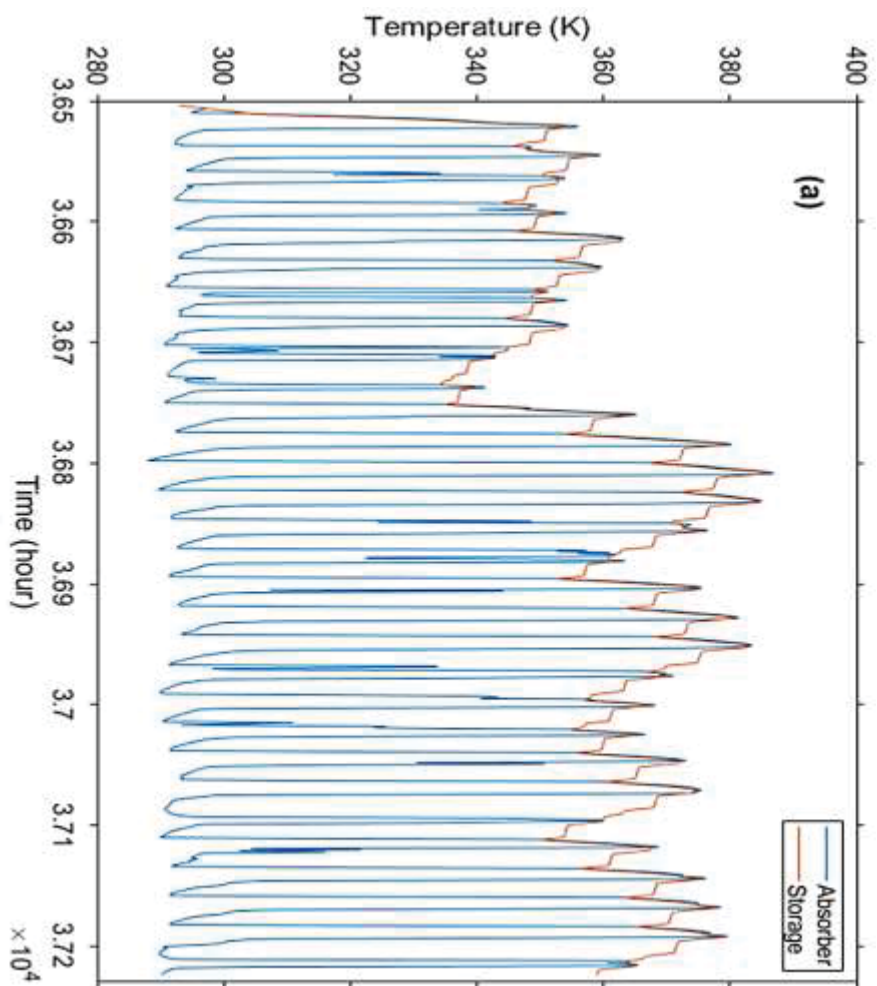


**Appendix 6.1:** Impact of solar intensity (SI) on the absorber and storage temperature for January 2019 (a) without and (b) with solar intensity relationship.

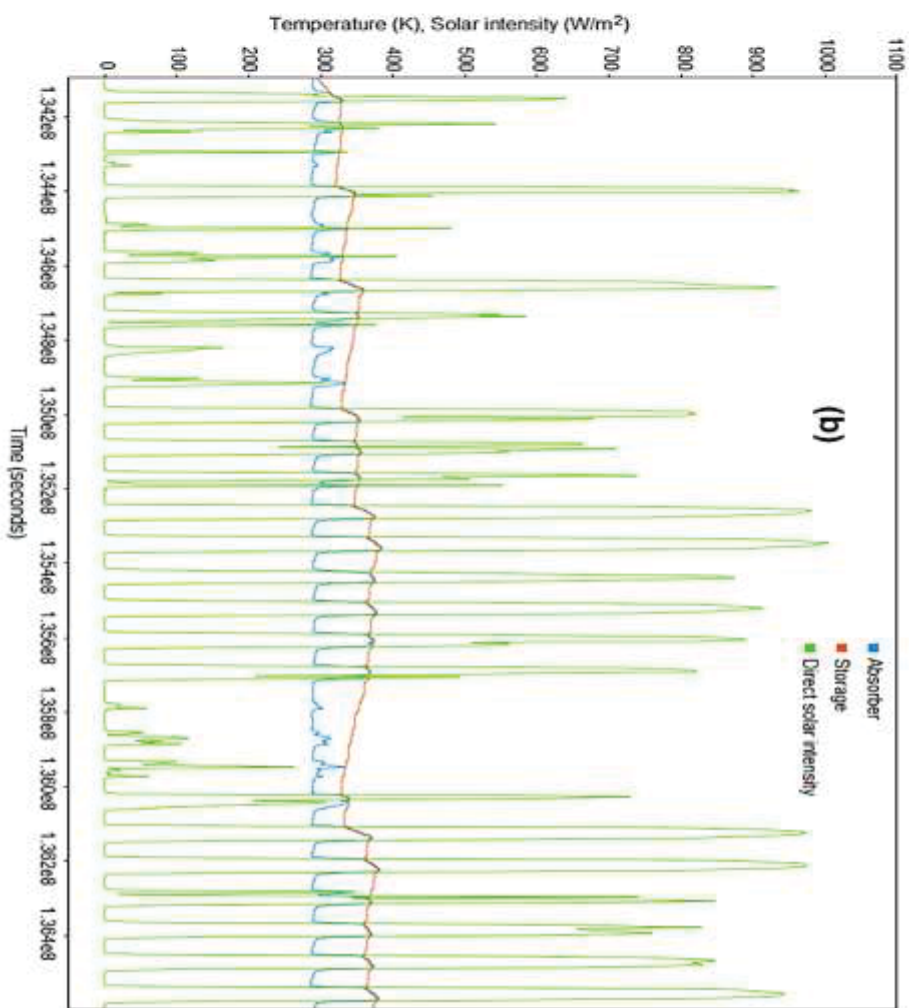
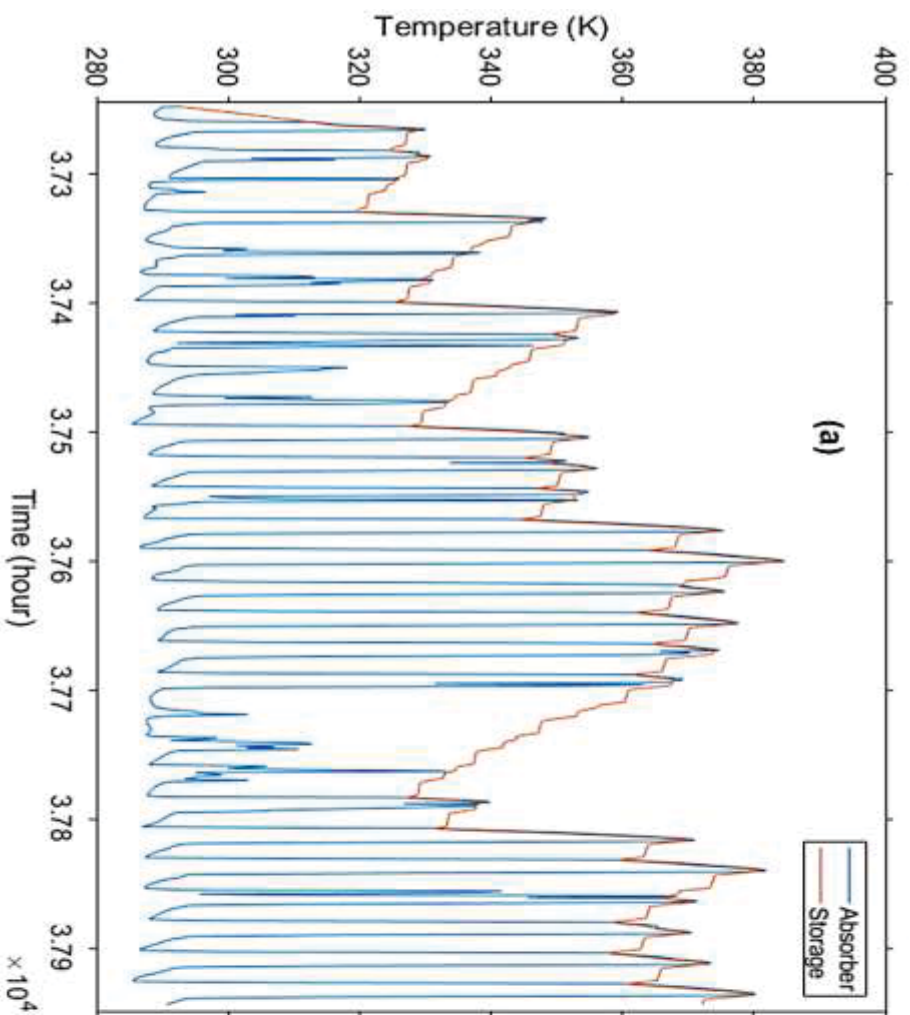




**Appendix 6.2:** Impact of solar intensity (SI) on the absorber and storage temperature for February 2019 (a) without and (b) with solar intensity relationship.

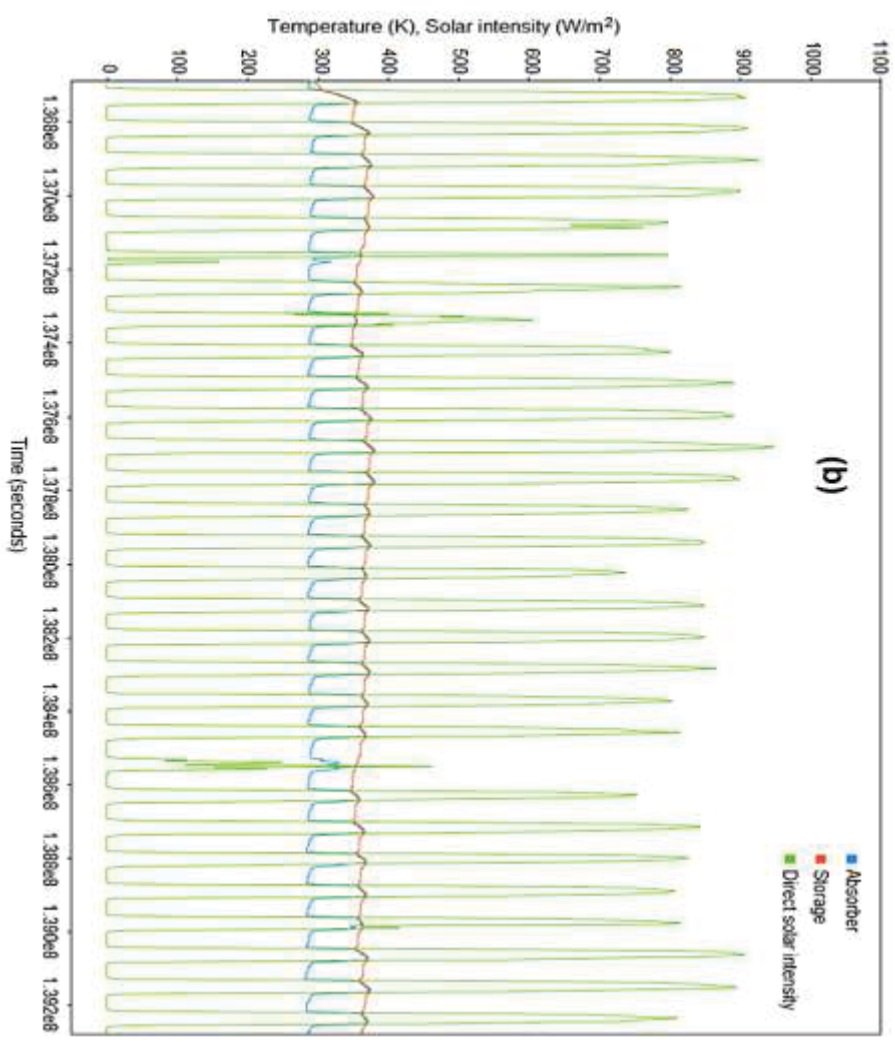
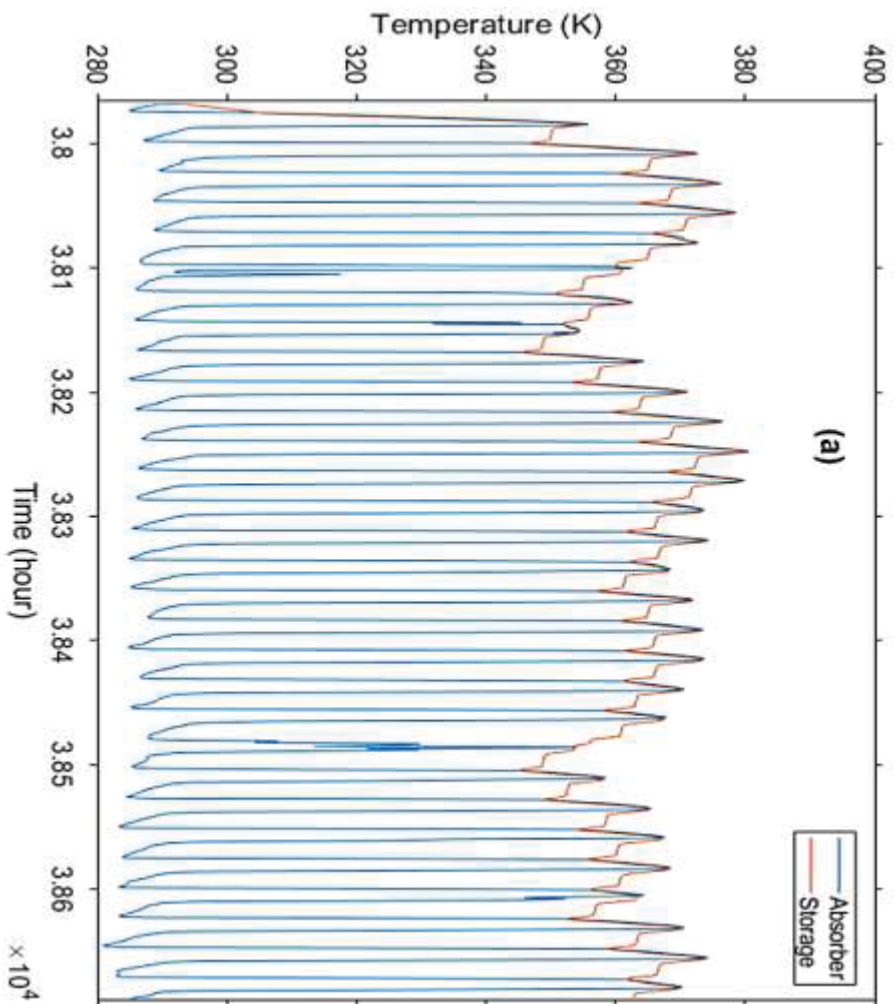


**Appendix 6.3:** Impact of solar intensity (SI) on the absorber and storage temperature for March 2019 (a) without and (b) with solar intensity relationship.

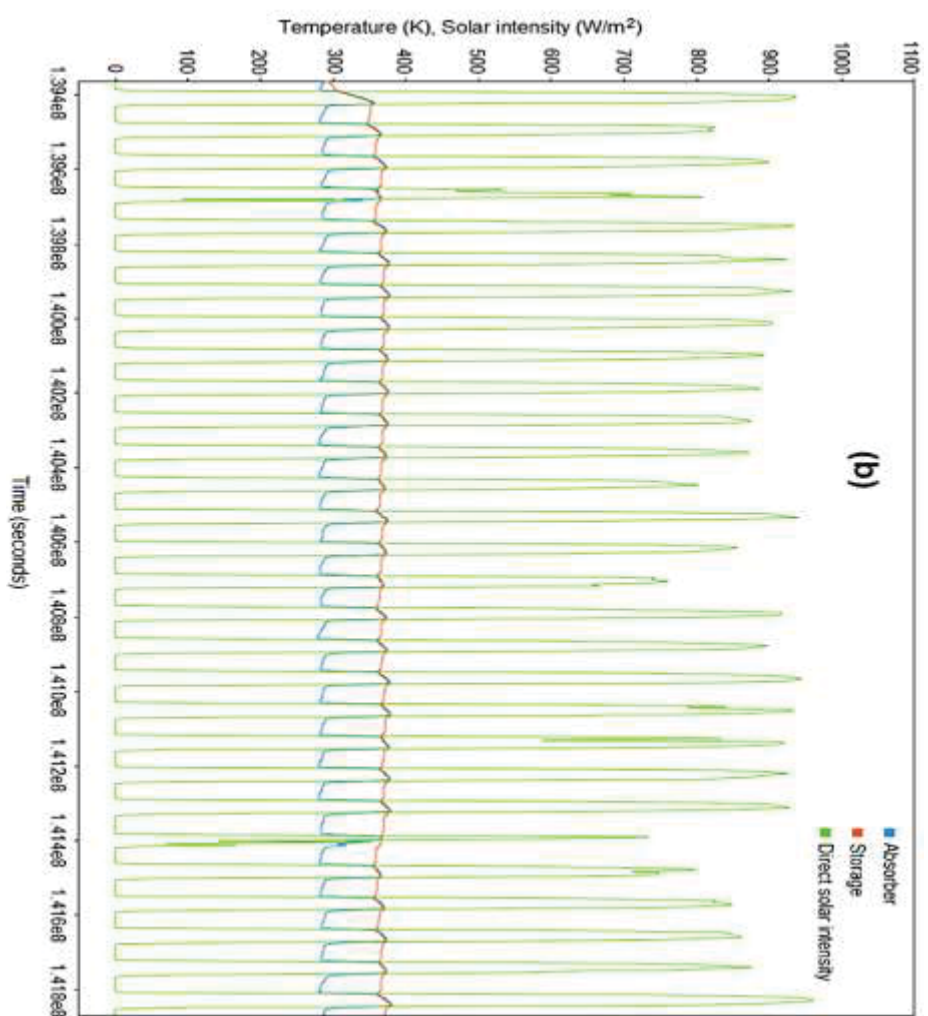
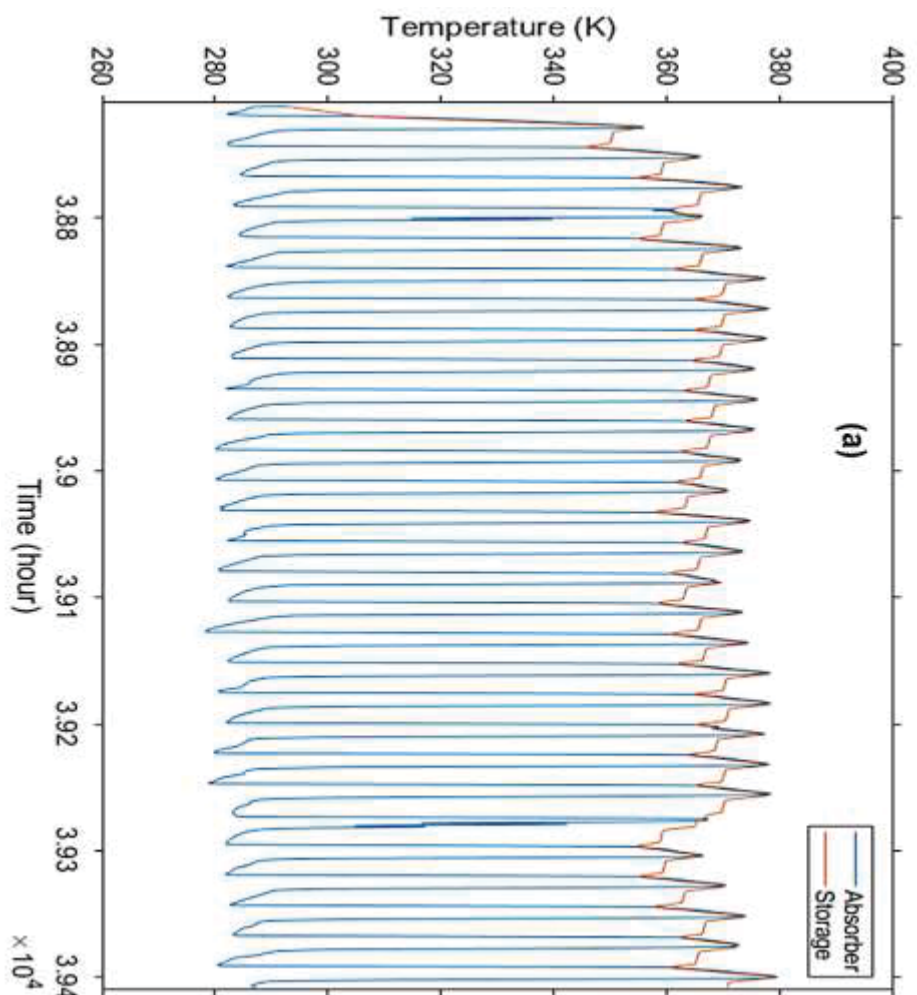


**Appendix 6.4:** Impact of solar intensity (SI) on the absorber and storage temperature for April 2019 (a) without and (b) with solar intensity relationship.

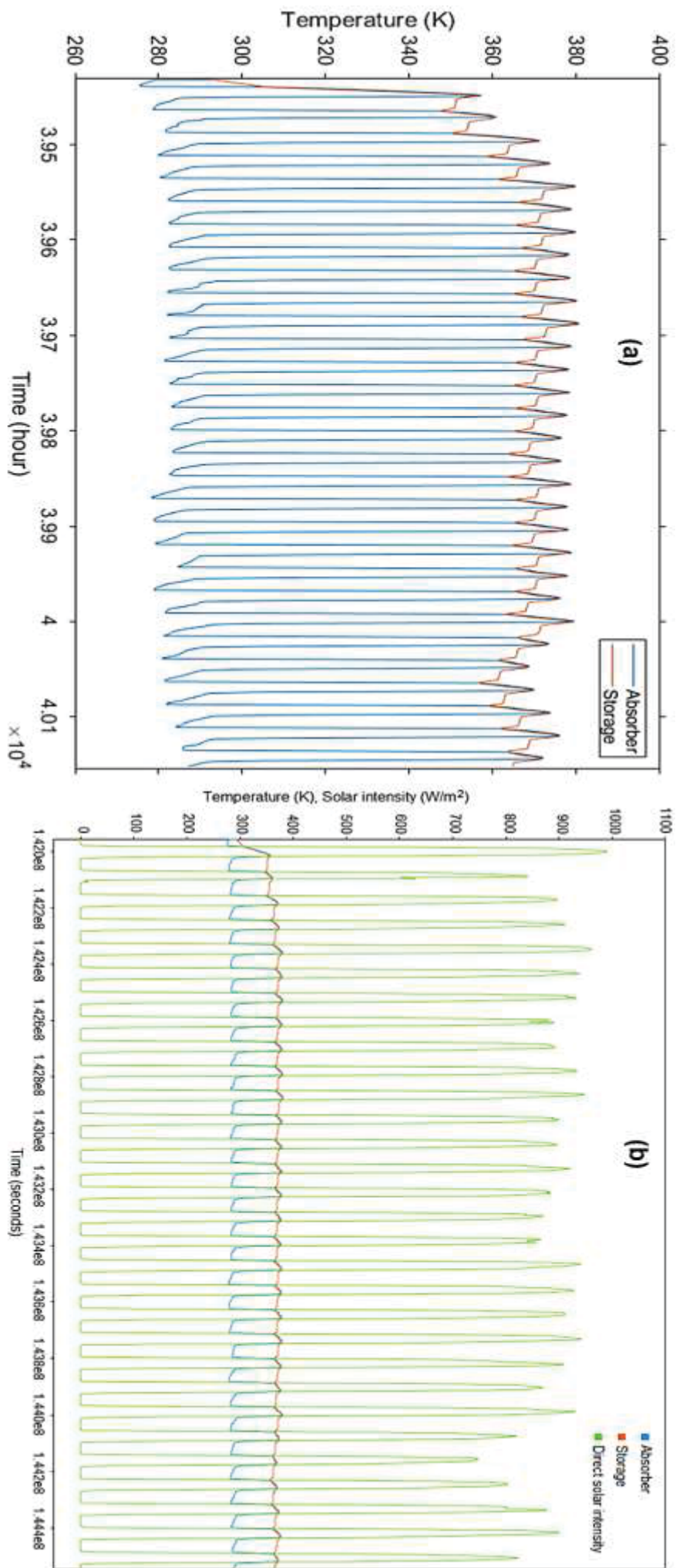




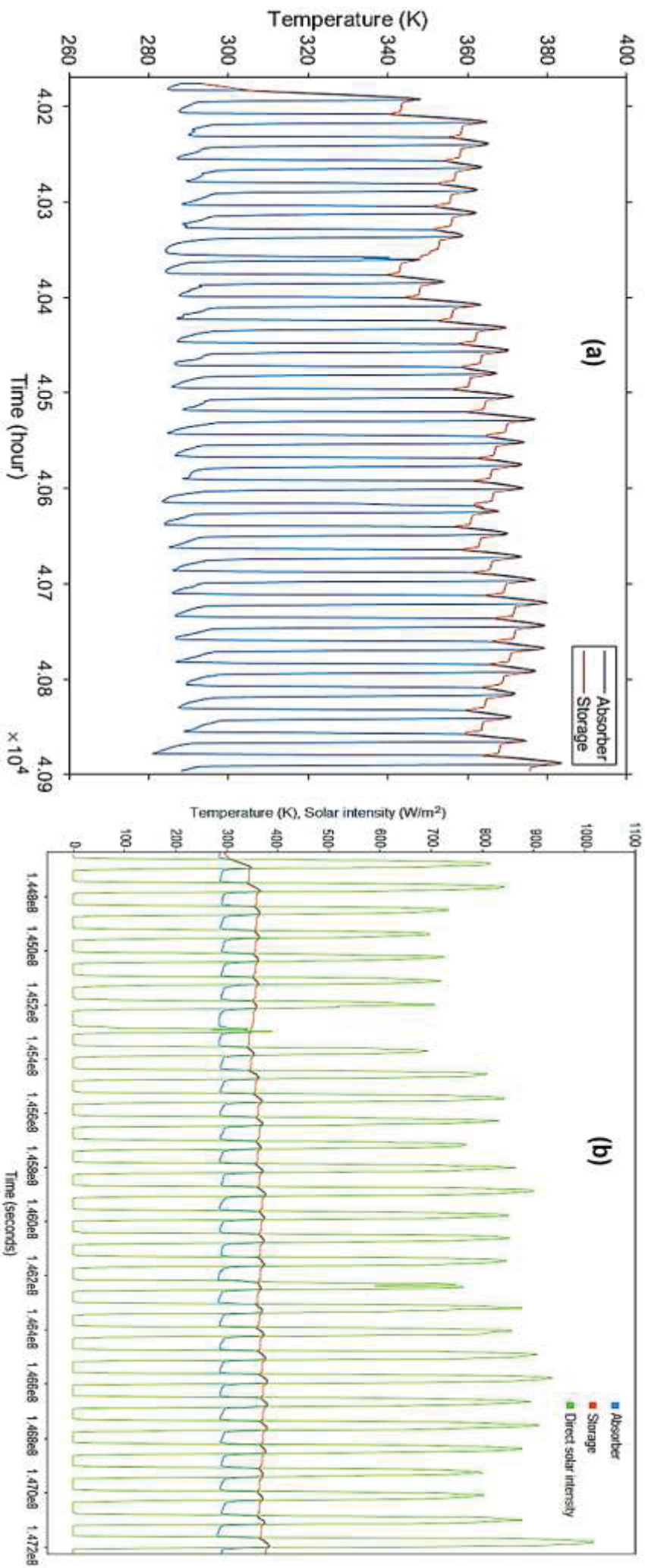
**Appendix 6.5:** Impact of solar intensity (SI) on the absorber and storage temperature for May 2019 (a) without and (b) with solar intensity relationship.



**Appendix 6.6:** Impact of solar intensity (SI) on the absorber and storage temperature for June 2019 (a) without and (b) with solar intensity relationship.

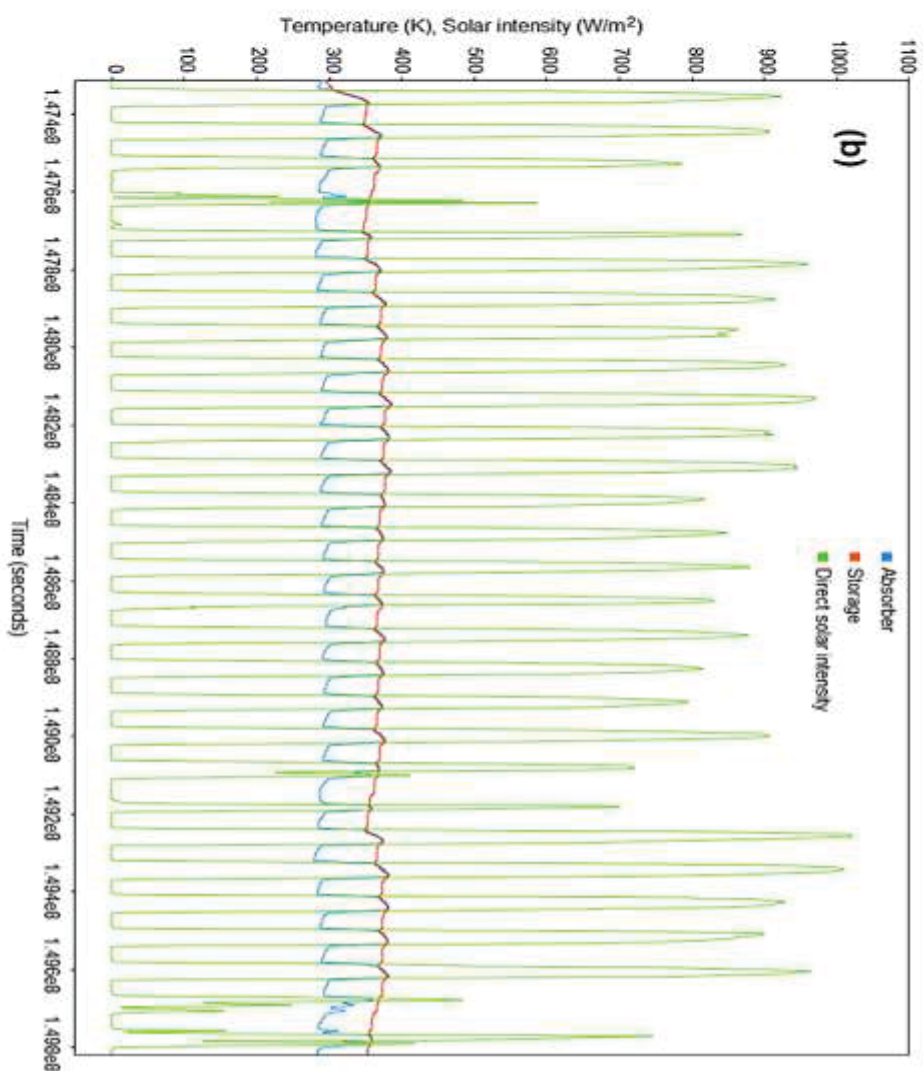
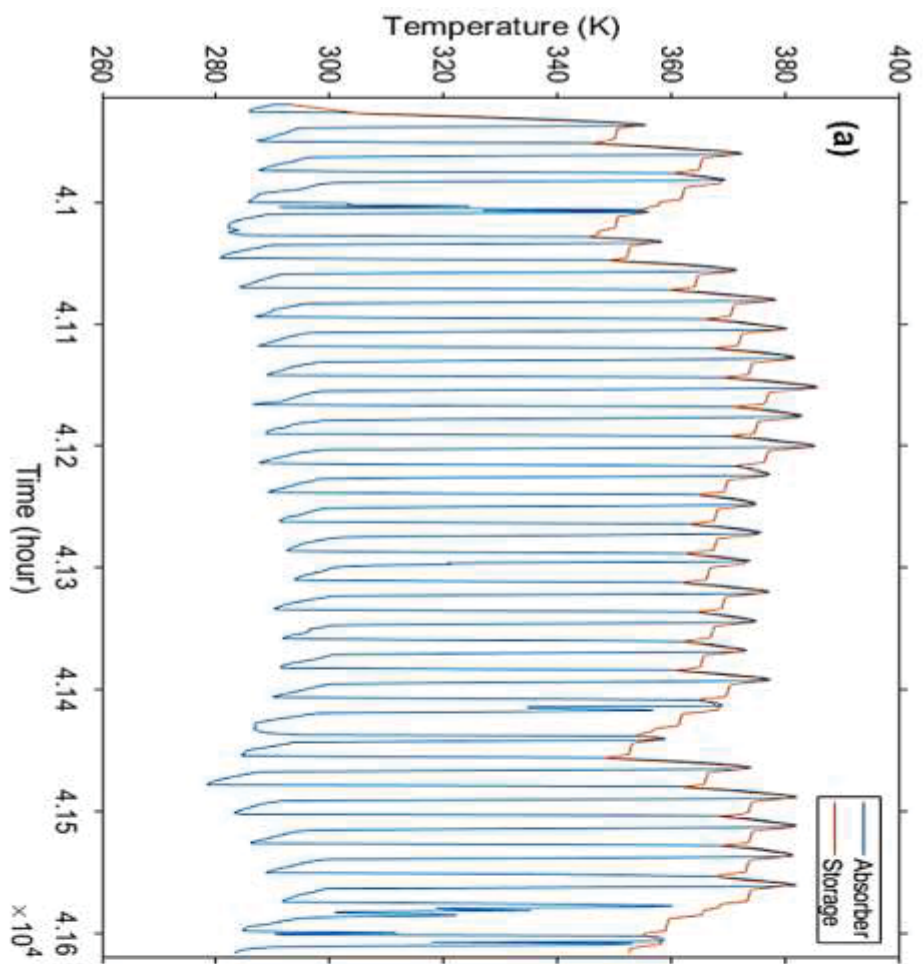


**Appendix 6.7:** Impact of solar intensity (SI) on the absorber and storage temperature for July 2019 (a) without and (b) with solar intensity relationship.

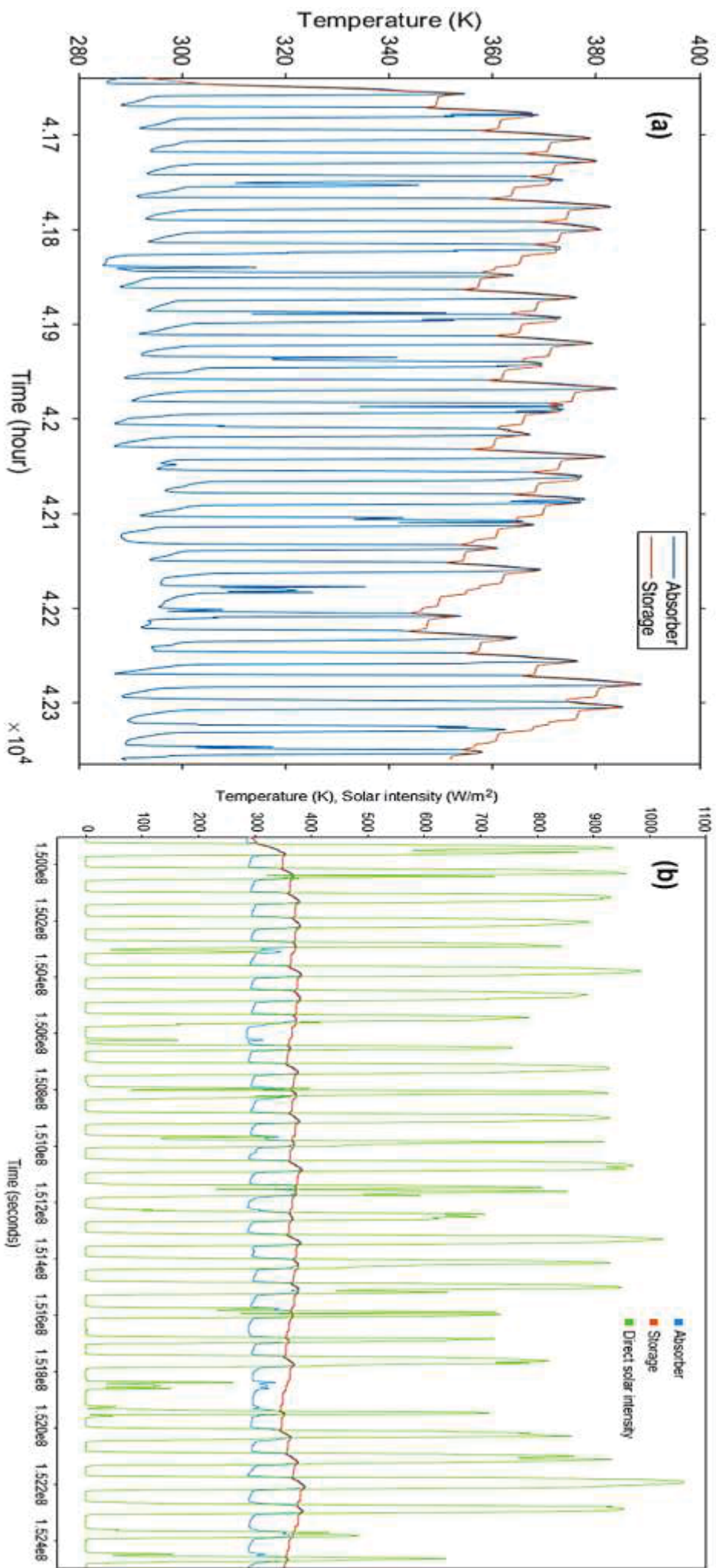


**Appendix 6.8:** Impact of solar intensity (SI) on the absorber and storage temperature for August 2019 (a) without and (b) with solar intensity relationship.

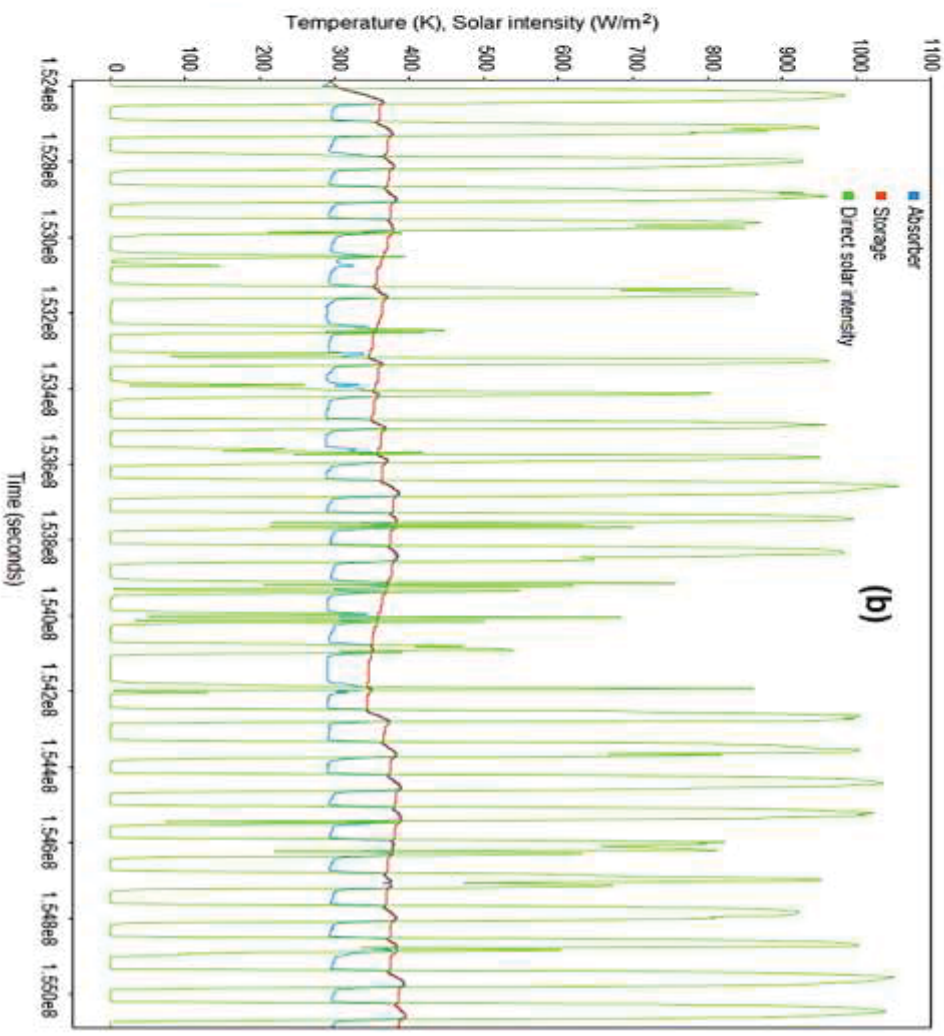
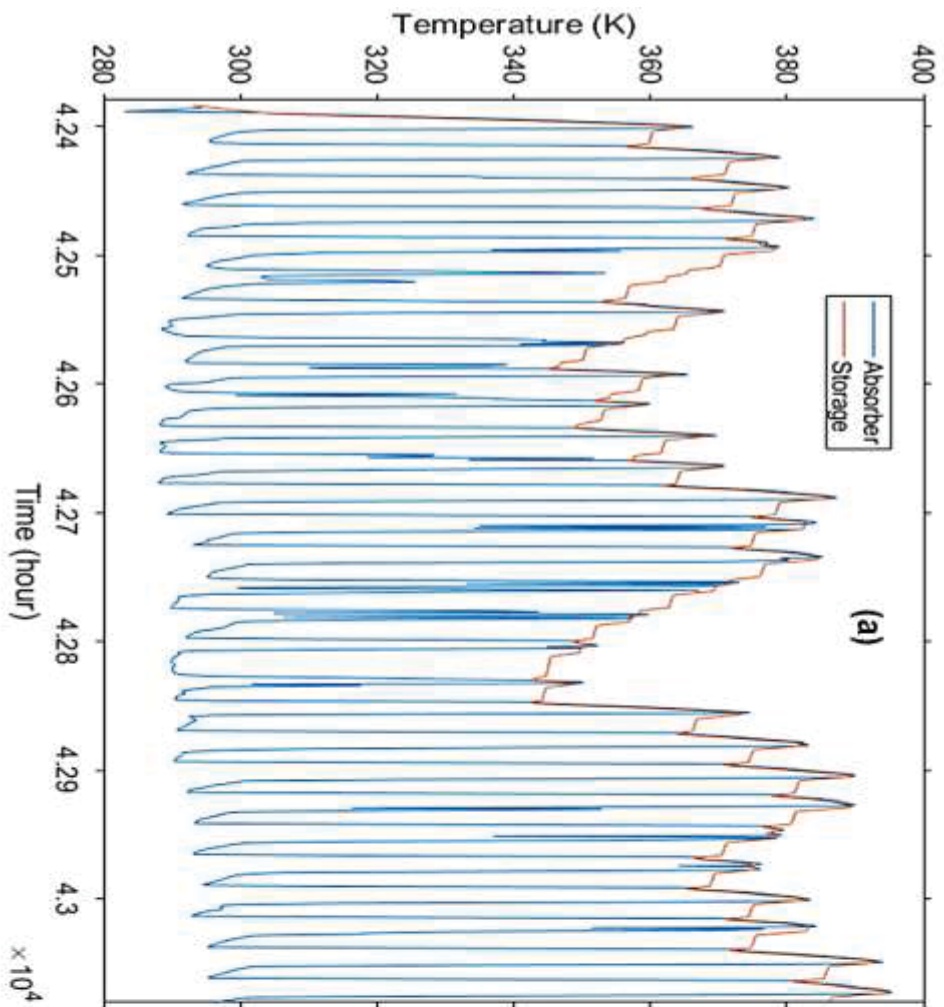




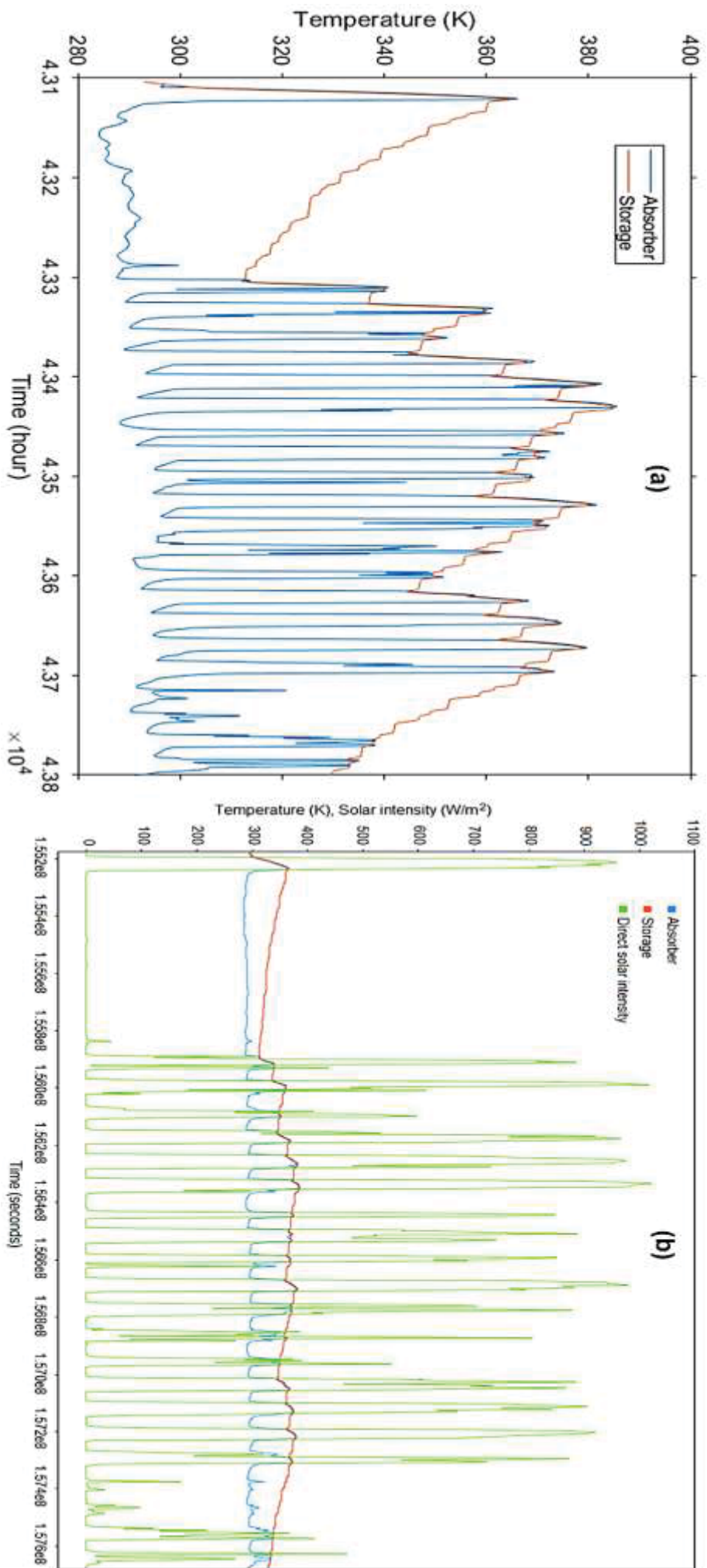
**Appendix 6.9:** Impact of solar intensity (SI) on the absorber and storage temperature for September 2019 (a) without and (b) with solar intensity relationship.



**Appendix 6.10:** Impact of solar intensity (SI) on the absorber and storage temperature for October 2019 (a) without and (b) with solar intensity relationship.



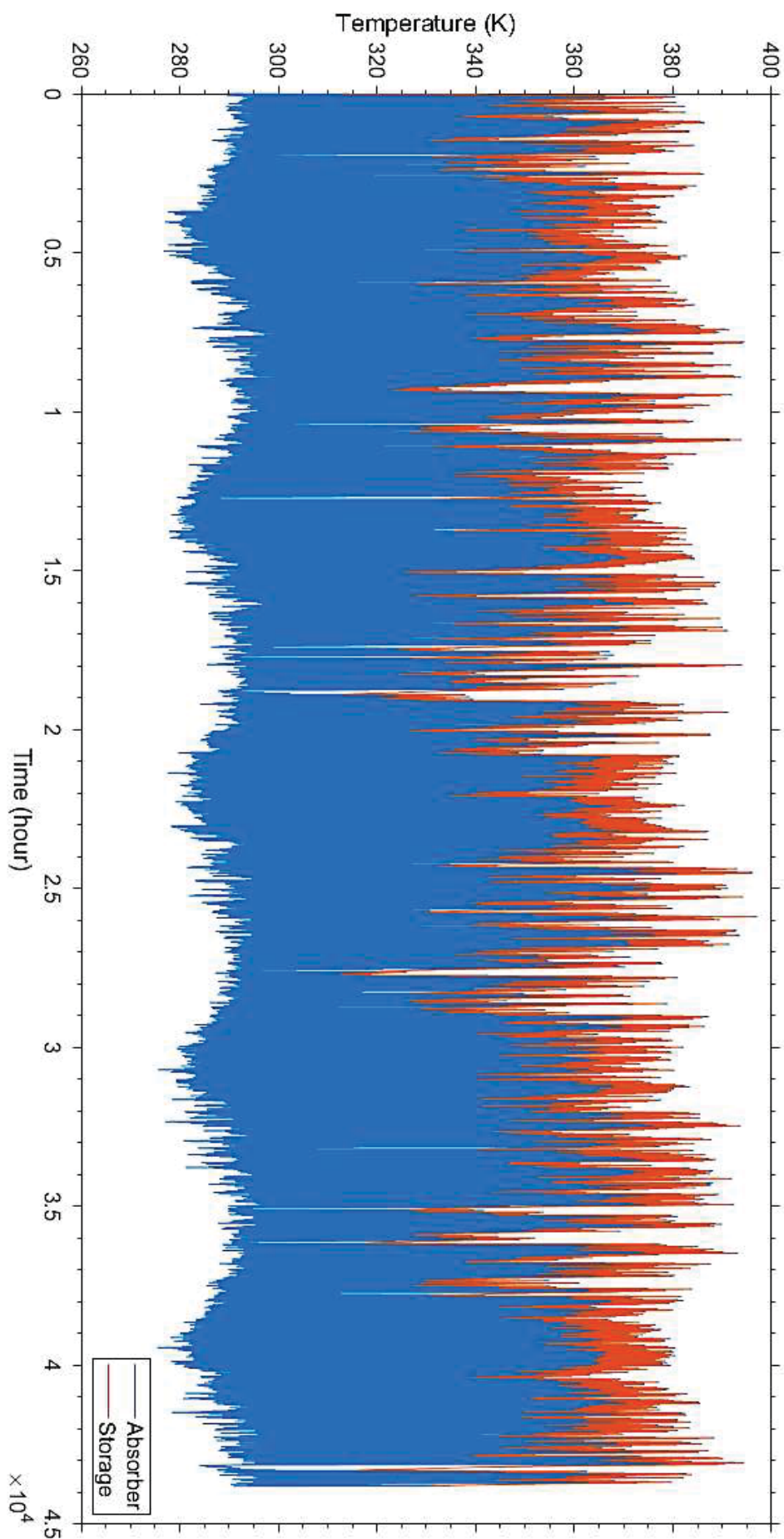
**Appendix 6.11:** Impact of solar intensity (SI) on the absorber and storage temperature for November 2019 (a) without and (b) with solar intensity relationship.



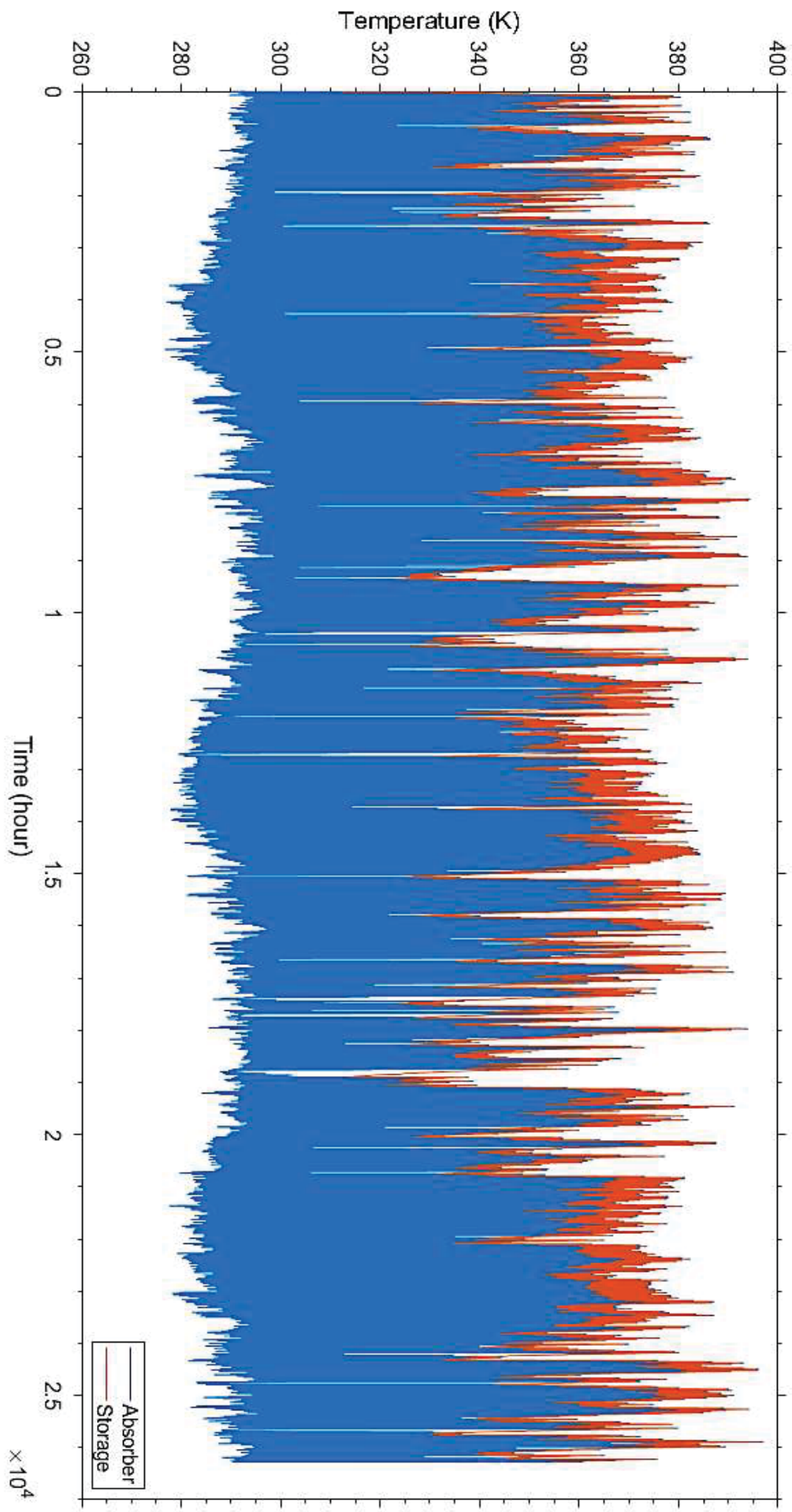
**Appendix 6.12:** Impact of solar intensity (S) on the absorber and storage temperature for December 2019 (a) without and (b) with solar intensity relationship.



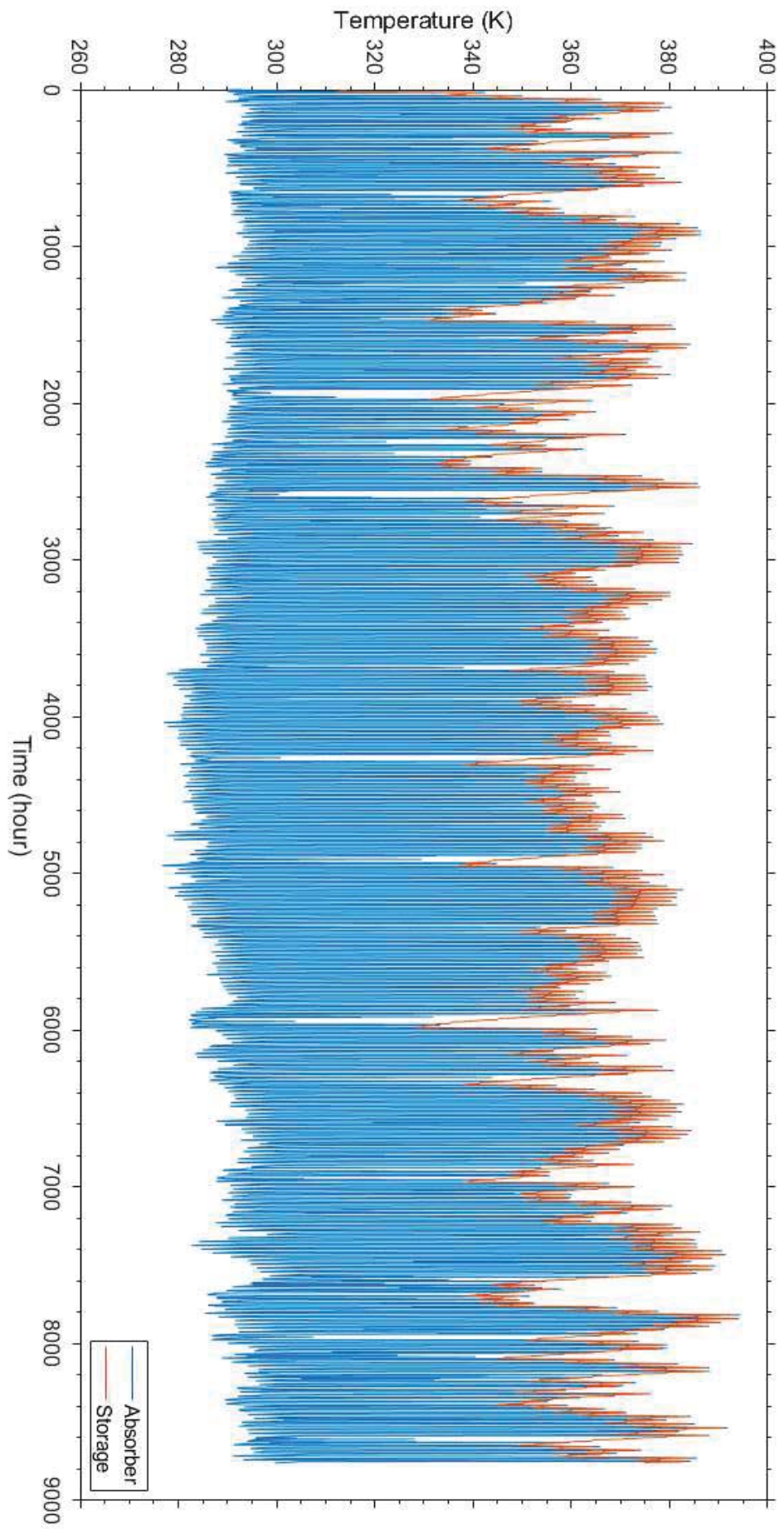
**Appendix 7:** Impact of solar intensity on the absorber and storage temperature for five years (January 2015 – December 2019).



**Appendix 8:** Impact of solar intensity on the absorber and storage temperature for three years (January 2015 – December 2017).

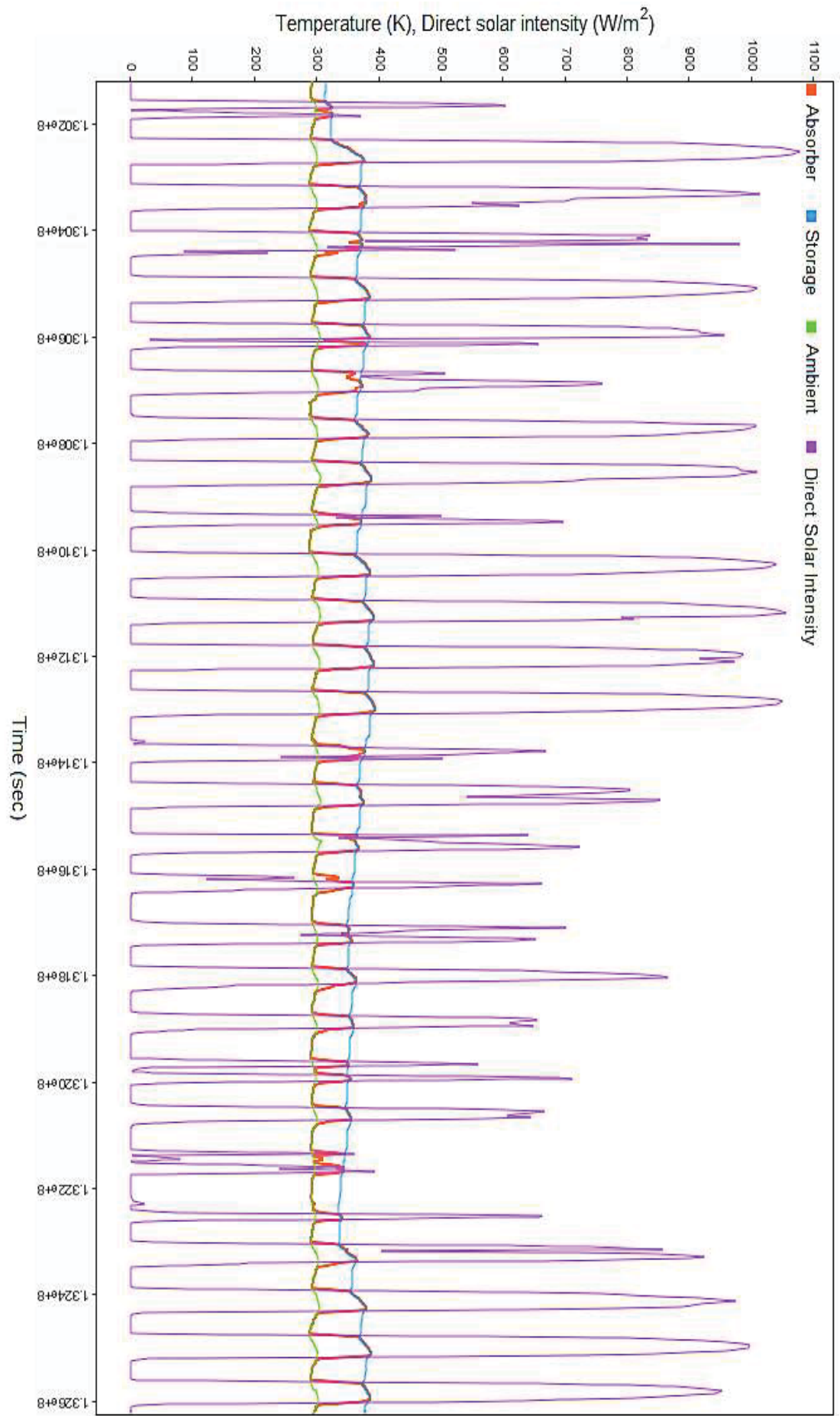


**Appendix 9:** Impact of solar intensity on the absorber and storage temperature for one years (January – December 2015).

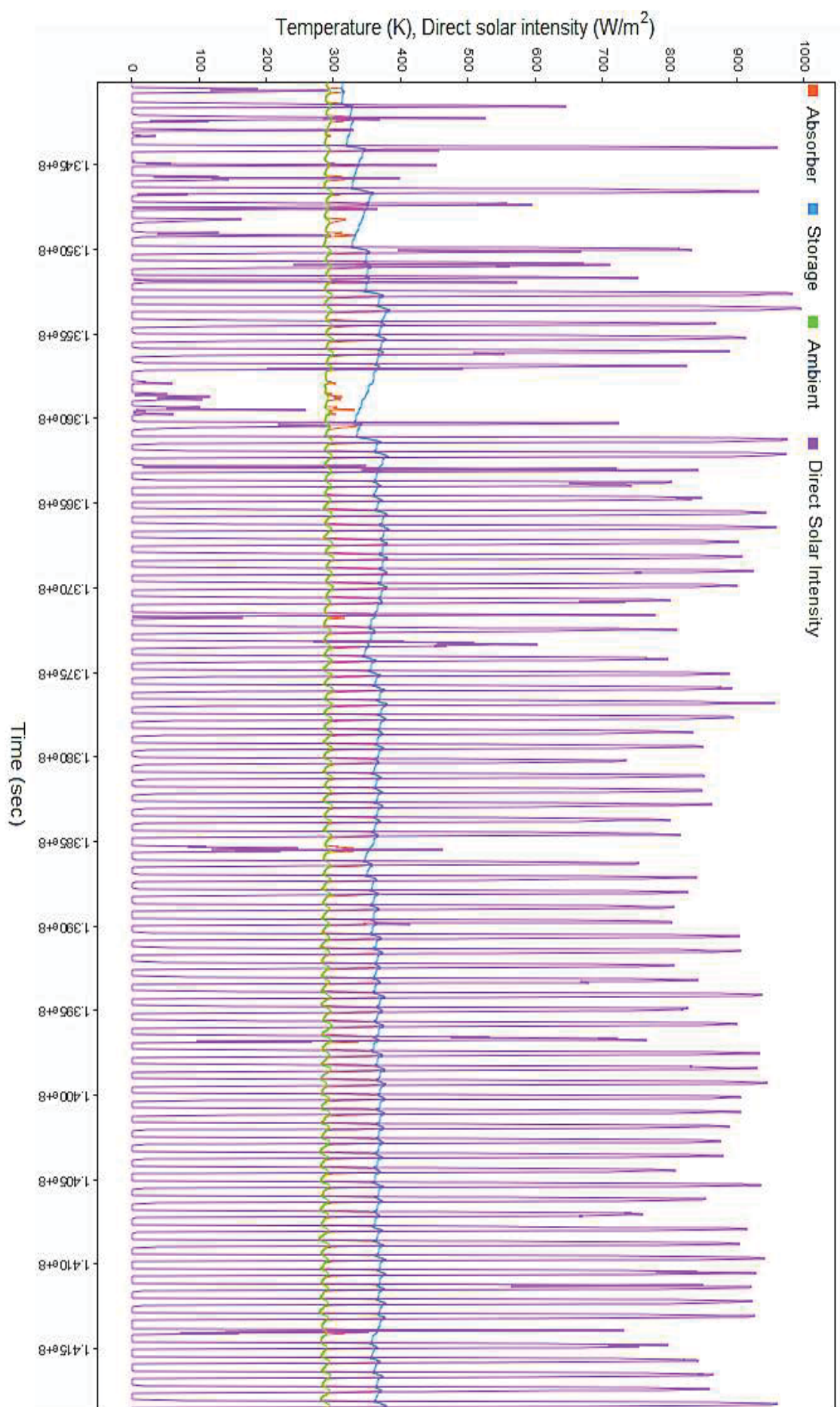




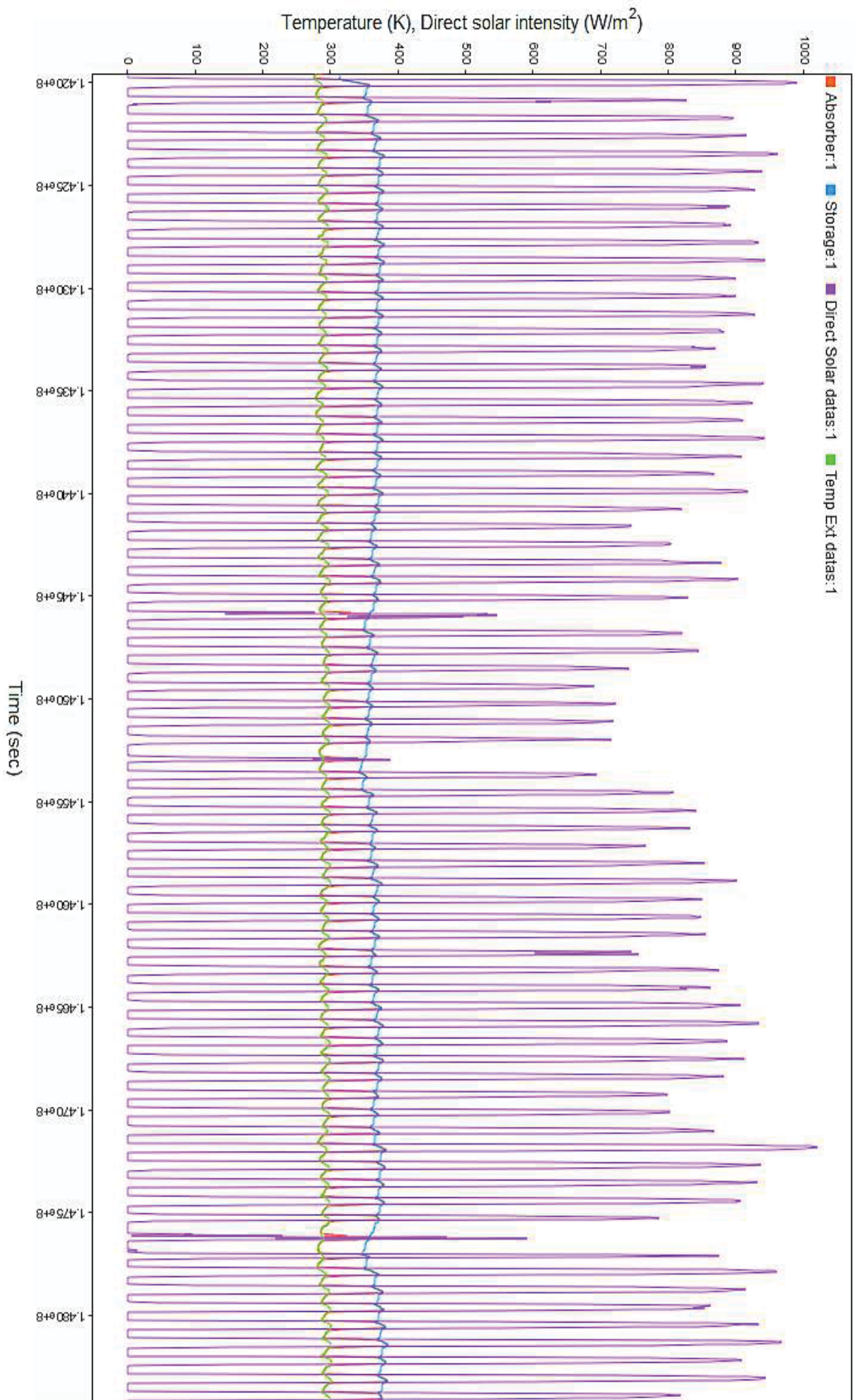
**Appendix 10:** Absorber and storage temperature during autumn (mid-February to April 2019).



**Appendix 11: Absorber and storage temperature during winter (May to July 2019).**

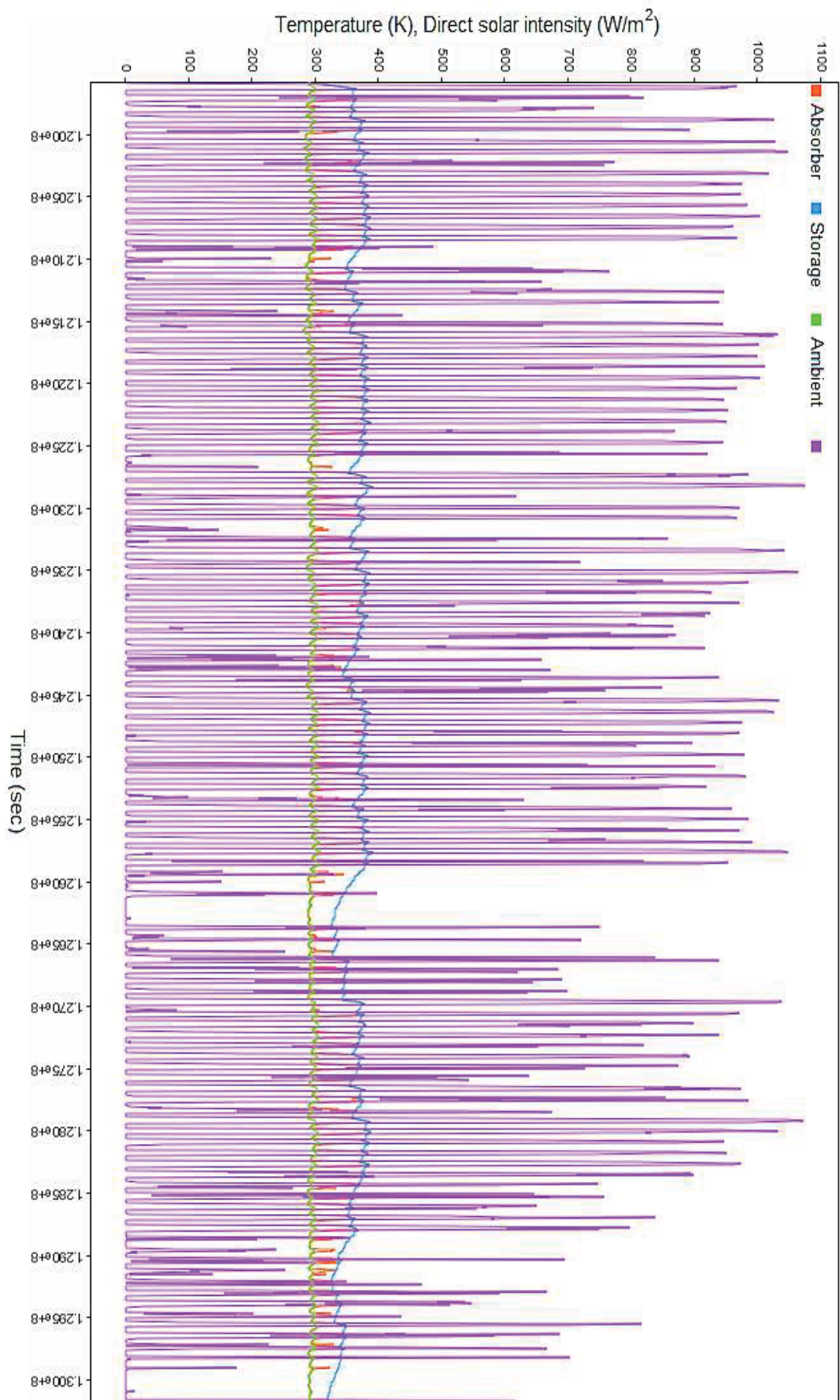


**Appendix 12: Absorber and storage temperature during spring (August to mid-October 2019).**





**Appendix 13: Absorber and storage temperature during summer (mid-October 2018 to mid-February 2019).**







**Titre :** Développement d'un Système Chauffe-Eau Solaire Avec Poursuite Pour la Maximisation du Rendement et Réservoir de Stockage avec Isolation en Matériaux composites

**Mots clés :** Modélisation, Développement de système, La performance du système, Énergie renouvelable

**Résumé :** Les sources d'énergies utilisées pour le chauffage de l'eau dans les bâtiments commerciaux et résidentielles sont multiples. Ces ressources sont essentiellement électriques dans les milieux urbains et utilisent le bois dans les milieux ruraux. Le pourcentage de l'énergie solaire utilisé reste assez faible. Les méthodes les utilisées pour produire l'eau chaude sont pour basés pour l'essentielle sur l'utilisation des résistances électrique ou des capteurs solaire plat. Le travail présenté dans cette thèse est basé sur l'utilisation des concentrateurs solaires pour chauffer des collecteurs d'énergie. Le rendement est augmenté par le développement de nouveau matériaux pour le stockage.

La structure pour le support du collecteur a été conçue et analysée utilisant le logiciel Solidworks®. Les forces agissant sur les éléments de la structure sont simulées pour assurer la fiabilité du support lors des différentes conditions de fonctionnement. L'analyse par la méthode des éléments finis a permis la vérification de la structure utilisée pour le réflecteur et son support.

Les performances énergétiques ont été simulées pour cinq ans d'opération utilisant le logiciel Matlab Simulink®.

Cette simulation a été basée sur l'utilisation de trois données différentes. La première est une base de données météorologique de cinq ans en Afrique du Sud dans la Ville de Tshwane. La deuxième est un profil d'utilisation pour un foyer type. La troisième est le coût de complément de chauffage en électricité dépendant de l'heure de l'utilisation. Cette simulation a permis la validation des choix de dimensions de différents éléments du système de chauffage.

Cette étude a permis le développement d'une approche pour la conception d'un système de chauffage solaire en optimisant les dimensions des différents éléments pour un foyer type et une région spécifique. De plus, nous avons conçu un autre réservoir d'eau chaude. Nous avons démontré que l'utilisation de matériaux polymères et d'autres matériaux comme le polyuréthane, le sel et l'aluminium est possible pour le développement d'un réservoir de stockage d'eau chaude en fonction de leurs propriétés inhérentes.

L'extension des résultats de cette thèse améliorera encore les conceptions des technologies de concentrateurs solaires et des systèmes de chauffage solaire de l'eau. Par conséquent, certaines recommandations et suggestions sont mises en évidence afin d'améliorer la conception, l'analyse et les performances globales du système.

**Title :** Development of Smart Parabolic Trough Solar Collector for Water Heating and Hybrid Polymeric Composite Water Storage Tank

**Keywords :** Modelling, System development, System performance, Renewable energy

**Abstract :** In recent years, various energy sources and methods have been used to heat water in domestic and commercial buildings. The known sources for water heating include electrical energy and solar radiation energy in the urban regions or burning of firewood in the rural areas. Several water heating methods may be used such as electrical heating elements, solar concentrators, flat plate collectors and evacuated tube collectors. This thesis focuses on ways to further improve the system's performance for water heating through the combined use of solar energy and solar concentrator technique. Furthermore, the study proposed an alternative design method for the hot water storage tank.

The solar collector-supporting frame was designed and analysed using Solidworks<sup>®</sup>. The forces acting on the structural members were simulated to determine the capacity of the frame to sustain the load, and the possible regions on the supporting frame, which could potentially fail while in operation. Energy performance was simulated for five years of operation using Matlab Simulink<sup>®</sup> software.

This simulation was based on the use of three different data. The first is a five-year weather database of the City of Tshwane in South Africa. The second is a hot water consumption profile for a typical household. The third is the cost of additional heating with electricity depending on the time of use. This simulation allowed the validation of the choices of the different elements of the heating system.

This study allowed the development of an approach for the design of a solar heating system by optimising the dimensions of the different elements for a typical household and a specific region. In addition, the use of polymeric materials and other materials like polyurethane, salt and aluminium is possible for the development of a hot water storage tank based on their inherent properties.

Extending the findings in this thesis will further improve the designs for solar concentrator technologies and solar water heating systems. Therefore, some recommendations and suggestions are highlighted in order to improve the overall system design, analysis and performance.